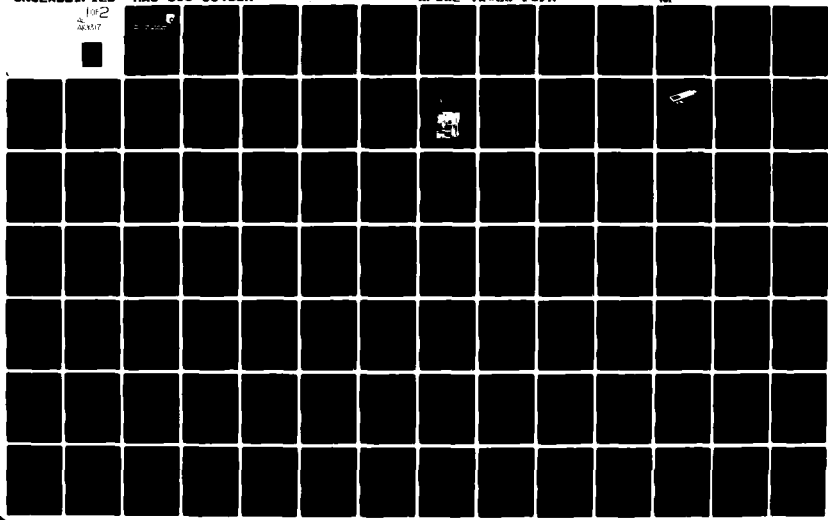


AD-A101 317

HUGHES AIRCRAFT CO LOS ANGELES CALIF SPACE AND COMMU--ETC F/8 10/2  
HIGH EFFICIENCY SOLAR PANEL, PHASE II. GALLIUM ARSENIDE.(U)  
MAR 81 G WOLFF, S S KAMATH, G J VENDURA F33615-77-C-3150  
HAC-SC8-00453R AFVAL-Tr-80-212A NI

UNCLASSIFIED

for 2  
4307



AD A101317



AFWAL-TR-80-2128

# HIGH EFFICIENCY SOLAR PANEL, PHASE II, GALLIUM ARSENIDE

George Wolff, Sanjiv S Kamath, George J Vendura, et al  
Hughes Aircraft Company  
Space and Communications Group  
P.O. Box 92426  
Los Angeles, California 90009

MARCH 1981

TECHNICAL REPORT AFWAL-TR-80-2128

**Final Report for Period  
September 1977 – September 1980**

Approved for Public Release, Distribution Unlimited

ERIC  
RECEIVED  
JUL 14 1981

A

AERO PROPULSION LABORATORY  
AIR FORCE WRIGHT AERONAUTICAL LABORATORIES  
AIR FORCE SYSTEMS COMMAND  
WRIGHT PATTISON AIR FORCE BASE, OHIO 45433

817 13 020

AD A101317



AFWAL-TR-80-2128

# HIGH EFFICIENCY SOLAR PANEL, PHASE II, GALLIUM ARSENIDE

George Wolff, Sanjiv S Kamath, George J Vendura, et al  
Hughes Aircraft Company  
Space and Communications Group  
P.O. Box 92426  
Los Angeles, California 90009

MARCH 1981

TECHNICAL REPORT AFWAL-TR-80-2128

**Final Report for Period  
September 1977 – September 1980**

Approved for Public Release, Distribution Unlimited

ERIC  
RECEIVED  
JUL 14 1981

A

AERO PROPULSION LABORATORY  
AIR FORCE WRIGHT AERONAUTICAL LABORATORIES  
AIR FORCE SYSTEMS COMMAND  
WRIGHT PATTISON AIR FORCE BASE, OHIO 45433

817 13 020

**NOTICE**

*When Government drawings, specifications, or other data are used for any purpose other than in connection with a definitely related Government procurement operation, the United States Government thereby incurs no responsibility nor any obligation whatsoever; and the fact that the government may have formulated, furnished, or in any way supplied the said drawings, specifications, or other data, is not to be regarded by implication or otherwise as in any manner licensing the holder or any person or corporation, or conveying any rights or permission to manufacture, use, or sell any patented invention that may in any way be related thereto.*

*This report has been reviewed by the Office of Public Affairs (ASD/PA) and is releasable to the National Technical Information Service (NTIS). At NTIS it will be available to the general public, including foreign nations.*

*This technical report has been reviewed and is approved for publication.*

Kenneth T. Masloski

KENNETH T. MASLOSKI, 2Lt, USAF  
Project Engineer  
Energy Conversion Branch

Joseph F. Wise

JOSEPH F. WISE  
TAM, Solar/thermal Power  
Energy Conversion Branch  
Aerospace Power Division

**FOR THE COMMANDER**

J.D. Reams

JAMES D. REAMS  
Chief, Aerospace Power Division  
Aero Propulsion Laboratory

*"If your address has changed, if you wish to be removed from our mailing list, or if the addressee is no longer employed by your organization, please notify AFWAL/POOC, W-PAFB, OH 45433 to help us maintain a current mailing list."*

*Copies of this report should not be returned unless return is required by security considerations, contractual obligations, or notice on a specific document.*

**NOTICE**

*When Government drawings, specifications, or other data are used for any purpose other than in connection with a definitely related Government procurement operation, the United States Government thereby incurs no responsibility nor any obligation whatsoever; and the fact that the government may have formulated, furnished, or in any way supplied the said drawings, specifications, or other data, is not to be regarded by implication or otherwise as in any manner licensing the holder or any person or corporation, or conveying any rights or permission to manufacture, use, or sell any patented invention that may in any way be related thereto.*

*This report has been reviewed by the Office of Public Affairs (ASD/PA) and is releasable to the National Technical Information Service (NTIS). At NTIS it will be available to the general public, including foreign nations.*

*This technical report has been reviewed and is approved for publication.*

Kenneth T. Masloski

KENNETH T. MASLOSKI, 2Lt, USAF  
Project Engineer  
Energy Conversion Branch

Joseph F. Wise

JOSEPH F. WISE  
TAM, Solar/thermal Power  
Energy Conversion Branch  
Aerospace Power Division

**FOR THE COMMANDER**

J.D. Reams

JAMES D. REAMS  
Chief, Aerospace Power Division  
Aero Propulsion Laboratory

*"If your address has changed, if you wish to be removed from our mailing list, or if the addressee is no longer employed by your organization, please notify AFWAL/POOC, W-PAFB, OH 45433 to help us maintain a current mailing list."*

*Copies of this report should not be returned unless return is required by security considerations, contractual obligations, or notice on a specific document.*

SECURITY CLASSIFICATION OF THIS PAGE (When Data Entered)

REPORT DOCUMENTATION PAGE		READ INSTRUCTIONS BEFORE COMPLETING FORM
1. REPORT NUMBER <i>(18) AFWAL-TR-SD-2128</i>	2. GOVT ACCESSION NO. <i>AD-A101 327</i>	3. RECIPIENT'S CATALOG NUMBER
4. TITLE (and Subtitle) <i>HIGH EFFICIENCY SOLAR PANEL PHASE II GALLIUM ARSENIDE.</i>	5. TYPE OF REPORT & PERIOD COVERED Final <i>Rept.</i> 45 Sept.- 1977 <i>to</i> Sept. 1980	
7. AUTHOR(s) <i>George Wolff, Sanjiv S. Kamath, George J. Vendura</i>	8. PERFORMING ORGANIZATION REPORT NUMBER <i>SCG-00453R</i>	
9. PERFORMING ORGANIZATION NAME AND ADDRESS Hughes Aircraft Company, SCG P.O. Box 92426 Los Angeles, CA 90009	10. PROGRAM ELEMENT, PROJECT, TASK AREA & WORK UNIT NUMBERS <i>63401 F 16/682J0406 17 04</i>	
11. CONTROLLING OFFICE NAME AND ADDRESS Aero-Propulsion Laboratory (AFWAL/POOC) Air Force Wright Aeronautical Laboratories (AFSC) Wright-Patterson AFB, Ohio 45433	12. REPORT DATE <i>11 March 1981</i>	
14. MONITORING AGENCY NAME & ADDRESS (if different from Controlling Office)	13. NUMBER OF PAGES <i>124</i>	
	15. SECURITY CLASS. (of this report) <i>UNCLASSIFIED</i>	
	16. DECLASSIFICATION/DOWNGRADING SCHEDULE	
16. DISTRIBUTION STATEMENT (of this Report)  Approved for public release, distribution unlimited		
17. DISTRIBUTION STATEMENT (of the abstract entered in Block 20, if different from Report)		
18. SUPPLEMENTARY NOTES		
19. KEY WORDS (Continue on reverse side if necessary and identify by block number)  Gallium Arsenide Solar Cells; 2 x 2 cm GaAs Solar Cells; 2 x 4 cm GaAs Solar Cells; Welded Interconnects; Liquid Phase Epitaxy Growth Process; Horizontal Bridgman Crystal Growth		
20. ABSTRACT (Continue on reverse side if necessary and identify by block number)  The goals of the GaAs High Efficiency Solar Panel Program were to demonstrate experimentally that space cells with efficiencies of 16% or better can be consistently produced. In developing the cells, fabrication processes were to be streamlined and perfected so cells are readily producible in large quantities. All the goals of the program were met in that the process for growing cells with efficiencies greater than 16% was fully developed. Cells with efficiencies greater than 18% were produced. A comprehensive qualification test program was successfully conducted, and the GaAs cells are now fully space qualified.		

DD FORM 1 JAN 73 1473

*312403-51*

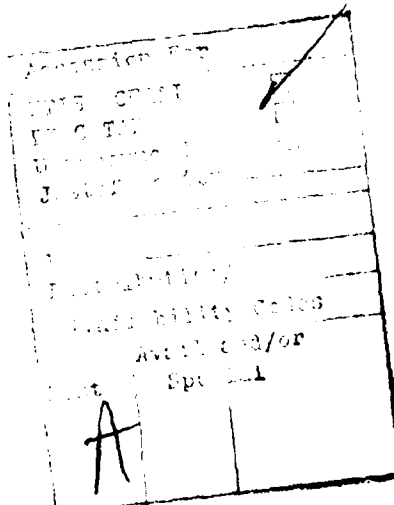
SECURITY CLASSIFICATION OF THIS PAGE (When Data Entered)

## PREFACE

The work described in this report was conducted between 15 September 1977 and 30 September 1980 under the direction of the Aero-Propulsion Laboratory, Wright-Patterson Air Force Base, Ohio; Contract No. F33615-77-C-3150; Program Element, Project, Task Area, and Work Unit number 63401 F 682J0406. J. Beam (AFWAL/POOC) was the Air Force Project Engineer.

This report was submitted to AFWAL/POOC on 17 November 1980.

The authors of this report were J. Ewan, S. Kamath, R. Knechtli, R. Loo, G. Vendura and G. Wolff. The program was managed by George Wolff with the valuable assistance of George Vendura of the Hughes Space and Communications Group, and Ron Knechtli of the Hughes Malibu Research Laboratories.



## PREFACE

The work described in this report was conducted between 15 September 1977 and 30 September 1980 under the direction of the Aero-Propulsion Laboratory, Wright-Patterson Air Force Base, Ohio; Contract No. F33615-77-C-3150; Program Element, Project, Task Area, and Work Unit number 63401 F 682J0406. J. Beam (AFWAL/POOC) was the Air Force Project Engineer.

This report was submitted to AFWAL/POOC on 17 November 1980.

The authors of this report were J. Ewan, S. Kamath, R. Knechtli, R. Loo, G. Vendura and G. Wolff. The program was managed by George Wolff with the valuable assistance of George Vendura of the Hughes Space and Communications Group, and Ron Knechtli of the Hughes Malibu Research Laboratories.

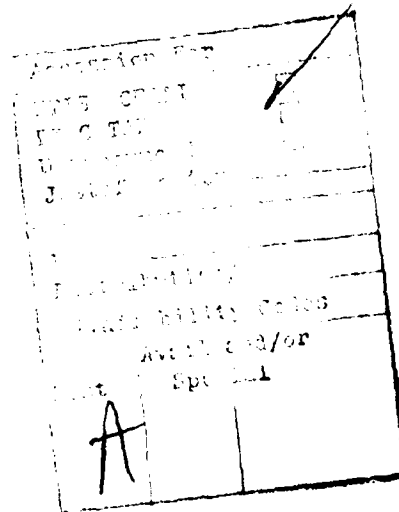


## TABLE OF CONTENTS

	<u>Page</u>
1. PROGRAM SUMMARY	1
1.1 Program Objectives and Results	1
1.2 Schedule	1
1.3 Key Elements	3
2. BASELINE CELL DESIGN	7
3. GaAs CELL PROCESSES	11
3.1 GaAs Growth Method	11
3.2 Epitaxial Process Development	13
3.3 LPE Solution Parameter Control	16
3.4 Cell Fabrication	18
3.5 Cell Production and Delivery	19
4. GaAs CELL METALLIZATION	23
4.1 General Background	23
4.2 Contact Metallization Techniques	24
4.3 Welding	25
5. GaAs SUBSTRATE	31
5.1 Introduction	31
5.2 Horizontal Bridgman Crystal Growth	31
5.3 Large Area GaAs Substrates - Assessment	33
5.4 Sawing and Polishing Process - Assessment	36
5.5 Thin GaAs Substrates - Assessment	37
6. TEST RESULTS	41
6.1 Group A - Contact Welding and Temperature Cycling Test	41
6.2 Group B - Radiation Resistance Test	43
6.3 Group C - Contact Integrity After Weld Test	49
6.4 Group D - High Temperature Vacuum and Humidity Test	53
6.5 Group E - Electrical Output Before Glassing and Radiometric Properties Test	57
6.6 Special Tests - Single Cell and Cell Module Thermal Tests	59
6.7 Spectrolab Documentation	61
6.8 Spectrolab Test Results	65
7. CONCLUSIONS	71
APPENDICES	
A. Radiation Test Results	75
B. GaAs Manufacturing Control Documentation	87
C. Safety Plan	127

## TABLE OF CONTENTS

	<u>Page</u>
1. PROGRAM SUMMARY	1
1.1 Program Objectives and Results	1
1.2 Schedule	1
1.3 Key Elements	3
2. BASELINE CELL DESIGN	7
3. GaAs CELL PROCESSES	11
3.1 GaAs Growth Method	11
3.2 Epitaxial Process Development	13
3.3 LPE Solution Parameter Control	16
3.4 Cell Fabrication	18
3.5 Cell Production and Delivery	19
4. GaAs CELL METALLIZATION	23
4.1 General Background	23
4.2 Contact Metallization Techniques	24
4.3 Welding	25
5. GaAs SUBSTRATE	31
5.1 Introduction	31
5.2 Horizontal Bridgman Crystal Growth	31
5.3 Large Area GaAs Substrates - Assessment	33
5.4 Sawing and Polishing Process - Assessment	36
5.5 Thin GaAs Substrates - Assessment	37
6. TEST RESULTS	41
6.1 Group A - Contact Welding and Temperature Cycling Test	41
6.2 Group B - Radiation Resistance Test	43
6.3 Group C - Contact Integrity After Weld Test	49
6.4 Group D - High Temperature Vacuum and Humidity Test	53
6.5 Group E - Electrical Output Before Glassing and Radiometric Properties Test	57
6.6 Special Tests - Single Cell and Cell Module Thermal Tests	59
6.7 Spectrolab Documentation	61
6.8 Spectrolab Test Results	65
7. CONCLUSIONS	71
APPENDICES	
A. Radiation Test Results	75
B. GaAs Manufacturing Control Documentation	87
C. Safety Plan	127

## LIST OF ILLUSTRATIONS

	<u>Page</u>
1. GaAs HESP II Program schedule	2
2. GaAs solar cell baseline design	7
3. LPE fabrication of GaAs solar cells	12
4. Hughes infinite solution epitaxy system with 3000 gm capacity	12
5. New substrate holder with large rectangular GaAs substrate	16
6. Cell yield for September 1977 through December 1978	20
7. GaAs solar cell fabrication process	25
8. Parallel gap welder: working area	25
9. Silver foil pattern with six tabs	26
10. Top view schematic of ultrasonic seam welder and supporting equipment	27
11. Horizontal Bridgman growth	32
12. Boat supports	32
13. HESP II test plan	42
14. Cell performance histograms	46
15. Neutron irradiation test results	48
16. Electron irradiation test results	49
17. Temperature coefficient curves	51
18. Pull strength histograms	54
19. Antireflection coating and glassing results	59
20. Cell 3465 spectral reflectance	60
21. Intensity variation test	66
22. Temperature variation test	66

### Appendix A Illustrations

1. The (AlGa) As-GaAs solar cell	77
2. Maximum power as a function of 1 MeV electron fluence	79
3. (AlGa) As-GaAs solar cell spectral response before and after 1 MeV electron irradiation	79
4. Short circuit current density versus 1 MeV electron radiation fluence, electrons/cm <sup>2</sup>	79
5. Predicted (AlGa) As-GaAs solar cell short circuit current density versus 1 MeV electron radiation fluence (AlGa)As layer thickness = 1.0 $\mu$ m, initial diffusion length $L_{po}$ = 2 $\mu$ m, $L_{no}$ = 5 $\mu$ m, and diffusion length damage constant $K_L$ = $7 \times 10^{-8}$ )	80
6. Short circuit current versus electron fluence level (1 MeV)	80
7. Maximum output power versus 1 MeV electron fluence	80
8(a). (AlGa)As-GaAs solar cell spectral response versus 1 MeV electron radiation fluences	81
8(b). (AlGa)As-GaAs solar cell spectral response versus 1 MeV electron radiation fluence	81

## LIST OF ILLUSTRATIONS

	<u>Page</u>
1. GaAs HESP II Program schedule	2
2. GaAs solar cell baseline design	7
3. LPE fabrication of GaAs solar cells	12
4. Hughes infinite solution epitaxy system with 3000 gm capacity	12
5. New substrate holder with large rectangular GaAs substrate	16
6. Cell yield for September 1977 through December 1978	20
7. GaAs solar cell fabrication process	25
8. Parallel gap welder: working area	25
9. Silver foil pattern with six tabs	26
10. Top view schematic of ultrasonic seam welder and supporting equipment	27
11. Horizontal Bridgman growth	32
12. Boat supports	32
13. HESP II test plan	42
14. Cell performance histograms	46
15. Neutron irradiation test results	48
16. Electron irradiation test results	49
17. Temperature coefficient curves	51
18. Pull strength histograms	54
19. Antireflection coating and glassing results	59
20. Cell 3465 spectral reflectance	60
21. Intensity variation test	66
22. Temperature variation test	66

### Appendix A Illustrations

1. The (AlGa) As-GaAs solar cell	77
2. Maximum power as a function of 1 MeV electron fluence	79
3. (AlGa) As-GaAs solar cell spectral response before and after 1 MeV electron irradiation	79
4. Short circuit current density versus 1 MeV electron radiation fluence, electrons/cm <sup>2</sup>	79
5. Predicted (AlGa) As-GaAs solar cell short circuit current density versus 1 MeV electron radiation fluence (AlGa)As layer thickness = 1.0 $\mu$ m, initial diffusion length $L_{po}$ = 2 $\mu$ m, $L_{no}$ = 5 $\mu$ m, and diffusion length damage constant $K_L$ = $7 \times 10^{-8}$ )	80
6. Short circuit current versus electron fluence level (1 MeV)	80
7. Maximum output power versus 1 MeV electron fluence	80
8(a). (AlGa)As-GaAs solar cell spectral response versus 1 MeV electron radiation fluences	81
8(b). (AlGa)As-GaAs solar cell spectral response versus 1 MeV electron radiation fluence	81

LIST OF ILLUSTRATIONS (Concluded)

8(c).	(AlGa)As-GaAs solar cell spectral response for several electron energies	81
9.	Dark I-V characteristics before and after electron irradiation	81
10(a).	Solar cell maximum output power versus 15.4 MeV proton irradiation fluence	82
10(b).	Solar cell maximum output power versus 40 MeV proton irradiation fluence	82
11.	(AlGa)As-GaAs solar cell spectral response before and after 15.4 MeV proton irradiation	82
12.	(AlGa)As-GaAs solar cell spectral response before and after 40 MeV proton irradiation	83
13.	Dark I-V characteristics before and after proton irradiation	83
14.	Unannealed fraction versus annealing time	84
15(a).	Spectral response before and after thermal annealing cell 1222	84
15(b).	Spectral response before and after thermal annealing cell 1008	84
15(c).	Spectral response before and after irradiation and after annealing cell 1278	84
16(a).	Dark I-V characteristic before and after thermal annealing cell 1222	85
16(b).	Dark I-V characteristic before and after thermal annealing cell 1008	85
16(c).	Dark I-V characteristic before and after thermal annealing cell 1278	85

LIST OF ILLUSTRATIONS (Concluded)

8(c).	(AlGa)As-GaAs solar cell spectral response for several electron energies	81
9.	Dark I-V characteristics before and after electron irradiation	81
10(a).	Solar cell maximum output power versus 15.4 MeV proton irradiation fluence	82
10(b).	Solar cell maximum output power versus 40 MeV proton irradiation fluence	82
11.	(AlGa)As-GaAs solar cell spectral response before and after 15.4 MeV proton irradiation	82
12.	(AlGa)As-GaAs solar cell spectral response before and after 40 MeV proton irradiation	83
13.	Dark I-V characteristics before and after proton irradiation	83
14.	Unannealed fraction versus annealing time	84
15(a).	Spectral response before and after thermal annealing cell 1222	84
15(b).	Spectral response before and after thermal annealing cell 1008	84
15(c).	Spectral response before and after irradiation and after annealing cell 1278	84
16(a).	Dark I-V characteristic before and after thermal annealing cell 1222	85
16(b).	Dark I-V characteristic before and after thermal annealing cell 1008	85
16(c).	Dark I-V characteristic before and after thermal annealing cell 1278	85

## LIST OF TABLES

	<u>Page</u>
1. GaAs HESP II Solar Cell Physical Specifications	8
2. GaAs HESP II Solar Cell Material Specifications	9
3. GaAs HESP II Solar Cell Electrical Specifications	10
4. Characteristics of Early GaAs Solar Cells Grown in Successive LPE Runs in December 1977	14
5. Characteristics of GaAs Solar Cells Grown in Successive LPE Runs in May 1978	14
6. Characteristics of GaAs Solar Cells Grown in Successive LPE Runs in December 1978	14
7. Characteristics of GaAs Solar Cells Grown in Successive LPE Runs in July 1979	15
8. Early GaAs Cells Grown in a Single Run (Two Substrates)	17
9. Later GaAs Cells Grown in a Single Run (Four Substrates)	17
10. Large Area (2 x 4 cm) (AlGa)As - GaAs Solar Cell Characteristics	18
11. GaAs Solar Cell Yield Versus Efficiency, September 1977 to December 1978	20
12. GaAs Solar Cell Characteristics With AgZn Contacts on P Side	25
13. Typical Ultrasonic Seam Weld Results	28
14. Typical Gap Weld Results	29
15. Large Area GaAs Substrates Growth Runs	34
16. Saw and Yield Data	38
17. Cell Performance Before and After Welding	44
18. Cell Performance Before and After Temperature Cycling	45
19. Pull Strength Test Results for GaAs Solar Cell Tabs	46
20. Neutron Irradiation Test	46
21. Cell Characteristics Before and After Neutron Irradiation	47
22. Neutron Irradiation $P_{max}$ Results	48
23. (AlGa)As - GaAs Solar Cell Characteristics Before and After 1 MeV Electron Irradiation (HESP II Cells)	50
24. GaAs Solar Cell Electrical Characteristics Before and After Welding	52
25. Pull Strength Test Results for GaAs Solar Cell Tabs (17 Cells)(Gap Weld)	53
26. Cell Electrical Characteristics Before and After Humidity Test	55
27. Cell Electrical Characteristics Before and After 120°C High Temperature at Vacuum Test	56
28. Effects of Antireflection Coating and Glassing on Cell Electrical Characteristics	58
29. Cell Solar Absorptance and Emittance	60
30. High Temperature Vacuum Test	60
31. Cell Module Thermal Test Results	62
32. GaAs Solar Cell Module Electrical Characteristics	64

## LIST OF TABLES

	<u>Page</u>
1. GaAs HESP II Solar Cell Physical Specifications	8
2. GaAs HESP II Solar Cell Material Specifications	9
3. GaAs HESP II Solar Cell Electrical Specifications	10
4. Characteristics of Early GaAs Solar Cells Grown in Successive LPE Runs in December 1977	14
5. Characteristics of GaAs Solar Cells Grown in Successive LPE Runs in May 1978	14
6. Characteristics of GaAs Solar Cells Grown in Successive LPE Runs in December 1978	14
7. Characteristics of GaAs Solar Cells Grown in Successive LPE Runs in July 1979	15
8. Early GaAs Cells Grown in a Single Run (Two Substrates)	17
9. Later GaAs Cells Grown in a Single Run (Four Substrates)	17
10. Large Area (2 x 4 cm) (AlGa)As - GaAs Solar Cell Characteristics	18
11. GaAs Solar Cell Yield Versus Efficiency, September 1977 to December 1978	20
12. GaAs Solar Cell Characteristics With AgZn Contacts on P Side	25
13. Typical Ultrasonic Seam Weld Results	28
14. Typical Gap Weld Results	29
15. Large Area GaAs Substrates Growth Runs	34
16. Saw and Yield Data	38
17. Cell Performance Before and After Welding	44
18. Cell Performance Before and After Temperature Cycling	45
19. Pull Strength Test Results for GaAs Solar Cell Tabs	46
20. Neutron Irradiation Test	46
21. Cell Characteristics Before and After Neutron Irradiation	47
22. Neutron Irradiation $P_{max}$ Results	48
23. (AlGa)As - GaAs Solar Cell Characteristics Before and After 1 MeV Electron Irradiation (HESP II Cells)	50
24. GaAs Solar Cell Electrical Characteristics Before and After Welding	52
25. Pull Strength Test Results for GaAs Solar Cell Tabs (17 Cells)(Gap Weld)	53
26. Cell Electrical Characteristics Before and After Humidity Test	55
27. Cell Electrical Characteristics Before and After 120°C High Temperature at Vacuum Test	56
28. Effects of Antireflection Coating and Glassing on Cell Electrical Characteristics	58
29. Cell Solar Absorptance and Emittance	60
30. High Temperature Vacuum Test	60
31. Cell Module Thermal Test Results	62
32. GaAs Solar Cell Module Electrical Characteristics	64

LIST OF TABLES (concluded)

33.	Process Fabrication Documentation	64
34.	Test Procedure Documentation	65
35.	Spectral Response ATP	66
36.	Temperature Humidity Test Results	67
37.	Thermal Shock Test Results	68
38.	High Temperature Vacuum Test Results	69
39.	Eighty Day Humidity Test Results	70
40.	GaAs Solar Cells Delivered	73

LIST OF TABLES (concluded)

33.	Process Fabrication Documentation	64
34.	Test Procedure Documentation	65
35.	Spectral Response ATP	66
36.	Temperature Humidity Test Results	67
37.	Thermal Shock Test Results	68
38.	High Temperature Vacuum Test Results	69
39.	Eighty Day Humidity Test Results	70
40.	GaAs Solar Cells Delivered	73

## 1. PROGRAM SUMMARY

This final report describes the work done during the period 15 September 1977 to 30 September 1980 by Hughes Aircraft Company on GaAs solar cells for the High Efficiency Solar Panel (HESP), Phase II (Contract F33615-77-C-3150).

1.1 Program Objectives and Results. The objective of this program was the development of space qualified solar cells having a beginning of life lot median efficiency of 16 percent at 25°C under air mass zero (AM0) illumination. The solar cell assembly was to be capable of withstanding both laser and nuclear weapons effects as well as the natural space environment at synchronous earth orbit. Also, the cells were to be readily producible in large quantities.

The end results of the program are high efficiency GaAs solar cells capable of being produced in large quantities; documentation of the qualification testing performed on the cells; a process identification document describing the cell production processes; documentation of facility, material, and personnel requirements for sustained high volume production; and trained production engineering personnel who can assume responsibility for any subsequent high volume production. In addition, the contract called for delivery of a number of both 2 x 2 cm and 2 x 4 cm GaAs solar cells, some of which were to be equipped with welded interconnects.

1.2 Schedule. The program schedule, shown in Figure 1, outlines the specific program tasks and milestones. These, in turn, can be roughly grouped into three chronological categories:

- 1) Development
- 2) Manufacturing control/qualification testing
- 3) Delivery

The first category involved extensive research and development of the basic GaAs cell over a period of 15 months. This in turn required preliminary testing to ensure proper characteristics. For instance, contacts to the cells were required to be low resistance, weldable, and capable of meeting the contract's temperature specifications; the cells themselves were

## 1. PROGRAM SUMMARY

This final report describes the work done during the period 15 September 1977 to 30 September 1980 by Hughes Aircraft Company on GaAs solar cells for the High Efficiency Solar Panel (HESP), Phase II (Contract F33615-77-C-3150).

1.1 Program Objectives and Results. The objective of this program was the development of space qualified solar cells having a beginning of life lot median efficiency of 16 percent at 25°C under air mass zero (AM0) illumination. The solar cell assembly was to be capable of withstanding both laser and nuclear weapons effects as well as the natural space environment at synchronous earth orbit. Also, the cells were to be readily producible in large quantities.

The end results of the program are high efficiency GaAs solar cells capable of being produced in large quantities; documentation of the qualification testing performed on the cells; a process identification document describing the cell production processes; documentation of facility, material, and personnel requirements for sustained high volume production; and trained production engineering personnel who can assume responsibility for any subsequent high volume production. In addition, the contract called for delivery of a number of both 2 x 2 cm and 2 x 4 cm GaAs solar cells, some of which were to be equipped with welded interconnects.

1.2 Schedule. The program schedule, shown in Figure 1, outlines the specific program tasks and milestones. These, in turn, can be roughly grouped into three chronological categories:

- 1) Development
- 2) Manufacturing control/qualification testing
- 3) Delivery

The first category involved extensive research and development of the basic GaAs cell over a period of 15 months. This in turn required preliminary testing to ensure proper characteristics. For instance, contacts to the cells were required to be low resistance, weldable, and capable of meeting the contract's temperature specifications; the cells themselves were

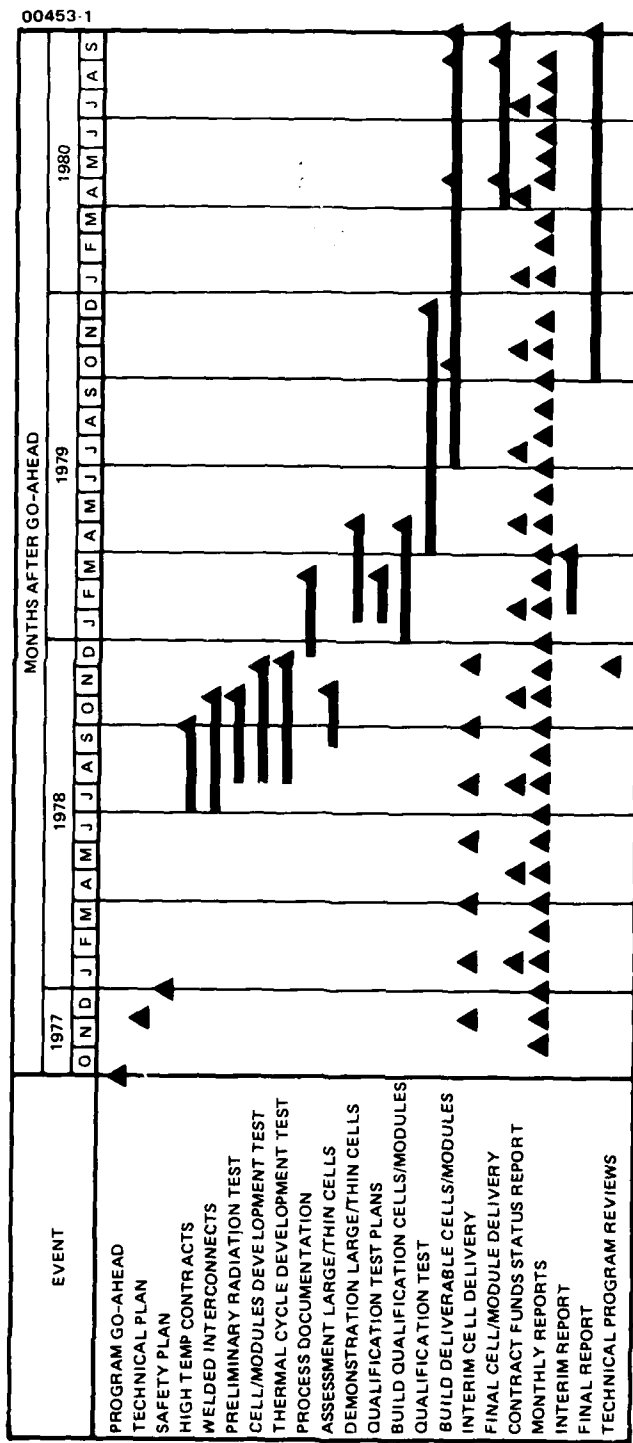


Figure 1. GaAs HESP II Program schedule

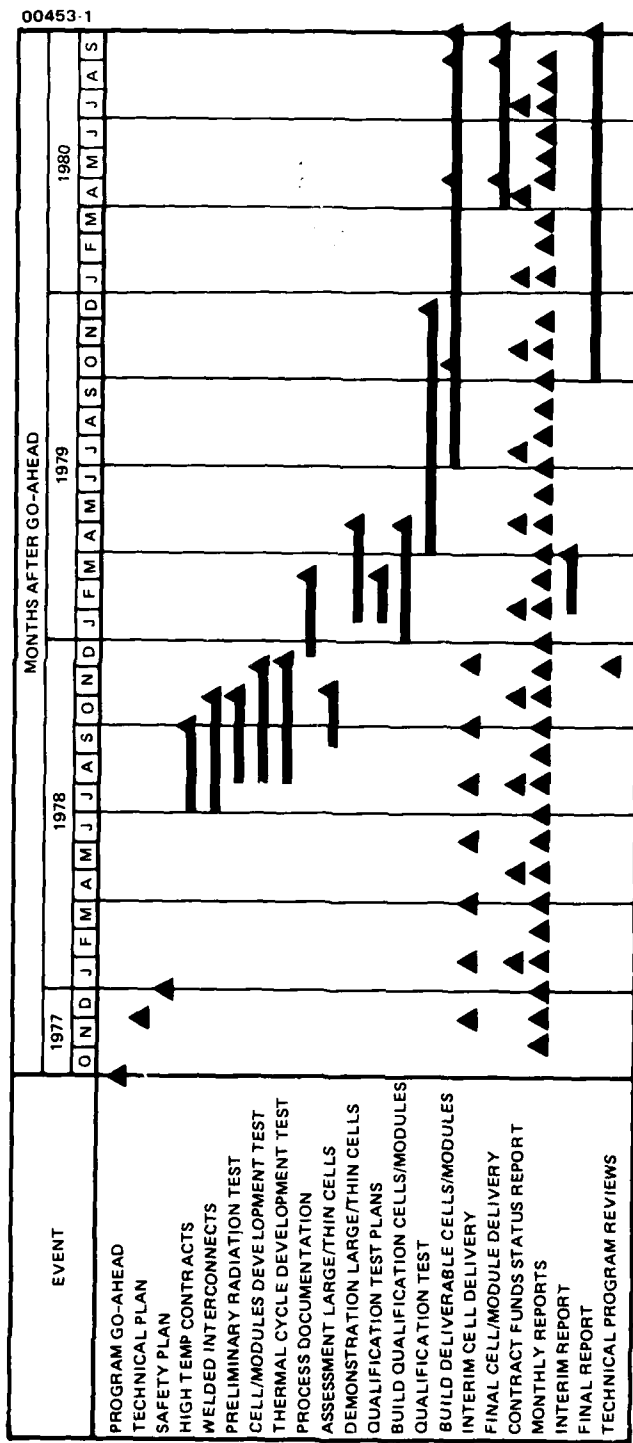


Figure 1. GaAs HESP II Program schedule

required to exhibit significant radiation hardness and to be capable of withstanding specific temperature extremes. During this stage of the contract, fabrication processes were significantly altered several times to arrive at an optimized cell design.

The second period, involving manufacturing control and qualification testing lasted about 6 months and entailed freezing all fabrication processes. At that point, the cell had become sufficiently standardized that finished devices were as close to identical as possible. This standardization process was followed by elaborate qualification testing covering all aspects of the final solar cell design. Test criteria included electrical, mechanical, radiation, and thermal suitability. In addition, the effects or characteristics of the cover glass, the antireflection coating, and the contacts and interconnects were examined.

After manufacturing control documentation and qualification testing were successfully completed, the final phase of the contract began, during which larger quantities of individual cells were fabricated in accordance with the processes developed during the earlier stages. A number of these cells were delivered as individual cells and a number were delivered after interconnection into modules. In addition to the 2 x 2 cm cells, a number of 2 x 4 cm cells were made and delivered, as well as a number of thin, 8 mil GaAs cells. Total cells delivered under this contract were 370 2 x 2 cm cells and 270 2 x 4 cm cells, including the cells in the delivered interconnected modules. These numbers do not include the limited number of 8 mil thick cells.

1.3 Key Elements. Of central importance in the program was the growth of the GaAs buffer and window layers, which, in turn, determine the depth of the junction. For this determination, control of the solution characteristics and the temperature and time dependence of the epitaxial growth are critical. In Section 3, details of the liquid phase epitaxy (LPE) process are presented, along with the resulting cell characteristics.

Another key element involves the metallizations applied to the GaAs cell. This phase of the program actually had two aspects: contact metallization and interconnect methods. The former concerns the layer or layers of metals deposited on both the p type and n type cell surfaces. Ideally, such contacts must have excellent mechanical strength as well as low electrical resistance. An additional criterion, stipulated by the HESP II contract, is specific high temperature survivability. Interconnect methods, on the other hand, address the task of applying connectors onto the various contact metallizations for subsequent building of cells into arrays. For HESP II, the feasibility of both ultrasonic seam and parallel gap welding tabs were studied. Both were found to be feasible. Areas of interest included the visual and electrical characteristics of individual cells after the welding operations as well as the mechanical strength of the resulting bonds. Details of both the contact metallizations and the interconnecting method are given in Section 4.

Since a critical goal of the HESP II program was production readiness, ways were investigated to minimize the costs associated with cell fabrication. As a result, attention was centered on the substrate cell geometry. Relatively large area rectangular GaAs substrates are desirable so that more than one

required to exhibit significant radiation hardness and to be capable of withstanding specific temperature extremes. During this stage of the contract, fabrication processes were significantly altered several times to arrive at an optimized cell design.

The second period, involving manufacturing control and qualification testing lasted about 6 months and entailed freezing all fabrication processes. At that point, the cell had become sufficiently standardized that finished devices were as close to identical as possible. This standardization process was followed by elaborate qualification testing covering all aspects of the final solar cell design. Test criteria included electrical, mechanical, radiation, and thermal suitability. In addition, the effects or characteristics of the cover glass, the antireflection coating, and the contacts and interconnects were examined.

After manufacturing control documentation and qualification testing were successfully completed, the final phase of the contract began, during which larger quantities of individual cells were fabricated in accordance with the processes developed during the earlier stages. A number of these cells were delivered as individual cells and a number were delivered after interconnection into modules. In addition to the 2 x 2 cm cells, a number of 2 x 4 cm cells were made and delivered, as well as a number of thin, 8 mil GaAs cells. Total cells delivered under this contract were 370 2 x 2 cm cells and 270 2 x 4 cm cells, including the cells in the delivered interconnected modules. These numbers do not include the limited number of 8 mil thick cells.

1.3 Key Elements. Of central importance in the program was the growth of the GaAs buffer and window layers, which, in turn, determine the depth of the junction. For this determination, control of the solution characteristics and the temperature and time dependence of the epitaxial growth are critical. In Section 3, details of the liquid phase epitaxy (LPE) process are presented, along with the resulting cell characteristics.

Another key element involves the metallizations applied to the GaAs cell. This phase of the program actually had two aspects: contact metallization and interconnect methods. The former concerns the layer or layers of metals deposited on both the p type and n type cell surfaces. Ideally, such contacts must have excellent mechanical strength as well as low electrical resistance. An additional criterion, stipulated by the HESP II contract, is specific high temperature survivability. Interconnect methods, on the other hand, address the task of applying connectors onto the various contact metallizations for subsequent building of cells into arrays. For HESP II, the feasibility of both ultrasonic seam and parallel gap welding tabs were studied. Both were found to be feasible. Areas of interest included the visual and electrical characteristics of individual cells after the welding operations as well as the mechanical strength of the resulting bonds. Details of both the contact metallizations and the interconnecting method are given in Section 4.

Since a critical goal of the HESP II program was production readiness, ways were investigated to minimize the costs associated with cell fabrication. As a result, attention was centered on the substrate cell geometry. Relatively large area rectangular GaAs substrates are desirable so that more than one

cell can be made on a single substrate during any single LPE growth process. The rectangular shape is useful to reduce losses due to excess material cut away when the rectangular cell is cleaved from the processed substrates. Section 5 outlines the most economical way to grow such substrates — a way which involved extensive experimentation with various boat materials. This study, in turn, expanded into a search for suitable boat liners and both new growth and slicing orientations.

Section 5 also includes results of the attempt to reduce the initial thickness of the GaAs substrate in an effort to eventually minimize both the cost and overall weight of the individual cell. This effort involved not merely slicing single crystal ingots into thinner substrates but doing so in a speedy, economical fashion with respectable yields. The study therefore expanded into a comparison of two different sectioning methods involving both inner diameter (ID) and multiblade saws. The ID cell method was found to be preferable for good yield and reproducibility. In addition, postsaw processing (involving mechanical grinding, chemical etching, and handling) becomes significant for complete assessment of fabrication breakage and for the establishment of the ultimate yield figures.

Thorough testing of the fabricated GaAs cells was carried out throughout the test program. Generally, these experiments fall into one of three categories: developmental, special, and qualification. Developmental tests were performed during the earliest stages of the program while the 16 percent cell was in the process of being implemented. These were necessary to constantly monitor the behavior of the devices in order to intelligently establish improved fabrication processes and techniques. Once repeatable manufacturing capability was perfected, however, all procedures became frozen by extensive documentation, and the production of nearly identical GaAs solar cells followed. At this point special and qualification tests were conducted. Both types of tests are designed to characterize the cells produced and to ensure acceptable performance under specific conditions. Special testing involved thermal testing of single cells and small modules, while qualification testing consisted of five distinct categories:

- 1) Group A: contact welding and temperature cycling
- 2) Group B: contact integrity after welding
- 3) Group C: charged particle radiation resistance
- 4) Group D: high temperature vacuum and humidity
- 5) Group E: electrical before glassing and radiometric properties

Descriptions of all tests, with results, are given in Section 6.

cell can be made on a single substrate during any single LPE growth process. The rectangular shape is useful to reduce losses due to excess material cut away when the rectangular cell is cleaved from the processed substrates. Section 5 outlines the most economical way to grow such substrates — a way which involved extensive experimentation with various boat materials. This study, in turn, expanded into a search for suitable boat liners and both new growth and slicing orientations.

Section 5 also includes results of the attempt to reduce the initial thickness of the GaAs substrate in an effort to eventually minimize both the cost and overall weight of the individual cell. This effort involved not merely slicing single crystal ingots into thinner substrates but doing so in a speedy, economical fashion with respectable yields. The study therefore expanded into a comparison of two different sectioning methods involving both inner diameter (ID) and multiblade saws. The ID cell method was found to be preferable for good yield and reproducibility. In addition, postsaw processing (involving mechanical grinding, chemical etching, and handling) becomes significant for complete assessment of fabrication breakage and for the establishment of the ultimate yield figures.

Thorough testing of the fabricated GaAs cells was carried out throughout the test program. Generally, these experiments fall into one of three categories: developmental, special, and qualification. Developmental tests were performed during the earliest stages of the program while the 16 percent cell was in the process of being implemented. These were necessary to constantly monitor the behavior of the devices in order to intelligently establish improved fabrication processes and techniques. Once repeatable manufacturing capability was perfected, however, all procedures became frozen by extensive documentation, and the production of nearly identical GaAs solar cells followed. At this point special and qualification tests were conducted. Both types of tests are designed to characterize the cells produced and to ensure acceptable performance under specific conditions. Special testing involved thermal testing of single cells and small modules, while qualification testing consisted of five distinct categories:

- 1) Group A: contact welding and temperature cycling
- 2) Group B: contact integrity after welding
- 3) Group C: charged particle radiation resistance
- 4) Group D: high temperature vacuum and humidity
- 5) Group E: electrical before glassing and radiometric properties

Descriptions of all tests, with results, are given in Section 6.

An independent solar cell manufacturing company, Spectrolab Inc., was contracted to document the manufacturing procedure as practiced at Hughes Research Laboratories (HRL), document the qualification test procedure as practiced at Spectrolab, monitor cells manufactured at HRL, and qualify the

monitored GaAs solar cells. The qualification tests included a humidity test of unfiltered cells, an intensity and temperature variation test of filtered cells, and a humidity, thermal shock, and high temperature vacuum test of filtered cells, all of which were successfully completed.

Finally, Section 7 summarizes the accomplishments of the contract.

monitored GaAs solar cells. The qualification tests included a humidity test of unfiltered cells, an intensity and temperature variation test of filtered cells, and a humidity, thermal shock, and high temperature vacuum test of filtered cells, all of which were successfully completed.

Finally, Section 7 summarizes the accomplishments of the contract.

## 2. BASELINE CELL DESIGN

The basic GaAs cell structure, shown in Figure 2, consists of a highly doped (Te)  $n^+$  substrate upon which two separate layers are deposited. The first layer is a  $10\ \mu\text{m}$  (Sn) n type buffer upon which a  $0.5\ \mu\text{m}$  p (AlGa)As window is grown. The actual junction is formed by diffusion of Be dopant from the window into the buffer layer. The p GaAs thickness (junction depth,  $X_j$ ) is an extremely important parameter for radiation damage control and is therefore crucial to space cell performance.

The basic solar cell structure is further detailed in the specifications given in Tables 1 through 3. As shown in Table 2, the AuZn p contacts are about  $2000\ \text{\AA}$  thick with a silver overlay of about  $5\ \mu\text{m}$ ; the n contact is AuGeNi ( $\sim 2000\ \text{\AA}$ ) with a similar Ag overlay. The antireflection (AR) coating is  $\text{Ta}_2\text{O}_5$ , the thickness of which has been optimized to match the spectral response of the GaAs cell.

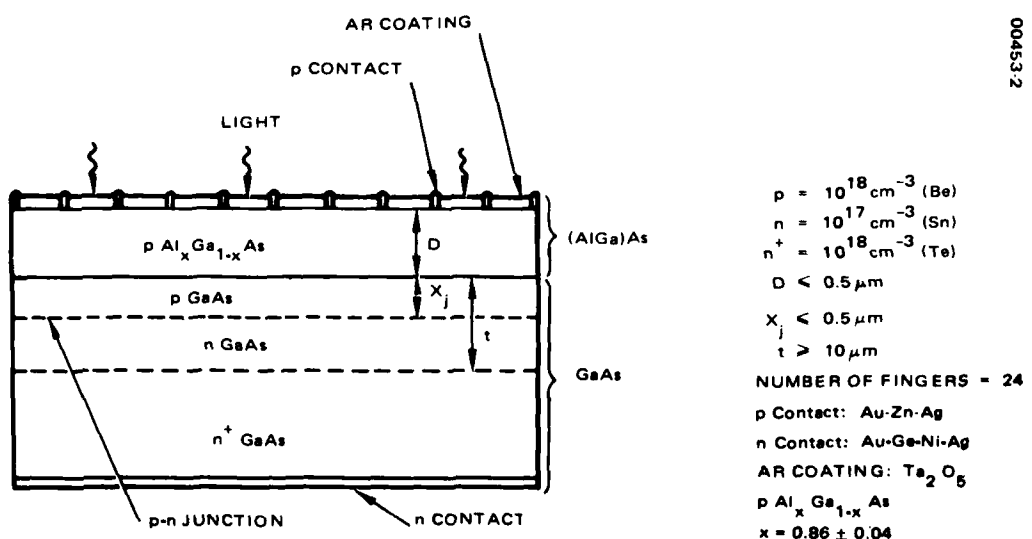


Figure 2. GaAs solar cell baseline design.

PRECEDING PAGE BLANK-NOT FILMED

## 2. BASELINE CELL DESIGN

The basic GaAs cell structure, shown in Figure 2, consists of a highly doped (Te)  $n^+$  substrate upon which two separate layers are deposited. The first layer is a  $10\ \mu\text{m}$  (Sn) n type buffer upon which a  $0.5\ \mu\text{m}$  p (AlGa)As window is grown. The actual junction is formed by diffusion of Be dopant from the window into the buffer layer. The p GaAs thickness (junction depth,  $X_j$ ) is an extremely important parameter for radiation damage control and is therefore crucial to space cell performance.

The basic solar cell structure is further detailed in the specifications given in Tables 1 through 3. As shown in Table 2, the AuZn p contacts are about  $2000\ \text{\AA}$  thick with a silver overlay of about  $5\ \mu\text{m}$ ; the n contact is AuGeNi ( $\sim 2000\ \text{\AA}$ ) with a similar Ag overlay. The antireflection (AR) coating is  $\text{Ta}_2\text{O}_5$ , the thickness of which has been optimized to match the spectral response of the GaAs cell.

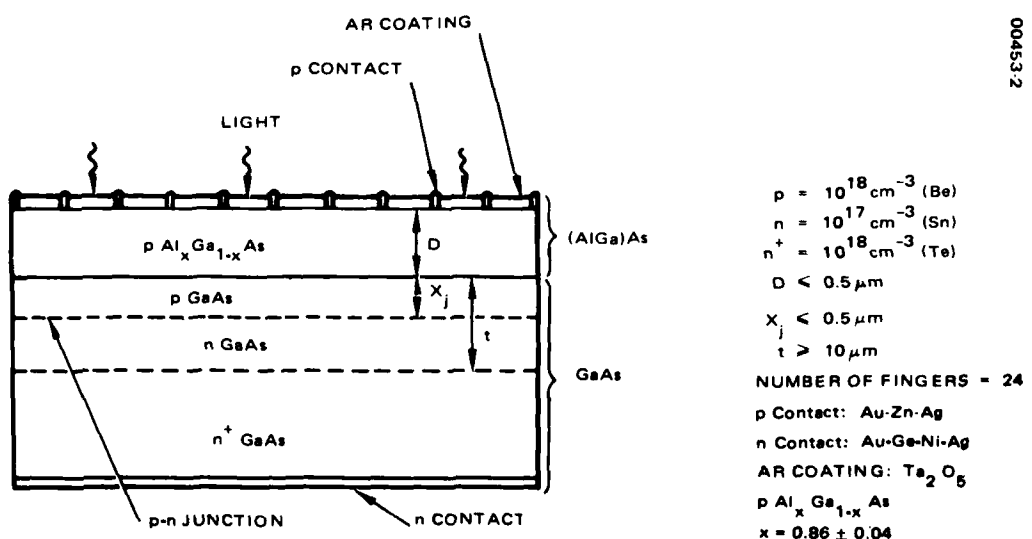


Figure 2. GaAs solar cell baseline design.

PRECEDING PAGE BLANK-NOT FILMED

TABLE 1. GaAs HESP II SOLAR CELL PHYSICAL SPECIFICATIONS

<b>Cell size</b>	
Length	0.79 in
Width	0.79 in
Height	0.030 in (with cover glass) 0.012 in (without cover glass)
<b>Cell area</b>	
Total	0.620 in <sup>2</sup>
Active	0.562 in <sup>2</sup>
<b>Cell weight</b>	
Without cover	0.67 gm
With cover	0.91 gm
<b>Upper contact</b>	
Number of gridlines	24 lines
Gridline length	0.74 in
Gridline width	0.0024 in
Contact bar length	0.753 in
Contact bar width	0.31 in
Gridline total thickness	~6.0 $\mu$ m
<b>Lower contact</b>	
Length	0.79 in
Width	0.79 in
Area	0.620 in <sup>2</sup>
Total thickness	~6.0 $\mu$ m
<b>Cover glass</b>	
Length	0.77 in
Width	0.80 in
Area	0.616 in <sup>2</sup>
Thickness	0.012 in

TABLE 1. GaAs HESP II SOLAR CELL PHYSICAL SPECIFICATIONS

<b>Cell size</b>	
Length	0.79 in
Width	0.79 in
Height	0.030 in (with cover glass) 0.012 in (without cover glass)
<b>Cell area</b>	
Total	0.620 in <sup>2</sup>
Active	0.562 in <sup>2</sup>
<b>Cell weight</b>	
Without cover	0.67 gm
With cover	0.91 gm
<b>Upper contact</b>	
Number of gridlines	24 lines
Gridline length	0.74 in
Gridline width	0.0024 in
Contact bar length	0.753 in
Contact bar width	0.31 in
Gridline total thickness	~6.0 $\mu$ m
<b>Lower contact</b>	
Length	0.79 in
Width	0.79 in
Area	0.620 in <sup>2</sup>
Total thickness	~6.0 $\mu$ m
<b>Cover glass</b>	
Length	0.77 in
Width	0.80 in
Area	0.616 in <sup>2</sup>
Thickness	0.012 in

TABLE 2. GaAs HESP II SOLAR CELL MATERIAL SPECIFICATIONS

Cell material	GaAs
Substrate	
Orientation	100
Type	n <sup>+</sup>
Dopant	Te
Concentration	>7 x 10 <sup>17</sup> cm <sup>-3</sup>
Thickness	0.015 in.
First epilayer	
Type	n
Dopant	Sn
Concentration	1 x 10 <sup>17</sup> cm <sup>-3</sup>
Thickness	10 μm
Resistivity	0.014 Ω·cm
Diffused layer	
Type	p
Dopant	Be
Concentration	1 x 10 <sup>18</sup> cm <sup>-3</sup>
Thickness	<0.5 μm
Second epilayer (window layer)	
Composition	(AlGa) As
Type	p <sup>+</sup>
Dopant	Be
Concentration	1 x 10 <sup>18</sup> cm <sup>-3</sup>
Thickness	<0.5 μm
Sheet resistivity	0.03 Ω·cm
Junction depth	<0.5 μm
Upper surface	
First metallization	
Metals	AuZn
Thickness	2000 Å
Second metallization	
Metal	Ag
Thickness	>3.0 μm
Antireflection coating	
Material	Ta <sub>2</sub> O <sub>5</sub>
Length	0.77 in.
Width	0.79 in.
Thickness	750 Å
Lower surface	
First metallization	
Metals	AuGeNi
Thickness	2000 Å
Second metallization	
Metal	Ag
Thickness	>3.0 μm
Cover glass	
Adhesive	Dow Corning 93-500
Material	Corning 7940 - fused silica
Length	0.77 in.
Width	0.80 in.
Thickness	0.012 in.
AR coating (on top of glass)	MgF <sub>2</sub>

TABLE 3. GaAs HESP II SOLAR CELL ELECTRICAL SPECIFICATIONS\*

$I_{sc}$ (short circuit current)	114 mA
$V_{oc}$ (open circuit voltage)	1.00 V
$I_{mp}$	102 mA
$V_{mp}$	0.87 V
$P_{max}$ (maximum power)	86.5 mW ( $4 \text{ cm}^2$ )
Energy conversion efficiency	16.0%

\*Average values.

TABLE 3. GaAs HESP II SOLAR CELL ELECTRICAL SPECIFICATIONS\*

$I_{sc}$ (short circuit current)	114 mA
$V_{oc}$ (open circuit voltage)	1.00 V
$I_{mp}$	102 mA
$V_{mp}$	0.87 V
$P_{max}$ (maximum power)	86.5 mW ( $4 \text{ cm}^2$ )
Energy conversion efficiency	16.0%

\*Average values.

### 3. GaAs CELL PROCESSES

3.1 GaAs Growth Method. A key element in the success of the GaAs solar cell program is the novel technology developed at Hughes Aircraft Company to grow large area GaAs and (AlGa)As layers reproducibly using infinite solution liquid phase epitaxy (LPE).

A schematic of the apparatus is shown in Figure 3. It features an all quartz growth tube connected to a stainless steel entry chamber through a high vacuum valve. A solution of high purity GaAs in either Ga or a mixture of Ga and Al serves as the growth solution. The Al:Ga ratio can be adjusted to give any composition from GaAs to AlAs for the epitaxial layer, and dopants such as Te, Sn, Ge, or Be can be used to produce a variety of doped layers. Once a solution is prepared, it is maintained in a pure graphite crucible under an ultrapure hydrogen ambient at close to the growth temperature for long periods while layers are grown.

The system has reproducibly grown layers with thicknesses down to  $0.5 \mu\text{m}$ , with a variation in thickness of less than  $\pm 10$  percent over substrates larger than  $6 \text{ cm}^2$  in area. The surfaces are specular and can be processed for devices as grown. Since a growth run takes only about an hour and the system can be scaled up for batch processing (simultaneous LPE growth on several substrates), the system can be adapted for large scale production of low cost cells.

A graphite substrate holder (Figure 3) is used to ensure good equilibration between the substrate and the growth solution prior to the start of growth. It enhances the capability of the infinite solution system for the growth of strain-free, large-area layers with a uniformity in carrier concentration and thickness that would be difficult without it.

The advantages of this technique stem from the use of a large, stable solution that permits the growth of epitaxial layers from the same solution for many months. This results in efficient use of gallium under extremely safe and reliable conditions. Measurements of cells fabricated under the HESP II program have attested to the success of the process. By modifying the graphite substrate holder it was possible for the method to be adapted for the growth of a number of GaAs cells ( $2 \times 2 \text{ cm}$ ) in a single epitaxial run in a total growth cycle time of less than 2 hours. Eight cells per run were made under the HESP II program. Further scale up to larger numbers of cells per run was found to be possible, if needed. Additionally, it was also demonstrated in an early phase of HESP II that the infinite solution technique can be used to tailor the cell parameters to yield a structure with very good control over both the window (AlGa)As layer thickness and the junction depth.

### 3. GaAs CELL PROCESSES

3.1 GaAs Growth Method. A key element in the success of the GaAs solar cell program is the novel technology developed at Hughes Aircraft Company to grow large area GaAs and (AlGa)As layers reproducibly using infinite solution liquid phase epitaxy (LPE).

A schematic of the apparatus is shown in Figure 3. It features an all quartz growth tube connected to a stainless steel entry chamber through a high vacuum valve. A solution of high purity GaAs in either Ga or a mixture of Ga and Al serves as the growth solution. The Al:Ga ratio can be adjusted to give any composition from GaAs to AlAs for the epitaxial layer, and dopants such as Te, Sn, Ge, or Be can be used to produce a variety of doped layers. Once a solution is prepared, it is maintained in a pure graphite crucible under an ultrapure hydrogen ambient at close to the growth temperature for long periods while layers are grown.

The system has reproducibly grown layers with thicknesses down to  $0.5 \mu\text{m}$ , with a variation in thickness of less than  $\pm 10$  percent over substrates larger than  $6 \text{ cm}^2$  in area. The surfaces are specular and can be processed for devices as grown. Since a growth run takes only about an hour and the system can be scaled up for batch processing (simultaneous LPE growth on several substrates), the system can be adapted for large scale production of low cost cells.

A graphite substrate holder (Figure 3) is used to ensure good equilibration between the substrate and the growth solution prior to the start of growth. It enhances the capability of the infinite solution system for the growth of strain-free, large-area layers with a uniformity in carrier concentration and thickness that would be difficult without it.

The advantages of this technique stem from the use of a large, stable solution that permits the growth of epitaxial layers from the same solution for many months. This results in efficient use of gallium under extremely safe and reliable conditions. Measurements of cells fabricated under the HESP II program have attested to the success of the process. By modifying the graphite substrate holder it was possible for the method to be adapted for the growth of a number of GaAs cells ( $2 \times 2 \text{ cm}$ ) in a single epitaxial run in a total growth cycle time of less than 2 hours. Eight cells per run were made under the HESP II program. Further scale up to larger numbers of cells per run was found to be possible, if needed. Additionally, it was also demonstrated in an early phase of HESP II that the infinite solution technique can be used to tailor the cell parameters to yield a structure with very good control over both the window (AlGa)As layer thickness and the junction depth.

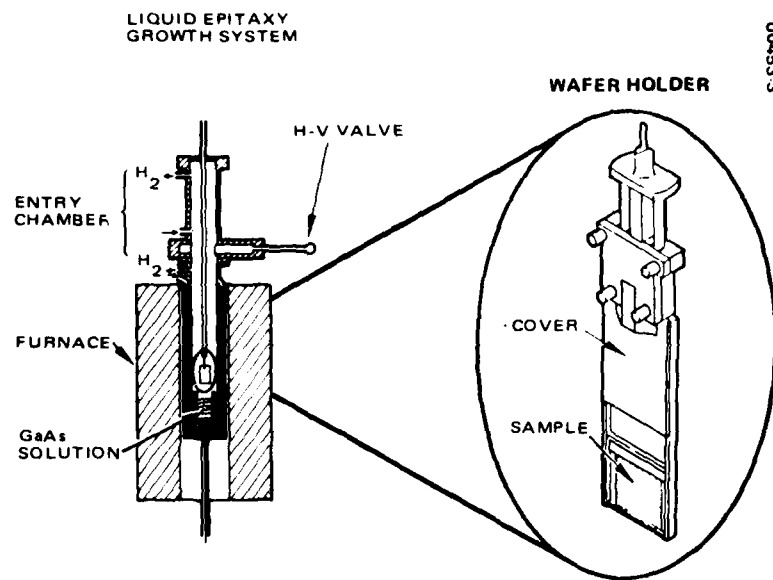


Figure 3. LPE fabrication of GaAs solar cells.

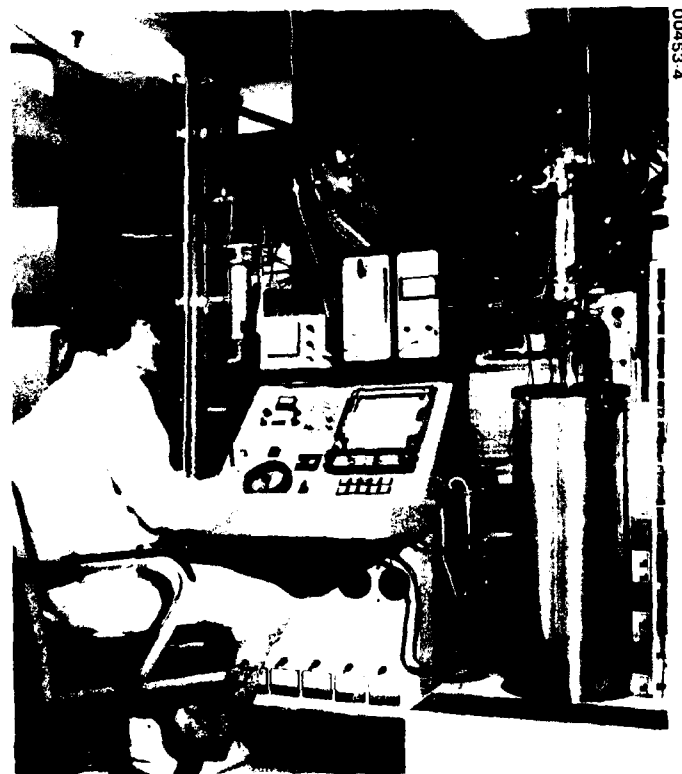


Figure 4. Hughes infinite solution epitaxy system with 3000 gm capacity (Photo M12175).

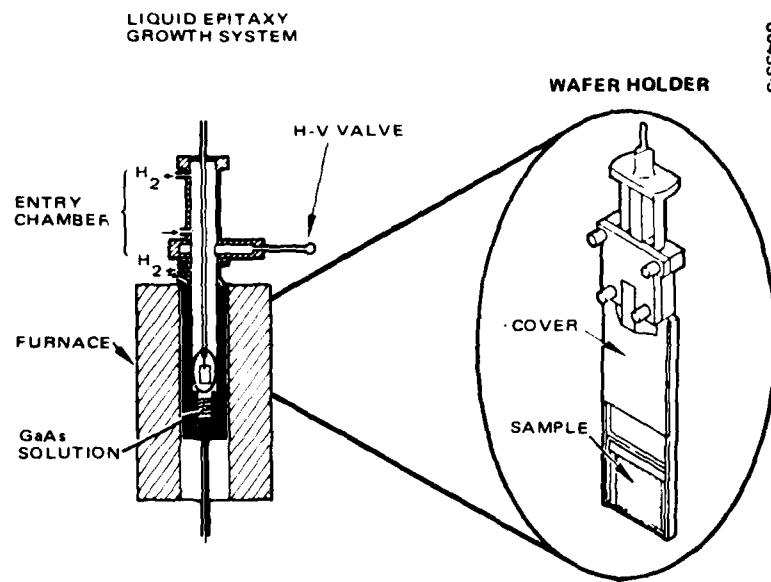


Figure 3. LPE fabrication of GaAs solar cells.

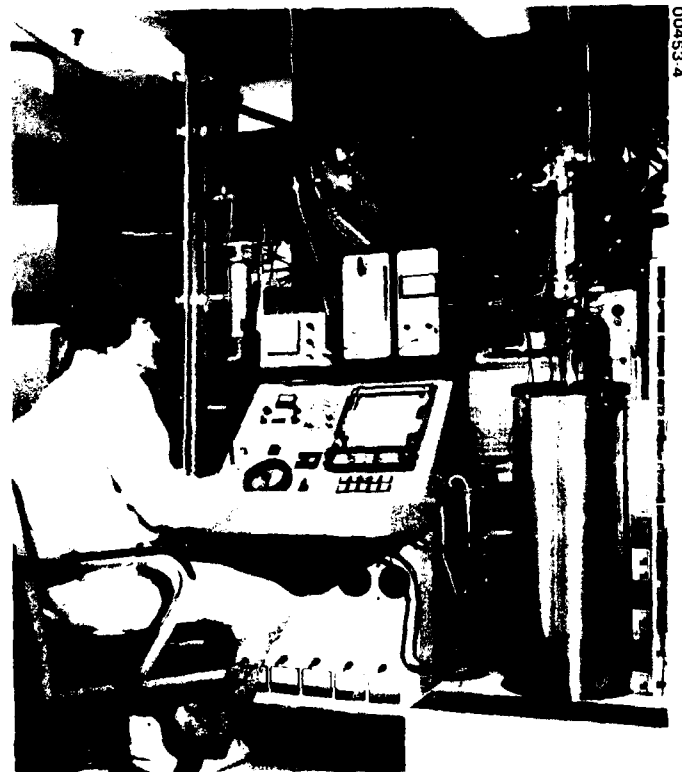


Figure 4. Hughes infinite solution epitaxy system with 3000 gm capacity (Photo M12175).

The cell characteristics have been measured in a large number of cases to prove that other relevant parameters that control the cell performance are well within operational control. These parameters include the (AlGa)As window layer composition, thicknesses, and doping levels as well as the interface behavior in the solar cell structure.

**3.2 Epitaxial Process Development.** The infinite solution epitaxial growth technique was chosen from several alternatives to produce the solar cell structure because of the quality of the resulting GaAs and (AlGa)As layers and because it is by far the most economical and best developed process available. On the other hand, since HESP II is expected to lead to large scale production of the cells, it was felt that the growth system had to be modified to permit the epitaxial growth of several substrates simultaneously, as indicated above.

The first step in this direction was taken in the early part of the program when the graphite substrate holder was modified to handle not a single substrate, but, instead, one substrate on either side of the holder. In addition, the LPE growth system itself was increased in size to hold a 3000 gm solution of GaAs in order to allow production of LPE layers in greater numbers. This system, shown in Figure 4, was checked out during a series of runs in which the layers grown using two substrates per holder were examined to determine both reproducibility and thickness uniformity. The results of these early tests led to modifications of the temperature profiles in the epitaxial reactor as well as to the determination of the proper cooling rates needed to permit the growth of  $0.5 \mu\text{m}$  window layers within a period of 2 to 5 minutes. The time was carefully chosen to be long enough to provide sufficient leeway for the system to attain reproducible conditions during growth, and at the same time short enough to reduce machine cycle time so as to minimize cost. In addition, mechanical tolerances in the substrate holder construction were tightened to increase the layer uniformity, and the temperature controls were refined by the use of a microprocessor that could control the temperature by a multistep program during the loading of the substrates and their introduction into the solution. With these modifications, it was possible to obtain extremely similar solar cell characteristics for the cells grown in each run, and reproducible characteristics from run to run. This is demonstrated in Tables 4 through 6, each of which shows the electrical parameters of cells grown together in individual runs but at different stages of the present contract. The reproducibility of cells within each run is excellent, while the overall quality of cells from run to run shows steady improvement.

These encouraging results resulted in an increase in the capacity of the substrate holder to four GaAs wafers. In addition, the size of each wafer was increased to 1 by 2 inches, allowing two  $2 \times 2 \text{ cm}$  cells per wafer to be grown. A series of runs was made using this arrangement and the system parameters were tailored to ensure uniform conditions of growth for all four substrates. As a result of this effort it was demonstrated that the infinite solution LPE system was successfully modified to fabricate eight solar cell structures at a time. Two such systems were used, one for buffer layers and one for the (AlGa)As window layers. They operated without any serious problems for more than a year. Typical characteristics of cells made with these modified LPE systems are shown in Table 6.

The cell characteristics have been measured in a large number of cases to prove that other relevant parameters that control the cell performance are well within operational control. These parameters include the (AlGa)As window layer composition, thicknesses, and doping levels as well as the interface behavior in the solar cell structure.

**3.2 Epitaxial Process Development.** The infinite solution epitaxial growth technique was chosen from several alternatives to produce the solar cell structure because of the quality of the resulting GaAs and (AlGa)As layers and because it is by far the most economical and best developed process available. On the other hand, since HESP II is expected to lead to large scale production of the cells, it was felt that the growth system had to be modified to permit the epitaxial growth of several substrates simultaneously, as indicated above.

The first step in this direction was taken in the early part of the program when the graphite substrate holder was modified to handle not a single substrate, but, instead, one substrate on either side of the holder. In addition, the LPE growth system itself was increased in size to hold a 3000 gm solution of GaAs in order to allow production of LPE layers in greater numbers. This system, shown in Figure 4, was checked out during a series of runs in which the layers grown using two substrates per holder were examined to determine both reproducibility and thickness uniformity. The results of these early tests led to modifications of the temperature profiles in the epitaxial reactor as well as to the determination of the proper cooling rates needed to permit the growth of  $0.5 \mu\text{m}$  window layers within a period of 2 to 5 minutes. The time was carefully chosen to be long enough to provide sufficient leeway for the system to attain reproducible conditions during growth, and at the same time short enough to reduce machine cycle time so as to minimize cost. In addition, mechanical tolerances in the substrate holder construction were tightened to increase the layer uniformity, and the temperature controls were refined by the use of a microprocessor that could control the temperature by a multistep program during the loading of the substrates and their introduction into the solution. With these modifications, it was possible to obtain extremely similar solar cell characteristics for the cells grown in each run, and reproducible characteristics from run to run. This is demonstrated in Tables 4 through 6, each of which shows the electrical parameters of cells grown together in individual runs but at different stages of the present contract. The reproducibility of cells within each run is excellent, while the overall quality of cells from run to run shows steady improvement.

These encouraging results resulted in an increase in the capacity of the substrate holder to four GaAs wafers. In addition, the size of each wafer was increased to 1 by 2 inches, allowing two  $2 \times 2 \text{ cm}$  cells per wafer to be grown. A series of runs was made using this arrangement and the system parameters were tailored to ensure uniform conditions of growth for all four substrates. As a result of this effort it was demonstrated that the infinite solution LPE system was successfully modified to fabricate eight solar cell structures at a time. Two such systems were used, one for buffer layers and one for the (AlGa)As window layers. They operated without any serious problems for more than a year. Typical characteristics of cells made with these modified LPE systems are shown in Table 6.

TABLE 4. CHARACTERISTICS OF EARLY GaAs SOLAR CELLS GROWN IN SUCCESSIVE LPE RUNS IN DECEMBER 1977

Cell No.	$I_{sc}$ , (mA)	$V_{oc}$ , (V)	FF	Efficiency AM0, (%)
1605	109	0.99	0.74	14.6
1606	104	1.01	0.77	14.8
1607	106	0.94	0.77	13.5
1609	101	1.03	0.82	15.7
1610	102	1.03	0.81	15.5
1611	100	1.03	0.83	15.8
1612	105	0.98	0.77	14.4
1614	100	1.02	0.83	15.7

TABLE 5. CHARACTERISTICS OF GaAs SOLAR CELLS GROWN IN SUCCESSIVE LPE RUNS IN MAY 1978

Cell No.	$I_{sc}$ , (mA)	$V_{oc}$ , (V)	FF	Efficiency AM0, (%)
2063	102	1.00	0.70	13.2
2064	110	1.01	0.74	15.2
2065	113	0.99	0.72	14.9
2066	109	1.01	0.76	15.4
2067	110	1.01	0.74	15.2
2068	115	1.01	0.75	16.0
2069	118	1.00	0.75	16.4
2070	113	1.01	0.73	15.4

TABLE 6. CHARACTERISTICS OF GaAs SOLAR CELLS GROWN IN SUCCESSIVE LPE RUNS IN DECEMBER 1978\*

Cell No.	$I_{sc}$ , (mA)	$V_{oc}$ , (V)	FF	Efficiency AM0, (%)
2684	119	1.02	0.77	17.2
2685	115	1.01	0.78	16.8
2686	111	1.01	0.77	16.0
2687	114	1.01	0.76	16.2
2688	118	1.02	0.77	17.2
2689	119	1.02	0.78	17.4
2690	119.5	1.02	0.74	16.4
2691	113	1.01	0.76	15.9

\*Two successive runs with smaller substrates that yielded an average of one cell per substrate.

The cells listed in Table 7 were fabricated with more rigorous control of the junction depth to ensure that it was less than 0.5  $\mu\text{m}$ , thus minimizing radiation damage to meet HESP II specifications. In addition, contact mechanical integrity had been enhanced by modifying the annealing process to ensure the contacts survivability during qualification tests.

In a later modification, a single substrate holder was enlarged to handle a 2 by 2 inch GaAs substrate that yielded four 2 x 2 cm cells as shown in Figure 5. The system handled this large holder with no problems. Subsequent studies showed that the substrate capacity can be further increased to hold at least eight wafers at a time, thus making 32 separate 2 x 2 cm cells per run. Such a scale-up effectively leads to mass production capabilities by reducing the LPE growth time per substrate and enabling batch processing in subsequent fabrication steps. Such batch processing capability is essential for mass production of space qualified solar cells for satellite power applications.

Several interesting factors emerged from experiments on larger systems. First, they proved to be more controllable than the smaller systems, largely because of the enhanced stability of the large solution and because a large number of layers can be grown in them without appreciably affecting the concentration of the solution. It was also observed that the large solutions were easier to bake out during the initial cleanup when the solutions were first made, and they maintained their purity for long periods without any subsequent cleaning. This advantage arose mainly from the lower surface-to-volume ratio of solution to the container and the substrate holder. Furthermore, lower growth temperatures could be maintained than in the case of smaller systems, and the temperature cycles could be reduced in range since a larger amount of solute is available ex-solution for a small drop in temperature. Since the cooling rate could be reduced, there was also less probability of spurious nucleation occurring in the solution during the long-term buffer layer growth. The combined result of all these factors was more reproducible control over the characteristics of the epitaxial layers and, hence, of the device itself.

TABLE 7. CHARACTERISTICS OF GaAs SOLAR CELLS GROWN IN SUCCESSIVE LPE RUNS IN JULY 1979

Cell No.	$I_{sc}$ (mA)	$V_{oc}$ (V)	FF	Efficiency AMO (%)
3562	117	1.0	0.77	16.7
3567	116	1.0	0.78	16.7
3568	114	1.0	0.77	16.3
3569	117	1.01	0.78	16.9
3570	117	1.0	0.79	17.2
3584	117	1.0	0.79	17.0
3585	119	1.01	0.77	17.2
3588	117	1.01	0.79	16.8

The cells listed in Table 7 were fabricated with more rigorous control of the junction depth to ensure that it was less than 0.5  $\mu\text{m}$ , thus minimizing radiation damage to meet HESP II specifications. In addition, contact mechanical integrity had been enhanced by modifying the annealing process to ensure the contacts survivability during qualification tests.

In a later modification, a single substrate holder was enlarged to handle a 2 by 2 inch GaAs substrate that yielded four 2 x 2 cm cells as shown in Figure 5. The system handled this large holder with no problems. Subsequent studies showed that the substrate capacity can be further increased to hold at least eight wafers at a time, thus making 32 separate 2 x 2 cm cells per run. Such a scale-up effectively leads to mass production capabilities by reducing the LPE growth time per substrate and enabling batch processing in subsequent fabrication steps. Such batch processing capability is essential for mass production of space qualified solar cells for satellite power applications.

Several interesting factors emerged from experiments on larger systems. First, they proved to be more controllable than the smaller systems, largely because of the enhanced stability of the large solution and because a large number of layers can be grown in them without appreciably affecting the concentration of the solution. It was also observed that the large solutions were easier to bake out during the initial cleanup when the solutions were first made, and they maintained their purity for long periods without any subsequent cleaning. This advantage arose mainly from the lower surface-to-volume ratio of solution to the container and the substrate holder. Furthermore, lower growth temperatures could be maintained than in the case of smaller systems, and the temperature cycles could be reduced in range since a larger amount of solute is available ex-solution for a small drop in temperature. Since the cooling rate could be reduced, there was also less probability of spurious nucleation occurring in the solution during the long-term buffer layer growth. The combined result of all these factors was more reproducible control over the characteristics of the epitaxial layers and, hence, of the device itself.

TABLE 7. CHARACTERISTICS OF GaAs SOLAR CELLS GROWN IN SUCCESSIVE LPE RUNS IN JULY 1979

Cell No.	$I_{sc}$ (mA)	$V_{oc}$ (V)	FF	Efficiency AM0 (%)
3562	117	1.0	0.77	16.7
3567	116	1.0	0.78	16.7
3568	114	1.0	0.77	16.3
3569	117	1.01	0.78	16.9
3570	117	1.0	0.79	17.2
3584	117	1.0	0.79	17.0
3585	119	1.01	0.77	17.2
3588	117	1.01	0.79	16.8

004535

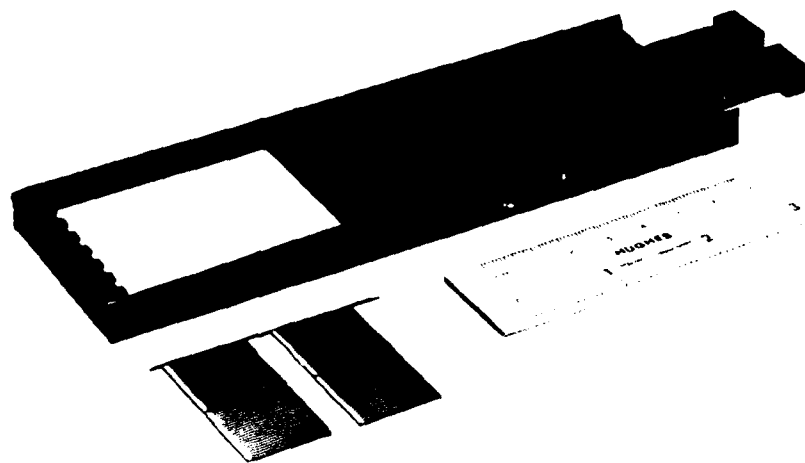


Figure 5. New substrate holder with large rectangular GaAs substrate.

3.3 LPE Solution Parameter Control. The larger solution made possible a more accurate study of the influence of various solution parameters. For example, the n type tin concentration for buffer layers was maintained  $> 1 \times 10^{17} \text{ cm}^{-3}$  in order to yield a grown layer with  $n = 1 \times 10^{17} \text{ cm}^{-3}$ . A solution maintained this concentration without any serious problem for a period of over 3 months at a time, during which over 500 layers were grown from it. At this stage, the solution level fell, and was brought back up by the simple addition of Ga, GaAs, and Sn in the original proportion.

The (AlGa)As solution acts similarly especially if only thin window layers are grown. The Al concentration in the solution tended to drop progressively because of the segregation coefficient of Al, which is approximately 50. However, the layer was so thin that several hundred layers could be grown from the large solution before the solution was observably depleted of Al. Furthermore, ways of growing the layers well below saturation temperatures were developed so that there was always an excess of (AlGa)As in the solution. Since the Al concentration of the solid was high, as it dissolved back it reestablished the equilibrium value of the solution at the growth temperature. This process made the window layers very reproducible in Al composition. Using this method in combination with the large solution, only the Be content needed to be replenished from time to time to permit the growth of several hundred layers.

The Be composition was controlled by adding about 5 mg of Be per 100 gm of solution to provide  $1 \times 10^{18} \text{ cm}^{-3}$  carriers in the epitaxial layer. Adding higher Be amounts can adversely affect the layer quality. Apparently, this level is close to the maximum that is normally incorporated in the GaAs lattice. Additions above  $2 \times 10^{18} \text{ cm}^{-3}$  result in precipitates and higher dislocations which are harmful. In cell processing they led to channeling of the contacting metals causing leakage in devices. At a level of  $1 \times 10^{18} \text{ cm}^{-3}$ ,

004535

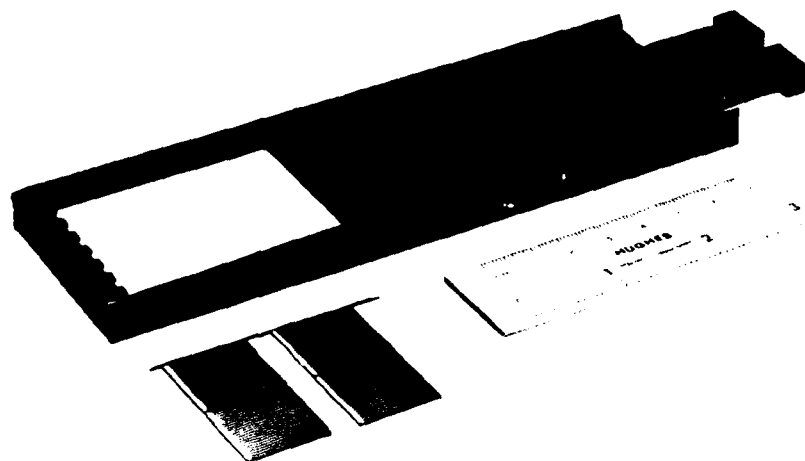


Figure 5. New substrate holder with large rectangular GaAs substrate.

3.3 LPE Solution Parameter Control. The larger solution made possible a more accurate study of the influence of various solution parameters. For example, the n type tin concentration for buffer layers was maintained  $> 1 \times 10^{17} \text{ cm}^{-3}$  in order to yield a grown layer with  $n = 1 \times 10^{17} \text{ cm}^{-3}$ . A solution maintained this concentration without any serious problem for a period of over 3 months at a time, during which over 500 layers were grown from it. At this stage, the solution level fell, and was brought back up by the simple addition of Ga, GaAs, and Sn in the original proportion.

The (AlGa)As solution acts similarly especially if only thin window layers are grown. The Al concentration in the solution tended to drop progressively because of the segregation coefficient of Al, which is approximately 50. However, the layer was so thin that several hundred layers could be grown from the large solution before the solution was observably depleted of Al. Furthermore, ways of growing the layers well below saturation temperatures were developed so that there was always an excess of (AlGa)As in the solution. Since the Al concentration of the solid was high, as it dissolved back it reestablished the equilibrium value of the solution at the growth temperature. This process made the window layers very reproducible in Al composition. Using this method in combination with the large solution, only the Be content needed to be replenished from time to time to permit the growth of several hundred layers.

The Be composition was controlled by adding about 5 mg of Be per 100 gm of solution to provide  $1 \times 10^{18} \text{ cm}^{-3}$  carriers in the epitaxial layer. Adding higher Be amounts can adversely affect the layer quality. Apparently, this level is close to the maximum that is normally incorporated in the GaAs lattice. Additions above  $2 \times 10^{18} \text{ cm}^{-3}$  result in precipitates and higher dislocations which are harmful. In cell processing they led to channeling of the contacting metals causing leakage in devices. At a level of  $1 \times 10^{18} \text{ cm}^{-3}$ ,

the layers were well behaved and did not develop surface degradation. As a result of these observations, the Be level was kept close to this concentration in the epitaxial layer. For similar reasons of layer stability, the Al composition was maintained at  $86 \pm 4$  percent in the (AlGa)As window layer. These parameters yielded cells with a  $V_{oc}$  of 1.0 volt and a short circuit current of  $115 \pm 5$  mA per  $4 \text{ cm}^2$  cell.

Table 8 presents the characteristics of four cells grown during a particular run using a single slide bar. Cells 1871 and 1872 came from the same substrate on one side of the slide bar, while the other two were cleaved from a substrate positioned on the opposite side. The lower efficiency of the latter two was traced to the fact that the slide bar was not properly centered in the solution. This centering was corrected and cells from subsequent growths were more uniform in efficiency. Table 9 shows the similar results obtained on seven cells fabricated later in the HESP II program using a double slide bar. This device consists of two separate graphite substrate holders nearly identical to the one used for the cells in Table 8, except that both are suspended and submerged in the solutions simultaneously. Thus, the capacity of the run was effectively doubled. The cells of Table 9 indicated not only enhanced production capability but also higher efficiencies.

TABLE 8. EARLY GaAs CELLS GROWN IN A SINGLE RUN  
(TWO SUBSTRATES)

Cell No.	$I_{sc}$ (mA)	$V_{oc}$ (V)	FF	Efficiency AMO (%)
* { 1871	112	1.0	0.77	15.8
1872	109	1.0	0.77	15.5
* { 1873	104	0.99	0.75	14.4
1874	104	0.98	0.74	14.0

\*Both cells from single substrate.

TABLE 9. LATER GaAs CELLS GROWN IN A SINGLE RUN  
(FOUR SUBSTRATES)

Cell No.	$I_{sc}$ (mA)	$V_{oc}$ (V)	$P_m$ (mW)	FF	Efficiency AMO (%)
*   Top 4461	117	0.99	87.2	0.75	16.1
Bottom 4462	116	0.91	71.8	0.70	13.5**
*   Top 4463	116	1.0	88	0.76	16.3
Bottom 4464	117	0.97	84.5	0.74	15.6
*   Top 4465	117	0.99	88.7	0.76	16.4
Bottom 4466	118	0.98	84.5	0.73	15.6
*   Top 4467	117	1.0	91.3	0.78	17.0
Bottom 4468	117	1.0	89.4	0.76	16.5

\*Cells from single substrate.

\*\*Visible flaw in top layer due to imperfect coverage.

the layers were well behaved and did not develop surface degradation. As a result of these observations, the Be level was kept close to this concentration in the epitaxial layer. For similar reasons of layer stability, the Al composition was maintained at  $86 \pm 4$  percent in the (AlGa)As window layer. These parameters yielded cells with a  $V_{oc}$  of 1.0 volt and a short circuit current of  $115 \pm 5$  mA per  $4 \text{ cm}^2$  cell.

Table 8 presents the characteristics of four cells grown during a particular run using a single slide bar. Cells 1871 and 1872 came from the same substrate on one side of the slide bar, while the other two were cleaved from a substrate positioned on the opposite side. The lower efficiency of the latter two was traced to the fact that the slide bar was not properly centered in the solution. This centering was corrected and cells from subsequent growths were more uniform in efficiency. Table 9 shows the similar results obtained on seven cells fabricated later in the HESP II program using a double slide bar. This device consists of two separate graphite substrate holders nearly identical to the one used for the cells in Table 8, except that both are suspended and submerged in the solutions simultaneously. Thus, the capacity of the run was effectively doubled. The cells of Table 9 indicated not only enhanced production capability but also higher efficiencies.

TABLE 8. EARLY GaAs CELLS GROWN IN A SINGLE RUN  
(TWO SUBSTRATES)

Cell No.	$I_{sc}$ (mA)	$V_{oc}$ (V)	FF	Efficiency AMO (%)
* { 1871	112	1.0	0.77	15.8
1872	109	1.0	0.77	15.5
* { 1873	104	0.99	0.75	14.4
1874	104	0.98	0.74	14.0

\*Both cells from single substrate.

TABLE 9. LATER GaAs CELLS GROWN IN A SINGLE RUN  
(FOUR SUBSTRATES)

Cell No.	$I_{sc}$ (mA)	$V_{oc}$ (V)	$P_m$ (mW)	FF	Efficiency AMO (%)
*   Top 4461	117	0.99	87.2	0.75	16.1
Bottom 4462	116	0.91	71.8	0.70	13.5**
*   Top 4463	116	1.0	88	0.76	16.3
Bottom 4464	117	0.97	84.5	0.74	15.6
*   Top 4465	117	0.99	88.7	0.76	16.4
Bottom 4466	118	0.98	84.5	0.73	15.6
*   Top 4467	117	1.0	91.3	0.78	17.0
Bottom 4468	117	1.0	89.4	0.76	16.5

\*Cells from single substrate.

\*\*Visible flaw in top layer due to imperfect coverage.

TABLE 10. LARGE AREA (2 x 4 cm) (AlGa) As-GaAs SOLAR CELL CHARACTERISTICS

Cell No.	$I_{sc}$ (mA)*	$V_{oc}$ (V)	FF	$P_m$ (mW)	Efficiency AMO (%)
1005	242	1.0	0.73	176	16.3
1008	250	1.01	0.71	180	16.6
1014	242	1.0	0.72	173.8	16.0
1015	246	1.0	0.70	172.2	15.9
1018	217	0.99	0.74	159	14.7
1019	226	0.99	0.71	159	14.7
1020	220	0.97	0.74	160	14.8
1021	228	1.01	0.76	174.7	16.1

\*After antireflective coating, 1 sun (AM0) measured at HRL

Table 10 lists the characteristics of 2 x 4 cm cells fabricated using the same techniques used for the 2 x 2 cm cells. The LPE system characteristics needed to be tailored somewhat more carefully to yield the uniformity of the window layer required for the larger cells. It was necessary to be more selective in the choice of the substrates, since any imperfections in the substrate resulted in a faulty cell. In the case of 2 x 2 cm cells, some cropping was possible. Our experience with the limited production of the 2 x 4 cm cells indicates, however, that they can be made with good yields when the substrate quality can be assured. The quality of the GaAs substrates available from Crystal Specialties has been steadily improving as they gain more experience with the rectangular shaped Bridgman ingots which they have been growing for the solar cells.

In addition, 8 mil cells were fabricated to show the feasibility of obtaining the lesser thicknesses to lower the cell weight. The characteristics of the cells are unaffected by the lesser thickness, but loss in material during polishing and subsequent handling is somewhat more pronounced. It must be stressed, however, that this loss is due in part to lack of experience in handling thin substrates and, in part, due to the quality (stress) of the substrates. Both these factors can be expected to improve with experience. Preliminary evidence indicates that GaAs cells much thinner than 8 mils can be made by the HRL technique.

**3.4 Cell Fabrication.** With the delivery of the GaAs substrate from a subcontractor, the cells were processed according to a sequence derived from both theoretical and empirical considerations. During HESP II this basic sequence was continually refined to enable the fabrication of 2 x 2 cm and 2 x 4 cm cells meeting the contract requirements. This perfected procedure was followed in the manufacture of qualification cells.

During the development period of the program, considerable attention was given to the problem of the epitaxial growth temperature. This is the temperature at which growth is initiated on the substrate. Earlier in the program this parameter was set at 800°C. Attempts were made to slow down

TABLE 10. LARGE AREA (2 x 4 cm) (AlGa) As-GaAs SOLAR CELL CHARACTERISTICS

Cell No.	$I_{sc}$ (mA)*	$V_{oc}$ (V)	FF	$P_m$ (mW)	Efficiency AMO (%)
1005	242	1.0	0.73	176	16.3
1008	250	1.01	0.71	180	16.6
1014	242	1.0	0.72	173.8	16.0
1015	246	1.0	0.70	172.2	15.9
1018	217	0.99	0.74	159	14.7
1019	226	0.99	0.71	159	14.7
1020	220	0.97	0.74	160	14.8
1021	228	1.01	0.76	174.7	16.1

\*After antireflective coating, 1 sun (AM0) measured at HRL

Table 10 lists the characteristics of 2 x 4 cm cells fabricated using the same techniques used for the 2 x 2 cm cells. The LPE system characteristics needed to be tailored somewhat more carefully to yield the uniformity of the window layer required for the larger cells. It was necessary to be more selective in the choice of the substrates, since any imperfections in the substrate resulted in a faulty cell. In the case of 2 x 2 cm cells, some cropping was possible. Our experience with the limited production of the 2 x 4 cm cells indicates, however, that they can be made with good yields when the substrate quality can be assured. The quality of the GaAs substrates available from Crystal Specialties has been steadily improving as they gain more experience with the rectangular shaped Bridgman ingots which they have been growing for the solar cells.

In addition, 8 mil cells were fabricated to show the feasibility of obtaining the lesser thicknesses to lower the cell weight. The characteristics of the cells are unaffected by the lesser thickness, but loss in material during polishing and subsequent handling is somewhat more pronounced. It must be stressed, however, that this loss is due in part to lack of experience in handling thin substrates and, in part, due to the quality (stress) of the substrates. Both these factors can be expected to improve with experience. Preliminary evidence indicates that GaAs cells much thinner than 8 mils can be made by the HRL technique.

**3.4 Cell Fabrication.** With the delivery of the GaAs substrate from a subcontractor, the cells were processed according to a sequence derived from both theoretical and empirical considerations. During HESP II this basic sequence was continually refined to enable the fabrication of 2 x 2 cm and 2 x 4 cm cells meeting the contract requirements. This perfected procedure was followed in the manufacture of qualification cells.

During the development period of the program, considerable attention was given to the problem of the epitaxial growth temperature. This is the temperature at which growth is initiated on the substrate. Earlier in the program this parameter was set at 800°C. Attempts were made to slow down

the layer formation in order to permit the reproducible growth of the critical ~0.5 μm window. However, the junction depth was found to vary and sometimes exceeded the desired value (also 0.5 μm). Since the junction depth is critical in determining the hardness of the cell to radiation environment, temperatures and growth times were varied in an attempt to establish guidelines for more controllable epitaxy. The final temperature selected was 750°C. At this temperature a layer approximately  $0.4 \pm 0.1$  μm could be formed in  $3 \pm 1$  minutes with a junction depth of less than 0.5 μm. Since this choice of parameters was suitable for fabrication of the HESP II baseline cell, it has been maintained in the present epitaxial process.

The influence of the n-type buffer layer thickness on overall cell performance was also studied. Early results showed that a buffer layer thickness greater than 7 μm was required to eliminate any noticeable substrate influence on cell efficiency. The n-layer thickness, therefore, was maintained at  $9 \pm 2$  μm.

Numerous other studies were conducted with respect to the ultimate quality of the epitaxial layers. In summary, the following requirements were found to be significant:

- 1) An oxygen-free ambient in the system
- 2) A Hall mobility of  $\sim 70$  cm<sup>2</sup> V<sup>-1</sup> sec<sup>-1</sup> for Be-doped (AlGa)As layers with a Be carrier concentration  $> 1 \times 10^{18}$  cm<sup>-3</sup>
- 3) Use of an etch and rinse procedure for substrates utilizing solvents and reagents of semiconductor purity
- 4) Use of deionized water with a resistivity greater than 15 megohms
- 5) Maintenance of an Al concentration in the (AlGa)As layer of  $85 \pm 5$  percent.

**3.5 Cell Production and Delivery.** During the first year of the HESP II program, 70 cells with power conversion efficiencies in excess of 15 percent AM0 were delivered to AFWAL. This met the delivery requirements of that period. During the last year, over 400 cells were delivered, partly for cell qualification. All the 2 x 2 cm cells and modules required by the program have been delivered, and the 2 x 4 cm cells and modules are being completed. Delivery of approximately 700 cells will be completed before the end of the program, thus meeting the HESP II contract requirements.

One of the important studies conducted during the program was to establish a rate of improvement in yield as a function of time. During the early part of the program, several parameters had to be optimized and the contacts were still causing some problems. As these problems were resolved and the process was streamlined, the yield of cells became more predictable. Table 11 shows the distribution of cells produced during 2 month periods at the beginning, the middle, and the end of the first year of HESP II. The

the layer formation in order to permit the reproducible growth of the critical ~0.5 μm window. However, the junction depth was found to vary and sometimes exceeded the desired value (also 0.5 μm). Since the junction depth is critical in determining the hardness of the cell to radiation environment, temperatures and growth times were varied in an attempt to establish guidelines for more controllable epitaxy. The final temperature selected was 750°C. At this temperature a layer approximately  $0.4 \pm 0.1$  μm could be formed in  $3 \pm 1$  minutes with a junction depth of less than 0.5 μm. Since this choice of parameters was suitable for fabrication of the HESP II baseline cell, it has been maintained in the present epitaxial process.

The influence of the n-type buffer layer thickness on overall cell performance was also studied. Early results showed that a buffer layer thickness greater than 7 μm was required to eliminate any noticeable substrate influence on cell efficiency. The n-layer thickness, therefore, was maintained at  $9 \pm 2$  μm.

Numerous other studies were conducted with respect to the ultimate quality of the epitaxial layers. In summary, the following requirements were found to be significant:

- 1) An oxygen-free ambient in the system
- 2) A Hall mobility of  $\sim 70$  cm<sup>2</sup> V<sup>-1</sup> sec<sup>-1</sup> for Be-doped (AlGa)As layers with a Be carrier concentration  $> 1 \times 10^{18}$  cm<sup>-3</sup>
- 3) Use of an etch and rinse procedure for substrates utilizing solvents and reagents of semiconductor purity
- 4) Use of deionized water with a resistivity greater than 15 megohms
- 5) Maintenance of an Al concentration in the (AlGa)As layer of  $85 \pm 5$  percent.

**3.5 Cell Production and Delivery.** During the first year of the HESP II program, 70 cells with power conversion efficiencies in excess of 15 percent AM0 were delivered to AFWAL. This met the delivery requirements of that period. During the last year, over 400 cells were delivered, partly for cell qualification. All the 2 x 2 cm cells and modules required by the program have been delivered, and the 2 x 4 cm cells and modules are being completed. Delivery of approximately 700 cells will be completed before the end of the program, thus meeting the HESP II contract requirements.

One of the important studies conducted during the program was to establish a rate of improvement in yield as a function of time. During the early part of the program, several parameters had to be optimized and the contacts were still causing some problems. As these problems were resolved and the process was streamlined, the yield of cells became more predictable. Table 11 shows the distribution of cells produced during 2 month periods at the beginning, the middle, and the end of the first year of HESP II. The

numbers in the table and the distribution curves shown in Figure 6 show the steady improvement both in the quality and the quantity of cells as a function of time. The yield of cells with efficiency higher than 16 percent approached 50 percent of all the cells processed.

We have maintained a record of the yield of cells during the last year of the HESP program and verified that when the solution parameters are

TABLE 11. GaAs SOLAR CELL YIELD VERSUS EFFICIENCY,  
SEPTEMBER 1977 TO DECEMBER 1978

Time	AMO efficiency, (%)	Yield/start, (%)
September to October 1977	≥15	22
	≥16	4
	≥17	0
May to June 1978	≥15	45
	≥16	21
	≥17	5
November to December 1978	≥15	61
	≥16	47
	≥17	18

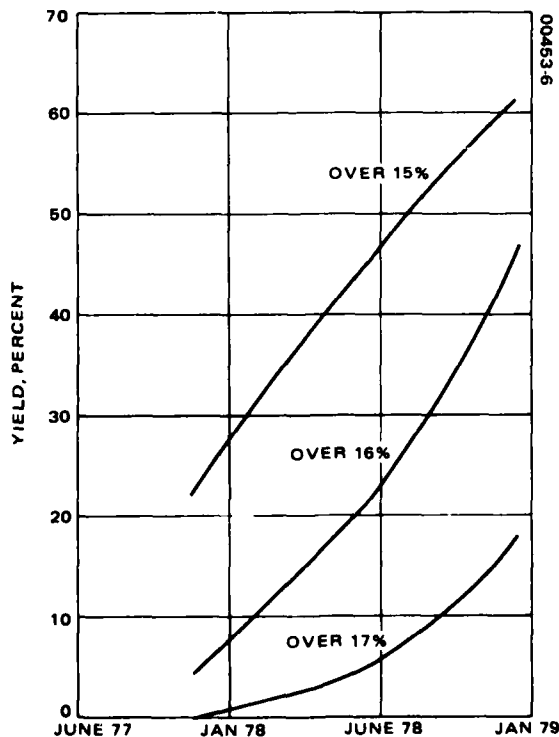


Figure 6. Cell yield for September 1977 through December 1978.

numbers in the table and the distribution curves shown in Figure 6 show the steady improvement both in the quality and the quantity of cells as a function of time. The yield of cells with efficiency higher than 16 percent approached 50 percent of all the cells processed.

We have maintained a record of the yield of cells during the last year of the HESP program and verified that when the solution parameters are

TABLE 11. GaAs SOLAR CELL YIELD VERSUS EFFICIENCY,  
SEPTEMBER 1977 TO DECEMBER 1978

Time	AMO efficiency, (%)	Yield/start, (%)
September to October 1977	≥15	22
	≥16	4
	≥17	0
May to June 1978	≥15	45
	≥16	21
	≥17	5
November to December 1978	≥15	61
	≥16	47
	≥17	18

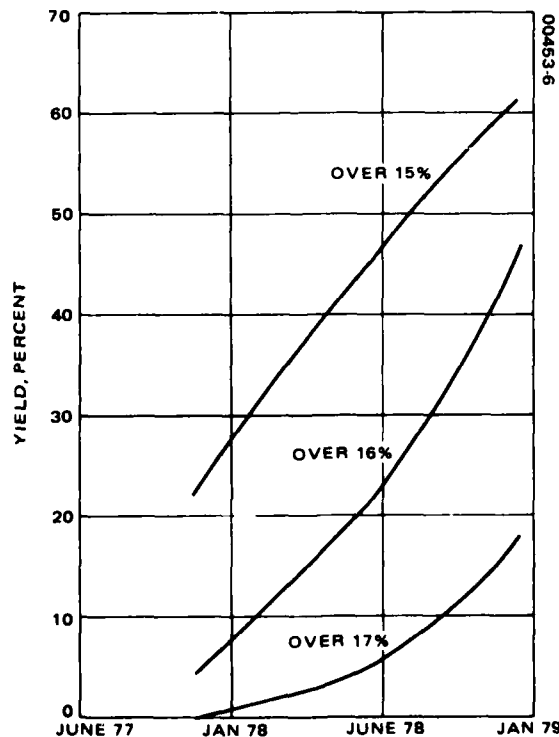


Figure 6. Cell yield for September 1977 through December 1978.

correctly controlled, yields of 50 percent can be expected from the system. In a production mode, the primary requirement would be to keep a regular schedule to replenish the solution in Al, Be, and the solute GaAs. The schedule can be worked out on the basis of experience and has enough latitude in the large solutions to be quite practical for uninterrupted production.

When the cells illustrated by Figure 6 and fabricated during the first year of HESP II were subjected to qualification tests, their stability degraded upon long time exposure to humidity at about 50°C. Some evidence of degradation was visible in earlier cells even at ordinary temperature after a long shelf life. The problem manifested itself in a slow deterioration of the cell surface (the AlGaAs window layer). Studies indicated that reducing the  $x$  value in  $\text{Al}_x\text{Ga}_{1-x}\text{As}$  to below 0.90 would eliminate the problem if the grown layers were kept dry through the processing sequence. The Al level was accordingly lowered to 86 +4 percent. The difference in output of the cells in this range of Al concentration is approximately 5 percent compared to that of cells with Al 90 percent or higher. Since the stability of the cells is a prime requirement for panel fabrication and shelf life, all the HESP II cells have been made with the Al concentration at ~86 percent.

correctly controlled, yields of 50 percent can be expected from the system. In a production mode, the primary requirement would be to keep a regular schedule to replenish the solution in Al, Be, and the solute GaAs. The schedule can be worked out on the basis of experience and has enough latitude in the large solutions to be quite practical for uninterrupted production.

When the cells illustrated by Figure 6 and fabricated during the first year of HESP II were subjected to qualification tests, their stability degraded upon long time exposure to humidity at about 50°C. Some evidence of degradation was visible in earlier cells even at ordinary temperature after a long shelf life. The problem manifested itself in a slow deterioration of the cell surface (the AlGaAs window layer). Studies indicated that reducing the  $x$  value in  $\text{Al}_x\text{Ga}_{1-x}\text{As}$  to below 0.90 would eliminate the problem if the grown layers were kept dry through the processing sequence. The Al level was accordingly lowered to 86 +4 percent. The difference in output of the cells in this range of Al concentration is approximately 5 percent compared to that of cells with Al 90 percent or higher. Since the stability of the cells is a prime requirement for panel fabrication and shelf life, all the HESP II cells have been made with the Al concentration at ~86 percent.

#### 4. GaAs CELL METALLIZATION

4.1 General Background. Aside from the epitaxial growth, the major emphasis on cell fabrication during the program was on the contacting procedures used. Forming reliable ohmic contacts that adhere to (AlGa)As proved to be a significant task.

The application of ohmic contacts to semiconductors consists of one or more metals applied to the semiconductor surface with a dopant, sometimes with a fluxing transition metal such as Ni, Cr, Pd, or Ti. For the n GaAs, some contacting systems were available. AuGeNi and AgSn are good examples, the former for a 450°C contact and the latter for one with somewhat higher temperature capability (600°C). AuGeNi was chosen as the first candidate since it is compatible with AuZn, which is the alloy most often used for p type GaAs contacts.

The alloys having been chosen, the next selection was the best technique. The two most commonly used methods are evaporation (either thermal or E beam) and sputtering (Rf or ion beam). The evaporation method is very reliable, but since the metals are so different in vapor pressures (Au and Zn), it was believed sputtering would have some advantages in control for the p contact.

Another consideration was the choice of contact grid patterns on the p side. The typical grid pattern used is a 24 finger pattern. It combines minimum shadowing (~ 5 to 8 percent) with good collection efficiency. This pattern can be produced using either photolithography or mechanical masks. HRL has been developing both techniques concurrently for use in a variety of applications. For a cell compatible with concentrated illumination, the photolithographic technique is especially useful since it provides the high resolution necessary for the closely spaced contact pattern required to minimize series resistance in high current operation. However, for high efficiency cells at low concentrations, a mechanical mask approach offers a technique that is compatible with silicon solar cell practice, which is a significant factor in establishing a rapid transition to production for GaAs solar cells. Thus, the mechanical mask approach was chosen utilizing the standard 24 finger mask used for silicon 2 x 2 cm space cells.

The feasibility of welding tabs onto the contacts deposited was also to be determined on the HESP II contract. Areas of concern included the electrical characteristics of cells upon the welding operation and the mechanical strength of the resulting bonds.

PRECEDING PAGE BLANK-NOT FILMED

#### 4. GaAs CELL METALLIZATION

4.1 General Background. Aside from the epitaxial growth, the major emphasis on cell fabrication during the program was on the contacting procedures used. Forming reliable ohmic contacts that adhere to (AlGa)As proved to be a significant task.

The application of ohmic contacts to semiconductors consists of one or more metals applied to the semiconductor surface with a dopant, sometimes with a fluxing transition metal such as Ni, Cr, Pd, or Ti. For the n GaAs, some contacting systems were available. AuGeNi and AgSn are good examples, the former for a 450°C contact and the latter for one with somewhat higher temperature capability (600°C). AuGeNi was chosen as the first candidate since it is compatible with AuZn, which is the alloy most often used for p type GaAs contacts.

The alloys having been chosen, the next selection was the best technique. The two most commonly used methods are evaporation (either thermal or E beam) and sputtering (Rf or ion beam). The evaporation method is very reliable, but since the metals are so different in vapor pressures (Au and Zn), it was believed sputtering would have some advantages in control for the p contact.

Another consideration was the choice of contact grid patterns on the p side. The typical grid pattern used is a 24 finger pattern. It combines minimum shadowing (~ 5 to 8 percent) with good collection efficiency. This pattern can be produced using either photolithography or mechanical masks. HRL has been developing both techniques concurrently for use in a variety of applications. For a cell compatible with concentrated illumination, the photolithographic technique is especially useful since it provides the high resolution necessary for the closely spaced contact pattern required to minimize series resistance in high current operation. However, for high efficiency cells at low concentrations, a mechanical mask approach offers a technique that is compatible with silicon solar cell practice, which is a significant factor in establishing a rapid transition to production for GaAs solar cells. Thus, the mechanical mask approach was chosen utilizing the standard 24 finger mask used for silicon 2 x 2 cm space cells.

The feasibility of welding tabs onto the contacts deposited was also to be determined on the HESP II contract. Areas of concern included the electrical characteristics of cells upon the welding operation and the mechanical strength of the resulting bonds.

PRECEDING PAGE BLANK-NOT FILMED

**4.2 Contact Metallization Techniques.** Figure 7 shows the complete GaAs solar cell fabrication process in which the ohmic contacts are given detailed attention.

The best results for applying the AuZn contacts to the p type (AlGa)As cell surface were achieved using a sputtering technique. The AuGeNi n type contacts were applied using thermal evaporation. These methods were used for the qualification cell contacts, and the cells successfully passed all tests.

The AuGeNi n type contacts are particularly easy to apply. The proportions involved are 12 percent Ge, 1.5 percent Ni, and 86.5 percent Au by weight. A coating approximately 2000 Å thick is used; this is covered by a 5 µm Ag overlay.

The AuZn contact consists of about 10 percent Zn and 90 percent Au by weight. Initially, the Au and Zn were sputtered onto the p surface from a composite target. However, a new sputtering system was acquired with multiple targets and a technique of sputtering from two targets of Au and Zn separately was perfected. This method provides considerably greater flexibility and reproducibility. The AuZn layer is also approximately 2000 Å thick and is covered with 5 µm of Ag.

After both the n and p type contacts are deposited, they are annealed at a temperature of 480°C in a furnace specially set up for this purpose. It was discovered early in the program that it is extremely important to eliminate oxygen from the annealing furnace to avoid deterioration of the (AlGa)As surface by oxidation and to prevent mechanical weakening of the contacts themselves. Any deterioration effect is significant, especially on the bar type contacts, since any weakening of these contacts leads to an increase in the series resistance (and sometimes increased leakage), which causes a lower power conversion efficiency. Use of a new annealing furnace with a Pd diffused hydrogen ambient, checked with an oxygen monitor, appreciably improved the contact conductance and contact adhesion, resulting in higher cell fabrication yields.

In addition to the AuZn and AuGeNi contact development work, AgZn and AgSn contacts were also investigated. The silver based contacts permitted higher temperature operation (600° versus 400°C). Also, they eliminate Au, which is costly. In addition to these direct benefits, there is another advantage in that the whole contact deposition can be handled in a sputtering system with three targets: Ag, Sn and Zn, thus reducing manufacturing process steps. The preliminary results obtained were encouraging. As shown in Table 12, the cells have reasonably good characteristics. However, the composition of the contacting alloys and the annealing cycles must be defined with much more precision to ensure reproducibility. Also, the mechanical integrity of these alternate contacts for welding, and under various ambient conditions must still be established.

In summary, the AuZn p type contact was developed for the HESP II cells in combination with the AuGeNi system for the n type. These contacts are both overlaid with 5.0 µm of Ag and are then annealed at 480°C. Sufficient

**4.2 Contact Metallization Techniques.** Figure 7 shows the complete GaAs solar cell fabrication process in which the ohmic contacts are given detailed attention.

The best results for applying the AuZn contacts to the p type (AlGa)As cell surface were achieved using a sputtering technique. The AuGeNi n type contacts were applied using thermal evaporation. These methods were used for the qualification cell contacts, and the cells successfully passed all tests.

The AuGeNi n type contacts are particularly easy to apply. The proportions involved are 12 percent Ge, 1.5 percent Ni, and 86.5 percent Au by weight. A coating approximately 2000 Å thick is used; this is covered by a 5 µm Ag overlay.

The AuZn contact consists of about 10 percent Zn and 90 percent Au by weight. Initially, the Au and Zn were sputtered onto the p surface from a composite target. However, a new sputtering system was acquired with multiple targets and a technique of sputtering from two targets of Au and Zn separately was perfected. This method provides considerably greater flexibility and reproducibility. The AuZn layer is also approximately 2000 Å thick and is covered with 5 µm of Ag.

After both the n and p type contacts are deposited, they are annealed at a temperature of 480°C in a furnace specially set up for this purpose. It was discovered early in the program that it is extremely important to eliminate oxygen from the annealing furnace to avoid deterioration of the (AlGa)As surface by oxidation and to prevent mechanical weakening of the contacts themselves. Any deterioration effect is significant, especially on the bar type contacts, since any weakening of these contacts leads to an increase in the series resistance (and sometimes increased leakage), which causes a lower power conversion efficiency. Use of a new annealing furnace with a Pd diffused hydrogen ambient, checked with an oxygen monitor, appreciably improved the contact conductance and contact adhesion, resulting in higher cell fabrication yields.

In addition to the AuZn and AuGeNi contact development work, AgZn and AgSn contacts were also investigated. The silver based contacts permitted higher temperature operation (600° versus 400°C). Also, they eliminate Au, which is costly. In addition to these direct benefits, there is another advantage in that the whole contact deposition can be handled in a sputtering system with three targets: Ag, Sn and Zn, thus reducing manufacturing process steps. The preliminary results obtained were encouraging. As shown in Table 12, the cells have reasonably good characteristics. However, the composition of the contacting alloys and the annealing cycles must be defined with much more precision to ensure reproducibility. Also, the mechanical integrity of these alternate contacts for welding, and under various ambient conditions must still be established.

In summary, the AuZn p type contact was developed for the HESP II cells in combination with the AuGeNi system for the n type. These contacts are both overlaid with 5.0 µm of Ag and are then annealed at 480°C. Sufficient

TABLE 12. GaAs SOLAR CELL CHARACTERISTICS  
WITH  $A_3Zn$  CONTACTS ON P SIDE

Cell No.	$V_{OC}$	$I_{SC}$ , (mA)	FF, (%)	Efficiency AMO (%) <sup>*</sup>
2393	1.01	119	78	17.3
2395	1.02	119	77	17.2
2451	0.99	111	77	15.6
2517	1.01	110	75	15.4

\*Efficiency with AR coating.

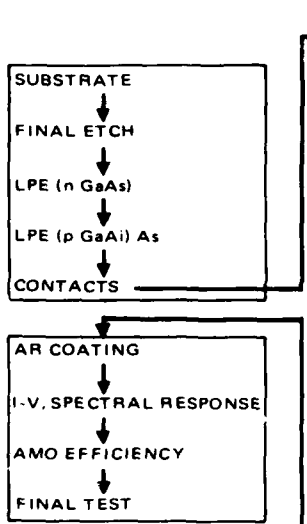


Figure 7. GaAs solar cell fabrication process.

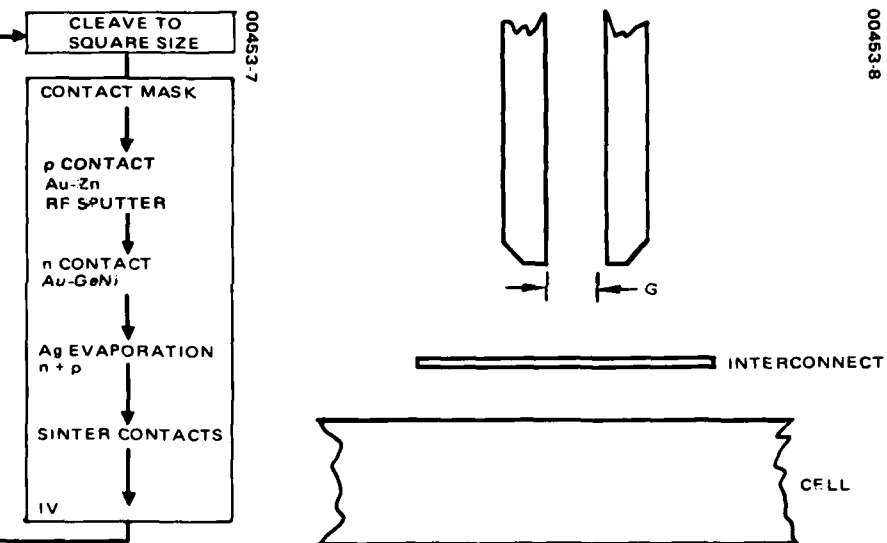


Figure 8. Parallel gap welder: working area

environmental tests were performed to prove their low resistance and good mechanical integrity, and their applicability to welded interconnection was demonstrated.

**4.3 Welding.** Two different methods of welding were developed under HESP II: ultrasonic seam welding and parallel gap welding. Since both involved highly specialized machinery, it was found that weld results were highly sensitive to the respective equipment controls.

**4.3.1 Parallel Gap Welding.** A simplified schematic of the working area of the parallel gap welder is shown in Figure 8. Here two electrodes, a set distance apart, are lowered onto an interconnect/cell assembly with a calibrated force. Activation of an electrical switch introduces a voltage and current pulse which produces a thermal weld in the discharge region. Optimum welds require adjustment of the following parameters:

TABLE 12. GaAs SOLAR CELL CHARACTERISTICS  
WITH  $A_3Zn$  CONTACTS ON P SIDE

Cell No.	$V_{OC}$	$I_{SC}$ , (mA)	FF, (%)	Efficiency AMO (%) <sup>*</sup>
2393	1.01	119	78	17.3
2395	1.02	119	77	17.2
2451	0.99	111	77	15.6
2517	1.01	110	75	15.4

\*Efficiency with AR coating.

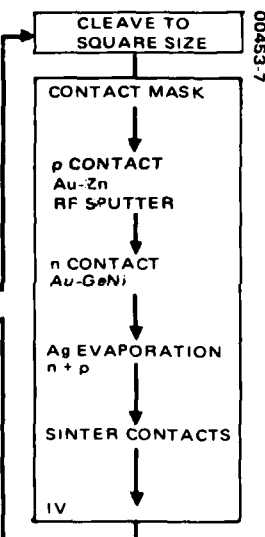
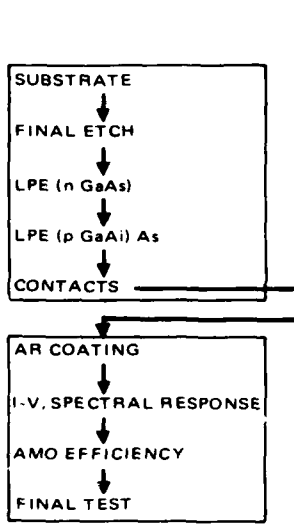


Figure 7. GaAs solar cell fabrication process.

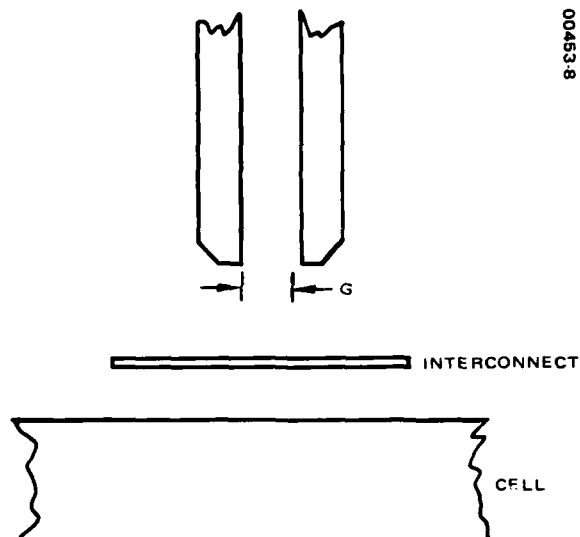


Figure 8. Parallel gap welder: working area

environmental tests were performed to prove their low resistance and good mechanical integrity, and their applicability to welded interconnection was demonstrated.

**4.3 Welding.** Two different methods of welding were developed under HESP II: ultrasonic seam welding and parallel gap welding. Since both involved highly specialized machinery, it was found that weld results were highly sensitive to the respective equipment controls.

**4.3.1 Parallel Gap Welding.** A simplified schematic of the working area of the parallel gap welder is shown in Figure 8. Here two electrodes, a set distance apart, are lowered onto an interconnect/cell assembly with a calibrated force. Activation of an electrical switch introduces a voltage and current pulse which produces a thermal weld in the discharge region. Optimum welds require adjustment of the following parameters:

- 1) F, contact force - This force is that which the electrodes exert on the tab/cell combination during welding. It is capable of being adjusted to several pounds, but, in actuality, minimal values are desirable.
- 2) V, voltage - This is the amplitude of the voltage pulse introduced into the weld area. Excessive voltage leads to blistering, while insufficient voltage results in poor or unsuccessful welds.
- 3) t, time - The duration of the voltage pulse is also significant. It, too, regulates the amount of energy delivered to the metal interface.
- 4) G, gap distance - This is the spacing between the electrode.

4.3.2 Ultrasonic Seam Welding. Interconnects were constructed from 99.99 percent Ag foil 1.0 mil thick. Units prepared for ultrasonic seam welding were made up of six tabs, each originally connected as shown in Figure 9. Welds were made by placing the fingers over the solar cell contact and running the weld wheel from A to A'. The foil was then cut along the dashed lines and individually separated following the welding operation. Thus, attached to the completed cell were 12 independent tabs, each approximately  $1.1 \times 6.5 \text{ mm}^2$  in area.

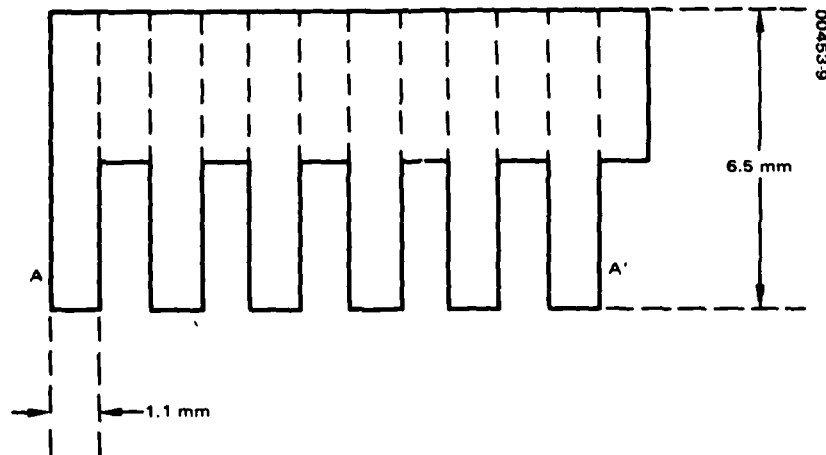


Figure 9. Silver foil pattern with six tabs

- 1) F, contact force - This force is that which the electrodes exert on the tab/cell combination during welding. It is capable of being adjusted to several pounds, but, in actuality, minimal values are desirable.
- 2) V, voltage - This is the amplitude of the voltage pulse introduced into the weld area. Excessive voltage leads to blistering, while insufficient voltage results in poor or unsuccessful welds.
- 3) t, time - The duration of the voltage pulse is also significant. It, too, regulates the amount of energy delivered to the metal interface.
- 4) G, gap distance - This is the spacing between the electrode.

4.3.2 Ultrasonic Seam Welding. Interconnects were constructed from 99.99 percent Ag foil 1.0 mil thick. Units prepared for ultrasonic seam welding were made up of six tabs, each originally connected as shown in Figure 9. Welds were made by placing the fingers over the solar cell contact and running the weld wheel from A to A'. The foil was then cut along the dashed lines and individually separated following the welding operation. Thus, attached to the completed cell were 12 independent tabs, each approximately  $1.1 \times 6.5 \text{ mm}^2$  in area.

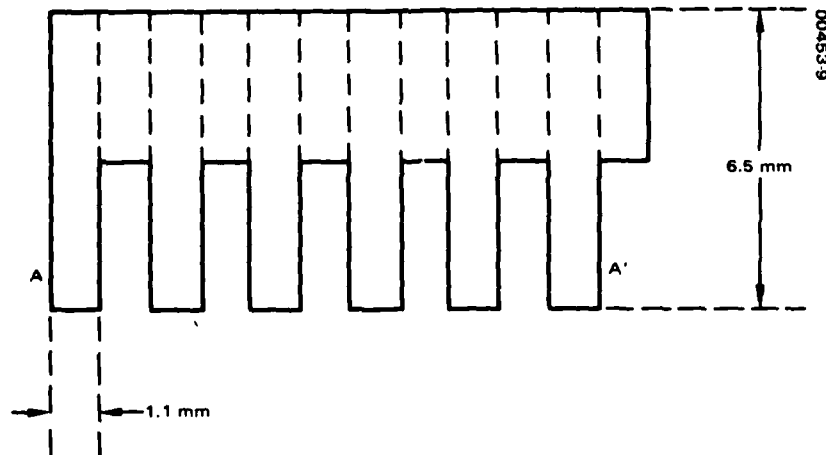


Figure 9. Silver foil pattern with six tabs

A simplified block schematic of the ultrasonic seam welder and supporting equipment is shown in Figure 10 (the horizontal plane is the surface of the figure; the vertical direction is into the diagram). Here the welding tool is a 0.71 inch diameter wheel machined from drill rod and attached to a 6 inch long tapered horn rigidly connected to a magnetostrictive (ferromagnetic) transducer. This entire unit is spring mounted to a block in such a way that the spring tension and thereby the contact force, ( $F_c$ ) of the wheel against the device can be increased or decreased in the vertical direction by means of set screws (not shown). The block, in turn, can be motor driven along a track in the horizontal plane at various speeds.

The transducer is controlled by a power source equipped with both amplitude and tuning adjustments. Meter scales associated with each ensures reproducibility of settings. Tuning is further facilitated by oscilloscope display of a Lissajous pattern resulting from simultaneously monitoring the current and voltage through the transducer.

The vacuum stage supports both the solar cell and tabs during welding, while the calibration stage is used to determine the contact force,  $F_c$ , of the wheel by means of a simple switch circuit.

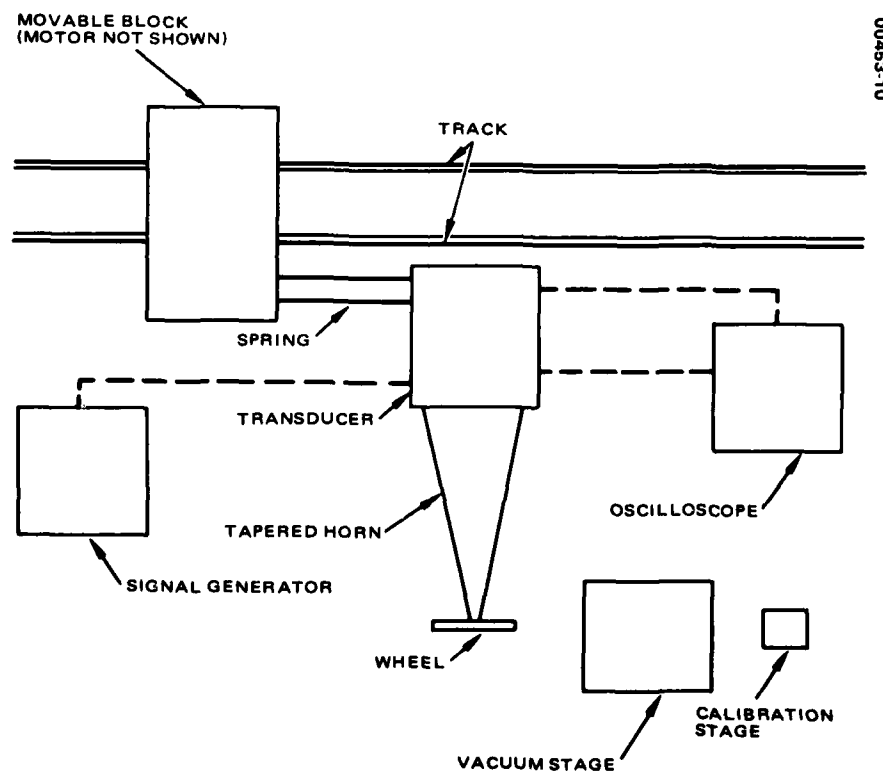


Figure 10. Top view schematic of ultrasonic seam welder and supporting equipment

A simplified block schematic of the ultrasonic seam welder and supporting equipment is shown in Figure 10 (the horizontal plane is the surface of the figure; the vertical direction is into the diagram). Here the welding tool is a 0.71 inch diameter wheel machined from drill rod and attached to a 6 inch long tapered horn rigidly connected to a magnetostrictive (ferromagnetic) transducer. This entire unit is spring mounted to a block in such a way that the spring tension and thereby the contact force, ( $F_c$ ) of the wheel against the device can be increased or decreased in the vertical direction by means of set screws (not shown). The block, in turn, can be motor driven along a track in the horizontal plane at various speeds.

The transducer is controlled by a power source equipped with both amplitude and tuning adjustments. Meter scales associated with each ensures reproducibility of settings. Tuning is further facilitated by oscilloscope display of a Lissajous pattern resulting from simultaneously monitoring the current and voltage through the transducer.

The vacuum stage supports both the solar cell and tabs during welding, while the calibration stage is used to determine the contact force,  $F_c$ , of the wheel by means of a simple switch circuit.

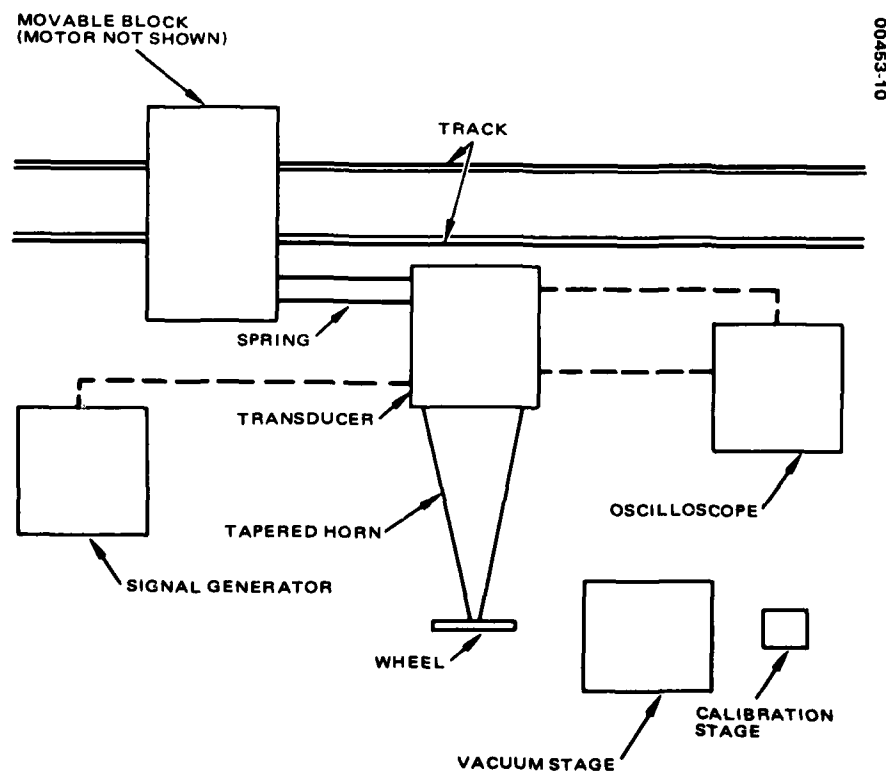


Figure 10. Top view schematic of ultrasonic seam welder and supporting equipment

Producing reliable bonds entailed optimizing a combination of the following key parameters:

- 1)  $F_c$ , contact force — This force is that which the weld wheel exerts upon the tab/cell combination during welding. It is capable of being adjusted through a range from zero to well over 450 grams.
- 2) P, relative power output of the source — This adjustment modifies the amplitude of the electromagnetic wave transformed by the transducer into mechanical oscillations eventually delivered to the weld area.
- 3) T, tuning of the source — Tuning alters the frequency of the electrical signal and thereby the mechanical energy transferred to the weld. By proper tuning, the energy delivered to the weld wheel can be maximized by matching the resonant frequency of the horn/wheel assembly.
- 4) V, velocity of the wheel — The speed at which the weld wheel travels over the weld area determines in part the total amount of energy imparted into the bond which, in turn, affects the quality of the bond.

4.3.3 Weld Results. Typical results of successful seam weld operations are submitted in Table 13. Pull strengths are excellent. However, there are some difficulties. First of all, the consistency of pull strengths is not the best: values range from as low as 0.70 to 1.35 pounds. Also, results from cell to cell are not as reproducible as desired. These difficulties are purely machine related, since similar results are noted when silicon solar cells are substituted for the GaAs cells.

TABLE 13. TYPICAL ULTRASONIC  
SEAM WELD RESULTS  
(Cell 4007)

Parameter	Front Contact	Back Contact
$F_c$ , gm	200	300
P	3.5	3.5
V	40	36
T	0.02	0
Pull Force, lb		
Tab	Front Contact	Back Contact
1	0.75	0.70
2	0.95	0.65
3	0.80	0.55
4	0.80	1.15
5	1.00	1.15
6	1.35	1.00

Producing reliable bonds entailed optimizing a combination of the following key parameters:

- 1)  $F_c$ , contact force — This force is that which the weld wheel exerts upon the tab/cell combination during welding. It is capable of being adjusted through a range from zero to well over 450 grams.
- 2) P, relative power output of the source — This adjustment modifies the amplitude of the electromagnetic wave transformed by the transducer into mechanical oscillations eventually delivered to the weld area.
- 3) T, tuning of the source — Tuning alters the frequency of the electrical signal and thereby the mechanical energy transferred to the weld. By proper tuning, the energy delivered to the weld wheel can be maximized by matching the resonant frequency of the horn/wheel assembly.
- 4) V, velocity of the wheel — The speed at which the weld wheel travels over the weld area determines in part the total amount of energy imparted into the bond which, in turn, affects the quality of the bond.

4.3.3 Weld Results. Typical results of successful seam weld operations are submitted in Table 13. Pull strengths are excellent. However, there are some difficulties. First of all, the consistency of pull strengths is not the best: values range from as low as 0.70 to 1.35 pounds. Also, results from cell to cell are not as reproducible as desired. These difficulties are purely machine related, since similar results are noted when silicon solar cells are substituted for the GaAs cells.

TABLE 13. TYPICAL ULTRASONIC  
SEAM WELD RESULTS  
(Cell 4007)

Parameter	Front Contact	Back Contact
$F_c$ , gm	200	300
P	3.5	3.5
V	40	36
T	0.02	0
Pull Force, lb		
Tab	Front Contact	Back Contact
1	0.75	0.70
2	0.95	0.65
3	0.80	0.55
4	0.80	1.15
5	1.00	1.15
6	1.35	1.00

Gap weld results are shown in Table 14. In general, consistency of pull strengths from tab to tab is superior, and reproducibility from cell to cell is also excellent. Pull strengths are well in excess of those required. In addition, no degradation of electrical parameters was noted.

In general then, the gap technique proved to be very reliable. All welding tasks involving cells for both qualification testing and ultimate delivery under the program employed this method.

TABLE 14. TYPICAL GAP  
WELD RESULTS  
(Cell 4184)

Parameter	Front Contact	Back Contact
F, lb	1.0	1.0
V, volts	0.46	0.45
t, ms	550	550
G, in.	0.015	0.015
Pull Force, lb		
Tab	Front Contact	Back Contact
1	0.71	0.71
2	0.65	0.69
3	0.74	0.68
4	0.72	0.69
5	0.76	0.61
6	0.76	0.69

Gap weld results are shown in Table 14. In general, consistency of pull strengths from tab to tab is superior, and reproducibility from cell to cell is also excellent. Pull strengths are well in excess of those required. In addition, no degradation of electrical parameters was noted.

In general then, the gap technique proved to be very reliable. All welding tasks involving cells for both qualification testing and ultimate delivery under the program employed this method.

TABLE 14. TYPICAL GAP  
WELD RESULTS  
(Cell 4184)

Parameter	Front Contact	Back Contact
F, lb	1.0	1.0
V, volts	0.46	0.45
t, ms	550	550
G, in.	0.015	0.015
Pull Force, lb		
Tab	Front Contact	Back Contact
1	0.71	0.71
2	0.65	0.69
3	0.74	0.68
4	0.72	0.69
5	0.76	0.61
6	0.76	0.69

## 5. GaAs SUBSTRATE

5.1 Introduction. Energy conversion in GaAs solar cells takes place in the uppermost layers. With the present process, these critical GaAs layers are grown by liquid phase epitaxy (LPE) upon a relatively inexpensive GaAs substrate that provides both electrical connection and mechanical support. An important program objective was to develop speedy, cost-effective methods of manufacturing large area, rectangular GaAs substrates.

To this end, we had a subcontract with Crystal Specialties Inc., (Monrovia, California) to study the horizontal Bridgman technique for producing GaAs single crystals with large area rectangular cross sections. A resulting slice with a 2.0 by 1.0 inch surface area would increase the usable material and thus reduce the cost. Wafers with cross sections as large as 2.0 by 2.0 inches would be even more effective.

Another area of concern was the reduction of the large GaAs crystals to appropriate substrate wafers. This process involves two major operations: sawing and polishing. Various methods of sawing and polishing were examined in an attempt to produce GaAs wafers in less time, with better mechanical characteristics, and with less breakage — in short, more economically.

Finally, attention was focused on processing thinner GaAs substrates. After successfully making 12 mil wafers, the feasibility of 8 mil wafers was studied. Such a reduction in thickness would result in lighter GaAs solar cells. In addition, if the 8 mil substrates could be sliced thinner from the beginning, more GaAs cells could be produced from a single crystal.

5.2 Horizontal Bridgman Crystal Growth. Growing crystals by the horizontal Bridgman technique usually involves the use of a two-zone furnace to produce a temperature gradient which is translated horizontally to cool a melt composed of the material which is being grown into a single crystal. However, for GaAs crystals, a third zone is used to control the arsenic temperature during reaction. Figure 11 is a schematic of the equipment required. The sealed quartz growth ampoule shown contains a boat loaded with a single crystal seed, GaAs melt, and quantities of elemental Te and As. The ampoule, in turn, is enclosed within the three-zone furnace, which can be translated.

## 5. GaAs SUBSTRATE

5.1 Introduction. Energy conversion in GaAs solar cells takes place in the uppermost layers. With the present process, these critical GaAs layers are grown by liquid phase epitaxy (LPE) upon a relatively inexpensive GaAs substrate that provides both electrical connection and mechanical support. An important program objective was to develop speedy, cost-effective methods of manufacturing large area, rectangular GaAs substrates.

To this end, we had a subcontract with Crystal Specialties Inc., (Monrovia, California) to study the horizontal Bridgman technique for producing GaAs single crystals with large area rectangular cross sections. A resulting slice with a 2.0 by 1.0 inch surface area would increase the usable material and thus reduce the cost. Wafers with cross sections as large as 2.0 by 2.0 inches would be even more effective.

Another area of concern was the reduction of the large GaAs crystals to appropriate substrate wafers. This process involves two major operations: sawing and polishing. Various methods of sawing and polishing were examined in an attempt to produce GaAs wafers in less time, with better mechanical characteristics, and with less breakage — in short, more economically.

Finally, attention was focused on processing thinner GaAs substrates. After successfully making 12 mil wafers, the feasibility of 8 mil wafers was studied. Such a reduction in thickness would result in lighter GaAs solar cells. In addition, if the 8 mil substrates could be sliced thinner from the beginning, more GaAs cells could be produced from a single crystal.

5.2 Horizontal Bridgman Crystal Growth. Growing crystals by the horizontal Bridgman technique usually involves the use of a two-zone furnace to produce a temperature gradient which is translated horizontally to cool a melt composed of the material which is being grown into a single crystal. However, for GaAs crystals, a third zone is used to control the arsenic temperature during reaction. Figure 11 is a schematic of the equipment required. The sealed quartz growth ampoule shown contains a boat loaded with a single crystal seed, GaAs melt, and quantities of elemental Te and As. The ampoule, in turn, is enclosed within the three-zone furnace, which can be translated.

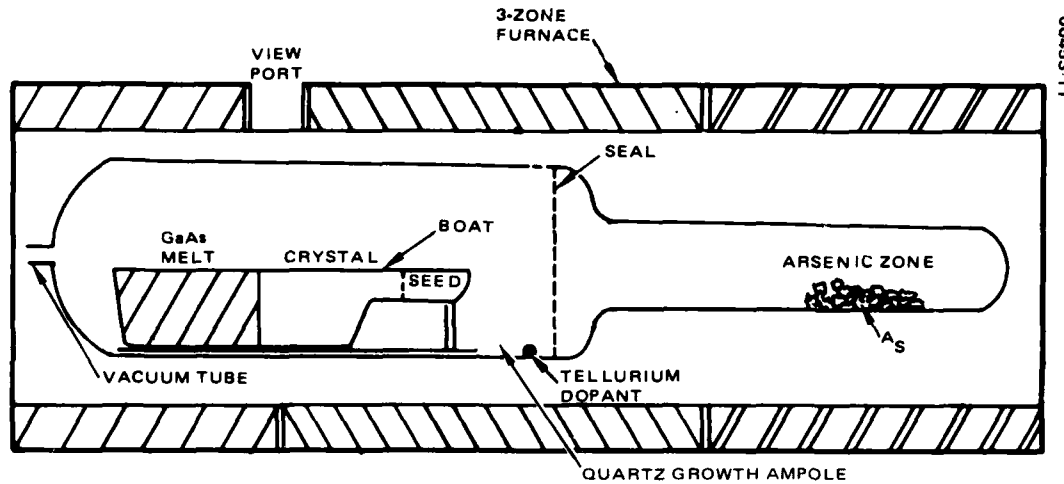


Figure 11. Horizontal Bridgman growth.

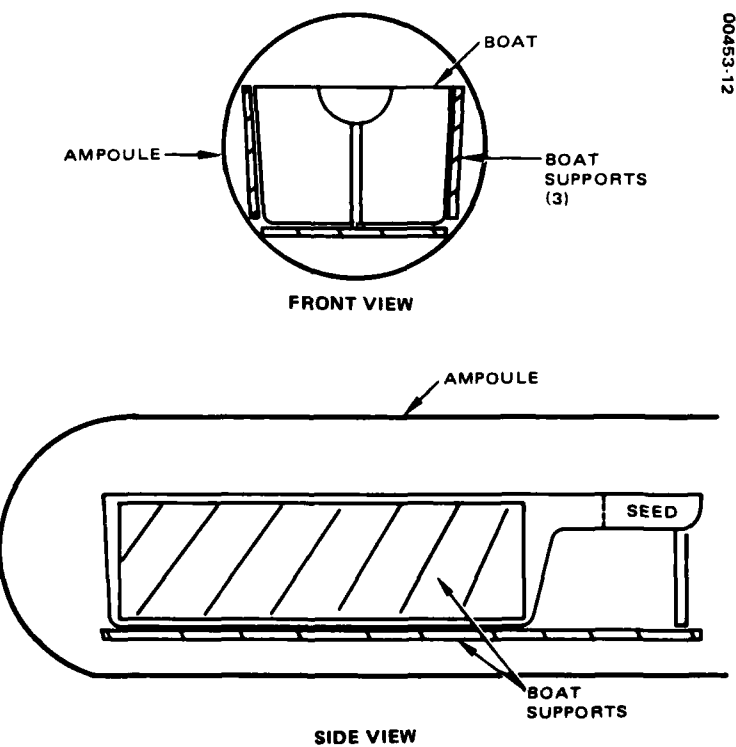


Figure 12. Boat supports.

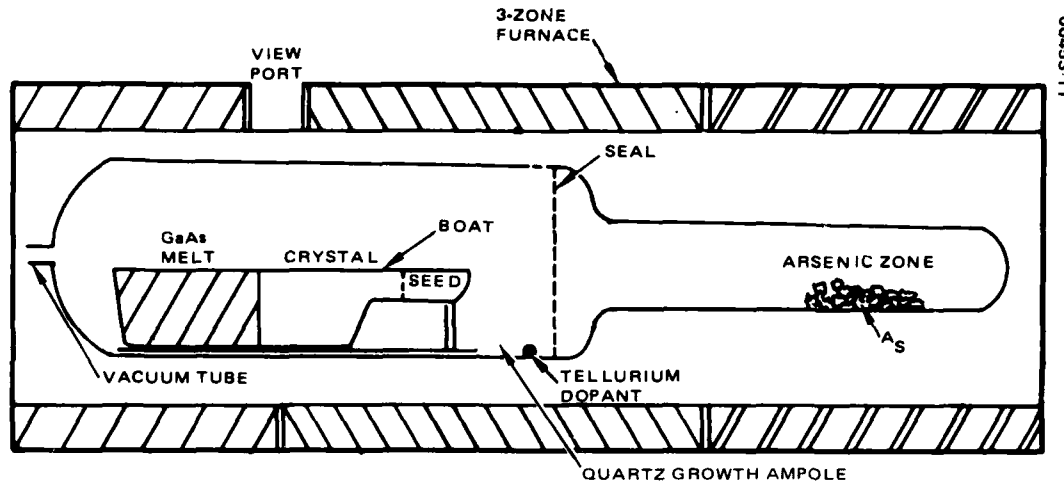


Figure 11. Horizontal Bridgman growth.

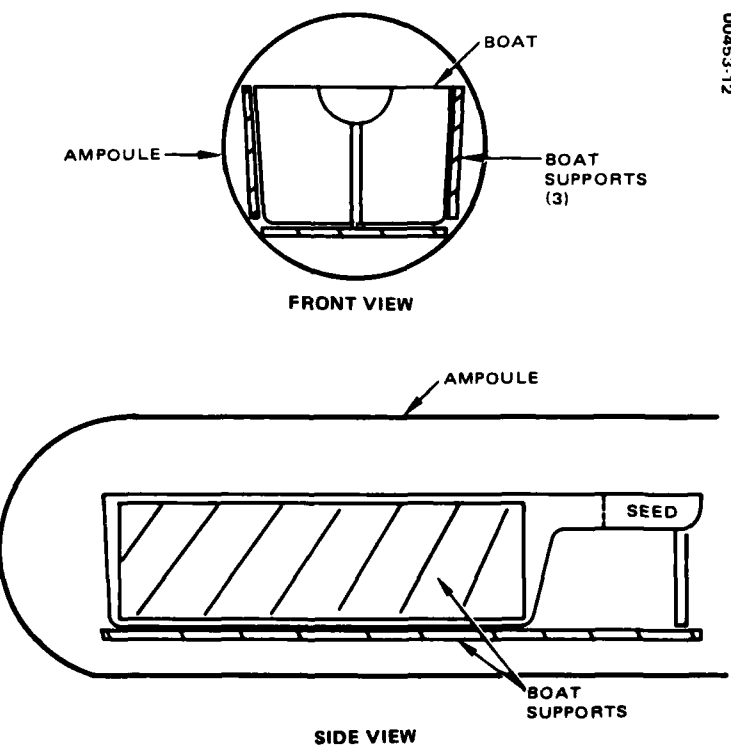


Figure 12. Boat supports.

The first step in actual GaAs growth involves the complete cleaning of all materials that come in contact with the gallium and arsenic during growth. Materials such as the boat (quartz, graphite, or vitreous carbon), the quartz growth ampoule, and the support liners are etched using a 1:1 mixture of nitric and hydrochloric acids. Afterward, these materials are thoroughly washed in deionized water.

The gallium is placed in the boat with a seed crystal in the front portion of the vessel. The support liners are placed on the sides and under the boat (if a quartz boat is used). A small amount of tellurium dopant is placed on the growth ampoule in front of the boat. A stoichiometric amount of arsenic is then placed in the other end of the growth ampoule. The quartz growth end and arsenic end are sealed with a quartz rod to form the growth ampoule. The ampoule is subsequently evacuated and sealed at the front of the growth end by collapsing and removing the quartz vacuum tube.

After this, the ampoule is placed in the furnace, and the gallium and arsenic are reacted by heating the gallium to the melting point of GaAs ( $1247^{\circ}\text{C}$ ) while the arsenic temperature is held at  $600^{\circ}\text{C}$ . At this temperature the arsenic sublimes and reacts with the gallium, forming the GaAs melt. The GaAs melt is then allowed to soak for 24 hours to aid single crystal growth. After adjusting the melt and growth zone temperature to a level where the molten GaAs just melts into the seed, the furnace is caused to travel, thus slowly cooling the material below the melting point of GaAs. The rate of travel of the furnace is about 0.5 inch per hour.

After the crystal is grown, it is taken from the furnace, and slices from the front and back of the crystal are removed to obtain EPD and Hall data. After these measurements are made the crystal is cut to the desired size and mounted in preparation for wafering on either the ID saw or multiblade saw.

5.3 Large Area GaAs Substrates - Assessment. To obtain rectangular GaAs crystals, a boat material had to be found which could physically hold the weight of the melt and at the same time be compatible with good crystal growth. This endeavor eventually led to the evaluation of fused quartz, graphite, and vitreous carbon boats. In addition, to support the bottom and sides of the rectangular quartz boats, liners made of silicon carbide, boron nitride, and fused quartz were assessed. The placement of such liners about the boat is illustrated in Figure 12. The effects of these materials, in various combinations, on crystal perfection and crystal uniformity were studied on resulting GaAs ingots with a minimum cross section of 1.0 by 2.0 inches and a preferred cross section of 2.0 by 2.0 inches.

Table 15 summarizes the growth runs and results. The resulting assessment of boat and liner materials and of the feasibility of large area substrate growth is given below the table.

TABLE 15. LARGE AREA GaAs SUBSTRATES GROWTH RUNS

Run	Boat size, (in.)	Material	Liner	Orientation	Results
2	1.0 x 2.0	Quartz	Silicon carbide	(100) 110 up	Poly - oxides
3	1.0 x 2.0	Quartz	Quartz	(100) 110 up	Single
5	2.0 x 2.0	Quartz	Quartz	(100) 110 up	Poly - steep thermal gradients
6	1.0 x 2.0	Quartz	Boron nitride (BN)	(100) 110 up	Poly - boat wet
8	1.0 x 2.0	Graphite	None	(100) 110 up	Poly - oxides, boat wet
9	1.0 x 2.0	Quartz	BN	(110) 100 up	Single
11	1.0 x 2.0	Quartz	BN	(110) 100 up	Single
12	2.0 x 2.0	Quartz	BN	(110) 100 up	Poly - steep thermal gradients
15	1.0 x 2.0	Quartz	BN	(110) 100 up	Single
16	1.0 x 2.0	Quartz	None	(110) 100 up	Single - bo. t sagged
19	1.0 x 2.0	Quartz	BN and Quartz	(110) 100 up	Single
20	1.0 x 2.0	Quartz	BN	(110) 100 up	Poly - oxides
22	1.0 x 2.0	Vitreous carbon	None	(110) 100 up	Poly - boat wet
23	1.0 x 2.0	Quartz	BN	(110) 100 up	Single
24	2.75 x 1.0	Quartz	BN	(110) 100 up	Poly
25	2.0 x 2.0	Quartz	BN	(100) 110 up	Poly - steep thermal gradients
26	2.0 x 2.0	Quartz	BN	(100) 100 up	Poly - steep thermal gradients
27	2.75 x 1.0	Quartz	BN	(110) 100 up	Single
28	1.0 x 2.0	Quartz	BN	(110) 100 up	Poly - melted seed
29	1.0 x 2.0	Quartz	BN	(110) 100 up	Poly - oxides
30	1.0 x 2.0	Quartz	BN	(110) 100 up	Single
31	1.0 x 2.0	Quartz	BN	(110) 100 up	Single
32	1.75 x 1.5	Quartz	BN	(110)	Single
33	1.0 x 2.0	Quartz	BN	(110) 100 up	Poly - oxides
34	1.0 x 2.0	Quartz	BN	(110)	Single
35	1.75 x 1.5	Quartz	BN	(110)	Single

5.3.1 Quartz Boats and Liners. Very early growth attempts in quartz encountered considerable difficulty attributed to boat wetting. With changes in cleaning techniques, however, such wetting was significantly reduced. Especially good single crystals were obtained in 1.0 by 2.0 inch quartz boats using boron nitride liners (runs 9, 11, 15, 23, 30, 31, and 34 of Table 13).

For support, silicon carbide liners were used in run 2. However, this resulted in the formation of a crystalline residue on the inside walls of the ampoule. In addition, a scum accumulated on the surface of the melt. Silicon carbide, therefore, is not considered to be a good liner material.

Quartz plates and rods were also used as liners (runs 3, 5, and 19), and subsequent growths for the most part proved to be single crystals. However, due to the high growth temperature needed for GaAs, they became distorted and tended to fuse to the quartz boat and ampoule.

Ingots 5, 12, 25, and 26 were grown in 2.0 by 2.0 inch quartz boats, but the material proved to be polycrystalline. This was probably due to the thermal gradients throughout the 2.0 inch depth of the boat. On the other hand, single crystals resulted in runs 32 and 35 which were grown in boats 1.75 inches wide and only 1.5 inches deep.

Therefore, 2.0 by 1.0 inch and 1.75 by 1.5 inch quartz boats with boron nitride support liners seem to be the most feasible way of growing single rectangular GaAs crystals. By cutting these selectively, substrate wafers with four surface areas can be regularly produced: 2.0 by 1.0 inches, 2.0 by 2.0 inches, 2.25 by 1.5 inches, and 1.75 by 1.5 inches.

The 2.0 by 1.0 inch and 1.75 by 1.5 inch boats come from standard size rectangular quartz stock. For boats with cross sections other than these dimensions, specially drawn quartz is required.

5.3.2 Graphite Boats. Run 8 was done in a 2.0 by 1.0 inch high purity graphite boat. A single crystal could not be grown because of a dross which floated upon the surface of the melt. Upon removal of the crystal from the furnace:

- 1) The top of the crystal was coated with many particles. These bubble-like deposits were scattered over the entire upper surface area. The particles probably came from the carbon boat. Historically, growth in carbon boats has not been successful, mainly because of these particles.
- 2) Difficulty was experienced in removing the crystal from the boat. This boat wetting effect usually occurs in quartz boats (primarily due to moisture in the quartz itself) and in the past has not been a problem with carbon boats.

Because of these effects, graphite is not considered to be a suitable boat material.

5.3.3 Vitreous Carbon Boats. Crystal 22 was grown in a 1.0 by 2.0 inch vitreous carbon boat made at Tylan Corporation by placing a high purity vitreous coating over a carbon boat. Single growth was attempted four separate times but could not be attained. There were no bubble-like particles on the surface of the crystal as was the case with the carbon boat. Apparently the vitreous (glassy) coating helped prevent carbon from leaving the boat and entering the melt. However, the crystal adhered severely to the boat, again indicating wetting.

**5.3.4 Summary.** As a result of this study, carbon and vitreous carbon boats were determined to be unsuitable for GaAs crystal growth. Quartz boats were found to be the best material, after proper cleaning to minimize boat wetting. However, at and above the melting point of gallium arsenide ( $1247^{\circ}\text{C}$ ), the quartz will soften and begin to sag under the weight of the growing crystal. To properly support growth, high temperature resistant liners are necessary. Boron nitride liners were found to be the most suitable liners.

Using the quartz and boron nitride combination, GaAs ingots can be grown that are capable of being processed into large area rectangular substrates having surfaces of 2.0 by 1.0 inches, 2.0 by 2.0 inches, 2.25 by 1.5 inches, and 1.75 by 1.5 inches.

**5.4 Sawing and Polishing Process - Assessment.** After the GaAs crystal is grown, it must be cut into wafers using either of two techniques - the inner diameter (ID) saw or the multiblade saw. A description of each follows.

**5.4.1 Sawing Methods.** The ID saw incorporates special orientation fixtures designed for unusual cutting angles which are necessary with GaAs crystals. The saw blade itself remains stationary while the mounted ingot moves through the blade. Blade flutter, the prime cause of gross subsurface damage in semiconductor wafers, is held to a minimum, and extremely close mechanical tolerance is possible. Saw marks and surface imperfections are not discernible if the machine is properly maintained.

The multiblade saw employs up to 240 thin oscillating steel bands. An abrasive slurry does the actual cutting, usually resulting in an extremely smooth surface ready for lapping and polishing. It was felt that with the use of such a machine, with blades that produce a kerf loss of 0.007 inch, the waste due to cutting and polishing could be reduced to about 54 percent of the present figure. Other savings in breakage and labor might also be realized.

**5.4.2 Post-Saw Processing.** After the crystal is sliced, the wafers are ultrasonically cleaned in sulfuric acid and then mounted on a flat stainless steel plate using a high purity microcrystalline wax. Five micron platelet alumina grit is used for precision lapping of the wafers to the desired thickness. This process is followed by polishing.

Mechanical polishing produces extremely flat wafers. However, there is always attendant subsurface damage. Chemical polishing, on the other hand, produces wafers that are relatively free of subsurface damage but are not optically flat. Chemomechanical polishing is the happy compromise. A chlorine bleaching solution acts as a mild chemical etchant while a polishing pad gently planes the surface, resulting in a flat surface with virtually no damage.

After polishing, the wafers are cleaned by boiling them in trichloroethylene. The wafers are then inspected for correct thickness and any physical damage before being accepted for LPE growth.

**5.3.4 Summary.** As a result of this study, carbon and vitreous carbon boats were determined to be unsuitable for GaAs crystal growth. Quartz boats were found to be the best material, after proper cleaning to minimize boat wetting. However, at and above the melting point of gallium arsenide ( $1247^{\circ}\text{C}$ ), the quartz will soften and begin to sag under the weight of the growing crystal. To properly support growth, high temperature resistant liners are necessary. Boron nitride liners were found to be the most suitable liners.

Using the quartz and boron nitride combination, GaAs ingots can be grown that are capable of being processed into large area rectangular substrates having surfaces of 2.0 by 1.0 inches, 2.0 by 2.0 inches, 2.25 by 1.5 inches, and 1.75 by 1.5 inches.

**5.4 Sawing and Polishing Process - Assessment.** After the GaAs crystal is grown, it must be cut into wafers using either of two techniques - the inner diameter (ID) saw or the multiblade saw. A description of each follows.

**5.4.1 Sawing Methods.** The ID saw incorporates special orientation fixtures designed for unusual cutting angles which are necessary with GaAs crystals. The saw blade itself remains stationary while the mounted ingot moves through the blade. Blade flutter, the prime cause of gross subsurface damage in semiconductor wafers, is held to a minimum, and extremely close mechanical tolerance is possible. Saw marks and surface imperfections are not discernible if the machine is properly maintained.

The multiblade saw employs up to 240 thin oscillating steel bands. An abrasive slurry does the actual cutting, usually resulting in an extremely smooth surface ready for lapping and polishing. It was felt that with the use of such a machine, with blades that produce a kerf loss of 0.007 inch, the waste due to cutting and polishing could be reduced to about 54 percent of the present figure. Other savings in breakage and labor might also be realized.

**5.4.2 Post-Saw Processing.** After the crystal is sliced, the wafers are ultrasonically cleaned in sulfuric acid and then mounted on a flat stainless steel plate using a high purity microcrystalline wax. Five micron platelet alumina grit is used for precision lapping of the wafers to the desired thickness. This process is followed by polishing.

Mechanical polishing produces extremely flat wafers. However, there is always attendant subsurface damage. Chemical polishing, on the other hand, produces wafers that are relatively free of subsurface damage but are not optically flat. Chemomechanical polishing is the happy compromise. A chlorine bleaching solution acts as a mild chemical etchant while a polishing pad gently planes the surface, resulting in a flat surface with virtually no damage.

After polishing, the wafers are cleaned by boiling them in trichloroethylene. The wafers are then inspected for correct thickness and any physical damage before being accepted for LPE growth.

**5.4.3 Evaluation of Saw Methods.** The initial tests using the multiblade saw were very positive; results are shown in Table 16. Crystal 11 was cut using 0.004 inch blades and 0.021 inch spacers. Crystals 15 and 16 were cut with 0.004 inch blades and 0.023 inch spacers. Each of these crystals was sandwiched between two glass plates in a gypsum cement mold. The objective in using the plates was to reduce wandering and to dress the blades as they cut through the GaAs crystal. There were very few broken slices as a result of the cutting operation. The multiblade saw provides for a more uniform wafer thickness with less kerf loss than the ID saw. Most of the wafers sliced on the multiblade saw varied  $\pm 0.0005$  inch per slice as compared with a  $\pm 0.002$  inch variance on the ID saw. Kerf loss on the multi-blade saw was also substantially reduced: from 0.013 inch on the ID saw (runs 23, 30, 31, 32, 34) down to about 0.007 inch (runs 11, 15, 16) on the multiblade saw.

On the other hand, the setup time for orientation, mold fabrication, and alignment of the crystal in the multiblade saw is 3 or 4 hours longer than the setup time for the ID saw. Maximum cutting time of 2.0 by 2.0 inch wafers on the multiblade saw, based on a 16 hour run to cut an entire crystal (with setup time), amounts to approximately 12 slices per hour. This compares with 20 slices per hour on the ID saw. Also, after the multiblade saw was used, damage was detected that penetrated the entire thickness of many of the wafers. This damage was probably due to vibrations in the saw during direction changes of the blade head which forced the crystal to oscillate vertically. To correct the problem, the saw would have to be run at about half its current speed, and this would be too slow to be of practical use.

**5.4.4 Summary.** Because of the damage it created in the wafers, the multiblade saw was deemed an unacceptable tool for slicing GaAs crystals, and its use was terminated. Crystals processed after run 30 (Table 15) were sliced with the ID saw. The wafers coming off this saw had a flatness of  $0.021 \pm 0.002$  inch. This was greater than the 0.0005 inch variance of the multiblade saw. This variance, however, can be reduced during the lapping and polishing operation. The advantages in using the ID saw, as compared with the multiblade saw, are that it takes less time to slice ingots and there is less subsurface damage.

After slicing and lapping, a polishing process is required to finish the wafers. Simple mechanical polishing was found to induce subsurface damage in the GaAs, while the simple chemical technique yielded substrates not sufficiently flat. A chemomechanical polishing process was therefore developed to minimize the disadvantages of both of these methods.

**5.5 Thin GaAs Substrates - Assessment.** The last column of Table 16 indicates that both 12 and 8 mil substrates were processed. However, yields and causes of breakage differ for the two thicknesses. An assessment of both groups follows.

**5.4.3 Evaluation of Saw Methods.** The initial tests using the multiblade saw were very positive; results are shown in Table 16. Crystal 11 was cut using 0.004 inch blades and 0.021 inch spacers. Crystals 15 and 16 were cut with 0.004 inch blades and 0.023 inch spacers. Each of these crystals was sandwiched between two glass plates in a gypsum cement mold. The objective in using the plates was to reduce wandering and to dress the blades as they cut through the GaAs crystal. There were very few broken slices as a result of the cutting operation. The multiblade saw provides for a more uniform wafer thickness with less kerf loss than the ID saw. Most of the wafers sliced on the multiblade saw varied  $\pm 0.0005$  inch per slice as compared with a  $\pm 0.002$  inch variance on the ID saw. Kerf loss on the multi-blade saw was also substantially reduced: from 0.013 inch on the ID saw (runs 23, 30, 31, 32, 34) down to about 0.007 inch (runs 11, 15, 16) on the multiblade saw.

On the other hand, the setup time for orientation, mold fabrication, and alignment of the crystal in the multiblade saw is 3 or 4 hours longer than the setup time for the ID saw. Maximum cutting time of 2.0 by 2.0 inch wafers on the multiblade saw, based on a 16 hour run to cut an entire crystal (with setup time), amounts to approximately 12 slices per hour. This compares with 20 slices per hour on the ID saw. Also, after the multiblade saw was used, damage was detected that penetrated the entire thickness of many of the wafers. This damage was probably due to vibrations in the saw during direction changes of the blade head which forced the crystal to oscillate vertically. To correct the problem, the saw would have to be run at about half its current speed, and this would be too slow to be of practical use.

**5.4.4 Summary.** Because of the damage it created in the wafers, the multiblade saw was deemed an unacceptable tool for slicing GaAs crystals, and its use was terminated. Crystals processed after run 30 (Table 15) were sliced with the ID saw. The wafers coming off this saw had a flatness of  $0.021 \pm 0.002$  inch. This was greater than the  $0.0005$  inch variance of the multiblade saw. This variance, however, can be reduced during the lapping and polishing operation. The advantages in using the ID saw, as compared with the multiblade saw, are that it takes less time to slice ingots and there is less subsurface damage.

After slicing and lapping, a polishing process is required to finish the wafers. Simple mechanical polishing was found to induce subsurface damage in the GaAs, while the simple chemical technique yielded substrates not sufficiently flat. A chemomechanical polishing process was therefore developed to minimize the disadvantages of both of these methods.

**5.5 Thin GaAs Substrates - Assessment.** The last column of Table 16 indicates that both 12 and 8 mil substrates were processed. However, yields and causes of breakage differ for the two thicknesses. An assessment of both groups follows.

TABLE 16. SAW AND YIELD DATA

Run No.	Saw used	Wafers cut	Saw damage	Average kerf loss, (in.)	Lapping and polishing damage	Cleaning and mounting damage	Final inspection (cracks, inclusions, handling)	Good (shipped to Hughes) to Hughes)	Good thickness (in.)
11	Multiblade	23	1	0.0005	3	3	—	16	0.012
15	Multiblade	26	1	0.0007	1	2	2	20	0.012
16	Multiblade	26	2	0.0008	2	3	1	18	0.012
23	ID saw	24	3	0.012	—	—	4	17	0.012
30	ID saw	<u>29</u>	—	0.014	—	—	<u>4</u>	<u>25</u>	0.012
		<u>128</u>					<u>11</u> (9 %)	<u>96</u> (75%)	
31	ID saw	24	2	0.014	—	3	8	11	0.008
32	ID saw	25	2	0.013	1	2	17	3	0.008
34	ID saw	<u>24</u>	2	0.014	—	6	<u>4</u>	<u>12</u>	0.008
		<u>73</u>					<u>29</u> (43%)	<u>26</u> (39%)	

TABLE 16. SAW AND YIELD DATA

Run No.	Saw used	Wafers cut	Saw damage	Average kerf loss, (in.)	Lapping and polishing damage	Cleaning and mounting damage	Final inspection (cracks, inclusions, handling)	Good (shipped to Hughes) to Hughes)	Good thickness (in.)
11	Multiblade	23	1	0.0005	3	3	—	16	0.012
15	Multiblade	26	1	0.0007	1	2	2	20	0.012
16	Multiblade	26	2	0.0008	2	3	1	18	0.012
23	ID saw	24	3	0.012	—	—	4	17	0.012
30	ID saw	<u>29</u>	—	0.014	—	—	<u>4</u>	<u>25</u>	0.012
		<u>128</u>					<u>11</u> (9 %)	<u>96</u> (75%)	
31	ID saw	24	2	0.014	—	3	8	11	0.008
32	ID saw	25	2	0.013	1	2	17	3	0.008
34	ID saw	<u>24</u>	2	0.014	—	6	<u>4</u>	<u>12</u>	0.008
		<u>73</u>					<u>29</u> (43%)	<u>26</u> (39%)	

5.5.1 Evaluation of 12 Mil Wafers. Wafers that were sliced on either the ID or multiblade saw were approximately 0.021 inch thick as they came directly off the saw.

The damaged wafers that were lapped and polished down to 0.012 inch (runs 11, 15, 16, 23, and 30) were rejected for various reasons: breakage during sawing, damage during lapping and polishing, breakage during cleaning and mounting, and cracks or inclusions discovered during final inspection.

Of the 121 wafers that were lapped and polished to 12 mils, 96 (75 percent) were acceptable for subsequent LPE growth. Most of the 11 rejected wafers were those with cracks and inclusions. Eight wafers were damaged during cleaning and mounting. Seven wafers were broken on the saw, and six wafers were damaged during lapping and polishing.

5.5.2 Evaluation of 8 Mil Wafers. The wafers that were lapped and polished down to 0.008 inch (runs 31, 32, and 34) had a higher rate of wafer breakage during cleaning and handling operations.

Of the 67 wafers so processed, only 26 (39 percent) were good. More than half of the damage was a result of breakage during the handling of these very thin sections in final inspection. Breakage of 11 others occurred during cleaning and polishing. In addition, six were damaged by the ID saw, and only one was damaged during lapping and polishing. This higher breakage rate can be reduced with modifications in the techniques used for the cleaning and handling.

The conclusion to be drawn from the subcontract with Crystal Specialties is that thinner GaAs substrates (8 mils thick) will require more careful handling than the simple techniques used at present. Using present techniques, however, substrates 12 mils or thicker, with the rectangular geometry, can be routinely produced. With the acquisition of special rectangular cross section quartz (2 by 2 inches), substrates capable of producing four 2 x 2 cm substrates with a minimum of waste can be fabricated by the Bridgman technique for low cost production of spaceworthy solar cells.

5.5.1 Evaluation of 12 Mil Wafers. Wafers that were sliced on either the ID or multiblade saw were approximately 0.021 inch thick as they came directly off the saw.

The damaged wafers that were lapped and polished down to 0.012 inch (runs 11, 15, 16, 23, and 30) were rejected for various reasons: breakage during sawing, damage during lapping and polishing, breakage during cleaning and mounting, and cracks or inclusions discovered during final inspection.

Of the 121 wafers that were lapped and polished to 12 mils, 96 (75 percent) were acceptable for subsequent LPE growth. Most of the 11 rejected wafers were those with cracks and inclusions. Eight wafers were damaged during cleaning and mounting. Seven wafers were broken on the saw, and six wafers were damaged during lapping and polishing.

5.5.2 Evaluation of 8 Mil Wafers. The wafers that were lapped and polished down to 0.008 inch (runs 31, 32, and 34) had a higher rate of wafer breakage during cleaning and handling operations.

Of the 67 wafers so processed, only 26 (39 percent) were good. More than half of the damage was a result of breakage during the handling of these very thin sections in final inspection. Breakage of 11 others occurred during cleaning and polishing. In addition, six were damaged by the ID saw, and only one was damaged during lapping and polishing. This higher breakage rate can be reduced with modifications in the techniques used for the cleaning and handling.

The conclusion to be drawn from the subcontract with Crystal Specialties is that thinner GaAs substrates (8 mils thick) will require more careful handling than the simple techniques used at present. Using present techniques, however, substrates 12 mils or thicker, with the rectangular geometry, can be routinely produced. With the acquisition of special rectangular cross section quartz (2 by 2 inches), substrates capable of producing four 2 x 2 cm substrates with a minimum of waste can be fabricated by the Bridgman technique for low cost production of spaceworthy solar cells.

## 6. TEST RESULTS

The overall HESP II test plan consisted of five individual qualification tests and two special tests. Details of the program are shown in Figure 13. The five major qualification tests are:

- 1) Group A - Contact Welding and Temperature Cycling Test
- 2) Group B - Radiation Resistance Test
- 3) Group C - Contact Integrity After Welding Test
- 4) Group D - High Temperature Vacuum and Humidity Test
- 5) Group E - Electrical Before Glassing and Radiometric Properties Test

The two special tests are:

- 1) Single Cell Thermal Test (Contract Section F4.3.4)
- 2) Cell Module Thermal Test (Contract Section F4.6)

Each of the tests is described in the following sections.

6.1 Group A - Contact Welding and Temperature Cycling Test. The contact welding and temperature cycling test is described in the contract as follows:

Facilities: HAC Solar Panel Lab and Culver City Labs.

Cell Description: Sixteen cells minimum, as required in Figure 1, each complete with cover glass.

Test Description: After initial IV characterization, contact pull tabs shall be welded according to 3.5.4 and subsequently retested electrically to determine whether any damage to the cell resulted. After 1000 temperature cycles from -195°C (+10°C; -1°C) to +100°C (+10°C; -0°C), IV curves again shall be generated and any changes in output noted. Visual and microscopic examinations shall be applied as necessary. Final pull strength tests shall follow 3.5.4.2.

## 6. TEST RESULTS

The overall HESP II test plan consisted of five individual qualification tests and two special tests. Details of the program are shown in Figure 13. The five major qualification tests are:

- 1) Group A - Contact Welding and Temperature Cycling Test
- 2) Group B - Radiation Resistance Test
- 3) Group C - Contact Integrity After Welding Test
- 4) Group D - High Temperature Vacuum and Humidity Test
- 5) Group E - Electrical Before Glassing and Radiometric Properties Test

The two special tests are:

- 1) Single Cell Thermal Test (Contract Section F4.3.4)
- 2) Cell Module Thermal Test (Contract Section F4.6)

Each of the tests is described in the following sections.

6.1 Group A - Contact Welding and Temperature Cycling Test. The contact welding and temperature cycling test is described in the contract as follows:

Facilities: HAC Solar Panel Lab and Culver City Labs.

Cell Description: Sixteen cells minimum, as required in Figure 1, each complete with cover glass.

Test Description: After initial IV characterization, contact pull tabs shall be welded according to 3.5.4 and subsequently retested electrically to determine whether any damage to the cell resulted. After 1000 temperature cycles from -195°C (+10°C; -1°C) to +100°C (+10°C; -0°C), IV curves again shall be generated and any changes in output noted. Visual and microscopic examinations shall be applied as necessary. Final pull strength tests shall follow 3.5.4.2.

00453-13

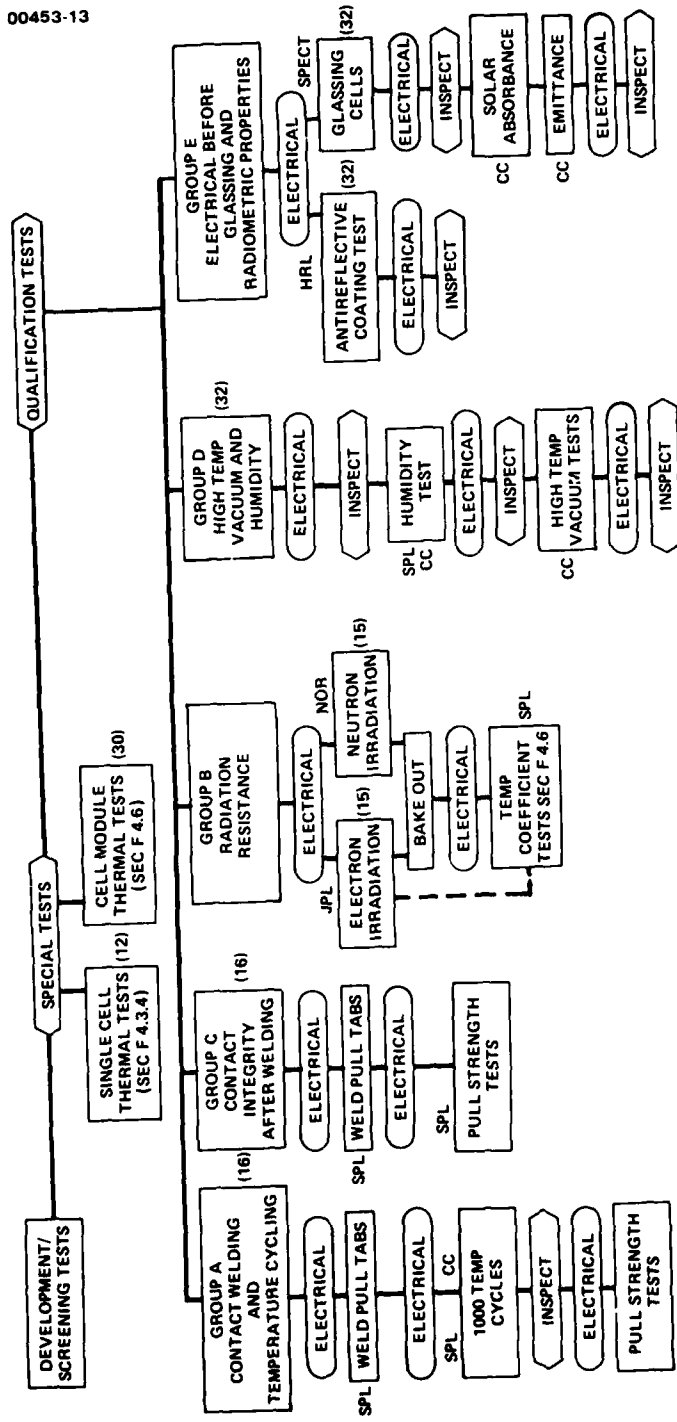


Figure 13. HESP II test plan.

00453-13

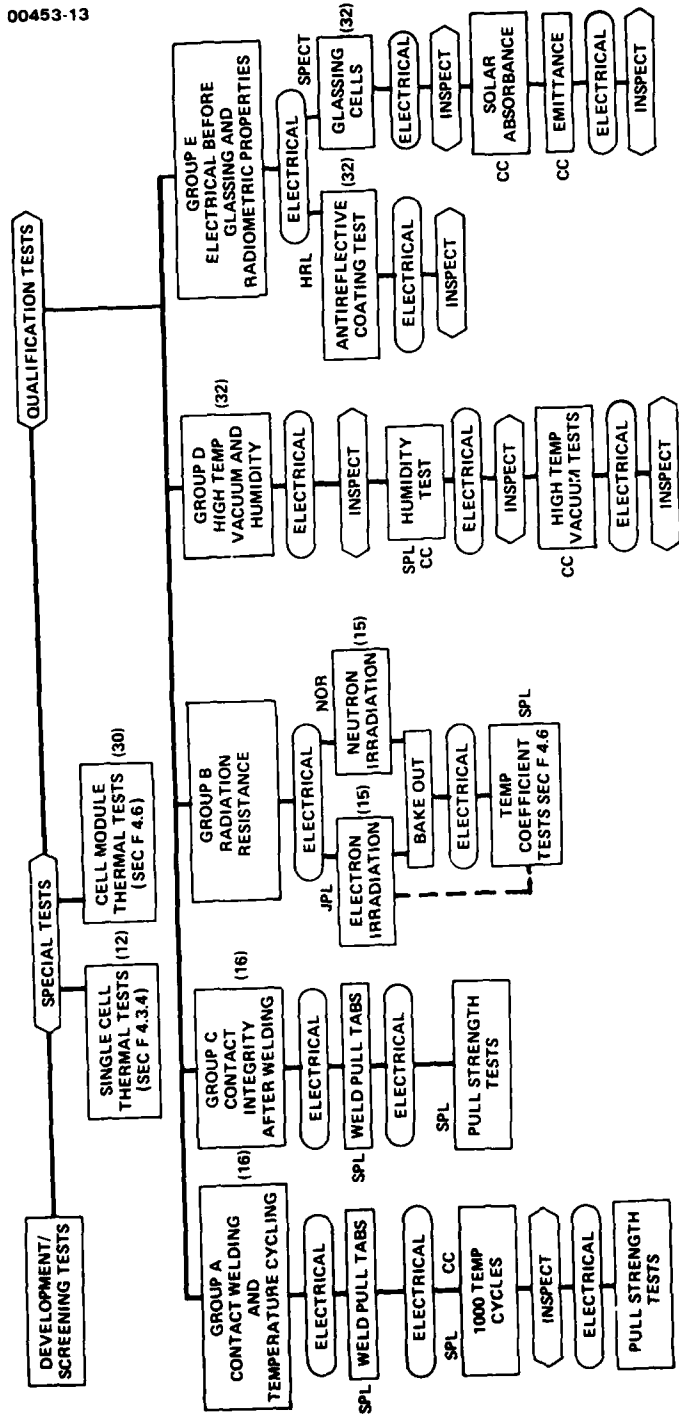


Figure 13. HESP II test plan.

As described in Section 4, two techniques developed by Hughes were considered for the welding task: parallel gap welding and ultrasonic seam welding. Parallel gap welding was chosen as the simpler method overall and was used for the tasks described in both Groups A and C. Table 14 shows typical gap weld results for the front and back cell contacts. In addition to the voltage, machine parameters for pulse duration,  $t$ , force of electrodes,  $F$ , and the gap width,  $G$ , are listed for both front and back contact operations.

The performance of the cells before and after tab welding is reflected in the electrical parameters given in Table 17. It can be seen that performance does not degrade as a result of the welding phase.

Results of the specified 1000 cycle temperature tests are shown in Table 18. Cells were tested through the upper weld tabs and through the back metallization. As Table 18 shows, there was no degradation due to the thermal cycling.

After cycling and the above-described electrical testing, each of the six upper and lower cell tabs was individually pulled. The histograms of the results for front and back surfaces are shown in Figure 14. Here, the number of tabs pulled is plotted against various pull strengths. The pull strength was analyzed statistically and is shown in Table 19.

6.2 Group B – Radiation Resistance Test. In the submitted Qualification Test Plan, the charged particle radiation resistance test is described as follows:

Facilities: Hughes Solar Panel Lab, JPL Dynamatron and Northrop TRIGA Reactor.

Cell Description: Twenty cells minimum shall be required for electron and 15 for neutron irradiation.

Test Description: After IV characterization, cells shall be either electron or neutron irradiated as described in military specification 3.5.5. Annealing at 60°C for 48 hours shall follow, and changes in the electrical output noted. In addition, temperature coefficients shall be determined as described in Section F, paragraph 4.4 of the contract. IV curves taken before, immediately after irradiation, and after annealing, shall be compared.

The radiation resistance tests were performed to observe how the GaAs solar cells degraded after varying levels of neutron and electron irradiation fluences.

6.2.1 Neutron Irradiation Test. Twenty-three cells were selected for the neutron irradiation test and were irradiated to the levels indicated in Table 20. Immediate post-neutron electrical characterization was not

As described in Section 4, two techniques developed by Hughes were considered for the welding task: parallel gap welding and ultrasonic seam welding. Parallel gap welding was chosen as the simpler method overall and was used for the tasks described in both Groups A and C. Table 14 shows typical gap weld results for the front and back cell contacts. In addition to the voltage, machine parameters for pulse duration,  $t$ , force of electrodes,  $F$ , and the gap width,  $G$ , are listed for both front and back contact operations.

The performance of the cells before and after tab welding is reflected in the electrical parameters given in Table 17. It can be seen that performance does not degrade as a result of the welding phase.

Results of the specified 1000 cycle temperature tests are shown in Table 18. Cells were tested through the upper weld tabs and through the back metallization. As Table 18 shows, there was no degradation due to the thermal cycling.

After cycling and the above-described electrical testing, each of the six upper and lower cell tabs was individually pulled. The histograms of the results for front and back surfaces are shown in Figure 14. Here, the number of tabs pulled is plotted against various pull strengths. The pull strength was analyzed statistically and is shown in Table 19.

6.2 Group B – Radiation Resistance Test. In the submitted Qualification Test Plan, the charged particle radiation resistance test is described as follows:

Facilities: Hughes Solar Panel Lab, JPL Dynamatron and Northrop TRIGA Reactor.

Cell Description: Twenty cells minimum shall be required for electron and 15 for neutron irradiation.

Test Description: After IV characterization, cells shall be either electron or neutron irradiated as described in military specification 3.5.5. Annealing at 60°C for 48 hours shall follow, and changes in the electrical output noted. In addition, temperature coefficients shall be determined as described in Section F, paragraph 4.4 of the contract. IV curves taken before, immediately after irradiation, and after annealing, shall be compared.

The radiation resistance tests were performed to observe how the GaAs solar cells degraded after varying levels of neutron and electron irradiation fluences.

6.2.1 Neutron Irradiation Test. Twenty-three cells were selected for the neutron irradiation test and were irradiated to the levels indicated in Table 20. Immediate post-neutron electrical characterization was not

**TABLE 17. CELL PERFORMANCE BEFORE AND AFTER WELDING**  
**(Before Temperature Cycling)**

Cell		I <sub>sc</sub> (mA)	V <sub>oc</sub> (V)	P <sub>max</sub> (mW)	η (%)	FF		Cell	I <sub>sc</sub> (mA)	V <sub>oc</sub> (V)	P <sub>max</sub> (mW)	η (%)	FF	
4219	B*	112	1.0	84.8	15.7	0.76		4443	B	115	0.98	84.0	15.5	0.75
	A*	113	0.99	85.2	15.7	0.76		A	114	0.99	84.0	15.5	0.75	
4222	B	114	1.0	85.7	15.8	0.75		4444	B	117	0.99	84.0	15.5	0.73
	A	114	1.0	85.6	15.8	0.75		A	114	0.99	83.4	15.4	0.74	
4227	B	116	0.99	85.5	15.8	0.74		4447	B	117	0.98	85.0	15.7	0.74
	A	116	0.98	85.1	15.6	0.75		A	116	0.98	84.0	15.5	0.74	
4228	B	114	1.0	84.6	15.6	0.74		4449	B	115	0.98	86.0	15.9	0.75
	A	114	0.99	84.0	15.5	0.74		A	114	0.99	85.7	15.8	0.76	
4254	B	114	0.99	85.0	15.7	0.75		4450	B	115	1.0	86.0	15.9	0.75
	A	111	0.99	82.5	15.2	0.75		A	115	1.0	85.3	15.8	0.74	
4259	B	111	1.0	84.7	15.6	0.76		4464	B	118	0.97	84.5	15.6	0.74
	A	111	1.0	84.1	15.5	0.76		A	115	0.97	82.8	15.3	0.74	
4313	B	113	0.99	86.1	15.9	0.77		4466	B	118	0.98	84.5	15.6	0.73
	A	112	0.99	86.8	16.0	0.78		A	116	0.98	82.8	15.3	0.73	
4325	B	110	0.98	83.8	15.5	0.78		4474	B	114	0.98	84.8	15.7	0.76
	A	110	0.99	85.0	15.7	0.78		A	111	0.98	82.2	15.2	0.76	
4336	B	111	0.98	83.8	15.5	0.78		4475	B	117	0.98	85.3	15.8	0.74
	A	111	0.99	85.5	15.8	0.78		A	114	0.97	81.4	15.0	0.74	
4376	B	114	0.97	84.2	15.6	0.76		4483	B	113	0.99	85.9	15.9	0.77
	A	112	0.98	83.5	15.4	0.76		A	110	0.98	83.4	15.4	0.77	
4382	B	118	0.97	85.3	15.8	0.75		4481	B	113	0.99	85.3	15.8	0.76
	A	116	0.975	84.2	15.6	0.74		A	110	0.98	82.0	15.2	0.76	
4411	B	116	0.98	84.9	15.7	0.75		4538	B	113	0.97	84.0	15.5	0.77
	A	113	0.99	83.8	15.5	0.75		A	113	0.97	83.4	15.4	0.76	
4438	B	113	0.98	83.8	15.5	0.76		4508	B	117	0.98	86.1	15.9	0.75
	A	113	0.98	82.4	15.2	0.74		A	115	0.98	85.1	15.7	0.75	
4441	B	115	0.98	85.1	15.7	0.76		4522	B	116	0.98	85.1	15.7	0.75
	A	115	0.99	84.0	15.5	0.74		A	116	0.98	83.3	15.4	0.73	
4439	B	114	0.98	84.5	15.6	0.76		4558	B	117	0.97	85.9	15.9	0.76
	A	113	0.99	83.6	15.5	0.75		A	115	0.97	84.8	15.7	0.76	

\*B = Before welding.

A = After welding, before glassing.

**TABLE 17. CELL PERFORMANCE BEFORE AND AFTER WELDING**  
**(Before Temperature Cycling)**

Cell		I <sub>sc</sub> (mA)	V <sub>oc</sub> (V)	P <sub>max</sub> (mW)	η (%)	FF	Cell		I <sub>sc</sub> (mA)	V <sub>oc</sub> (V)	P <sub>max</sub> (mW)	η (%)	FF
4219	B*	112	1.0	84.8	15.7	0.76	4443	B	115	0.98	84.0	15.5	0.75
	A*	113	0.99	85.2	15.7	0.76		A	114	0.99	84.0	15.5	0.75
4222	B	114	1.0	85.7	15.8	0.75	4444	B	117	0.99	84.0	15.5	0.73
	A	114	1.0	85.6	15.8	0.75		A	114	0.99	83.4	15.4	0.74
4227	B	116	0.99	85.5	15.8	0.74	4447	B	117	0.98	85.0	15.7	0.74
	A	116	0.98	85.1	15.6	0.75		A	116	0.98	84.0	15.5	0.74
4228	B	114	1.0	84.6	15.6	0.74	4449	B	115	0.98	86.0	15.9	0.75
	A	114	0.99	84.0	15.5	0.74		A	114	0.99	85.7	15.8	0.76
4254	B	114	0.99	85.0	15.7	0.75	4450	B	115	1.0	86.0	15.9	0.75
	A	111	0.99	82.5	15.2	0.75		A	115	1.0	85.3	15.8	0.74
4259	B	111	1.0	84.7	15.6	0.76	4464	B	118	0.97	84.5	15.6	0.74
	A	111	1.0	84.1	15.5	0.76		A	115	0.97	82.8	15.3	0.74
4313	B	113	0.99	86.1	15.9	0.77	4466	B	118	0.98	84.5	15.6	0.73
	A	112	0.99	86.8	16.0	0.78		A	116	0.98	82.8	15.3	0.73
4325	B	110	0.98	83.8	15.5	0.78	4474	B	114	0.98	84.8	15.7	0.76
	A	110	0.99	85.0	15.7	0.78		A	111	0.98	82.2	15.2	0.76
4336	B	111	0.98	83.8	15.5	0.78	4475	B	117	0.98	85.3	15.8	0.74
	A	111	0.99	85.5	15.8	0.78		A	114	0.97	81.4	15.0	0.74
4376	B	114	0.97	84.2	15.6	0.76	4483	B	113	0.99	85.9	15.9	0.77
	A	112	0.98	83.5	15.4	0.76		A	110	0.98	83.4	15.4	0.77
4382	B	118	0.97	85.3	15.8	0.75	4481	B	113	0.99	85.3	15.8	0.76
	A	116	0.975	84.2	15.6	0.74		A	110	0.98	82.0	15.2	0.76
4411	B	116	0.98	84.9	15.7	0.75	4538	B	113	0.97	84.0	15.5	0.77
	A	113	0.99	83.8	15.5	0.75		A	113	0.97	83.4	15.4	0.76
4438	B	113	0.98	83.8	15.5	0.76	4508	B	117	0.98	86.1	15.9	0.75
	A	113	0.98	82.4	15.2	0.74		A	115	0.98	85.1	15.7	0.75
4441	B	115	0.98	85.1	15.7	0.76	4522	B	116	0.98	85.1	15.7	0.75
	A	115	0.99	84.0	15.5	0.74		A	116	0.98	83.3	15.4	0.73
4439	B	114	0.98	84.5	15.6	0.76	4558	B	117	0.97	85.9	15.9	0.76
	A	113	0.99	83.6	15.5	0.75		A	115	0.97	84.8	15.7	0.76

\*B = Before welding.

A = After welding, before glassing.

TABLE 18. CELL PERFORMANCE BEFORE AND AFTER TEMPERATURE CYCLING

Cell		I <sub>sc</sub> (mA)	V <sub>oc</sub> (V)	P <sub>max</sub> (mW)	η (%)	FF	Cell	I <sub>sc</sub> (mA)	V <sub>oc</sub> (V)	P <sub>max</sub> (mW)	η (%)	FF	
4219	B*	117	0.99	88.2	16.3	0.76	4443	B	118	0.98	88.0	16.3	0.76
	A*	115	0.99	86.6	16.0	0.76		A	118	0.99	88.0	16.3	0.75
4222	B	118	1.0	88.6	16.4	0.75	4444	B	118	0.98	86.3	15.9	0.75
	A	116	0.99	87.2	16.1	0.76		A	118	0.99	85.9	15.9	0.74
4227	B	119	0.99	88.3	16.3	0.75	4447	B	120	0.98	86.6	16.0	0.74
	A	117	0.99	87.6	16.2	0.74		A	119	0.98	86.4	16.0	0.74
4228	B	117	0.99	86.6	16.0	0.75	4449	B	120	0.99	90.2	16.7	0.76
	A	117	0.99	86.7	16.0	0.75		A	117	1.00	90.2	16.7	0.77
4254	B	111	0.99	86.6	16.0	0.79	4450	B	119	1.0	89.4	16.5	0.75
	A	114	0.99	85.6	15.8	0.76		A	119	1.0	90.1	16.6	0.76
4259	B	116	1.0	87.2	16.1	0.75	4464	B	121	0.97	86.9	16.1	0.74
	A							A	119	0.97	86.7	16.0	0.75
4313	B	115	0.99	89.0	16.5	0.78	4466	B	120	0.98	85.4	15.8	0.73
	A	115	0.99	89.0	16.5	0.75		A	119	0.98	84.6	15.6	0.73
4325	B	115	0.99	86.1	15.9	0.76	4474	B	116	0.98	86.3	15.9	0.76
	A	113	0.99	86.5	16.0	0.77		A	116	0.98	86.9	16.1	0.76
4336	B	115	0.99	88.8	16.4	0.78	4475	B	121	0.97	85.8	15.9	0.73
	A							A	120	0.97	86.4	16.0	0.74
4376	B	116	0.98	86.4	15.9	0.76	4483	B	116	0.99	87.7	16.2	0.76
	A							A	115	0.99	87.2	16.1	0.77
4382	B	120	0.975	86.9	16.0	0.74	4481	B	116	0.98	85.3	15.8	0.75
	A							A	115	0.98	84.8	15.7	0.75
4411	B	117	0.99	87.1	16.1	0.75	4538	B	117	0.98	85.7	15.8	0.75
	A							A	116	0.98	85.3	15.8	0.75
4438	B	118	0.98	86.4	16.0	0.75	4508	B	120	0.98	88.0	16.3	0.75
	A	116	0.98	85.2	15.7	0.75		A	118	0.98	86.3	15.9	0.75
4441	B	120	0.99	87.2	16.1	0.73	4522	B	119	0.98	86.5	16.0	0.74
	A							A	117	0.98	86.1	15.9	0.75
4439	B	118	0.99	86.9	16.0	0.74	4558	B	119	0.98	87.7	16.2	0.75
	A	118	0.99	87.2	16.1	0.75		A	119	0.98	87.2	16.1	0.75

\*B = After welding, after glassing, before temperature cycling.

A = After temperature cycling.

TABLE 18. CELL PERFORMANCE BEFORE AND AFTER TEMPERATURE CYCLING

Cell		I <sub>sc</sub> (mA)	V <sub>oc</sub> (V)	P <sub>max</sub> (mW)	η (%)	FF	Cell	I <sub>sc</sub> (mA)	V <sub>oc</sub> (V)	P <sub>max</sub> (mW)	η (%)	FF	
4219	B*	117	0.99	88.2	16.3	0.76	4443	B	118	0.98	88.0	16.3	0.76
	A*	115	0.99	86.6	16.0	0.76		A	118	0.99	88.0	16.3	0.75
4222	B	118	1.0	88.6	16.4	0.75	4444	B	118	0.98	86.3	15.9	0.75
	A	116	0.99	87.2	16.1	0.76		A	118	0.99	85.9	15.9	0.74
4227	B	119	0.99	88.3	16.3	0.75	4447	B	120	0.98	86.6	16.0	0.74
	A	117	0.99	87.6	16.2	0.74		A	119	0.98	86.4	16.0	0.74
4228	B	117	0.99	86.6	16.0	0.75	4449	B	120	0.99	90.2	16.7	0.76
	A	117	0.99	86.7	16.0	0.75		A	117	1.00	90.2	16.7	0.77
4254	B	111	0.99	86.6	16.0	0.79	4450	B	119	1.0	89.4	16.5	0.75
	A	114	0.99	85.6	15.8	0.76		A	119	1.0	90.1	16.6	0.76
4259	B	116	1.0	87.2	16.1	0.75	4464	B	121	0.97	86.9	16.1	0.74
	A							A	119	0.97	86.7	16.0	0.75
4313	B	115	0.99	89.0	16.5	0.78	4466	B	120	0.98	85.4	15.8	0.73
	A	115	0.99	89.0	16.5	0.75		A	119	0.98	84.6	15.6	0.73
4325	B	115	0.99	86.1	15.9	0.76	4474	B	116	0.98	86.3	15.9	0.76
	A	113	0.99	86.5	16.0	0.77		A	116	0.98	86.9	16.1	0.76
4336	B	115	0.99	88.8	16.4	0.78	4475	B	121	0.97	85.8	15.9	0.73
	A							A	120	0.97	86.4	16.0	0.74
4376	B	116	0.98	86.4	15.9	0.76	4483	B	116	0.99	87.7	16.2	0.76
	A							A	115	0.99	87.2	16.1	0.77
4382	B	120	0.975	86.9	16.0	0.74	4481	B	116	0.98	85.3	15.8	0.75
	A							A	115	0.98	84.8	15.7	0.75
4411	B	117	0.99	87.1	16.1	0.75	4538	B	117	0.98	85.7	15.8	0.75
	A							A	116	0.98	85.3	15.8	0.75
4438	B	118	0.98	86.4	16.0	0.75	4508	B	120	0.98	88.0	16.3	0.75
	A	116	0.98	85.2	15.7	0.75		A	118	0.98	86.3	15.9	0.75
4441	B	120	0.99	87.2	16.1	0.73	4522	B	119	0.98	86.5	16.0	0.74
	A							A	117	0.98	86.1	15.9	0.75
4439	B	118	0.99	86.9	16.0	0.74	4558	B	119	0.98	87.7	16.2	0.75
	A	118	0.99	87.2	16.1	0.75		A	119	0.98	87.2	16.1	0.75

\*B = After welding, after glassing, before temperature cycling.

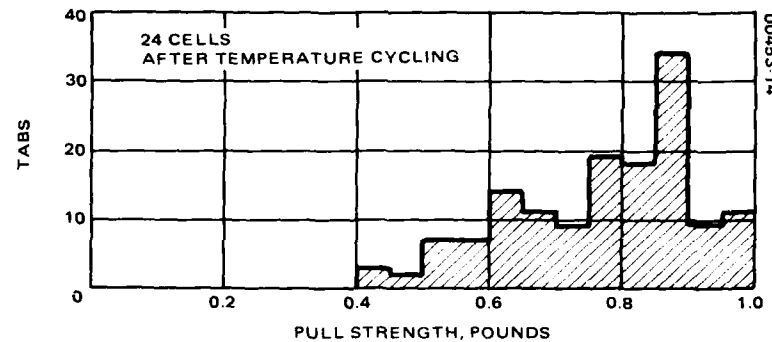
A = After temperature cycling.

TABLE 19. PULL STRENGTH TEST RESULTS FOR GaAs SOLAR CELL TABS  
(24 CELLS) (GAP WELD)

Separation Type	Front Tabs				Back Tabs			
	Strength, lb	Standard Deviation	Occurrences		Strength, lb	Standard Deviation	Occurrences	
			Number	Percent			Number	Percent
Break at weld	0.75	0.14	134	93	0.59	0.12	90	62.5
Partial break at weld	0.55	0	1	1	0.64	0.07	15	10.5
Tab off completely	0.72	0.11	6	4	0.49	0.17	32	22
Tab broke	0.92	0.45	3	2	0	0	0	0
Tab already off	-	-	0	0	-	-	7	5

TABLE 20. NEUTRON IRRADIATION TEST

Number of Cells	1 MeV Equivalent neutrons/cm <sup>2</sup>	Fluence
[6]	[None (control cells)]	
6	$1 \times 10^{11}$	
5	$1 \times 10^{12}$	
6	$1 \times 10^{13}$	



a) Front surface

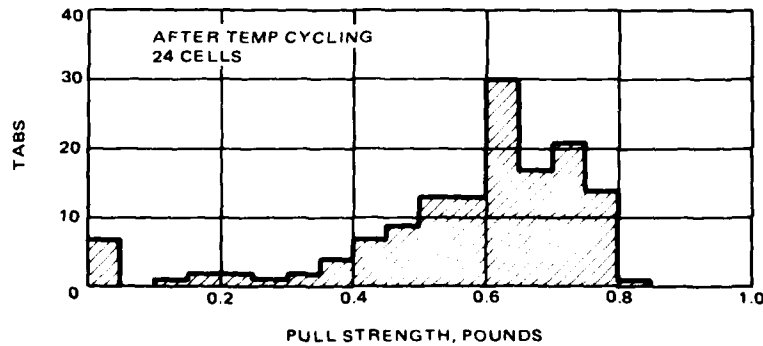


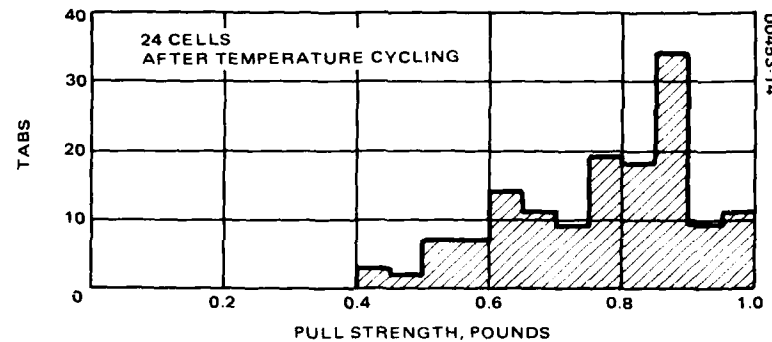
Figure 14. Cell performance histograms

TABLE 19. PULL STRENGTH TEST RESULTS FOR GaAs SOLAR CELL TABS  
(24 CELLS) (GAP WELD)

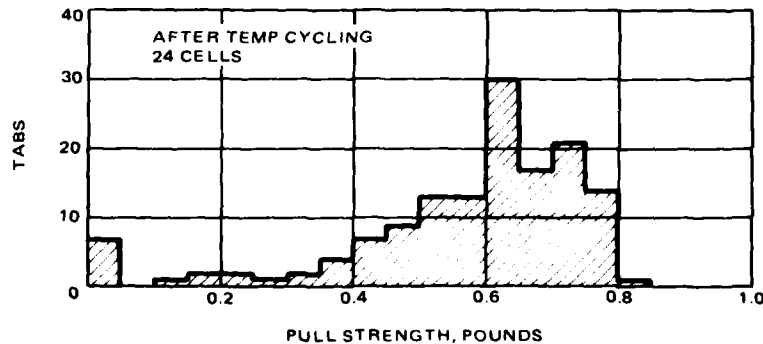
Separation Type	Front Tabs				Back Tabs			
	Strength, lb	Standard Deviation	Occurrences		Strength, lb	Standard Deviation	Occurrences	
			Number	Percent			Number	Percent
Break at weld	0.75	0.14	134	93	0.59	0.12	90	62.5
Partial break at weld	0.55	0	1	1	0.64	0.07	15	10.5
Tab off completely	0.72	0.11	6	4	0.49	0.17	32	22
Tab broke	0.92	0.45	3	2	0	0	0	0
Tab already off	-	-	0	0	-	-	7	5

TABLE 20. NEUTRON IRRADIATION TEST

Number of Cells	1 MeV Equivalent neutrons/cm <sup>2</sup>	Fluence
[6]	[None (control cells)]	
6	$1 \times 10^{11}$	
5	$1 \times 10^{12}$	
6	$1 \times 10^{13}$	



a) Front surface



b) Back surface

Figure 14. Cell performance histograms

possible until the residual radioactivity decreased to levels permitting handling and electrical testing. Cell electrical characterization before and after irradiation are shown in Table 21; the last column shows the power ratio in which the input is divided by output. For convenience, Table 22 compares the different fluences, the contract requirements, and the actual power figures. Values are far above the minimum required. For these results, no annealing step was necessary to relax out damage since the cells had been stored for a full month during radioactive cooldown. The results, shown

TABLE 21. CELL CHARACTERISTICS BEFORE AND AFTER  
NEUTRON IRRADIATION

Cell No.	Energy (MeV)	Fluence (n/cm <sup>2</sup> )	I <sub>sc</sub> (mA)	V <sub>oc</sub> (V)	FF	P <sub>max</sub> (mW)	η (%)	P <sub>i</sub> /P <sub>o</sub>
3482	0	0	115	1.00	0.79	90.3	16.7	—
	1	1 × 10 <sup>11</sup>	115	1.00	0.79	90.3	16.7	100
3505	0	0	116	1.00	0.76	87.9	16.2	—
	1	1 × 10 <sup>11</sup>	116	1.00	0.76	87.9	16.2	100
3512	0	0	115	0.98	0.78	88.2	16.3	—
	1	1 × 10 <sup>11</sup>	115	0.98	0.78	88.2	16.3	100
3513	0	0	115	0.99	0.79	89.9	16.6	—
	1	1 × 10 <sup>11</sup>	115	0.99	0.79	89.9	16.6	100
3520	0	0	112	1.00	0.77	86.7	16.0	—
	1	1 × 10 <sup>11</sup>	112	1.00	0.77	86.7	16.0	100
3521	0	0	115	1.00	0.78	90.1	16.7	—
	1	1 × 10 <sup>11</sup>	115	1.00	0.78	90.1	16.7	100
<hr/>								
3488	0	0	119	1.00	0.76	90.7	16.8	—
	1	1 × 10 <sup>12</sup>	115	0.99	0.78	85.9	15.9	94.7
3492	0	0	117	1.01	0.76	89.6	16.6	—
	1	1 × 10 <sup>12</sup>	116	0.98	0.78	88.1	16.3	98.3
3499	0	0	116	1.00	0.77	89.5	16.5	—
	1	1 × 10 <sup>12</sup>	116	0.98	0.77	88.0	16.2	98.0
3517	0	0	114	0.99	0.77	87.3	16.1	—
	1	1 × 10 <sup>12</sup>	112	0.98	0.78	85.6	15.8	98.0
3523	0	0	113	1.00	0.78	87.7	16.2	—
	1	1 × 10 <sup>12</sup>	111	0.98	0.76	82.2	15.2	94.0
<hr/>								
3485	0	0	120	1.00	0.76	91.0	16.8	—
	1	1 × 10 <sup>13</sup>	109	0.93	0.75	76.4	14.1	84.0
3493	0	0	117	1.00	0.76	88.8	16.4	—
	1	1 × 10 <sup>13</sup>	105	0.93	0.77	74.7	13.8	84.1
3501	0	0	111	0.99	0.78	86.9	16.1	—
	1	1 × 10 <sup>13</sup>	105	0.93	0.77	75.5	13.9	87.0
3503	0	0	116	0.99	0.77	88.6	16.4	—
	1	1 × 10 <sup>13</sup>	105	0.93	0.77	75.5	14.0	85.2
3516	0	0	114	0.99	0.78	88.0	16.3	—
	1	1 × 10 <sup>13</sup>	104	0.93	0.77	74.7	13.8	85.0
3524	0	0	114	1.00	0.78	88.5	16.4	—
	1	1 × 10 <sup>13</sup>	103	0.93	0.78	74.5	13.8	84.0

possible until the residual radioactivity decreased to levels permitting handling and electrical testing. Cell electrical characterization before and after irradiation are shown in Table 21; the last column shows the power ratio in which the input is divided by output. For convenience, Table 22 compares the different fluences, the contract requirements, and the actual power figures. Values are far above the minimum required. For these results, no annealing step was necessary to relax out damage since the cells had been stored for a full month during radioactive cooldown. The results, shown

TABLE 21. CELL CHARACTERISTICS BEFORE AND AFTER  
NEUTRON IRRADIATION

Cell No.	Energy (MeV)	Fluence (n/cm <sup>2</sup> )	I <sub>sc</sub> (mA)	V <sub>oc</sub> (V)	FF	P <sub>max</sub> (mW)	η (%)	P <sub>i</sub> /P <sub>o</sub>
3482	0	0	115	1.00	0.79	90.3	16.7	—
	1	1 × 10 <sup>11</sup>	115	1.00	0.79	90.3	16.7	100
3505	0	0	116	1.00	0.76	87.9	16.2	—
	1	1 × 10 <sup>11</sup>	116	1.00	0.76	87.9	16.2	100
3512	0	0	115	0.98	0.78	88.2	16.3	—
	1	1 × 10 <sup>11</sup>	115	0.98	0.78	88.2	16.3	100
3513	0	0	115	0.99	0.79	89.9	16.6	—
	1	1 × 10 <sup>11</sup>	115	0.99	0.79	89.9	16.6	100
3520	0	0	112	1.00	0.77	86.7	16.0	—
	1	1 × 10 <sup>11</sup>	112	1.00	0.77	86.7	16.0	100
3521	0	0	115	1.00	0.78	90.1	16.7	—
	1	1 × 10 <sup>11</sup>	115	1.00	0.78	90.1	16.7	100
<hr/>								
3488	0	0	119	1.00	0.76	90.7	16.8	—
	1	1 × 10 <sup>12</sup>	115	0.99	0.78	85.9	15.9	94.7
3492	0	0	117	1.01	0.76	89.6	16.6	—
	1	1 × 10 <sup>12</sup>	116	0.98	0.78	88.1	16.3	98.3
3499	0	0	116	1.00	0.77	89.5	16.5	—
	1	1 × 10 <sup>12</sup>	116	0.98	0.77	88.0	16.2	98.0
3517	0	0	114	0.99	0.77	87.3	16.1	—
	1	1 × 10 <sup>12</sup>	112	0.98	0.78	85.6	15.8	98.0
3523	0	0	113	1.00	0.78	87.7	16.2	—
	1	1 × 10 <sup>12</sup>	111	0.98	0.76	82.2	15.2	94.0
<hr/>								
3485	0	0	120	1.00	0.76	91.0	16.8	—
	1	1 × 10 <sup>13</sup>	109	0.93	0.75	76.4	14.1	84.0
3493	0	0	117	1.00	0.76	88.8	16.4	—
	1	1 × 10 <sup>13</sup>	105	0.93	0.77	74.7	13.8	84.1
3501	0	0	111	0.99	0.78	86.9	16.1	—
	1	1 × 10 <sup>13</sup>	105	0.93	0.77	75.5	13.9	87.0
3503	0	0	116	0.99	0.77	88.6	16.4	—
	1	1 × 10 <sup>13</sup>	105	0.93	0.77	75.5	14.0	85.2
3516	0	0	114	0.99	0.78	88.0	16.3	—
	1	1 × 10 <sup>13</sup>	104	0.93	0.77	74.7	13.8	85.0
3524	0	0	114	1.00	0.78	88.5	16.4	—
	1	1 × 10 <sup>13</sup>	103	0.93	0.78	74.5	13.8	84.0

TABLE 22. NEUTRON IRRADIATION  
P<sub>MAX</sub> RESULTS

Fluence (n/cm <sup>2</sup> )	Power Required (mW)	Power Actual* (mW)
1 X 10 <sup>11</sup>	79	88.9
1 X 10 <sup>12</sup>	66	86.9
1 X 10 <sup>13</sup>	50	75.2

\*Average from Table 21.

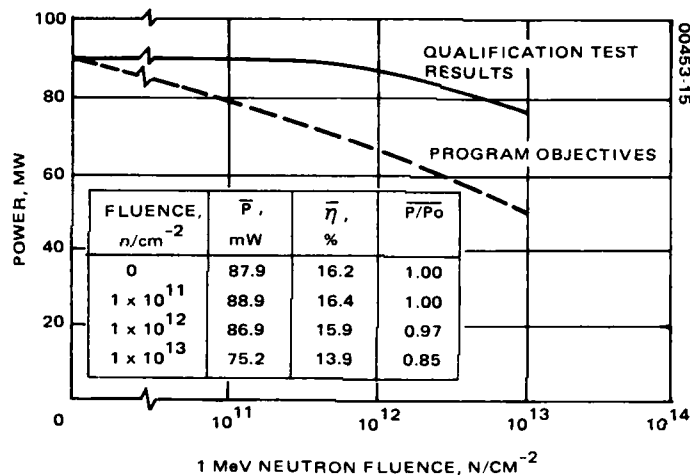


Figure 15. Neutron irradiation test results.

graphically and in tabular form in Figure 15, demonstrate how the actual degraded cell power (solid line) far exceeds that set by the qualification test program (dashed line).

6.2.2 Electron Irradiation Test. Thirty-three GaAs cells were electron irradiated at JPL using the following fluences:

$$3 \times 10^{14} \text{ e/cm}^2$$

$$1 \times 10^{15} \text{ e/cm}^2$$

$$1 \times 10^{16} \text{ e/cm}^2$$

Afterwards, the group was broken into two batches of 18 and 15 cells. The first was stored at room temperature and tested electrically daily. The second, after original current-voltage characterization, underwent bakeout at 60°C for 48 hours. This parallel test was to determine the existence of any relaxation effects.

TABLE 22. NEUTRON IRRADIATION  
 $P_{MAX}$  RESULTS

Fluence (n/cm <sup>2</sup> )	Power Required (mW)	Power Actual* (mW)
$1 \times 10^{11}$	79	88.9
$1 \times 10^{12}$	66	86.9
$1 \times 10^{13}$	50	75.2

\*Average from Table 21.

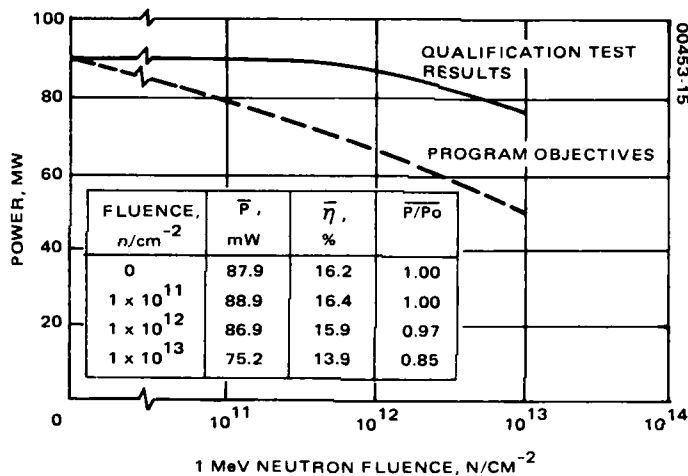


Figure 15. Neutron irradiation test results.

graphically and in tabular form in Figure 15, demonstrate how the actual degraded cell power (solid line) far exceeds that set by the qualification test program (dashed line).

6.2.2 Electron Irradiation Test. Thirty-three GaAs cells were electron irradiated at JPL using the following fluences:

$$3 \times 10^{14} \text{ e/cm}^2$$

$$1 \times 10^{15} \text{ e/cm}^2$$

$$1 \times 10^{16} \text{ e/cm}^2$$

Afterwards, the group was broken into two batches of 18 and 15 cells. The first was stored at room temperature and tested electrically daily. The second, after original current-voltage characterization, underwent bakeout at 60°C for 48 hours. This parallel test was to determine the existence of any relaxation effects.

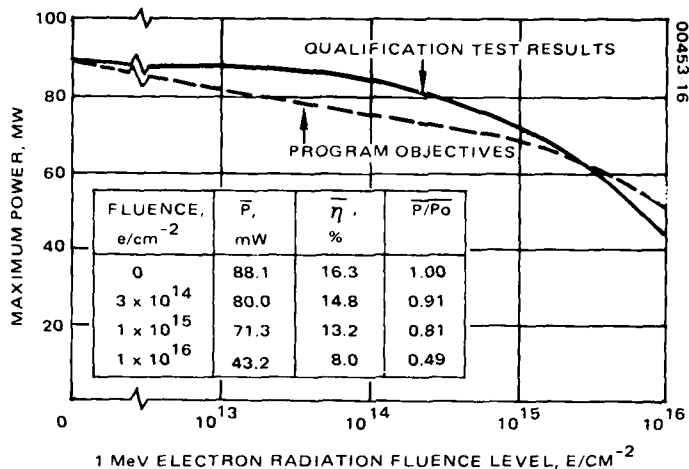


Figure 16. Electron irradiation test results.

The 18 room temperature cells were tested daily for five consecutive days. No significant differences in the average electrical parameters at any of the fluences were noted with respect to the 15 that had undergone bakeout. Results are shown graphically and in tabular form in Figure 16 and Table 23. For  $3 \times 10^{14}$  and  $1 \times 10^{15} e/cm^2$ ,  $P_{max}$  exceeded contract specifications, and for the case  $1 \times 10^{16} e/cm^2$ , the value was slightly below, as shown.

Twenty-five of the electron irradiated cells were then electrically tested for their temperature coefficient characteristics. Great care was taken to ensure proper vacuum and temperature control of the containing test fixture in order to obtain meaningful results. Such control is required because temperature drifts as little as a few degrees in either direction of the specified point can significantly confuse results. Another consideration was the choice of simulators beneath which the test was performed. Since the present temperature coefficient test fixture contained six separate cells, a simulator beaming a large area of light maintained the constant intensity. Thus, all such testing was conducted at the more suitably equipped solar panel laboratory facility. Four major electrical parameters ( $I_{sc}$ ,  $V_{oc}$ ,  $I_{mp}$ ,  $V_{mp}$ ) were measured over a temperature range from  $-60^\circ$  to  $100^\circ C$ . These parameters were averaged according to temperature and radiation level. Figure 17 shows the curves that best interpret the data.

In summary the degraded irradiated cell performance was better than expected except for a slight drop at the extreme  $1 \times 10^{16} e/cm^2$  dosage. This drop can be moved farther out by a reduction in the junction depth to 0.3  $\mu m$ .

**6.3 Group C - Contact Integrity After Weld Test.** The contact integrity after welding test is described in the Qualification Test Plan as follows:

Facilities: HAC Solar Panel Lab

Cell Description: Sixteen cells minimum, as required in Figure 1.

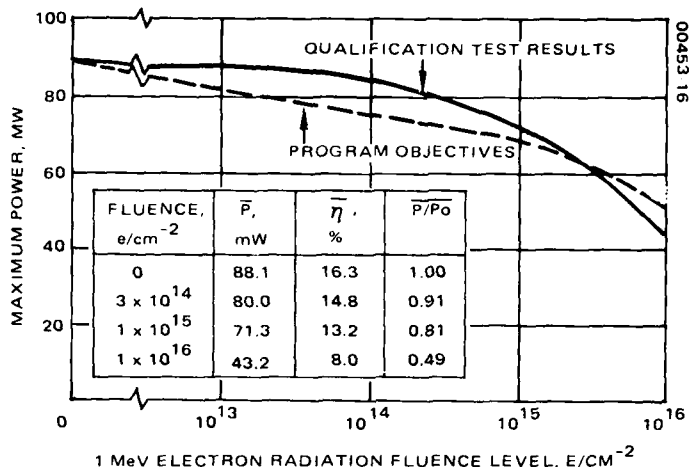


Figure 16. Electron irradiation test results.

The 18 room temperature cells were tested daily for five consecutive days. No significant differences in the average electrical parameters at any of the fluences were noted with respect to the 15 that had undergone bakeout. Results are shown graphically and in tabular form in Figure 16 and Table 23. For  $3 \times 10^{14}$  and  $1 \times 10^{15} e/cm^2$ ,  $P_{max}$  exceeded contract specifications, and for the case  $1 \times 10^{16} e/cm^2$ , the value was slightly below, as shown.

Twenty-five of the electron irradiated cells were then electrically tested for their temperature coefficient characteristics. Great care was taken to ensure proper vacuum and temperature control of the containing test fixture in order to obtain meaningful results. Such control is required because temperature drifts as little as a few degrees in either direction of the specified point can significantly confuse results. Another consideration was the choice of simulators beneath which the test was performed. Since the present temperature coefficient test fixture contained six separate cells, a simulator beaming a large area of light maintained the constant intensity. Thus, all such testing was conducted at the more suitably equipped solar panel laboratory facility. Four major electrical parameters ( $I_{sc}$ ,  $V_{oc}$ ,  $I_{mp}$ ,  $V_{mp}$ ) were measured over a temperature range from  $-60^\circ$  to  $100^\circ C$ . These parameters were averaged according to temperature and radiation level. Figure 17 shows the curves that best interpret the data.

In summary the degraded irradiated cell performance was better than expected except for a slight drop at the extreme  $1 \times 10^{16} e/cm^2$  dosage. This drop can be moved farther out by a reduction in the junction depth to 0.3  $\mu m$ .

**6.3 Group C - Contact Integrity After Weld Test.** The contact integrity after welding test is described in the Qualification Test Plan as follows:

Facilities: HAC Solar Panel Lab

Cell Description: Sixteen cells minimum, as required in Figure 1.

TABLE 23. (AlGa)As-GaAs SOLAR CELL CHARACTERISTICS BEFORE AND AFTER  
1 MeV ELECTRON IRRADIATION (HESP II CELLS)

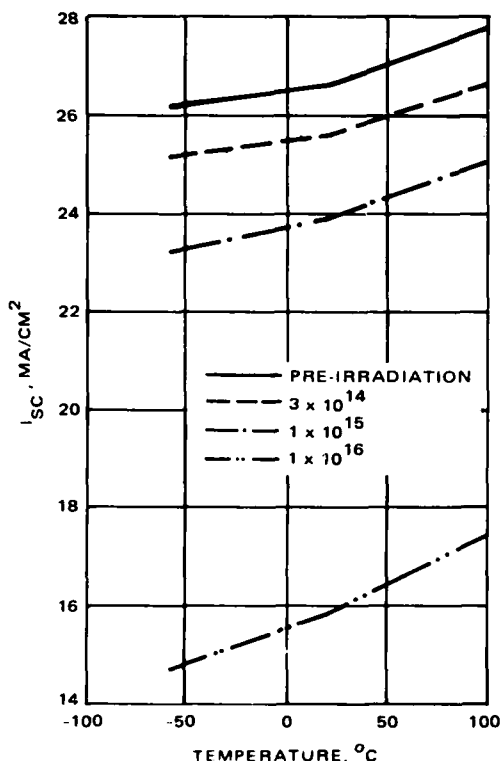
Cell No.	Fluence, e/cm <sup>2</sup>	I <sub>sc</sub> , mA	V <sub>oc</sub> , V	P <sub>m</sub> , mW	FF	$\eta$ Percent
3655	0	113	0.99	87.2	0.78	16.1
	3 x 10 <sup>14</sup>	106	0.94	79.6	0.80	14.7
3638	0	114	0.99	86.5	0.76	16.0
	3 x 10 <sup>14</sup>	108	0.93	79.4	0.79	14.7
3623	0	111	1.0	85.7	0.77	15.8
	3 x 10 <sup>14</sup>	105	0.94	78.4	0.80	14.5
3794	0	116	1.0	91.4	0.79	16.9
	3 x 10 <sup>14</sup>	108	0.94	81.2	0.80	15.0
3704*	0	114	0.99	86.1	0.76	15.9
	3 x 10 <sup>14</sup>	106	0.94	79.4	0.80	14.7
3643*	0	117	1.0	90.5	0.77	16.7
	3 x 10 <sup>14</sup>	108	0.94	81.8	0.81	15.1
3635	0	118	1.0	89.9	0.755	16.6
	3 x 10 <sup>14</sup>	109	0.94	80.4	0.785	15.0
3644	0	116	1.0	90.3	0.77	16.7
	1 x 10 <sup>15</sup>	95	0.91	69.6	0.81	12.9
3697	0	116	1.0	88.8	0.77	16.4
	1 x 10 <sup>15</sup>	100	0.91	72.7	0.80	13.4
3682	0	112	0.99	86.3	0.77	16.0
	1 x 10 <sup>15</sup>	97	0.91	70.2	0.80	13.0
3631	0	118	0.99	89.4	0.77	16.5
	1 x 10 <sup>15</sup>	100	0.91	72.7	0.80	13.4
3698*	0	116	1.0	89	0.77	16.4
	1 x 10 <sup>15</sup>	99	0.91	72	0.80	13.3
3627*	0	114	1.0	87.6	0.77	16.2
	1 x 10 <sup>15</sup>	98	0.91	70.7	0.79	13.1
3625*	0	112	1.0	86.5	0.77	16.6
	1 x 10 <sup>15</sup>	97	0.91	71.5	0.81	13.2
3612	0	114	1.0	85.8	0.75	15.9
	1 x 10 <sup>16</sup>	65	0.83	40.1	0.76	7.4
3696	0	116	0.99	86.4	0.75	16.0
	1 x 10 <sup>16</sup>	70	0.83	44	0.75	8.1
3634	0	116	1.0	88.6	0.76	16.4
	1 x 10 <sup>16</sup>	66	0.83	42.1	0.77	7.8
3797	0	117	1.0	92.4	0.79	17.0
	1 x 10 <sup>16</sup>	72	0.83	46.8	0.78	8.6
3633	0	118	1.0	90.2	0.76	16.7
	1 x 10 <sup>16</sup>	67	0.83	43.2	0.78	8.0
3732	0	114	0.99	85.1	0.75	15.7
	1 x 10 <sup>16</sup>	69	0.83	44.5	0.78	8.2
3695*	0	116	1.0	89.5	0.77	16.5
	1 x 10 <sup>16</sup>	69	0.83	44.7	0.78	8.3
3636*	0	115	1.0	86.7	0.75	16.0
	1 x 10 <sup>16</sup>	65	0.83	41.4	0.77	7.6
3700*	0	113	1.0	85.7	0.77	15.8
	1 x 10 <sup>16</sup>	67	0.83	41.9	0.75	7.7

\*Cells that were baked out

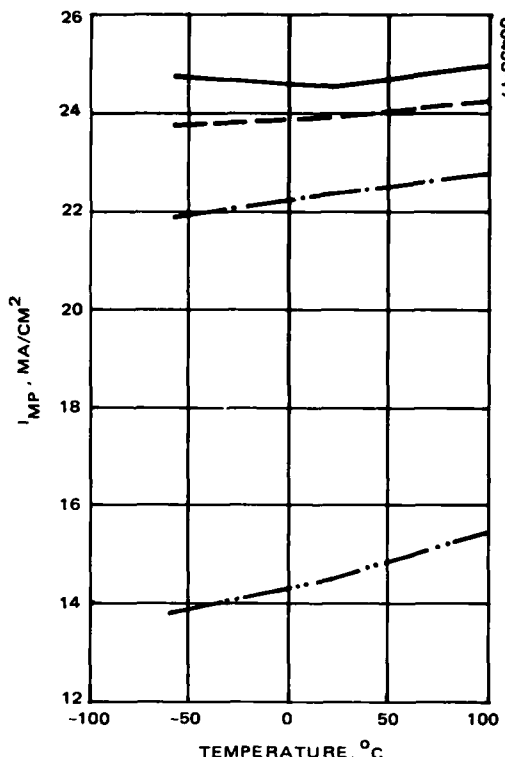
TABLE 23. (AlGa)As-GaAs SOLAR CELL CHARACTERISTICS BEFORE AND AFTER  
1 MeV ELECTRON IRRADIATION (HESP II CELLS)

Cell No.	Fluence, e/cm <sup>2</sup>	I <sub>sc</sub> , mA	V <sub>oc</sub> , V	P <sub>m</sub> , mW	FF	$\eta$ Percent
3655	0	113	0.99	87.2	0.78	16.1
	3 x 10 <sup>14</sup>	106	0.94	79.6	0.80	14.7
3638	0	114	0.99	86.5	0.76	16.0
	3 x 10 <sup>14</sup>	108	0.93	79.4	0.79	14.7
3623	0	111	1.0	85.7	0.77	15.8
	3 x 10 <sup>14</sup>	105	0.94	78.4	0.80	14.5
3794	0	116	1.0	91.4	0.79	16.9
	3 x 10 <sup>14</sup>	108	0.94	81.2	0.80	15.0
3704*	0	114	0.99	86.1	0.76	15.9
	3 x 10 <sup>14</sup>	106	0.94	79.4	0.80	14.7
3643*	0	117	1.0	90.5	0.77	16.7
	3 x 10 <sup>14</sup>	108	0.94	81.8	0.81	15.1
3635	0	118	1.0	89.9	0.755	16.6
	3 x 10 <sup>14</sup>	109	0.94	80.4	0.785	15.0
3644	0	116	1.0	90.3	0.77	16.7
	1 x 10 <sup>15</sup>	95	0.91	69.6	0.81	12.9
3697	0	116	1.0	88.8	0.77	16.4
	1 x 10 <sup>15</sup>	100	0.91	72.7	0.80	13.4
3682	0	112	0.99	86.3	0.77	16.0
	1 x 10 <sup>15</sup>	97	0.91	70.2	0.80	13.0
3631	0	118	0.99	89.4	0.77	16.5
	1 x 10 <sup>15</sup>	100	0.91	72.7	0.80	13.4
3698*	0	116	1.0	89	0.77	16.4
	1 x 10 <sup>15</sup>	99	0.91	72	0.80	13.3
3627*	0	114	1.0	87.6	0.77	16.2
	1 x 10 <sup>15</sup>	98	0.91	70.7	0.79	13.1
3625*	0	112	1.0	86.5	0.77	16.6
	1 x 10 <sup>15</sup>	97	0.91	71.5	0.81	13.2
3612	0	114	1.0	85.8	0.75	15.9
	1 x 10 <sup>16</sup>	65	0.83	40.1	0.76	7.4
3696	0	116	0.99	86.4	0.75	16.0
	1 x 10 <sup>16</sup>	70	0.83	44	0.75	8.1
3634	0	116	1.0	88.6	0.76	16.4
	1 x 10 <sup>16</sup>	66	0.83	42.1	0.77	7.8
3797	0	117	1.0	92.4	0.79	17.0
	1 x 10 <sup>16</sup>	72	0.83	46.8	0.78	8.6
3633	0	118	1.0	90.2	0.76	16.7
	1 x 10 <sup>16</sup>	67	0.83	43.2	0.78	8.0
3732	0	114	0.99	85.1	0.75	15.7
	1 x 10 <sup>16</sup>	69	0.83	44.5	0.78	8.2
3695*	0	116	1.0	89.5	0.77	16.5
	1 x 10 <sup>16</sup>	69	0.83	44.7	0.78	8.3
3636*	0	115	1.0	86.7	0.75	16.0
	1 x 10 <sup>16</sup>	65	0.83	41.4	0.77	7.6
3700*	0	113	1.0	85.7	0.77	15.8
	1 x 10 <sup>16</sup>	67	0.83	41.9	0.75	7.7

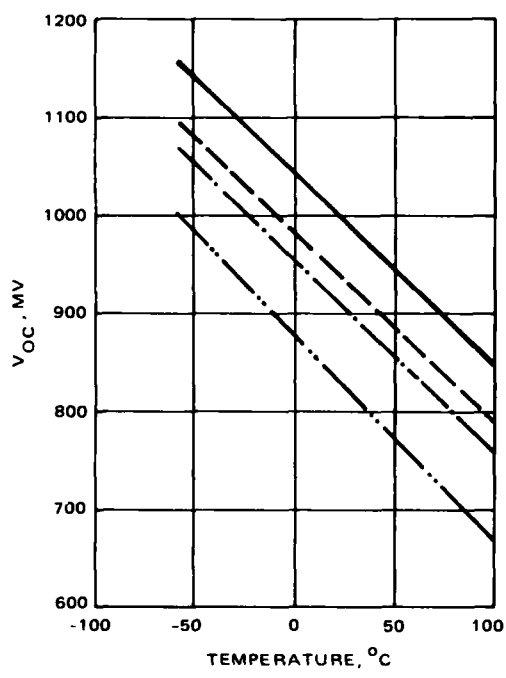
\*Cells that were baked out



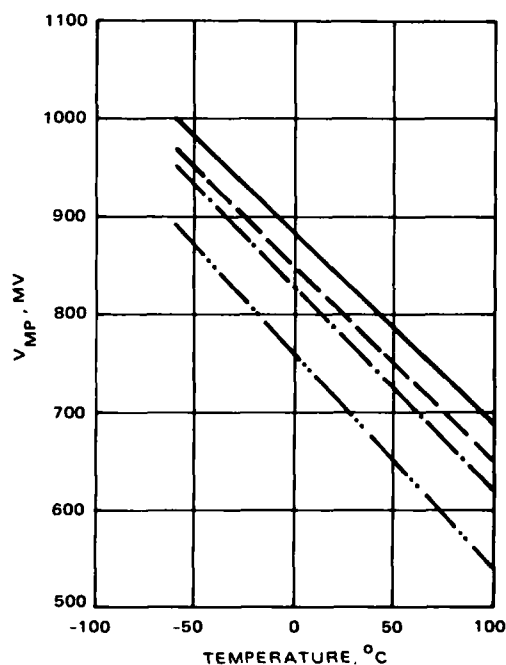
a) For  $I_{SC}$



c) For  $I_{MP}$

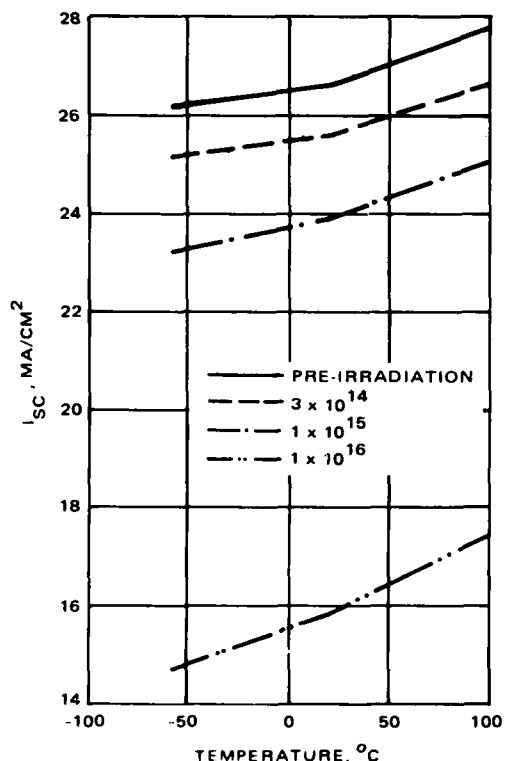


b) For  $V_{OC}$

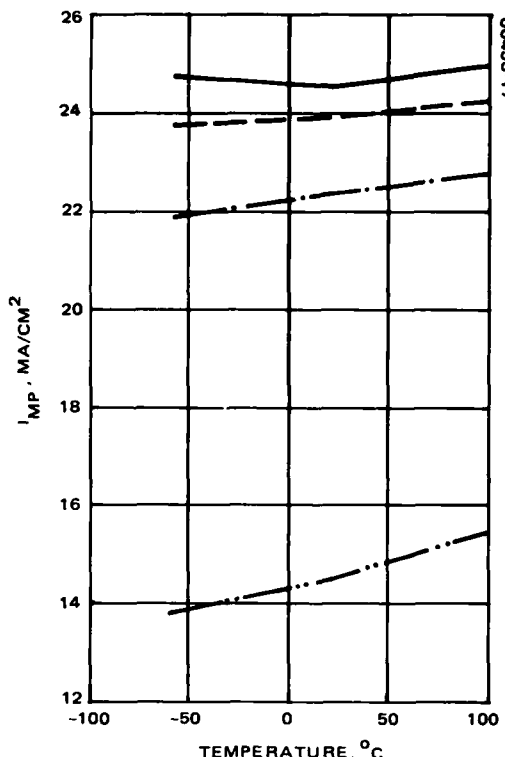


d) For  $V_{MP}$

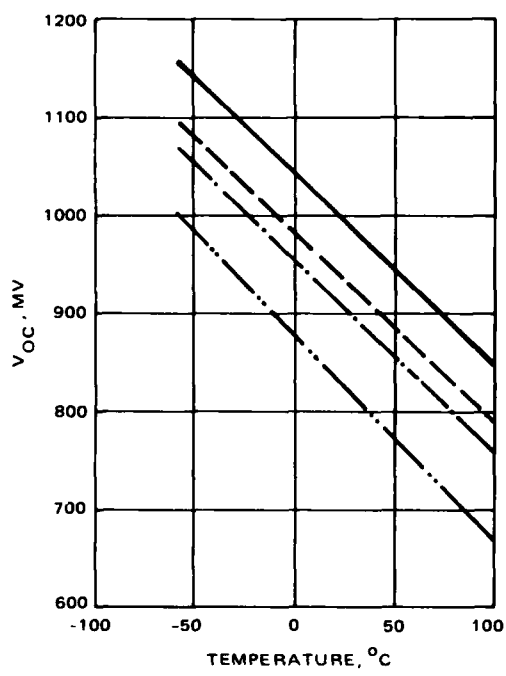
Figure 17. Temperature coefficient curves.



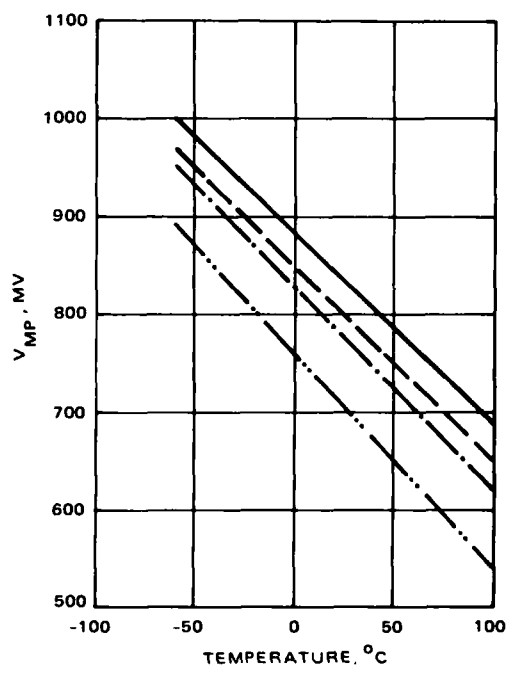
a) For  $I_{SC}$



c) For  $I_{MP}$



b) For  $V_{OC}$



d) For  $V_{MP}$

Figure 17. Temperature coefficient curves.

**Test Description:** IV curves shall be prepared for tested cells before and after welding contacts according to 3.4.5.7. Pull strength shall then be recorded as required in 3.4.5.7.1.

This test was performed to demonstrate the feasibility of the selected tab welding technique. Since we had better control over parallel gap welding than ultrasonic welding, we proceeded with the gap welder and the digitated test tab. The before and after weld cell parameters, given in Table 24, show that the parameters do not degrade after welding.

TABLE 24. GaAs SOLAR CELL ELECTRICAL CHARACTERISTICS BEFORE AND AFTER WELDING

Cell No.		I <sub>sc</sub> (mA)	V <sub>oc</sub> (V)	P <sub>max</sub> (mW)	FF	η (%)
4065	P*	111.5	1.05	84.2	0.72	15.6
	B*	114.0	1.10	88.8	0.71	16.4
	A*	115.0	1.04	89.3	0.75	16.5
4100	P	110.5	1.00	82.0	0.74	15.2
	B	116.0	1.00	88.4	0.76	16.3
	A	117.0	1.00	88.7	0.76	16.4
4112	P	112.0	0.99	81.2	0.73	15.0
	B	118.0	1.00	88.2	0.75	16.3
	A	119.0	1.00	88.6	0.75	16.4
4117	P	115.0	0.99	84.5	0.74	15.6
	B	117.0	0.99	87.5	0.76	16.2
	A	118.0	0.99	86.7	0.74	16.0
4128	P	114.0	0.98	81.6	0.73	15.1
	B	115.5	0.98	83.4	0.74	15.4
	A	117.0	0.98	84.2	0.73	15.6
4135	P**					
	B	117.0	1.00	88.4	0.76	16.3
	A	118.0	1.00	88.6	0.75	16.4
4136	P	114.0	1.00	88.0	0.77	16.3
	B	117.0	1.00	90.8	0.78	16.8
	A	117.0	1.05	91.4	0.74	16.9
4141	P**					
	B	113.5	0.98	83.8	0.75	15.5
	A	114.0	0.99	84.5	0.75	15.6
4143	P	115.5	1.01	86.7	0.75	16.0
	B	116.0	1.00	87.7	0.76	16.2
	A	117.0	1.00	88.8	0.76	16.4
4146	P	114.0	0.99	81.6	0.72	15.1
	B	113.5	0.99	82.4	0.74	15.2
	A	115.0	0.98	82.0	0.73	15.2
4149	P	118.0	0.98	83.2	0.72	15.4
	B	118.0	0.98	84.2	0.73	15.6
	A	120.0	0.98	84.8	0.72	15.7

\*P = before glassing; B = before welding;

A = after welding.

\*\* = data missing.

**Test Description:** IV curves shall be prepared for tested cells before and after welding contacts according to 3.4.5.7. Pull strength shall then be recorded as required in 3.4.5.7.1.

This test was performed to demonstrate the feasibility of the selected tab welding technique. Since we had better control over parallel gap welding than ultrasonic welding, we proceeded with the gap welder and the digitated test tab. The before and after weld cell parameters, given in Table 24, show that the parameters do not degrade after welding.

TABLE 24. GaAs SOLAR CELL ELECTRICAL CHARACTERISTICS BEFORE AND AFTER WELDING

Cell No.		I <sub>sc</sub> (mA)	V <sub>oc</sub> (V)	P <sub>max</sub> (mW)	FF	η (%)
4065	P*	111.5	1.05	84.2	0.72	15.6
	B*	114.0	1.10	88.8	0.71	16.4
	A*	115.0	1.04	89.3	0.75	16.5
4100	P	110.5	1.00	82.0	0.74	15.2
	B	116.0	1.00	88.4	0.76	16.3
	A	117.0	1.00	88.7	0.76	16.4
4112	P	112.0	0.99	81.2	0.73	15.0
	B	118.0	1.00	88.2	0.75	16.3
	A	119.0	1.00	88.6	0.75	16.4
4117	P	115.0	0.99	84.5	0.74	15.6
	B	117.0	0.99	87.5	0.76	16.2
	A	118.0	0.99	86.7	0.74	16.0
4128	P	114.0	0.98	81.6	0.73	15.1
	B	115.5	0.98	83.4	0.74	15.4
	A	117.0	0.98	84.2	0.73	15.6
4135	P**					
	B	117.0	1.00	88.4	0.76	16.3
	A	118.0	1.00	88.6	0.75	16.4
4136	P	114.0	1.00	88.0	0.77	16.3
	B	117.0	1.00	90.8	0.78	16.8
	A	117.0	1.05	91.4	0.74	16.9
4141	P**					
	B	113.5	0.98	83.8	0.75	15.5
	A	114.0	0.99	84.5	0.75	15.6
4143	P	115.5	1.01	86.7	0.75	16.0
	B	116.0	1.00	87.7	0.76	16.2
	A	117.0	1.00	88.8	0.76	16.4
4146	P	114.0	0.99	81.6	0.72	15.1
	B	113.5	0.99	82.4	0.74	15.2
	A	115.0	0.98	82.0	0.73	15.2
4149	P	118.0	0.98	83.2	0.72	15.4
	B	118.0	0.98	84.2	0.73	15.6
	A	120.0	0.98	84.8	0.72	15.7

\*P = before glassing; B = before welding;

A = after welding.

\*\* = data missing.

Following this electrical characterization, the pull strength test was performed on the individual GaAs solar cell tabs. Test data were taken for 17 cells, each having 12 tabs (6 front, 6 back), and were statistically treated. Table 25 shows the results of the analysis. The results of front and back

Following this electrical characterization, the pull strength test was performed on the individual GaAs solar cell tabs. Test data were taken for 17 cells, each having 12 tabs (6 front, 6 back), and were statistically treated. Table 25 shows the results of the analysis. The results of front and back tabs are compared. The first column identifies the manner in which the tab separated from the solar cell. The next three columns for each contact list the average pull strength, the standard deviation, and the number and percentage occurrence of each particular separation. Pull strengths averaged 0.77 pound per individual tab. The total strength of the entire interconnect (6 tabs) is obviously much more.

Pull strength histograms for the front and back tabs are shown in Figure 18. This figure shows the number of occurrences in each pull strength range. As can be seen, the distributions reveal reasonable concentrations around average values. With additional refinement and experience, GaAs cells should be routinely weldable for panel construction.

**6.4 Group D – High Temperature Vacuum and Humidity Test.** The high temperature vacuum and humidity test is described in the Qualification Test Plan as follows:

**Facilities:** Hughes Solar Panel Lab and Culver City Labs.

**Cell Description:** Thirty-two cells minimum, as required, each complete with cover glass.

**Test Description:** Cells shall be inspected and electrically tested before and after humidity and high temperature vacuum treatments outlined in military specifications 3.5.3 and 3.5.2. Final visual or microscopic examination shall be performed as necessary. Physical and electrical output changes shall be recorded.

The humidity portion of this test lasted 30 days. Thirty-five GaAs cells were placed in a closed chamber being maintained at a minimum temperature of 45°C and a relative humidity of at least 90 percent. The cells were arranged and

TABLE 25. PULL STRENGTH TEST RESULTS FOR GaAs SOLAR CELL TABS (17 CELLS) (GAP WELD)

Separation Type*	Front Tabs				Back Tabs			
	Strength (lbs)	Standard Deviation	Occurrences		Strength (lbs)	Standard Deviation	Occurrences	
			No.	%			No.	%
BAW	0.87	0.16	102	100	0.69	0.12	72	70.6
BAWX	–	–	0	0	0.68	0.12	17	16.6
TO	–	–	0	0	0.54	0.11	13	12.7

\*BAW = Break at weld

BAWX = Partial break at weld

TO = Tab off completely

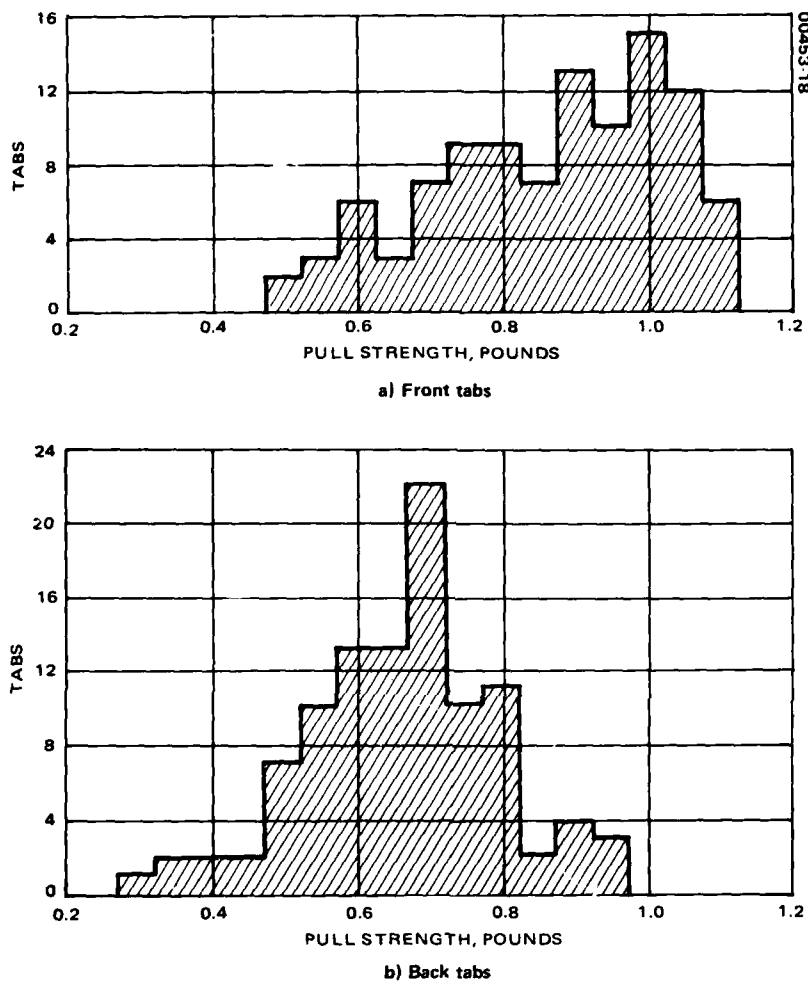


Figure 18. Pull strength histograms.

shielded to avoid direct dripping of condensate onto the test item surfaces. Meanwhile, temperature and humidity were continually monitored using 24 hour circular charts. In addition, cells were visually examined for oxide growth, spotting, or any other obvious cosmetic defects at least once daily; no such degradation was detected. After 30 days, the cells were further inspected and electrically examined to determine the effects, if any, on initial power and efficiency. Table 26 gives electrical results; no electrical degradation of any parameter resulted from the humidity test. In addition, no cosmetic changes were noted during visual inspection.

The high temperature test involved cells at  $1 \times 10^{-5}$  Torr (maximum) and 120°C maintained for 168 hours. This test was conducted in series with

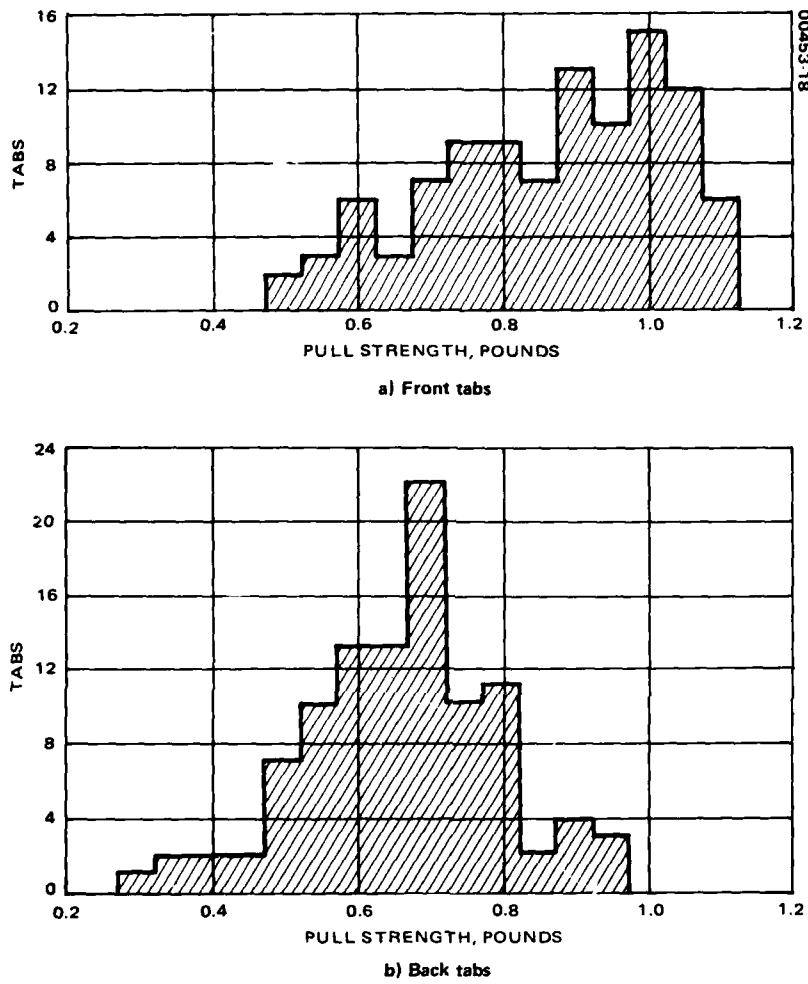


Figure 18. Pull strength histograms.

shielded to avoid direct dripping of condensate onto the test item surfaces. Meanwhile, temperature and humidity were continually monitored using 24 hour circular charts. In addition, cells were visually examined for oxide growth, spotting, or any other obvious cosmetic defects at least once daily; no such degradation was detected. After 30 days, the cells were further inspected and electrically examined to determine the effects, if any, on initial power and efficiency. Table 26 gives electrical results; no electrical degradation of any parameter resulted from the humidity test. In addition, no cosmetic changes were noted during visual inspection.

The high temperature test involved cells at  $1 \times 10^{-5}$  Torr (maximum) and 120°C maintained for 168 hours. This test was conducted in series with

TABLE 26. CELL ELECTRICAL CHARACTERISTICS BEFORE AND AFTER HUMIDITY TEST

Cell No.		I <sub>sc</sub> (mA)	V <sub>oc</sub> (V)	FF	P <sub>max</sub> (mW)	η (%)		Cell No.	I <sub>sc</sub> (mA)	V <sub>oc</sub> (V)	FF	P <sub>max</sub> (mW)	η (%)	
3550	B*	115	1.01	0.79	89.40	16.5		3586	B	118	1.00	0.76	89.60	16.6
	A*	115	1.01	0.79	89.40	16.5		A	118	1.00	0.76	89.60	16.6	
3551	B	117	1.00	0.76	89.50	16.5		3587	B	117	1.00	0.77	89.90	16.6
	A	117	1.00	0.76	89.50	16.5		A	117	1.00	0.77	89.90	16.6	
3554	B	117	1.00	0.76	89.50	16.5		3597	B	114	1.00	0.77	88.00	16.3
	A	117	1.00	0.76	89.50	16.5		A	114	1.00	0.77	88.00	16.3	
3559	B	116	1.00	0.77	89.90	16.6		3598	B	112	1.01	0.77	87.00	16.1
	A	116	1.00	0.77	89.90	16.6		A	112	1.01	0.77	87.00	16.1	
3560	B	115	1.00	0.78	89.30	16.5		3599	B	112	1.00	0.78	87.00	16.1
	A	115	1.00	0.78	89.30	16.5		A	112	1.00	0.78	87.00	16.1	
3561	B	115	0.99	0.78	88.60	16.4		3602	B	113	1.00	0.78	88.00	16.4
	A	115	0.99	0.78	88.60	16.4		A	113	1.00	0.78	88.00	16.4	
3563	B	114	1.00	0.78	88.80	16.3		3605	B	115	1.00	0.76	87.20	16.1
	A	114	1.00	0.78	88.80	16.3		A	115	1.00	0.76	87.20	16.1	
3564	B	114	1.01	0.78	89.50	16.5		3607	B	114	1.00	0.77	87.60	16.2
	A	114	1.01	0.78	89.50	16.5		A	114	1.00	0.77	87.60	16.2	
3573	B	116	1.00	0.76	87.98	16.3		3606	B	114	1.01	0.78	89.44	16.5
	A	116	1.00	0.76	87.98	16.3		A	114	1.01	0.78	89.44	16.5	
3574	B	113	1.01	0.78	88.80	16.4		3610	B	114	1.00	0.77	88.20	16.3
	A	113	1.01	0.78	88.80	16.4		A	114	1.00	0.77	88.20	16.3	
3575	B	116	1.01	0.77	89.64	16.6		3611	B	116	1.00	0.78	89.90	16.6
	A	116	1.01	0.77	89.64	16.6		A	116	1.00	0.78	89.90	16.6	
3577	B	116	1.01	0.76	89.00	16.5		3613	B	116	1.00	0.78	90.10	16.7
	A	116	1.01	0.76	89.00	16.5		A	116	1.00	0.78	90.10	16.7	
3579	B	116	1.00	0.77	88.80	16.4		3614	B	112	1.00	0.774	86.70	16.1
	A	116	1.00	0.77	88.80	16.4		A	112	1.00	0.774	86.70	16.1	
3580	B	115	1.01	0.75	87.36	16.1		3617	B	113	1.00	0.78	88.20	16.3
	A	115	1.01	0.75	87.36	16.1		A	113	1.00	0.78	88.20	16.3	
3582	B	116	1.00	0.78	90.00	16.6		3618	B	113	1.00	0.78	88.00	16.3
	A	116	1.00	0.78	90.00	16.6		A	113	1.00	0.78	88.00	16.3	
3583	B	116	1.00	0.77	89.00	16.5		3619	B	115	1.00	0.77	88.60	16.4
	A	116	1.00	0.77	89.00	16.5		A	115	1.00	0.77	88.60	16.4	

\*B = Before humidity test.

A = After humidity test.

the special RFP test 4.3.4., requiring similar vacuum for cells raised to 400°C and 260°C and maintained for 100 seconds and 16 hours, respectively. The full listing of results for all three temperatures is shown under the RFP test in Table 30. However, for clarity, data for the 120°C test alone was reduced and is presented separately as Table 27. As shown, there was no degradation in cell output as a result of the test. Visual inspection showed no changes whatsoever in cell appearance.

TABLE 26. CELL ELECTRICAL CHARACTERISTICS BEFORE AND AFTER HUMIDITY TEST

Cell No.		I <sub>sc</sub> (mA)	V <sub>oc</sub> (V)	FF	P <sub>max</sub> (mW)	η (%)		Cell No.	I <sub>sc</sub> (mA)	V <sub>oc</sub> (V)	FF	P <sub>max</sub> (mW)	η (%)	
3550	B*	115	1.01	0.79	89.40	16.5		3586	B	118	1.00	0.76	89.60	16.6
	A*	115	1.01	0.79	89.40	16.5		A	118	1.00	0.76	89.60	16.6	
3551	B	117	1.00	0.76	89.50	16.5		3587	B	117	1.00	0.77	89.90	16.6
	A	117	1.00	0.76	89.50	16.5		A	117	1.00	0.77	89.90	16.6	
3554	B	117	1.00	0.76	89.50	16.5		3597	B	114	1.00	0.77	88.00	16.3
	A	117	1.00	0.76	89.50	16.5		A	114	1.00	0.77	88.00	16.3	
3559	B	116	1.00	0.77	89.90	16.6		3598	B	112	1.01	0.77	87.00	16.1
	A	116	1.00	0.77	89.90	16.6		A	112	1.01	0.77	87.00	16.1	
3560	B	115	1.00	0.78	89.30	16.5		3599	B	112	1.00	0.78	87.00	16.1
	A	115	1.00	0.78	89.30	16.5		A	112	1.00	0.78	87.00	16.1	
3561	B	115	0.99	0.78	88.60	16.4		3602	B	113	1.00	0.78	88.00	16.4
	A	115	0.99	0.78	88.60	16.4		A	113	1.00	0.78	88.00	16.4	
3563	B	114	1.00	0.78	88.80	16.3		3605	B	115	1.00	0.76	87.20	16.1
	A	114	1.00	0.78	88.80	16.3		A	115	1.00	0.76	87.20	16.1	
3564	B	114	1.01	0.78	89.50	16.5		3607	B	114	1.00	0.77	87.60	16.2
	A	114	1.01	0.78	89.50	16.5		A	114	1.00	0.77	87.60	16.2	
3573	B	116	1.00	0.76	87.98	16.3		3606	B	114	1.01	0.78	89.44	16.5
	A	116	1.00	0.76	87.98	16.3		A	114	1.01	0.78	89.44	16.5	
3574	B	113	1.01	0.78	88.80	16.4		3610	B	114	1.00	0.77	88.20	16.3
	A	113	1.01	0.78	88.80	16.4		A	114	1.00	0.77	88.20	16.3	
3575	B	116	1.01	0.77	89.64	16.6		3611	B	116	1.00	0.78	89.90	16.6
	A	116	1.01	0.77	89.64	16.6		A	116	1.00	0.78	89.90	16.6	
3577	B	116	1.01	0.76	89.00	16.5		3613	B	116	1.00	0.78	90.10	16.7
	A	116	1.01	0.76	89.00	16.5		A	116	1.00	0.78	90.10	16.7	
3579	B	116	1.00	0.77	88.80	16.4		3614	B	112	1.00	0.774	86.70	16.1
	A	116	1.00	0.77	88.80	16.4		A	112	1.00	0.774	86.70	16.1	
3580	B	115	1.01	0.75	87.36	16.1		3617	B	113	1.00	0.78	88.20	16.3
	A	115	1.01	0.75	87.36	16.1		A	113	1.00	0.78	88.20	16.3	
3582	B	116	1.00	0.78	90.00	16.6		3618	B	113	1.00	0.78	88.00	16.3
	A	116	1.00	0.78	90.00	16.6		A	113	1.00	0.78	88.00	16.3	
3583	B	116	1.00	0.77	89.00	16.5		3619	B	115	1.00	0.77	88.60	16.4
	A	116	1.00	0.77	89.00	16.5		A	115	1.00	0.77	88.60	16.4	

\*B = Before humidity test.

A = After humidity test.

the special RFP test 4.3.4., requiring similar vacuum for cells raised to 400°C and 260°C and maintained for 100 seconds and 16 hours, respectively. The full listing of results for all three temperatures is shown under the RFP test in Table 30. However, for clarity, data for the 120°C test alone was reduced and is presented separately as Table 27. As shown, there was no degradation in cell output as a result of the test. Visual inspection showed no changes whatsoever in cell appearance.

TABLE 27. CELL ELECTRICAL  
CHARACTERISTICS BEFORE  
AND AFTER 120°C HIGH  
TEMPERATURE AT  
VACUUM TEST

Cell No.		$I_{sc}$ (mA)	$V_{oc}$ (V)	FF	$P_{max}$ (mW)	$\eta$ (%)
3660	B *	114	0.99	0.78	88.2	16.3
	A *	115	0.99	0.79	90.1	16.7
3664	B	113	0.99	0.78	87.6	16.2
	A	114	1.00	0.79	88.8	16.4
3665	B	112	0.99	0.77	85.5	15.8
	A	114	0.99	0.77	87.6	16.2
3666	B	113	0.99	0.77	86.3	16.0
	A	113	0.99	0.78	87.2	16.1
3667	B	110	1.00	0.79	86.0	15.9
	A	113	1.00	0.79	88.8	16.4
3668	B	111	0.99	0.79	87.1	16.1
	A	114	0.99	0.80	90.1	16.7
3669	B	112	0.99	0.78	86.7	16.0
	A	115	0.99	0.79	89.6	16.6
3671	B	112	0.99	0.78	86.7	16.0
	A	113	0.99	0.78	86.9	16.1
3672	B	114	0.99	0.77	87.2	16.1
	A	115	0.99	0.78	88.4	16.3
3673	B	118	0.99	0.76	89.0	16.4
	A	118	0.99	0.76	89.3	16.5
3674	B	117	0.99	0.78	90.7	16.8
	A	116	0.99	0.79	90.8	16.8
3675	B	117	1.00	0.77	90.5	16.7
	A	115	1.00	0.77	89.0	16.4
3676	B	115	0.99	0.78	88.8	16.4
	A	115	0.99	0.78	88.8	16.4
3677	B	112	0.99	0.78	86.7	16.0
	A	112	0.99	0.78	86.9	16.0
3683	B	114	0.99	0.77	86.5	16.0
	A	115	0.99	0.77	87.1	16.1

\*B = Before 120°C high temperature at vacuum test.  
A = After 120°C high temperature at vacuum test.

TABLE 27. CELL ELECTRICAL  
CHARACTERISTICS BEFORE  
AND AFTER 120°C HIGH  
TEMPERATURE AT  
VACUUM TEST

Cell No.		$I_{sc}$ (mA)	$V_{oc}$ (V)	FF	$P_{max}$ (mW)	$\eta$ (%)
3660	B *	114	0.99	0.78	88.2	16.3
	A *	115	0.99	0.79	90.1	16.7
3664	B	113	0.99	0.78	87.6	16.2
	A	114	1.00	0.79	88.8	16.4
3665	B	112	0.99	0.77	85.5	15.8
	A	114	0.99	0.77	87.6	16.2
3666	B	113	0.99	0.77	86.3	16.0
	A	113	0.99	0.78	87.2	16.1
3667	B	110	1.00	0.79	86.0	15.9
	A	113	1.00	0.79	88.8	16.4
3668	B	111	0.99	0.79	87.1	16.1
	A	114	0.99	0.80	90.1	16.7
3669	B	112	0.99	0.78	86.7	16.0
	A	115	0.99	0.79	89.6	16.6
3671	B	112	0.99	0.78	86.7	16.0
	A	113	0.99	0.78	86.9	16.1
3672	B	114	0.99	0.77	87.2	16.1
	A	115	0.99	0.78	88.4	16.3
3673	B	118	0.99	0.76	89.0	16.4
	A	118	0.99	0.76	89.3	16.5
3674	B	117	0.99	0.78	90.7	16.8
	A	116	0.99	0.79	90.8	16.8
3675	B	117	1.00	0.77	90.5	16.7
	A	115	1.00	0.77	89.0	16.4
3676	B	115	0.99	0.78	88.8	16.4
	A	115	0.99	0.78	88.8	16.4
3677	B	112	0.99	0.78	86.7	16.0
	A	112	0.99	0.78	86.9	16.0
3683	B	114	0.99	0.77	86.5	16.0
	A	115	0.99	0.77	87.1	16.1

\*B = Before 120°C high temperature at vacuum test.  
A = After 120°C high temperature at vacuum test.

6.5 Group E – Electrical Output Before Glassing and Radiometric Properties Test. The submitted qualification test plan describes the electrical output before glassing and radiometric properties test as follows:

Facilities: Hughes Research Labs, Spectrolab, Hughes Solar Panel Lab and Culver City Labs.

Cell Description: Thirty-two cells (minimum) shall be required for the antireflective coating test and thirty-two for the glassing test.

Test Description: IV characteristics shall be taken before and after the application of the antireflection coating and changes in output noted. The same shall be done with respect to the application of cover glasses as outlined in military specification 3.4.4. In accordance with military specification 3.3.6, the average radiometric properties of the cells shall be determined.

The purpose of this task was to observe how the performance of the GaAs solar cells varied at the specified stages of fabrication. Thirty-five cells were electrically tested three separate times:

- 1) Before applying the antireflection coating (and glasses)
- 2) After applying the antireflection coatings (but before glassing)
- 3) After applying both the antireflection coatings and glasses

Complete results for each cell with respect to short circuit current, open circuit voltage, maximum power, fill factor, and ultimate efficiency are included in Table 28. As can be seen, fill factors remained basically the same while electrical output increased with each process (average final efficiency is 16.4 percent).

Typical results, using cell 3586 as an example, are shown in Figure 19.

Absorptance and emittance tests were performed at the Culver City facility. The absorptance test is nondestructive, but emittance characterization always entails breakage of cells owing to the size of the sample holder in the optical equipment used. As a result, the final electrical and inspection tasks could not be performed on the latter group. Were it not for the size of the sample holder, these tests would be nondestructive.

Twelve cells were tested for solar absorptance and emittance. Results are shown in Table 29. In addition, the reflectance spectrum of all cells was monitored from the visible to infrared regions (5 to 26  $\mu\text{m}$ ). Since the resulting curves looked similar in all cases, only that of cell 3465 is included in Figure 20. These results show excellent cell characteristics after the final fabrication stage.

6.5 Group E – Electrical Output Before Glassing and Radiometric Properties Test. The submitted qualification test plan describes the electrical output before glassing and radiometric properties test as follows:

Facilities: Hughes Research Labs, Spectrolab, Hughes Solar Panel Lab and Culver City Labs.

Cell Description: Thirty-two cells (minimum) shall be required for the antireflective coating test and thirty-two for the glassing test.

Test Description: IV characteristics shall be taken before and after the application of the antireflection coating and changes in output noted. The same shall be done with respect to the application of cover glasses as outlined in military specification 3.4.4. In accordance with military specification 3.3.6, the average radiometric properties of the cells shall be determined.

The purpose of this task was to observe how the performance of the GaAs solar cells varied at the specified stages of fabrication. Thirty-five cells were electrically tested three separate times:

- 1) Before applying the antireflection coating (and glasses)
- 2) After applying the antireflection coatings (but before glassing)
- 3) After applying both the antireflection coatings and glasses

Complete results for each cell with respect to short circuit current, open circuit voltage, maximum power, fill factor, and ultimate efficiency are included in Table 28. As can be seen, fill factors remained basically the same while electrical output increased with each process (average final efficiency is 16.4 percent).

Typical results, using cell 3586 as an example, are shown in Figure 19.

Absorptance and emittance tests were performed at the Culver City facility. The absorptance test is nondestructive, but emittance characterization always entails breakage of cells owing to the size of the sample holder in the optical equipment used. As a result, the final electrical and inspection tasks could not be performed on the latter group. Were it not for the size of the sample holder, these tests would be nondestructive.

Twelve cells were tested for solar absorptance and emittance. Results are shown in Table 29. In addition, the reflectance spectrum of all cells was monitored from the visible to infrared regions (5 to 26  $\mu\text{m}$ ). Since the resulting curves looked similar in all cases, only that of cell 3465 is included in Figure 20. These results show excellent cell characteristics after the final fabrication stage.

TABLE 28. EFFECTS OF ANTIREFLECTION COATING AND GLASSING  
ON CELL ELECTRICAL CHARACTERISTICS

Cell No.		$I_{sc}$ (mA)	$V_{oc}$ (V)	$P_{max}$ (mW)	FF	$\eta$ (%)	Cell No.		$I_{sc}$ (mA)	$V_{oc}$ (V)	$P_{max}$ (mW)	FF	$\eta$ (%)
3550	A*	86	0.99	67.3	0.79	12.4	3586	A	87	0.99	65.5	0.76	12.1
	B*	112	1.00	88.5	0.79	16.3		B	115	1.00	87.4	0.76	16.2
	C*	115	1.01	89.4	0.79	16.5		C	118	1.00	89.6	0.76	16.6
3551	A	88	0.99	66.2	0.76	12.2	3587	A	89	0.99	67.8	0.77	12.5
	B	113	1.00	86.0	0.76	15.9		B	113	1.00	87.0	0.77	16.1
	C	117	1.00	89.5	0.76	16.5		C	117	1.00	89.9	0.77	16.6
3554	A	89	0.99	67.0	0.76	12.4	3591	A	84	0.99	65.7	0.79	12.1
	B	113	1.00	86.0	0.76	15.9		B	109	1.00	86.1	0.79	15.9
	C	117	1.00	89.5	0.76	16.5		C	112	1.00	89.0	0.79	16.4
3559	A	89	0.99	67.5	0.77	12.5	3597	A	85	0.99	64.8	0.77	12.0
	B	112	1.00	86.2	0.77	15.9		B	109	1.00	83.9	0.77	15.5
	C	116	1.00	89.9	0.77	16.6		C	114	1.00	88.0	0.77	16.3
3560	A	88	0.99	68.0	0.78	12.6	3598	A	84	0.99	64.0	0.77	11.8
	B	112	1.00	87.4	0.78	16.1		B	107	1.00	82.4	0.77	15.2
	C	115	1.00	89.3	0.78	16.5		C	112	1.01	87.0	0.77	16.1
3561	A	86	0.98	65.7	0.78	12.1	3599	A	83	0.98	63.4	0.78	11.7
	B	111	0.99	85.7	0.78	15.8		B	108	1.00	84.2	0.78	15.6
	C	115	0.99	88.6	0.78	16.4		C	112	1.00	87.0	0.78	16.1
3563	A	85	0.99	65.6	0.78	12.1	3602	A	83	0.99	64.1	0.78	11.8
	B	111	1.00	86.6	0.78	16.0		B	110	1.00	85.8	0.78	15.9
	C	114	1.00	88.8	0.78	16.3		C	113	1.00	88.0	0.78	16.4
3564	A	86	0.99	66.4	0.78	12.3	3605	A	86	0.99	64.7	0.76	12.0
	B	111	1.00	86.6	0.78	16.0		B	113	1.00	85.9	0.76	15.9
	C	114	1.01	89.5	0.78	16.5		C	115	1.00	87.2	0.76	16.1
3567	A	87	0.99	67.2	0.78	12.4	3607	A	86	0.99	65.6	0.77	12.1
	B	113	1.00	88.1	0.78	16.3		B	114	1.00	65.6	0.77	12.1
	C	116	1.00	90.3	0.78	16.7		C	114	1.00	87.6	0.77	16.2
3572	A	86	0.99	65.6	0.77	12.1	3609	A	85	0.99	65.6	0.78	12.1
	B	110	1.00	84.7	0.77	15.7		B	109	1.00	85.0	0.78	15.7
	C	114	1.00	88.0	0.77	16.5		C	114	1.01	89.4	0.78	16.5
3573	A	88	0.98	65.5	0.76	12.1	3610	A	86	0.99	65.6	0.77	12.1
	B	112	0.99	84.3	0.76	15.6		B	114	1.00	65.6	0.77	12.1
	C	116	1.00	88.0	0.76	16.3		C	114	1.00	87.6	0.77	16.3
3574	A	84	0.99	64.9	0.78	12.0	3611	A	87	0.99	67.2	0.78	12.4
	B	111	1.00	86.6	0.78	16.0		B	113	1.00	88.2	0.78	16.3
	C	113	1.01	88.8	0.78	16.4		C	116	1.00	89.9	0.78	16.6
3575	A	87	0.99	66.3	0.77	12.3	3613	A	87	1.00	67.9	0.78	12.5
	B	114	1.00	87.8	0.77	16.2		B	113	1.00	88.1	0.78	16.3
	C	116	1.01	90.0	0.77	16.6		C	116	1.00	90.1	0.78	16.7
3577	A	87	0.99	65.5	0.76	12.1	3614	A	85	1.00	65.5	0.77	12.1
	B	114	1.00	86.7	0.76	16.0		B	107	1.00	82.4	0.77	15.2
	C	116	1.01	89.0	0.76	16.5		C	112	1.00	86.7	0.77	16.1
3579	A	86	0.99	65.6	0.77	12.1	3617	A	84	0.99	64.9	0.78	12.0
	B	113	1.00	87.0	0.77	16.1		B	109	1.00	85.0	0.78	15.7
	C	116	1.00	88.8	0.77	16.4		C	113	1.00	88.2	0.78	16.3
3580	A	85	0.98	62.5	0.75	11.5	3618	A	84	0.99	64.9	0.78	12.0
	B	112	1.00	84.0	0.75	15.5		B	110	1.00	85.8	0.78	15.9
	C	115	1.01	87.4	0.75	16.1		C	113	1.00	88.0	0.78	16.3
3582	A	86	0.99	66.4	0.78	12.3	3619	A	85	0.99	64.8	0.77	12.0
	B	112	1.00	87.4	0.78	16.1		B	111	1.00	85.5	0.77	15.8
	C	116	1.00	90.0	0.78	16.6		C	115	1.00	88.0	0.77	16.4
3583	A	87	0.99	66.3	0.77	12.3							
	B	112	1.00	86.2	0.77	15.9							
	C	116	1.00	89.0	0.77	16.5							

\*A = Characteristics without antireflection coating or glass.

B = Characteristics with antireflection coating but without glass.

C = Characteristics with both antireflection coating and glass.

TABLE 28. EFFECTS OF ANTIREFLECTION COATING AND GLASSING  
ON CELL ELECTRICAL CHARACTERISTICS

Cell No.		$I_{sc}$ (mA)	$V_{oc}$ (V)	$P_{max}$ (mW)	FF	$\eta$ (%)	Cell No.		$I_{sc}$ (mA)	$V_{oc}$ (V)	$P_{max}$ (mW)	FF	$\eta$ (%)
3550	A*	86	0.99	67.3	0.79	12.4	3586	A	87	0.99	65.5	0.76	12.1
	B*	112	1.00	88.5	0.79	16.3		B	115	1.00	87.4	0.76	16.2
	C*	115	1.01	89.4	0.79	16.5		C	118	1.00	89.6	0.76	16.6
3551	A	88	0.99	66.2	0.76	12.2	3587	A	89	0.99	67.8	0.77	12.5
	B	113	1.00	86.0	0.76	15.9		B	113	1.00	87.0	0.77	16.1
	C	117	1.00	89.5	0.76	16.5		C	117	1.00	89.9	0.77	16.6
3554	A	89	0.99	67.0	0.76	12.4	3591	A	84	0.99	65.7	0.79	12.1
	B	113	1.00	86.0	0.76	15.9		B	109	1.00	86.1	0.79	15.9
	C	117	1.00	89.5	0.76	16.5		C	112	1.00	89.0	0.79	16.4
3559	A	89	0.99	67.5	0.77	12.5	3597	A	85	0.99	64.8	0.77	12.0
	B	112	1.00	86.2	0.77	15.9		B	109	1.00	83.9	0.77	15.5
	C	116	1.00	89.9	0.77	16.6		C	114	1.00	88.0	0.77	16.3
3560	A	88	0.99	68.0	0.78	12.6	3598	A	84	0.99	64.0	0.77	11.8
	B	112	1.00	87.4	0.78	16.1		B	107	1.00	82.4	0.77	15.2
	C	115	1.00	89.3	0.78	16.5		C	112	1.01	87.0	0.77	16.1
3561	A	86	0.98	65.7	0.78	12.1	3599	A	83	0.98	63.4	0.78	11.7
	B	111	0.99	85.7	0.78	15.8		B	108	1.00	84.2	0.78	15.6
	C	115	0.99	88.6	0.78	16.4		C	112	1.00	87.0	0.78	16.1
3563	A	85	0.99	65.6	0.78	12.1	3602	A	83	0.99	64.1	0.78	11.8
	B	111	1.00	86.6	0.78	16.0		B	110	1.00	85.8	0.78	15.9
	C	114	1.00	88.8	0.78	16.3		C	113	1.00	88.0	0.78	16.4
3564	A	86	0.99	66.4	0.78	12.3	3605	A	86	0.99	64.7	0.76	12.0
	B	111	1.00	86.6	0.78	16.0		B	113	1.00	85.9	0.76	15.9
	C	114	1.01	89.5	0.78	16.5		C	115	1.00	87.2	0.76	16.1
3567	A	87	0.99	67.2	0.78	12.4	3607	A	86	0.99	65.6	0.77	12.1
	B	113	1.00	88.1	0.78	16.3		B	114	1.00	65.6	0.77	12.1
	C	116	1.00	90.3	0.78	16.7		C	114	1.00	87.6	0.77	16.2
3572	A	86	0.99	65.6	0.77	12.1	3609	A	85	0.99	65.6	0.78	12.1
	B	110	1.00	84.7	0.77	15.7		B	109	1.00	85.0	0.78	15.7
	C	114	1.00	88.0	0.77	16.5		C	114	1.01	89.4	0.78	16.5
3573	A	88	0.98	65.5	0.76	12.1	3610	A	86	0.99	65.6	0.77	12.1
	B	112	0.99	84.3	0.76	15.6		B	114	1.00	65.6	0.77	12.1
	C	116	1.00	88.0	0.76	16.3		C	114	1.00	87.6	0.77	16.3
3574	A	84	0.99	64.9	0.78	12.0	3611	A	87	0.99	67.2	0.78	12.4
	B	111	1.00	86.6	0.78	16.0		B	113	1.00	88.2	0.78	16.3
	C	113	1.01	88.8	0.78	16.4		C	116	1.00	89.9	0.78	16.6
3575	A	87	0.99	66.3	0.77	12.3	3613	A	87	1.00	67.9	0.78	12.5
	B	114	1.00	87.8	0.77	16.2		B	113	1.00	88.1	0.78	16.3
	C	116	1.01	90.0	0.77	16.6		C	116	1.00	90.1	0.78	16.7
3577	A	87	0.99	65.5	0.76	12.1	3614	A	85	1.00	65.5	0.77	12.1
	B	114	1.00	86.7	0.76	16.0		B	107	1.00	82.4	0.77	15.2
	C	116	1.01	89.0	0.76	16.5		C	112	1.00	86.7	0.77	16.1
3579	A	86	0.99	65.6	0.77	12.1	3617	A	84	0.99	64.9	0.78	12.0
	B	113	1.00	87.0	0.77	16.1		B	109	1.00	85.0	0.78	15.7
	C	116	1.00	88.8	0.77	16.4		C	113	1.00	88.2	0.78	16.3
3580	A	85	0.98	62.5	0.75	11.5	3618	A	84	0.99	64.9	0.78	12.0
	B	112	1.00	84.0	0.75	15.5		B	110	1.00	85.8	0.78	15.9
	C	115	1.01	87.4	0.75	16.1		C	113	1.00	88.0	0.78	16.3
3582	A	86	0.99	66.4	0.78	12.3	3619	A	85	0.99	64.8	0.77	12.0
	B	112	1.00	87.4	0.78	16.1		B	111	1.00	85.5	0.77	15.8
	C	116	1.00	90.0	0.78	16.6		C	115	1.00	88.0	0.77	16.4
3583	A	87	0.99	66.3	0.77	12.3							
	B	112	1.00	86.2	0.77	15.9							
	C	116	1.00	89.0	0.77	16.5							

\*A = Characteristics without antireflection coating or glass.

B = Characteristics with antireflection coating but without glass.

C = Characteristics with both antireflection coating and glass.

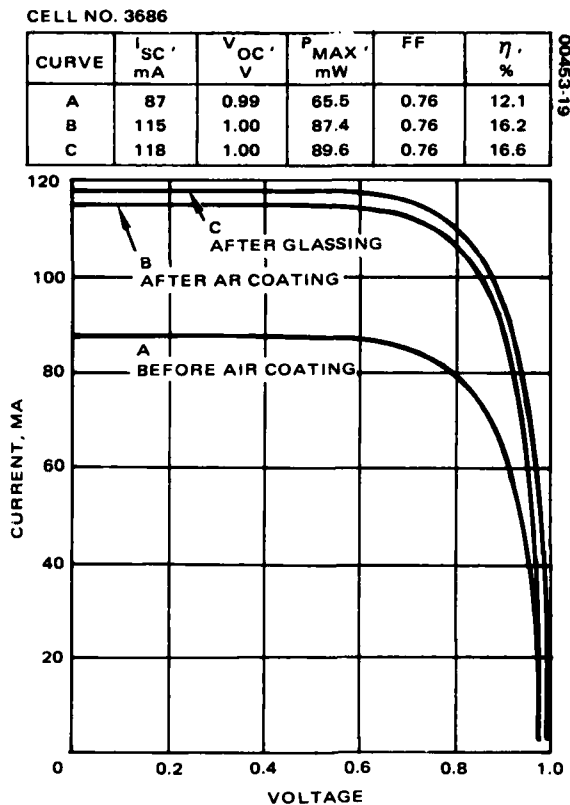


Figure 19. Antireflection coating and glassing results.

**6.6 Special Tests – Single Cell and Cell Module Thermal Tests.** The special tests consisted of the single cell thermal test and the cell module thermal test. The single cell thermal test was described in Section F 4.3.4 of the contract as follows:

Solar cell assemblies shall be designed for survival without adhesive debonding or power output degradation of more than 20 percent after being subjected to each of the following thermal conditions:

- 260°C for 16 hours in vacuum of  $1 \times 10^{-5}$  Torr
- 400°C for 100 seconds in vacuum of  $1 \times 10^{-5}$  Torr
- 500 cycles from -160°C to +100°C at a minimum rate of 30°C per minute in nitrogen

Twelve cell assemblies based on the final design configuration and including welded interconnect tabs shall be tested to each of the above thermal conditions. Pre- and post electrical performance measurements shall be made for all assemblies and results tabulated.

In practice, however, the additional high temperature test of Group D (120°C for 168 hours in vacuum of  $1 \times 10^{-5}$  Torr) was included in series with the same cells.

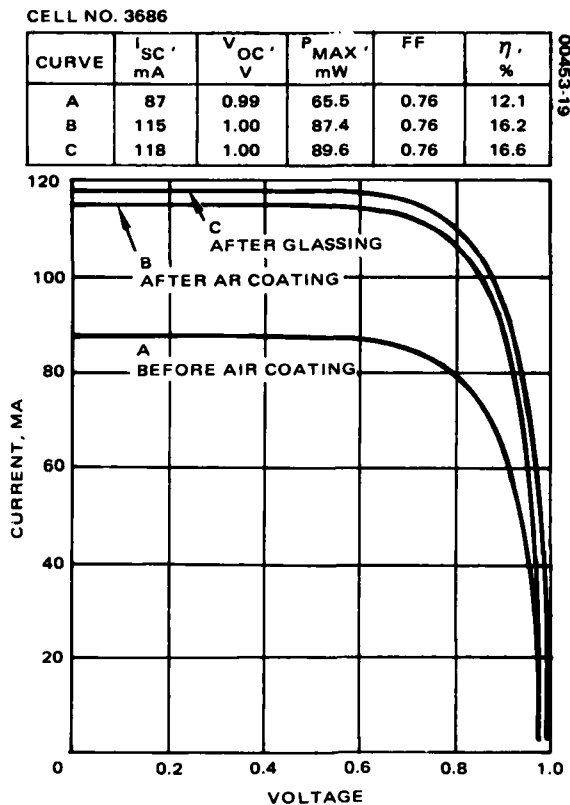


Figure 19. Antireflection coating and glassing results.

**6.6 Special Tests – Single Cell and Cell Module Thermal Tests.** The special tests consisted of the single cell thermal test and the cell module thermal test. The single cell thermal test was described in Section F 4.3.4 of the contract as follows:

Solar cell assemblies shall be designed for survival without adhesive debonding or power output degradation of more than 20 percent after being subjected to each of the following thermal conditions:

- 260°C for 16 hours in vacuum of  $1 \times 10^{-5}$  Torr
- 400°C for 100 seconds in vacuum of  $1 \times 10^{-5}$  Torr
- 500 cycles from -160°C to +100°C at a minimum rate of 30°C per minute in nitrogen

Twelve cell assemblies based on the final design configuration and including welded interconnect tabs shall be tested to each of the above thermal conditions. Pre- and post electrical performance measurements shall be made for all assemblies and results tabulated.

In practice, however, the additional high temperature test of Group D (120°C for 168 hours in vacuum of  $1 \times 10^{-5}$  Torr) was included in series with the same cells.

TABLE 29. CELL SOLAR ABSORPTANCE AND EMITTANCE

Cell No.	$\alpha$	$\epsilon$
3538	0.734	0.836
3539	0.727	0.836
3465	0.761	0.833
3471	0.776	0.817
3467	0.768	0.833
3477	0.751	0.836
3531	0.743	0.836
3537	0.752	0.837
3508	0.737	0.837
3526	0.746	0.835
3506	0.771	0.834
3504	0.740	0.840

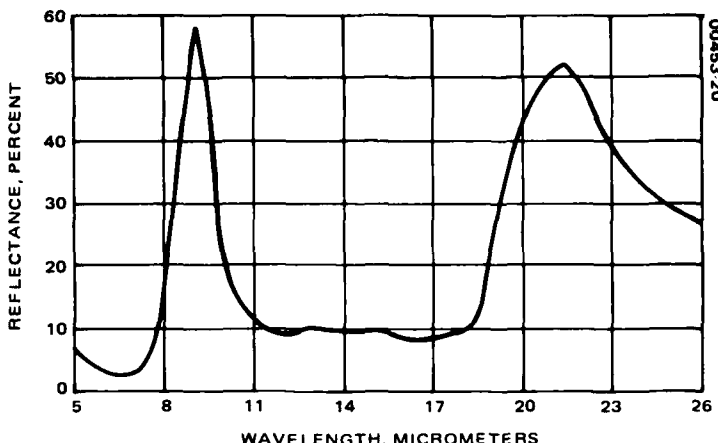


Figure 20. Cell 3465 spectral reflectance.

TABLE 30. HIGH TEMPERATURE VACUUM TEST

Test	Number of Cells	Vacuum (Torr)	Temperature (°C)	Duration
1	16	$10^{-5}$	400	100 sec
2	16	$10^{-5}$	260	16 hr
3	16	$10^{-5}$	120	168 hr

The high temperature vacuum tests were begun on a batch of 16 cells. The total test plan involved stressing the cells for the specified periods of time at the three separate temperatures in the order outlined in Table 30. Afterwards, the 500 cycles were to be performed.

For this series of tests, cells remained unglassed only for the 400°C test due to the high temperature involved and the softening level of the adhesive between the glass and cell surface. Immediately afterwards, however, cells were glassed and the test series was continued.

The procedure consisted of stacking the cells inside a small bell jar which was evacuated to  $1 \times 10^{-5}$  Torr. The cells were then heated to 400°C by means of resistor heater coils supported in a small hollow cylindrical oven placed around the stack. A thermocouple was inserted inside the oven in contact with the cells, and the temperature was monitored continually throughout the heating and cooling cycle. This temperature was found to be controllable to  $\pm 5^\circ\text{C}$ . After the cells were maintained at 400°C for 100 seconds, current to the oven was eliminated, and the cells were allowed to cool to room temperature. Subsequent electrical characterization revealed no degradation of power or efficiency whatsoever. After coverglasses were applied, all cells were again inserted into the oven and heated to 260°C for 16 hours. Afterwards they were electrically characterized. A similar operation was performed to accomplish the 120°C run for 168 hours. Afterwards cells were cycled 500 times as described previously.

TABLE 29. CELL SOLAR ABSORPTANCE AND EMITTANCE

Cell No.	$\alpha$	$\epsilon$
3538	0.734	0.836
3539	0.727	0.836
3465	0.761	0.833
3471	0.776	0.817
3467	0.768	0.833
3477	0.751	0.836
3531	0.743	0.836
3537	0.752	0.837
3508	0.737	0.837
3526	0.746	0.835
3506	0.771	0.834
3504	0.740	0.840

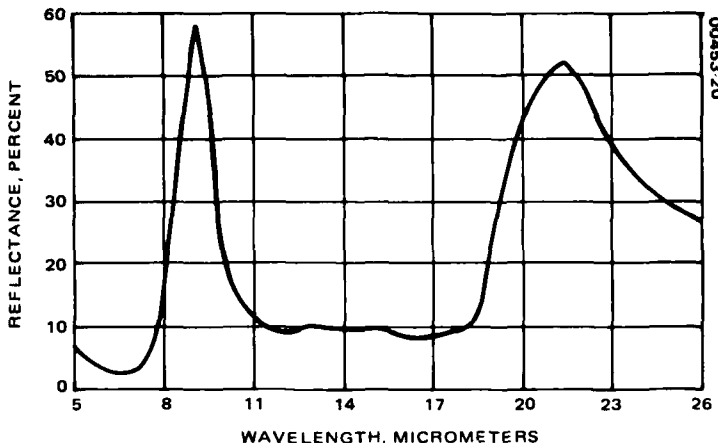


Figure 20. Cell 3465 spectral reflectance.

TABLE 30. HIGH TEMPERATURE VACUUM TEST

Test	Number of Cells	Vacuum (Torr)	Temperature (°C)	Duration
1	16	$10^{-5}$	400	100 sec
2	16	$10^{-5}$	260	16 hr
3	16	$10^{-5}$	120	168 hr

The high temperature vacuum tests were begun on a batch of 16 cells. The total test plan involved stressing the cells for the specified periods of time at the three separate temperatures in the order outlined in Table 30. Afterwards, the 500 cycles were to be performed.

For this series of tests, cells remained unglassed only for the 400°C test due to the high temperature involved and the softening level of the adhesive between the glass and cell surface. Immediately afterwards, however, cells were glassed and the test series was continued.

The procedure consisted of stacking the cells inside a small bell jar which was evacuated to  $1 \times 10^{-5}$  Torr. The cells were then heated to 400°C by means of resistor heater coils supported in a small hollow cylindrical oven placed around the stack. A thermocouple was inserted inside the oven in contact with the cells, and the temperature was monitored continually throughout the heating and cooling cycle. This temperature was found to be controllable to  $\pm 5^\circ\text{C}$ . After the cells were maintained at 400°C for 100 seconds, current to the oven was eliminated, and the cells were allowed to cool to room temperature. Subsequent electrical characterization revealed no degradation of power or efficiency whatsoever. After coverglasses were applied, all cells were again inserted into the oven and heated to 260°C for 16 hours. Afterwards they were electrically characterized. A similar operation was performed to accomplish the 120°C run for 168 hours. Afterwards cells were cycled 500 times as described previously.

Results for all four phases of this test are summarized in Table 31. No deterioration of electrical parameters resulted at any stage. In fact, the overall effect of the series was an enhancement of values in addition to that expected by the glassing operation alone.

The cell module thermal test is specified in the contract as follows:

The contractor shall design and develop weldable interconnects and the technique required to install them. To demonstrate this technique, five (5) modules of at least six (6) cell assemblies each shall be subjected to temperature cycling in accordance with para 4.5.11 of MIL-C-83443 A (USAF) except that 100 cycles rather than 1000 cycles will be used. Electrical degradation from this test shall not exceed 2.5% for any module and shall average 1.5% or less for the five (5) modules.

A 1 mil silver mesh interconnect was selected for the solar cell modules. The six-fingered tabs previously used were selected to demonstrate that the welding techniques would consistently produce strong welds. They were applied to individual cells that afterwards were to be destructively pull-tested. Interconnected cells in the form of modules require different treatment. The new mesh interconnect was chosen to ensure that the modules would undergo the least possible amount of thermal stress during cycling. Results are shown in Table 32. Modules survived cycling with no detectable degradation.

### 6.7 Spectrolab Documentation

**6.7.1 Process Fabrication Documentation.** At the beginning of the program, Hughes supplied Spectrolab with a set of GaAs solar cell fabrication procedures. These procedures and visits to Hughes Research Laboratories (HRL) were used as a basis to document all GaAs processes as practiced at HRL, Malibu, California. Additional procedures were documented describing the processes used at Spectrolab to bond coverslides to the GaAs solar cells. Table 33 lists the Manufacturing Process Procedure (MPP's) and Engineering Line Instructions (ELI's) documented during this program.

**6.7.2 Cell Test Procedure.** A preliminary test procedure for GaAs solar cells has been established by modifying silicon solar cell test procedures, leaving sections to be determined when necessary test data is not available. Table 34 lists the Mechanical Inspection, Manufacturing Control Document (MCD), Quality Assurance Program (QAP), Acceptance Test Plan (ATP), Type Approval Test (TAT), and Process Integration Document (PID) which have been established for GaAs cell testing, which were derived by modifying existing documentation for silicon solar cells.

**6.7.3 Monitoring Cell Fabrication Processes.** Following the documentation of the GaAs fabrication processes, qualified engineers were sent to HRL to monitor the processes. The cells which were monitored at various stages in the process were used as the test cells for the Acceptance and Type Approval tests.

Results for all four phases of this test are summarized in Table 31. No deterioration of electrical parameters resulted at any stage. In fact, the overall effect of the series was an enhancement of values in addition to that expected by the glassing operation alone.

The cell module thermal test is specified in the contract as follows:

The contractor shall design and develop weldable interconnects and the technique required to install them. To demonstrate this technique, five (5) modules of at least six (6) cell assemblies each shall be subjected to temperature cycling in accordance with para 4.5.11 of MIL-C-83443 A (USAF) except that 100 cycles rather than 1000 cycles will be used. Electrical degradation from this test shall not exceed 2.5% for any module and shall average 1.5% or less for the five (5) modules.

A 1 mil silver mesh interconnect was selected for the solar cell modules. The six-fingered tabs previously used were selected to demonstrate that the welding techniques would consistently produce strong welds. They were applied to individual cells that afterwards were to be destructively pull-tested. Interconnected cells in the form of modules require different treatment. The new mesh interconnect was chosen to ensure that the modules would undergo the least possible amount of thermal stress during cycling. Results are shown in Table 32. Modules survived cycling with no detectable degradation.

### 6.7 Spectrolab Documentation

**6.7.1 Process Fabrication Documentation.** At the beginning of the program, Hughes supplied Spectrolab with a set of GaAs solar cell fabrication procedures. These procedures and visits to Hughes Research Laboratories (HRL) were used as a basis to document all GaAs processes as practiced at HRL, Malibu, California. Additional procedures were documented describing the processes used at Spectrolab to bond coverslides to the GaAs solar cells. Table 33 lists the Manufacturing Process Procedure (MPP's) and Engineering Line Instructions (ELI's) documented during this program.

**6.7.2 Cell Test Procedure.** A preliminary test procedure for GaAs solar cells has been established by modifying silicon solar cell test procedures, leaving sections to be determined when necessary test data is not available. Table 34 lists the Mechanical Inspection, Manufacturing Control Document (MCD), Quality Assurance Program (QAP), Acceptance Test Plan (ATP), Type Approval Test (TAT), and Process Integration Document (PID) which have been established for GaAs cell testing, which were derived by modifying existing documentation for silicon solar cells.

**6.7.3 Monitoring Cell Fabrication Processes.** Following the documentation of the GaAs fabrication processes, qualified engineers were sent to HRL to monitor the processes. The cells which were monitored at various stages in the process were used as the test cells for the Acceptance and Type Approval tests.

TABLE 31. CELL MODULE THERMAL TEST RESULTS

Cell No.	Glass*	Temp (°C)	Time	I <sub>sc</sub> (mA)	V <sub>oc</sub> (V)	FF	P <sub>max</sub> (mW)	η (%)
3660	—	—	—	112	1.00	0.78	87.0	16.1
	X	400	100 sec	112	1.00	0.79	89.0	16.5
	X	—	—	114	1.00	0.78	88.6	16.4
	X	260	16 hr	114	0.99	0.78	88.2	16.3
	X	120	168 hr	115	0.99	0.79	90.1	16.7
	X	500 cycles		117	1.00	0.78	91.2	16.8
3664	—	—	—	112	1.00	0.77	85.9	15.9
	X	400	100 sec	112	1.00	0.78	87.9	16.2
	X	—	—	115	1.00	0.78	89.0	16.4
	X	260	16 hr	113	0.99	0.78	87.6	16.2
	X	120	168 hr	114	1.00	0.79	88.8	16.4
	X	500 cycles		115	1.00	0.78	89.6	16.6
3665	—	—	—	111	0.99	0.77	84.5	15.6
	X	400	100 sec	111	0.99	0.79	86.3	16.0
	X	—	—	113	0.99	0.77	85.9	15.9
	X	260	16 hr	112	0.99	0.77	85.5	15.8
	X	120	168 hr	114	0.99	0.77	87.6	16.2
	X	500 cycles		115	1.00	0.78	88.8	16.4
3666	—	—	—	109	1.00	0.78	84.8	15.7
	X	400	100 sec	109	1.00	0.78	84.8	15.7
	X	—	—	115	0.99	0.77	87.4	16.1
	X	260	16 hr	113	0.99	0.77	86.3	16.0
	X	230	168 hr	113	0.99	0.78	87.2	16.1
	X	500 cycles		115	0.99	0.77	87.8	16.2
3667	—	—	—	110	1.00	0.78	85.7	15.8
	X	400	100 sec	110	1.00	0.79	86.5	16.0
	X	—	—	114	1.00	0.78	88.8	16.4
	X	260	16 hr	110	1.00	0.79	86.0	15.9
	X	120	168 hr	113	1.00	0.79	88.8	16.4
	X	500 cycles		114	1.00	0.78	89.4	16.5
3668	—	—	—	112	1.00	0.78	86.7	16.0
	X	400	100 sec	112	1.00	0.80	88.4	16.3
	X	—	—	115	1.00	0.79	90.3	16.7
	X	260	16 hr	111	0.99	0.79	87.1	16.1
	X	120	168 hr	114	0.99	0.80	90.1	16.7
	X	500 cycles		116	1.00	0.79	91.6	16.9
3669	—	—	—	112	1.00	0.77	86.1	15.9
	X	400	100 sec	112	1.00	0.78	87.8	16.2
	X	—	—	116	1.00	0.77	89.7	16.6
	X	260	16 hr	112	0.99	0.78	86.7	16.0
	X	120	168 hr	115	0.99	0.79	89.6	16.6
	X	500 cycles		116	1.00	0.78	91.0	16.8
3671	—	—	—	111	1.00	0.77	85.0	15.7
	X	400	100 sec	112	1.00	0.78	87.8	16.2
	X	—	—	115	0.99	0.78	88.4	16.3
	X	260	16 hr	112	0.99	0.78	86.7	16.0
	X	120	168 hr	113	0.99	0.78	86.9	16.1
	X	500 cycles		116	1.00	0.77	89.0	16.5

TABLE 31. CELL MODULE THERMAL TEST RESULTS

Cell No.	Glass*	Temp (°C)	Time	I <sub>sc</sub> (mA)	V <sub>oc</sub> (V)	FF	P <sub>max</sub> (mW)	η (%)
3660	—	—	—	112	1.00	0.78	87.0	16.1
	X	400	100 sec	112	1.00	0.79	89.0	16.5
	X	—	—	114	1.00	0.78	88.6	16.4
	X	260	16 hr	114	0.99	0.78	88.2	16.3
	X	120	168 hr	115	0.99	0.79	90.1	16.7
	X	500 cycles		117	1.00	0.78	91.2	16.8
3664	—	—	—	112	1.00	0.77	85.9	15.9
	X	400	100 sec	112	1.00	0.78	87.9	16.2
	X	—	—	115	1.00	0.78	89.0	16.4
	X	260	16 hr	113	0.99	0.78	87.6	16.2
	X	120	168 hr	114	1.00	0.79	88.8	16.4
	X	500 cycles		115	1.00	0.78	89.6	16.6
3665	—	—	—	111	0.99	0.77	84.5	15.6
	X	400	100 sec	111	0.99	0.79	86.3	16.0
	X	—	—	113	0.99	0.77	85.9	15.9
	X	260	16 hr	112	0.99	0.77	85.5	15.8
	X	120	168 hr	114	0.99	0.77	87.6	16.2
	X	500 cycles		115	1.00	0.78	88.8	16.4
3666	—	—	—	109	1.00	0.78	84.8	15.7
	X	400	100 sec	109	1.00	0.78	84.8	15.7
	X	—	—	115	0.99	0.77	87.4	16.1
	X	260	16 hr	113	0.99	0.77	86.3	16.0
	X	230	168 hr	113	0.99	0.78	87.2	16.1
	X	500 cycles		115	0.99	0.77	87.8	16.2
3667	—	—	—	110	1.00	0.78	85.7	15.8
	X	400	100 sec	110	1.00	0.79	86.5	16.0
	X	—	—	114	1.00	0.78	88.8	16.4
	X	260	16 hr	110	1.00	0.79	86.0	15.9
	X	120	168 hr	113	1.00	0.79	88.8	16.4
	X	500 cycles		114	1.00	0.78	89.4	16.5
3668	—	—	—	112	1.00	0.78	86.7	16.0
	X	400	100 sec	112	1.00	0.80	88.4	16.3
	X	—	—	115	1.00	0.79	90.3	16.7
	X	260	16 hr	111	0.99	0.79	87.1	16.1
	X	120	168 hr	114	0.99	0.80	90.1	16.7
	X	500 cycles		116	1.00	0.79	91.6	16.9
3669	—	—	—	112	1.00	0.77	86.1	15.9
	X	400	100 sec	112	1.00	0.78	87.8	16.2
	X	—	—	116	1.00	0.77	89.7	16.6
	X	260	16 hr	112	0.99	0.78	86.7	16.0
	X	120	168 hr	115	0.99	0.79	89.6	16.6
	X	500 cycles		116	1.00	0.78	91.0	16.8
3671	—	—	—	111	1.00	0.77	85.0	15.7
	X	400	100 sec	112	1.00	0.78	87.8	16.2
	X	—	—	115	0.99	0.78	88.4	16.3
	X	260	16 hr	112	0.99	0.78	86.7	16.0
	X	120	168 hr	113	0.99	0.78	86.9	16.1
	X	500 cycles		116	1.00	0.77	89.0	16.5

Table 31 (continued)

Cell No.	Glass*	Temp (°C)	Time	I <sub>sc</sub> (mA)	V <sub>oc</sub> (V)	FF	P <sub>max</sub> (mW)	η (%)
3672	—	—		113	1.00	0.76	85.9	15.9
	X	400	100 sec	114	1.00	0.78	88.4	16.3
	X	—	—	116	1.00	0.76	88.4	16.3
	X	260	16 hr	114	0.99	0.77	87.2	16.3
	X	—	—	115	0.99	0.78	88.4	16.3
	X	—	500 cycles	117	1.00	0.78	90.7	16.8
3673	—	—		115	0.99	0.75	85.7	15.8
	X	400	100 sec	115	0.99	0.77	87.8	16.2
	X	—	—	118	0.99	0.75	88.0	16.3
	X	260	16 hr	118	0.99	0.76	89.0	16.4
	X	120	168 hr	118	0.99	0.76	89.3	16.5
	X	—	500 cycles	119	0.99	0.77	90.5	16.7
3674	—	—		113	1.00	0.78	87.6	16.2
	X	400	100 sec	114	1.00	0.78	89.5	16.5
	X	—	—	117	1.00	0.77	90.5	16.7
	X	260	16 hr	117	0.99	0.78	90.7	16.8
	X	120	168 hr	116	0.99	0.79	90.8	16.8
	X	—	500 cycles	118	1.00	0.78	91.6	16.9
3675	—	—		113	1.00	0.76	86.3	16.0
	X	400	100 sec	115	1.00	0.78	89.5	16.5
	X	—	—	117	1.00	0.77	90.5	16.7
	X	260	16 hr	117	1.00	0.77	90.5	16.7
	X	120	168 hr	115	1.00	0.77	89.0	16.4
	X	—	500 cycles	117	0.99	0.78	90.1	16.6
3676	—	—		112	1.00	0.77	85.9	15.9
	X	400	100 sec	113	1.00	0.78	87.8	16.2
	X	—	—	116	1.00	0.77	89.0	16.4
	X	260	16 hr	115	0.99	0.78	88.8	16.4
	X	120	168 hr	115	0.99	0.78	88.8	16.4
	X	—	500 cycles	116	1.00	0.78	89.8	16.6
3677	—	—		110	1.00	0.77	85.0	15.7
	X	400	100 sec	110	1.00	0.79	86.9	16.1
	X	—	—	114	1.00	0.77	88.2	16.3
	X	260	16 hr	112	0.99	0.78	86.7	16.0
	X	120	168 hr	112	0.99	0.78	86.9	16.1
	X	—	500 cycles	113	0.99	0.79	88.4	16.3
3678**	—	—		110	1.00	0.77	85.0	15.7
	X	400	100 sec	112	1.00	0.79	88.0	16.3
3683	—	—		113	0.99	0.76	84.7	15.6
	X	400	100 sec	114	0.99	0.77	87.2	16.1
	X	—	—	116	0.99	0.76	87.6	16.2
	X	260	16 hr	114	0.99	0.77	86.5	16.0
	X	120	168 hr	115	0.99	0.77	87.1	16.1
	X	—	500 cycles	116	0.99	0.77	88.8	16.4

\* An X in this column indicates that the cell was equipped with a cover glass.

\*\* Damaged during handling; data incomplete.

Table 31 (continued)

Cell No.	Glass*	Temp (°C)	Time	I <sub>sc</sub> (mA)	V <sub>oc</sub> (V)	FF	P <sub>max</sub> (mW)	η (%)
3672	—	—	—	113	1.00	0.76	85.9	15.9
	X	400	100 sec	114	1.00	0.78	88.4	16.3
	X	—	—	116	1.00	0.76	88.4	16.3
	X	260	16 hr	114	0.99	0.77	87.2	16.3
	X	—	—	115	0.99	0.78	88.4	16.3
	X	—	500 cycles	117	1.00	0.78	90.7	16.8
3673	—	—	—	115	0.99	0.75	85.7	15.8
	X	400	100 sec	115	0.99	0.77	87.8	16.2
	X	—	—	118	0.99	0.75	88.0	16.3
	X	260	16 hr	118	0.99	0.76	89.0	16.4
	X	120	168 hr	118	0.99	0.76	89.3	16.5
	X	—	500 cycles	119	0.99	0.77	90.5	16.7
3674	—	—	—	113	1.00	0.78	87.6	16.2
	X	400	100 sec	114	1.00	0.78	89.5	16.5
	X	—	—	117	1.00	0.77	90.5	16.7
	X	260	16 hr	117	0.99	0.78	90.7	16.8
	X	120	168 hr	116	0.99	0.79	90.8	16.8
	X	—	500 cycles	118	1.00	0.78	91.6	16.9
3675	—	—	—	113	1.00	0.76	86.3	16.0
	X	400	100 sec	115	1.00	0.78	89.5	16.5
	X	—	—	117	1.00	0.77	90.5	16.7
	X	260	16 hr	117	1.00	0.77	90.5	16.7
	X	120	168 hr	115	1.00	0.77	89.0	16.4
	X	—	500 cycles	117	0.99	0.78	90.1	16.6
3676	—	—	—	112	1.00	0.77	85.9	15.9
	X	400	100 sec	113	1.00	0.78	87.8	16.2
	X	—	—	116	1.00	0.77	89.0	16.4
	X	260	16 hr	115	0.99	0.78	88.8	16.4
	X	120	168 hr	115	0.99	0.78	88.8	16.4
	X	—	500 cycles	116	1.00	0.78	89.8	16.6
3677	—	—	—	110	1.00	0.77	85.0	15.7
	X	400	100 sec	110	1.00	0.79	86.9	16.1
	X	—	—	114	1.00	0.77	88.2	16.3
	X	260	16 hr	112	0.99	0.78	86.7	16.0
	X	120	168 hr	112	0.99	0.78	86.9	16.1
	X	—	500 cycles	113	0.99	0.79	88.4	16.3
3678**	—	—	—	110	1.00	0.77	85.0	15.7
	X	400	100 sec	112	1.00	0.79	88.0	16.3
3683	—	—	—	113	0.99	0.76	84.7	15.6
	X	400	100 sec	114	0.99	0.77	87.2	16.1
	X	—	—	116	0.99	0.76	87.6	16.2
	X	260	16 hr	114	0.99	0.77	86.5	16.0
	X	120	168 hr	115	0.99	0.77	87.1	16.1
	X	—	500 cycles	116	0.99	0.77	88.8	16.4

\* An X in this column indicates that the cell was equipped with a cover glass.

\*\* Damaged during handling; data incomplete.

TABLE 32. GaAs SOLAR CELL MODULE ELECTRICAL CHARACTERISTICS

Cell String No.		I <sub>sc</sub> (A)	V <sub>oc</sub> (V)	P <sub>m</sub> (W)
2	P	0.1038	5.93	0.464
	B	0.1026	5.94	0.461
	A	0.1046	5.93	0.470
3	P	0.1052	5.91	0.477
	B	0.1058	5.91	0.479
	A	0.1058	5.91	0.479
4	P	0.1042	5.91	0.471
	B	0.1064	5.92	0.483
	A	0.105	5.90	0.477
5	P	0.1076	5.95	0.488
	B	0.1046	5.91	0.476
	A	0.1070	5.93	0.481
6	P	0.1066	5.93	0.482
	B	0.1056	5.93	0.480
	A	0.1068	5.88	0.462

P - Before coupon fabrication

B - After coupon fabrication, before thermal cycling

A - After thermal cycling

TABLE 33. PROCESS FABRICATION DOCUMENTATION

Specification No.	Date	Document Title
024502 N/C	2-18-80	Gallium Arsenide Inspection
024503 N/C	2-18-80	Gallium Arsenide Substrate Sizing
024504 N/C	2-18-80	Gallium Arsenide Cleaning and Etching Substrate
024505 N/C	2-18-80	Gallium Arsenide Slide Bar Load
024506 N/C	2-18-80	Gallium Arsenide Reactor Load
024507 N/C	2-18-80	Gallium Arsenide Buffer Layer Reactor Run
024508 N/C	2-18-80	Gallium Arsenide Reactor Unload
024509 N/C	2-18-80	Gallium Arsenide Slide Bar Unload
024510 N/C	2-18-80	Gallium Arsenide Buffer Layer Measurement
024511 N/C	2-18-80	Gallium Arsenide Substrate Preparation for Window Layer
024512 N/C	2-18-80	Gallium Arsenide Reactor Run - Window Layer
024513 N/C	2-18-80	Gallium Arsenide Window Anneal
024514 N/C	2-18-80	Gallium Arsenide AuZn Sputtered Front Contact
024515 N/C	2-18-80	Gallium Arsenide Evaporated Front Contact
024516 N/C	2-18-80	Gallium Arsenide Evaporated Back Contact
024517 N/C	2-18-80	Gallium Arsenide Sintered Contacts
024518 N/C	2-28-80	Engineering Line Instruction (GaAs 2x2)
024553 N/C	3-14-80	Final Gallium Arsenide Wafer Sizing
024519 N/C	2-28-80	Antireflective Coating
024520 N/C	2-28-80	Coverslide and Cell Cleaning
024552 N/C	2-28-80	Coverslide and Cell Cleaning (ELI)
024521 N/C	2-28-80	Coverslide Bonding
024551 N/C	2-28-80	Coverslide Bonding (ELI)

TABLE 34. TEST PROCEDURE DOCUMENTATION

Specification No.	Date	Document Title
024560 N/C	3-12-80	Mechanical Inspection
024469 N/C	2-11-80	Manufacturing Control Document (MCD)
024470 N/C	2-11-80	Quality Assurance Program (QAP)
024471 N/C	2-11-80	Acceptance Test Plan (ATP)
024472 N/C	2-11-80	Type Approval Test Procedure (TAT)
024559 N/C	3-12-80	Process Integration Document (PID)

Except for five cells, all cells were processed in accordance with the MPPs and ELIs. In Procedure 024515 (GaAs Evaporated Front Contact) a tantalum boat was used to evaporate the silver overcoat for these five cells. The silver evaporation material alloyed with the boat and broke the boat (evaporation run 642). The run was stopped, and the broken tantalum boat was removed and replaced with the correct boat. The contacts were then completed in accordance with Procedure 024515.

6.8 Spectrolab Test Results. A sample of 45 cells were selected from the various groups of cells monitored during fabrication at HRL. All of these cells were required to pass the Acceptance Test Plan (ATP). Part of the ATP requirement is a cell response check over a narrow spectral range, data for which is given in Table 35. Spectrolab has no previous spectral response data for comparison.

The sample of 45 cells was divided into two major groups, 30 to receive a coverglass filter and 15 to remain unfiltered. Ten of the filtered cells were selected for the intensity variation test, per Section 4.3 of specification No. 024472. The cell temperature was maintained at 28°C throughout the test, and the current-voltage characteristics were measured with the varied illuminated intensity of 100, 115, 130 and 150 mW/cm<sup>2</sup>. The current-voltage characteristics were established at each of these intensities for each cell. Figure 21 is a current-voltage characteristic of a representative cell at each intensity.

Following the intensity variation test, the same ten cells were subjected to a temperature variation test (see Section 4.4 of specification No. 024472). The illuminated intensity was maintained at AM0 (135.3 mW/cm<sup>2</sup>) throughout the test, and the current-voltage characteristics were measured at -50°, 0°, 50° and 100°C. The current-voltage characteristics were established at each of these temperatures for each cell. Figure 22 is a current-voltage characteristic of a representative cell at each temperature. Inspection revealed some adhesive bubble defects after filtering, and cell chips after testing.

TABLE 35. SPECTRAL RESPONSE ATP

Cell No.	$I_{SC}$ , mA No Filter	$I_{SC}$ , mA Covered
1	114	63
2	115	63
3	116	63
4	115	61
5	115	62
6	118	64
7	117	63
8	115	63
9	117	63
10	117	63

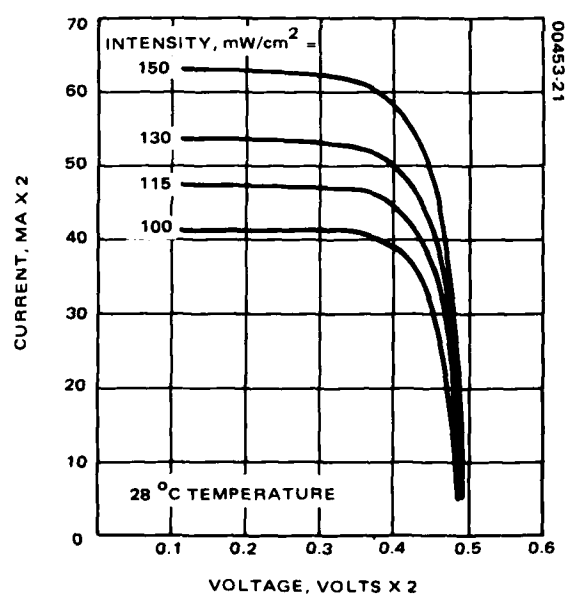


Figure 21. Intensity variation test

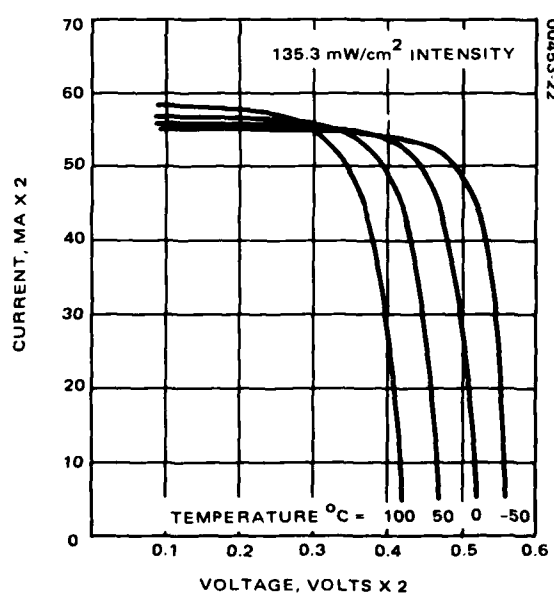


Figure 22. Temperature variation test

TABLE 34. TEST PROCEDURE DOCUMENTATION

Specification No.	Date	Document Title
024560 N/C	3-12-80	Mechanical Inspection
024469 N/C	2-11-80	Manufacturing Control Document (MCD)
024470 N/C	2-11-80	Quality Assurance Program (QAP)
024471 N/C	2-11-80	Acceptance Test Plan (ATP)
024472 N/C	2-11-80	Type Approval Test Procedure (TAT)
024559 N/C	3-12-80	Process Integration Document (PID)

Except for five cells, all cells were processed in accordance with the MPPs and ELIs. In Procedure 024515 (GaAs Evaporated Front Contact) a tantalum boat was used to evaporate the silver overcoat for these five cells. The silver evaporation material alloyed with the boat and broke the boat (evaporation run 642). The run was stopped, and the broken tantalum boat was removed and replaced with the correct boat. The contacts were then completed in accordance with Procedure 024515.

6.8 Spectrolab Test Results. A sample of 45 cells were selected from the various groups of cells monitored during fabrication at HRL. All of these cells were required to pass the Acceptance Test Plan (ATP). Part of the ATP requirement is a cell response check over a narrow spectral range, data for which is given in Table 35. Spectrolab has no previous spectral response data for comparison.

The sample of 45 cells was divided into two major groups, 30 to receive a coverglass filter and 15 to remain unfiltered. Ten of the filtered cells were selected for the intensity variation test, per Section 4.3 of specification No. 024472. The cell temperature was maintained at 28°C throughout the test, and the current-voltage characteristics were measured with the varied illuminated intensity of 100, 115, 130 and 150 mW/cm<sup>2</sup>. The current-voltage characteristics were established at each of these intensities for each cell. Figure 21 is a current-voltage characteristic of a representative cell at each intensity.

Following the intensity variation test, the same ten cells were subjected to a temperature variation test (see Section 4.4 of specification No. 024472). The illuminated intensity was maintained at AM0 (135.3 mW/cm<sup>2</sup>) throughout the test, and the current-voltage characteristics were measured at -50°, 0°, 50° and 100°C. The current-voltage characteristics were established at each of these temperatures for each cell. Figure 22 is a current-voltage characteristic of a representative cell at each temperature. Inspection revealed some adhesive bubble defects after filtering, and cell chips after testing.

The remaining 20 filtered cells, which had some bubbles after filtering, were exposed to a variety of environmental tests. The first of these tests was a temperature humidity test that consisted of a 2 hour raise to 52°C and 95 percent relative humidity, followed by a 6 hour soak and a 16 hour cool-down cycle to 37°C or /ESS (see Section 4.6 of specification No. 024472). The results of this test are given in Table 36. The cell performances were well within tolerance and only small visual defects were found. Five exposures to +145° and -194°C was the second thermal shock test conducted (see Section 4.9 of Specification 024472). The output of the cells was again well within acceptable limits (Table 37), and small antireflective (AR) coating voids were found. The third and final test these cells were exposed to was a high temperature-vacuum test, which consisted of a 168 hour soak at 140°C and 10<sup>-5</sup> Torr (see Section 4.12 of Specification 024472 for details). The performance of the cells after this test was well within acceptable limits (Table 38), and some additional AR coating voids were observed on one cell. The overall average change in current at load, 830 mV ( $I_p$ ), short circuit current ( $I_{sc}$ ), and open circuit voltage ( $V_{oc}$ ) was +1.3, +0.3 and 0.0 percent, respectively. These GaAs solar cells had no appreciable change except for small AR coating voids after undergoing these three environmental tests.

TABLE 36. TEMPERATURE HUMIDITY TEST RESULTS

Cell S/N	Pretest			Posttest			Percent Degradation		
	$I_p$ (mA)	$I_{sc}$ (mA)	$V_{oc}$ (mV)	$I_p$ (mA)	$I_{sc}$ (mA)	$V_{oc}$ (mV)	$I_p$	$I_{sc}$	$V_{oc}$
4874	108	116	988	106	116	992	-2	0	+0.4
4871	108	115	996	106	115	997	-2	0	0
4848	104	115	994	104	116	994	0	+1	0
4847	105	117	996	105	117	994	0	0	0
4846	106	116	994	105	117	992	-1	+1	0
4845	106	116	993	104	117	991	-2	+1	0
4843	103	115	992	104	116	994	+1	+1	0
4842	104	115	993	104	115	992	0	0	0
4841	106	114	996	105	115	998	-1	+1	0
4840	103	115	991	103	115	992	0	0	0
4839	104	115	994	103	115	992	-1	0	0
4818	105	114	988	103	114	992	-2	0	+0.4
4817	106	114	993	104	114	993	-2	0	0
4805	104	115	992	104	116	992	0	+1	0
4796	102	113	994	100	113	994	-2	0	0
4794	101	114	987	100	114	992	-1	0	+0.5
4793	103	113	992	102	114	992	-1	+1	0
4792	100	114	991	100	114	990	0	0	0
4791	103	114	994	101	115	994	-2	+1	0
4778	99	115	981	98	115	978	-1	0	0
Avg.	104.0	114.8	992.0	103.1	115.2	992.3	-0.9	+0.3	0

TABLE 35. SPECTRAL RESPONSE ATP

Cell No.	$I_{SC}$ , mA No Filter	$I_{SC}$ , mA Covered
1	114	63
2	115	63
3	116	63
4	115	61
5	115	62
6	118	64
7	117	63
8	115	63
9	117	63
10	117	63

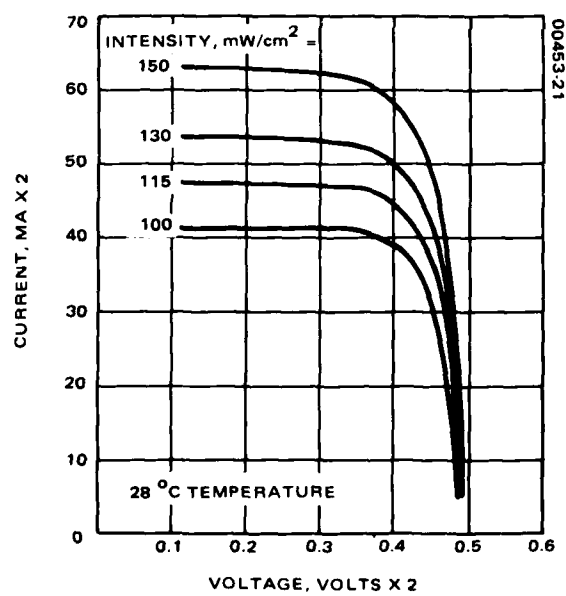


Figure 21. Intensity variation test

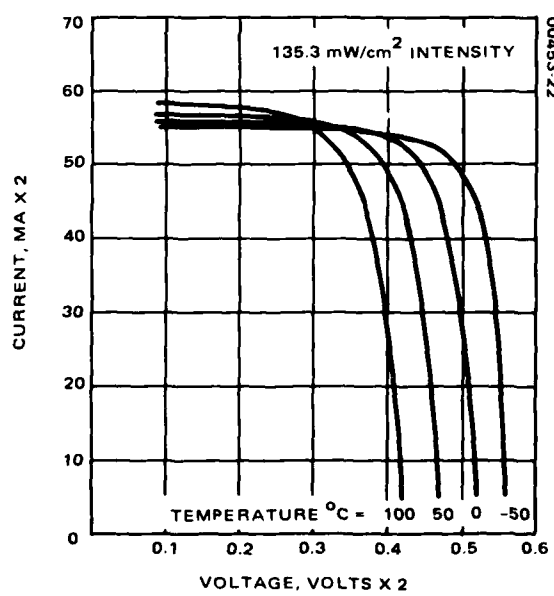


Figure 22. Temperature variation test

TABLE 37. THERMAL SHOCK TEST RESULTS

Cell S/N	Pretest			Posttest			Percent Degradation		
	I <sub>p</sub> (mA)	I <sub>sc</sub> (mA)	V <sub>oc</sub> (mV)	I <sub>p</sub> (mA)	I <sub>sc</sub> (mA)	V <sub>oc</sub> (mV)	I <sub>p</sub>	I <sub>sc</sub>	V <sub>oc</sub>
4874	106	116	992	109	117	992	+3	+1	0
4871	106	115	997	108	116	996	+2	+1	0
4848	104	116	994	104	116	991	0	0	0
4847	105	117	994	106	118	994	+1	+1	0
4846	105	117	992	106	117	993	+1	0	0
4845	104	117	991	106	117	996	+2	0	0.5
4843	104	116	994	105	116	993	+1	0	0
4842	104	115	992	106	116	992	+2	+1	0
4841	105	115	998	107	115	998	+2	0	0
4840	103	115	992	105	116	992	+2	+1	0
4839	103	115	992	104	116	993	+1	+1	0
4818	103	114	992	103	115	994	0	+1	0
4817	104	114	993	106	115	992	+2	+1	0
4805	104	116	992	104	116	992	0	0	0
4796	100	113	994	104	113	992	+4	0	0
4794	100	114	992	102	115	993	+2	+1	0
4793	102	114	992	103	115	992	+1	+1	0
4792	100	114	990	101	115	989	+1	+1	0
4791	101	115	994	104	115	993	+3	0	0
4778	98	115	978	98	115	979	0	0	0
Avg.	103.1	115.2	992.3	104.6	115.7	992.3	+1.5	+0.4	0

The remaining 20 filtered cells, which had some bubbles after filtering, were exposed to a variety of environmental tests. The first of these tests was a temperature humidity test that consisted of a 2 hour raise to 52°C and 95 percent relative humidity, followed by a 6 hour soak and a 16 hour cool-down cycle to 37°C or /ESS (see Section 4.6 of specification No. 024472). The results of this test are given in Table 36. The cell performances were well within tolerance and only small visual defects were found. Five exposures to +145° and -194°C was the second thermal shock test conducted (see Section 4.9 of Specification 024472). The output of the cells was again well within acceptable limits (Table 37), and small antireflective (AR) coating voids were found. The third and final test these cells were exposed to was a high temperature-vacuum test, which consisted of a 168 hour soak at 140°C and 10<sup>-5</sup> Torr (see Section 4.12 of Specification 024472 for details). The performance of the cells after this test was well within acceptable limits (Table 38), and some additional AR coating voids were observed on one cell. The overall average change in current at load, 830 mV ( $I_p$ ), short circuit current ( $I_{sc}$ ), and open circuit voltage ( $V_{oc}$ ) was +1.3, +0.3 and 0.0 percent, respectively. These GaAs solar cells had no appreciable change except for small AR coating voids after undergoing these three environmental tests.

TABLE 36. TEMPERATURE HUMIDITY TEST RESULTS

Cell S/N	Pretest			Posttest			Percent Degradation		
	$I_p$ (mA)	$I_{sc}$ (mA)	$V_{oc}$ (mV)	$I_p$ (mA)	$I_{sc}$ (mA)	$V_{oc}$ (mV)	$I_p$	$I_{sc}$	$V_{oc}$
4874	108	116	988	106	116	992	-2	0	+0.4
4871	108	115	996	106	115	997	-2	0	0
4848	104	115	994	104	116	994	0	+1	0
4847	105	117	996	105	117	994	0	0	0
4846	106	116	994	105	117	992	-1	+1	0
4845	106	116	993	104	117	991	-2	+1	0
4843	103	115	992	104	116	994	+1	+1	0
4842	104	115	993	104	115	992	0	0	0
4841	106	114	996	105	115	998	-1	+1	0
4840	103	115	991	103	115	992	0	0	0
4839	104	115	994	103	115	992	-1	0	0
4818	105	114	988	103	114	992	-2	0	+0.4
4817	106	114	993	104	114	993	-2	0	0
4805	104	115	992	104	116	992	0	+1	0
4796	102	113	994	100	113	994	-2	0	0
4794	101	114	987	100	114	992	-1	0	+0.5
4793	103	113	992	102	114	992	-1	+1	0
4792	100	114	991	100	114	990	0	0	0
4791	103	114	994	101	115	994	-2	+1	0
4778	99	115	981	98	115	978	-1	0	0
Avg.	104.0	114.8	992.0	103.1	115.2	992.3	-0.9	+0.3	0

TABLE 38. HIGH TEMPERATURE VACUUM TEST RESULTS

Cell S/N	Pretest			Posttest			Percent Degradation		
	I <sub>p</sub> (mA)	I <sub>sc</sub> (mA)	V <sub>oc</sub> (mV)	I <sub>p</sub> (mA)	I <sub>sc</sub> (mA)	V <sub>oc</sub> (mV)	I <sub>p</sub>	I <sub>sc</sub>	V <sub>oc</sub>
4874	109	117	992	107	117	990	-2	0	-0.2
4871	108	116	996	108	115	995	0	-1	-0.1
4848	104	116	991	105	116	993	+1	0	+0.3
4847	106	118	994	106	118	992	0	0	-0.2
4846	106	117	993	106	117	993	0	0	0
4845	106	117	996	106	117	995	0	0	-0.1
4843	105	116	993	105	116	992	0	0	-0.1
4842	106	116	992	105	116	991	-1	0	-0.1
4841	107	115	998	108	116	997	+1	+1	-0.1
4840	105	116	992	104	116	990	-1	0	-0.2
4839	104	116	993	105	116	992	+1	0	-0.1
4818	103	115	994	103	115	993	0	0	-0.1
4817	106	115	992	106	115	992	0	0	0
4805	104	116	992	105	116	991	+1	0	-0.1
4796	104	113	992	103	113	994	-1	0	+0.2
4794	102	115	993	102	115	992	0	0	-0.1
4793	103	115	992	103	114	991	0	-1	-0.1
4792	101	115	989	100	114	989	-1	-1	0
4791	104	115	993	102	115	992	-2	0	-0.1
4778	98	115	979	99	115	986	+1	0	+0.8
Avg.	104.6	115.7	992.3	104.4	115.6	992	-0.2	-0.1	0

The remaining 15 cells without filters were exposed to an 80 day temperature (45 °C) and humidity test (90 percent relative humidity) (see Section 4.6.8 of Specification 024472). Of the 15 cells, 10 were fabricated normally, and 5 cells were processed as described in 6.7.3. The cells processed normally were well within tolerance after the humidity treatment. The remaining five cells had a resultant average degradation of 3.3 percent in I<sub>p</sub> (see Table 39).

TABLE 37. THERMAL SHOCK TEST RESULTS

Cell S/N	Pretest			Posttest			Percent Degradation		
	I <sub>p</sub> (mA)	I <sub>sc</sub> (mA)	V <sub>oc</sub> (mV)	I <sub>p</sub> (mA)	I <sub>sc</sub> (mA)	V <sub>oc</sub> (mV)	I <sub>p</sub>	I <sub>sc</sub>	V <sub>oc</sub>
4874	106	116	992	109	117	992	+3	+1	0
4871	106	115	997	108	116	996	+2	+1	0
4848	104	116	994	104	116	991	0	0	0
4847	105	117	994	106	118	994	+1	+1	0
4846	105	117	992	106	117	993	+1	0	0
4845	104	117	991	106	117	996	+2	0	0.5
4843	104	116	994	105	116	993	+1	0	0
4842	104	115	992	106	116	992	+2	+1	0
4841	105	115	998	107	115	998	+2	0	0
4840	103	115	992	105	116	992	+2	+1	0
4839	103	115	992	104	116	993	+1	+1	0
4818	103	114	992	103	115	994	0	+1	0
4817	104	114	993	106	115	992	+2	+1	0
4805	104	116	992	104	116	992	0	0	0
4796	100	113	994	104	113	992	+4	0	0
4794	100	114	992	102	115	993	+2	+1	0
4793	102	114	992	103	115	992	+1	+1	0
4792	100	114	990	101	115	989	+1	+1	0
4791	101	115	994	104	115	993	+3	0	0
4778	98	115	978	98	115	979	0	0	0
Avg.	103.1	115.2	992.3	104.6	115.7	992.3	+1.5	+0.4	0

TABLE 39. EIGHTY DAY HUMIDITY TEST RESULTS

Cell S/N	Before Humidity			After Humidity			Percent Degradation		
	- Pre Test			Posttest					
	I <sub>p</sub> (mA)	I <sub>sc</sub> (mA)	V <sub>oc</sub> (mV)	I <sub>p</sub> (mA)	I <sub>sc</sub> (mA)	V <sub>oc</sub> (mV)	I <sub>p</sub>	I <sub>sc</sub>	V <sub>oc</sub>
4630	102	112	993	102	113	993	0	0	0

TABLE 38. HIGH TEMPERATURE VACUUM TEST RESULTS

Cell S/N	Pretest			Posttest			Percent Degradation		
	I <sub>p</sub> (mA)	I <sub>sc</sub> (mA)	V <sub>oc</sub> (mV)	I <sub>p</sub> (mA)	I <sub>sc</sub> (mA)	V <sub>oc</sub> (mV)	I <sub>p</sub>	I <sub>sc</sub>	V <sub>oc</sub>
4874	109	117	992	107	117	990	-2	0	-0.2
4871	108	116	996	108	115	995	0	-1	-0.1
4848	104	116	991	105	116	993	+1	0	+0.3
4847	106	118	994	106	118	992	0	0	-0.2
4846	106	117	993	106	117	993	0	0	0
4845	106	117	996	106	117	995	0	0	-0.1
4843	105	116	993	105	116	992	0	0	-0.1
4842	106	116	992	105	116	991	-1	0	-0.1
4841	107	115	998	108	116	997	+1	+1	-0.1
4840	105	116	992	104	116	990	-1	0	-0.2
4839	104	116	993	105	116	992	+1	0	-0.1
4818	103	115	994	103	115	993	0	0	-0.1
4817	106	115	992	106	115	992	0	0	0
4805	104	116	992	105	116	991	+1	0	-0.1
4796	104	113	992	103	113	994	-1	0	+0.2
4794	102	115	993	102	115	992	0	0	-0.1
4793	103	115	992	103	114	991	0	-1	-0.1
4792	101	115	989	100	114	989	-1	-1	0
4791	104	115	993	102	115	992	-2	0	-0.1
4778	98	115	979	99	115	986	+1	0	+0.8
Avg.	104.6	115.7	992.3	104.4	115.6	992	-0.2	-0.1	0

The remaining 15 cells without filters were exposed to an 80 day temperature (45 °C) and humidity test (90 percent relative humidity) (see Section 4.6.8 of Specification 024472). Of the 15 cells, 10 were fabricated normally, and 5 cells were processed as described in 6.7.3. The cells processed normally were well within tolerance after the humidity treatment. The remaining five cells had a resultant average degradation of 3.3 percent in I<sub>p</sub> (see Table 39).

## 7. CONCLUSIONS

The process used at Hughes is readily adaptable to pilot line production.

The GaAs HESP II program has been completed and its major goals accomplished. Space qualified solar cells were developed with a beginning-of-life lot median efficiency of 16 percent of 25°C under air mass zero (AM0) illumination. The solar cell assemblies show good thermal and radiation resistance.

Specific accomplishments are as follows:

- Efficient GaAs Solar Cells — The fabrication processing was perfected for 16 percent efficient cells. The end-of-line yield using the developed technique is approximately 30 to 50 percent of the starting number. Cell efficiencies as high as 18 percent have been achieved by cells fabricated by the Hughes process.
- Thin GaAs Solar Cells — Cells as thin as 8 mils were fabricated on an experimental basis. The conclusion of this tangential study was that the manufacture of thin cells is feasible.
- Large Area GaAs Solar Cells — The 2.0 x 2.0 cm GaAs cells of the earlier part of the program led to the fabrication of 2.0 x 4.0 cm devices with an identical cross section and comparable performance.
- Batch Processing — The liquid phase reactors grew in size to accommodate fabrication batches including as many as eight individual 2.0 x 2.0 cm GaAs cells. This was made possible in part by using larger solutions and double graphite substrate holders.
- Contact Metallization — A sputtered AuZn contact was developed for the upper p-type face of the GaAs solar cell. The bottom, n-type metallization consisted of evaporated NiGeAu. Both contacts were covered with relatively thick layers of evaporated Ag. The metallizations have been demonstrated to withstand temperature excursions up to 400°C for several hours without adverse effect on the solar cell performance.

TABLE 39. EIGHTY DAY HUMIDITY TEST RESULTS

Cell S/N	Before Humidity			After Humidity			Percent Degradation		
	- Pre Test			Posttest					
	I <sub>p</sub> (mA)	I <sub>sc</sub> (mA)	V <sub>oc</sub> (mV)	I <sub>p</sub> (mA)	I <sub>sc</sub> (mA)	V <sub>oc</sub> (mV)	I <sub>p</sub>	I <sub>sc</sub>	V <sub>oc</sub>
4630	102	112	993	102	113	993	0	0	0
4631	103	114	989	100	115	983	-3	0	-0.6
4635	104	114	981	103	115	980	+1	0	0
4636	102	115	984	102	116	985	0	0	0
4724	101	114	987	103	115	994	0	0	0
4732	101	115	991	100	115	989	-1	0	0
4733	100	114	983	99	115	984	-1	0	0
4734	101	114	992	101	115	991	0	0	0
4735	98	113	976	95	114	975	-3.0	+1	0
4736	99	115	982	96	116	974	-4	0	-1
4743	98	111	987	89	105	980	-9	-5.4	-0.7
4744	99	112	994	92	103	991	-7	-9	0
4765	97	111	984	92	106	980	-5	-5	-0.4
4776	98	115	989	90	107	984	-8	-8	-0.5
4779	98	113	987	88	106	976	-10	-7	-1.0
Avg. 1st 10 cells	101.1	114.0	985.8	100.1	114.9	984.8	-1.0	-0.8	-0.1
15 cells	100.1	113.5	989.9	96.8	111.7	983.9	-3.3	-1.6	-0.6

- Welding Capability - Two separate welding techniques were successfully developed: ultrasonic seam welding and parallel gap welding. The latter was used more extensively. This effort proved the compatibility of welding methods with the GaAs/metallization systems developed under the HESP II contract.

- Radiation Hardness - GaAs solar cells were irradiated with both neutrons and electrons of various fluences. Electrical characteristics of the cells are shown to meet HESP II requirements.

- Manufacturing Control Documentation - All processes and techniques in the fabrication of the GaAs solar cell were recorded. This documentation ensures that all processes are sufficiently controlled to manufacture cells. The manufacturing control documentation also brings the development of GaAs solar cells as close to pilot line production as possible under the HESP II program. Support documentation is submitted as Appendix B of this report.

- Qualification Testing - Extensive testing was executed on GaAs cells in the following areas:

- 1) Glassing
- 2) Radiometric properties
- 3) High temperature
- 4) Humidity
- 5) Radiation resistance
- 6) Temperature coefficients
- 7) Temperature cycling
- 8) Welding
- 9) Interconnecting
- 10) Single cell thermal tests
- 11) Cell module thermal tests

As reported in detail in Section 6, GaAs solar cells produced under the HESP II contract performed favorably throughout this rigorous testing program.

## 7. CONCLUSIONS

The process used at Hughes is readily adaptable to pilot line production.

The GaAs HESP II program has been completed and its major goals accomplished. Space qualified solar cells were developed with a beginning-of-life lot median efficiency of 16 percent of 25°C under air mass zero (AM0) illumination. The solar cell assemblies show good thermal and radiation resistance.

Specific accomplishments are as follows:

- Efficient GaAs Solar Cells — The fabrication processing was perfected for 16 percent efficient cells. The end-of-line yield using the developed technique is approximately 30 to 50 percent of the starting number. Cell efficiencies as high as 18 percent have been achieved by cells fabricated by the Hughes process.
- Thin GaAs Solar Cells — Cells as thin as 8 mils were fabricated on an experimental basis. The conclusion of this tangential study was that the manufacture of thin cells is feasible.
- Large Area GaAs Solar Cells — The 2.0 x 2.0 cm GaAs cells of the earlier part of the program led to the fabrication of 2.0 x 4.0 cm devices with an identical cross section and comparable performance.
- Batch Processing — The liquid phase reactors grew in size to accommodate fabrication batches including as many as eight individual 2.0 x 2.0 cm GaAs cells. This was made possible in part by using larger solutions and double graphite substrate holders.
- Contact Metallization — A sputtered AuZn contact was developed for the upper p-type face of the GaAs solar cell. The bottom, n-type metallization consisted of evaporated NiGeAu. Both contacts were covered with relatively thick layers of evaporated Ag. The metallizations have been demonstrated to withstand temperature excursions up to 400°C for several hours without adverse effect on the solar cell performance.

• Solar Cell Deliveries - Under the HESP II plan several hundred  $2.0 \times 2.0$  cm  $2.0 \times 4.0$  cm GaAs solar cells were delivered to the Air Force. The specific descriptions are given in Table 40. All deliverables exhibited an average lot efficiency of 16.0 percent as specified in the contract.

TABLE 40. GaAs SOLAR CELLS DELIVERED

Description	Quantities	
	$2.0 \times 2.0$ cm	$2.0 \times 4.0$ cm
Glassed, no interconnects	150	150
Glassed, with interconnects	85	75
Unglassed, with interconnects	90	-
Glassed, interconnected into modules	45	45
Total	370	270

- Welding Capability - Two separate welding techniques were successfully developed: ultrasonic seam welding and parallel gap welding. The latter was used more extensively. This effort proved the compatibility of welding methods with the GaAs/metallization systems developed under the HESP II contract.

- Radiation Hardness - GaAs solar cells were irradiated with both neutrons and electrons of various fluences. Electrical characteristics of the cells are shown to meet HESP II requirements.

- Manufacturing Control Documentation - All processes and techniques in the fabrication of the GaAs solar cell were recorded. This documentation ensures that all processes are sufficiently controlled to manufacture cells. The manufacturing control documentation also brings the development of GaAs solar cells as close to pilot line production as possible under the HESP II program. Support documentation is submitted as Appendix B of this report.

- Qualification Testing - Extensive testing was executed on GaAs cells in the following areas:

- 1) Glassing
- 2) Radiometric properties
- 3) High temperature
- 4) Humidity
- 5) Radiation resistance
- 6) Temperature coefficients
- 7) Temperature cycling
- 8) Welding
- 9) Interconnecting
- 10) Single cell thermal tests
- 11) Cell module thermal tests

As reported in detail in Section 6, GaAs solar cells produced under the HESP II contract performed favorably throughout this rigorous testing program.

## APPENDIX A. RADIATION TEST RESULTS

R. Loo, L. Goldhammer, B. Anspaugh,  
R. C. Knechtli, and G. S. Kamath, "Electron  
and Proton Degradation in (AlGa)As -GaAs  
Solar Cells," Proc. 13th Photovoltaic  
Specialists Conference, June 1978.

PRECEDING PAGE BLANK-NOT FILMED

• Solar Cell Deliveries - Under the HESP II plan several hundred  $2.0 \times 2.0$  cm  $2.0 \times 4.0$  cm GaAs solar cells were delivered to the Air Force. The specific descriptions are given in Table 40. All deliverables exhibited an average lot efficiency of 16.0 percent as specified in the contract.

TABLE 40. GaAs SOLAR CELLS DELIVERED

Description	Quantities	
	$2.0 \times 2.0$ cm	$2.0 \times 4.0$ cm
Glassed, no interconnects	150	150
Glassed, with interconnects	85	75
Unglassed, with interconnects	90	-
Glassed, interconnected into modules	45	45
Total	370	270

## ELECTRON AND PROTON DEGRADATION IN (AlGa)As-GaAs SOLAR CELLS

R. Loo, L. Goldammer \* S. Anspaugh, \*\* R.C. Knechtli and G.S. Kamath

Hughes Research Laboratories  
Malibu, California 90265

### ABSTRACT

Results on radiation damage in (AlGa)As-GaAs solar cells by 1 MeV electron fluences up to  $1 \times 10^{16} \text{ e/cm}^2$  and by 15, 20, 30 and 40 MeV proton fluences up to  $5 \times 10^{11} \text{ p/cm}^2$  are presented. The damage is compared with data on state-of-the-art silicon cells which were irradiated along with the gallium arsenide cells. We verified experimentally our theoretical expectation that the junction depth has to be kept relatively shallow, to minimize radiation damage. The damage to the GaAs cells as a function of irradiation, is correlated with the change in their spectral response and dark I-V characteristics. The effect of thermal annealing on the (AlGa)As-GaAs solar cells was also investigated. This data is used to predict further avenues of optimization of the GaAs cells.

### INTRODUCTION

The behavior of solar cells under radiation environment is of great importance for space application. Previous studies have shown that the (AlGa)As-GaAs solar cells have achieved an efficiency of 18.5% AMO (1) with a radiation resistance equal to or better than that observed in violet silicon cells (2). In this paper, we report the radiation effect on large-area ( $2 \text{ cm} \times 2 \text{ cm}$ ) (AlGa)As-GaAs solar cells fabricated at Hughes Research Laboratories (HRL) using the infinite melt liquid phase epitaxial (LPE) growth system. Our best cell to date has an AMO efficiency of 18%, and our improved shallow-junction cells show more radiation resistance than silicon cells.

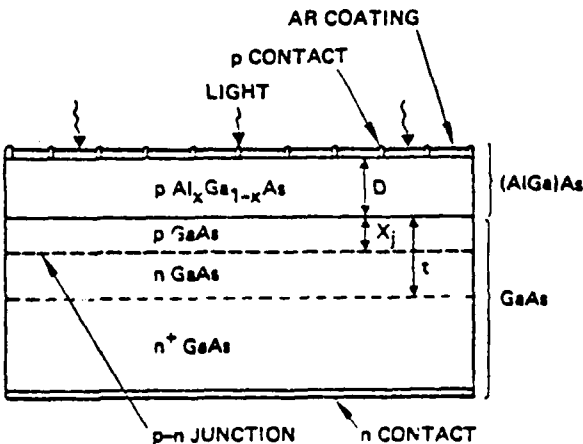
GaAs has a large optical absorption constant and a short diffusion length; essentially, all the photovoltaic response is close to the GaAs surface. The radiation damage beyond this active region has a negligible effect on cell performance. Consequently, the reduction in the required minority carrier diffusion length and the relative shallowness of the active region are the key factors that can be exploited to make GaAs solar cells more radiation resistant. Data consistent with these observations is presented below.

\* Hughes Research Laboratories, Malibu, California  
\*\* J.P.L., Pasadena, California

### EXPERIMENTAL

Figure 1 shows the (AlGa)As-GaAs solar cell structure. The  $n^+$  concentration for the substrate is fixed at  $> 5 \times 10^{17} \text{ cm}^{-3}$  with Te as the dopant. The n buffer layer concentration is  $1 \times 10^{17} \text{ cm}^{-3}$ . (At this doping level, the open-circuit voltage is 1 V.) The thickness of this layer was fixed at 10  $\mu\text{m}$  or more because results indicated that the substrate visibility is minimized at a buffer layer thickness of 10  $\mu\text{m}$ . A thickness less than this is not always sufficient to remove the effect of the substrate on cell performance.

7645-6



NUMBER OF FINGERS = 24

p CONTACT: Au-Zn-Ag

n CONTACT: Au-Ge-Ni-Ag

AR COATING:  $Ta_2O_5$

$p Al_xGa_{1-x}As: X \geq 0.95$

CELL SIZE =  $2 \times 2 \text{ CM}^2$

Figure 1. The (AlGa)As-GaAs solar cell

## APPENDIX A. RADIATION TEST RESULTS

R. Loo, L. Goldhammer, B. Anspaugh,  
R. C. Knechtli, and G. S. Kamath, "Electron  
and Proton Degradation in (AlGa)As -GaAs  
Solar Cells," Proc. 13th Photovoltaic  
Specialists Conference, June 1978.

PRECEDING PAGE BLANK-NOT FILMED

## ELECTRON AND PROTON DEGRADATION IN (AlGa)As-GaAs SOLAR CELLS

R. Loo, L. Goldhammer \* S. Anspaugh, \*\* R.C. Knechtli and G.S. Kamath

Hughes Research Laboratories  
Malibu, California 90265

### ABSTRACT

Results on radiation damage in (AlGa)As-GaAs solar cells by 1 MeV electron fluences up to  $1 \times 10^{16} \text{ e/cm}^2$  and by 15, 20, 30 and 40 MeV proton fluences up to  $5 \times 10^{11} \text{ p/cm}^2$  are presented. The damage is compared with data on state-of-the-art silicon cells which were irradiated along with the gallium arsenide cells. We verified experimentally our theoretical expectation that the junction depth has to be kept relatively shallow, to minimize radiation damage. The damage to the GaAs cells as a function of irradiation, is correlated with the change in their spectral response and dark I-V characteristics. The effect of thermal annealing on the (AlGa)As-GaAs solar cells was also investigated. This data is used to predict further avenues of optimization of the GaAs cells.

### INTRODUCTION

The behavior of solar cells under radiation environment is of great importance for space application. Previous studies have shown that the (AlGa)As-GaAs solar cells have achieved an efficiency of 18.5% AMO (1) with a radiation resistance equal to or better than that observed in violet silicon cells (2). In this paper, we report the radiation effect on large-area ( $2 \text{ cm} \times 2 \text{ cm}$ ) (AlGa)As-GaAs solar cells fabricated at Hughes Research Laboratories (HRL) using the infinite melt liquid phase epitaxial (LPE) growth system. Our best cell to date has an AMO efficiency of 18%, and our improved shallow-junction cells show more radiation resistance than silicon cells.

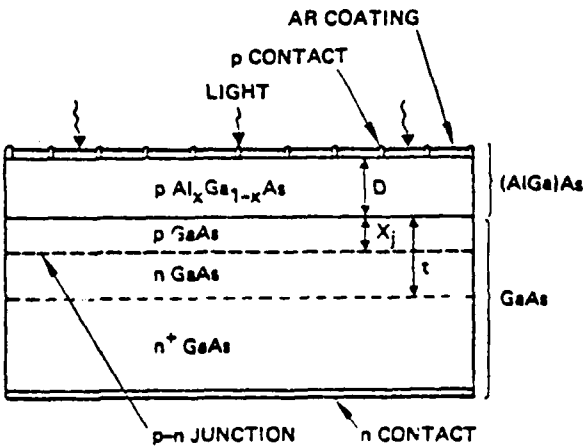
GaAs has a large optical absorption constant and a short diffusion length; essentially, all the photovoltaic response is close to the GaAs surface. The radiation damage beyond this active region has a negligible effect on cell performance. Consequently, the reduction in the required minority carrier diffusion length and the relative shallowness of the active region are the key factors that can be exploited to make GaAs solar cells more radiation resistant. Data consistent with these observations is presented below.

\* Hughes Research Laboratories, Malibu, California  
\*\* J.P.L., Pasadena, California

### EXPERIMENTAL

Figure 1 shows the (AlGa)As-GaAs solar cell structure. The  $n^+$  concentration for the substrate is fixed at  $> 5 \times 10^{17} \text{ cm}^{-3}$  with Te as the dopant. The n buffer layer concentration is  $1 \times 10^{17} \text{ cm}^{-3}$ . (At this doping level, the open-circuit voltage is 1 V.) The thickness of this layer was fixed at 10  $\mu\text{m}$  or more because results indicated that the substrate visibility is minimized at a buffer layer thickness of 10  $\mu\text{m}$ . A thickness less than this is not always sufficient to remove the effect of the substrate on cell performance.

7645-6



NUMBER OF FINGERS = 24

p CONTACT: Au-Zn-Ag

n CONTACT: Au-Ge-Ni-Ag

AR COATING:  $Ta_2O_5$

$p Al_xGa_{1-x}As: X \geq 0.95$

CELL SIZE =  $2 \times 2 \text{ CM}^2$

Figure 1. The (AlGa)As-GaAs solar cell

The window layer of  $(Al_xGa_{1-x})As$  is grown by LPE on GaAs. Our layer has  $x > 0.90$ , making the bandgap and hence the optical transmission as high as possible. The dopant is beryllium (Be). The concentration is  $1 \times 10^{18} \text{ cm}^{-3}$ . During  $(AlGa)As$  window layer growth, a p-n homojunction is formed by Be diffusion from the  $(AlGa)As$  layer into the n buffer layer. The carrier concentration of the p-diffused region is also  $1 \times 10^{18} \text{ cm}^{-3}$ .

The remaining parts of the baseline structure are self-explanatory. The Au-Zn contacts are about 3000 to 4000 Å with a silver overlay about 4 µm thick, and the n contact is AuGeNi (~ 5000 Å) with an Ag overlay. The AR coating is  $Ta_2O_5$ .

The Dynamitron particle accelerator at JPL was used as the electron source for high-energy electron irradiation; the irradiations were performed in vacuum at room temperature. The uniformity over the test plane was  $\pm 4\%$  with no areas of discontinuity. Fluxes and fluences were measured with a Faraday cup the current of which was integrated to establish electron fluences and to automatically stop the irradiation at the desired fluence levels.

High-energy proton irradiation was performed at the Crocker Nuclear Laboratory at the University of California at Davis. This cyclotron can produce a primary proton beam at energies between approximately 8 and 68 MeV. The solar cells were mounted with small pieces of double-face masking tape to aluminum plates. Each plate was irradiated separately in air at specific proton energies and fluences.\* The fluence over the target plane was uniform within  $\pm 5\%$ . The cell temperature during irradiation was kept at 30°C.

The full matrix of tests performed on the  $(AlGa)As$ -GaAs solar cells and on several representative silicon solar cells are given in Tables 1 and 2.

Table 1. Electron Irradiation Experiments

ELECTRON ENERGY MeV	ELECTRON FLUENCE E/cm <sup>2</sup>	TYPE AND NUMBER OF CELLS		
		(AlGa)As-GaAs	Si CONVENTIONAL	Si HIGH EFFICIENCY
1.0	$1 \times 10^{13}$	3	3	3
	$4 \times 10^{14}$	3	3	3
	$1 \times 10^{15}$	3	3	3
	$5 \times 10^{15}$	3	3	3
	$1 \times 10^{16}$	3	3	3
0.7	$1 \times 10^{15}$	2		
1.9	$1 \times 10^{15}$	2		

\*By comparing the results from previous solar cells irradiated both in air and in vacuum, we found that the ionized gases in air surrounding the cell during irradiation have no effect on the cells.

Table 2. High-Energy Proton Irradiation Experiments

7545-5

ELECTRON ENERGY MeV	ELECTRON FLUENCE E/cm <sup>2</sup>	TYPE AND NUMBER OF CELLS		
		(AlGa)As-GaAs	Si HIGH EFFICIENCY	Si CONVENTIONAL
15.4	$5 \times 10^{10}$	3	5	4
15.4	$5 \times 10^{11}$	3	4	4
22	$5 \times 10^{10}$	3	2	3
22	$5 \times 10^{11}$	3	2	3
30	$5 \times 10^{10}$	3	2	3
30	$5 \times 10^{11}$	3	2	3
40	$5 \times 10^{10}$	3	2	3
40	$5 \times 10^{11}$	3	2	3

## RESULTS AND DISCUSSION

### Electron Damage

A group of cells were fabricated early in the program for electron radiation tests. These cells were designed to have high efficiency with no attempt at optimizing the design parameters to increase radiation hardness. Figure 2 shows the maximum power obtained from the cells plotted against 1 MeV electron radiation fluence. These results were then compared with those for two types of silicon cells as shown in Table 1. This showed the need to improve these early cells for better resistance to electron radiation damage at fluences in excess of  $4 \times 10^{14}/\text{cm}^2$ .

Figure 3 shows the spectral response before and after electron irradiation. The results show that in these cells the spectral response in the short wavelength region shows greater damage compared to the longwavelength region. Since the optical absorption coefficient is greater for short wave lengths, most of the absorption in this region will be close to the surface of the cell. The photo generated carriers, therefore, must travel farther to reach the junction than do those generated by longer wavelengths. We suspected from the spectral response of the damaged cells that their junctions had to be relatively deep compared to the minority carrier diffusion length in the damaged layer. Our suspicion was confirmed by the measured junction depth of  $> 1 \mu\text{m}$ . These observation led us to examine the influence of the junction depth on radiation damage more carefully.

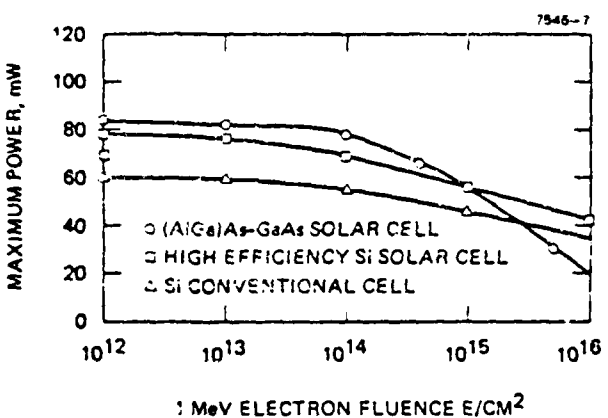


Figure 2. Maximum power as a function of 1 MeV electron fluence

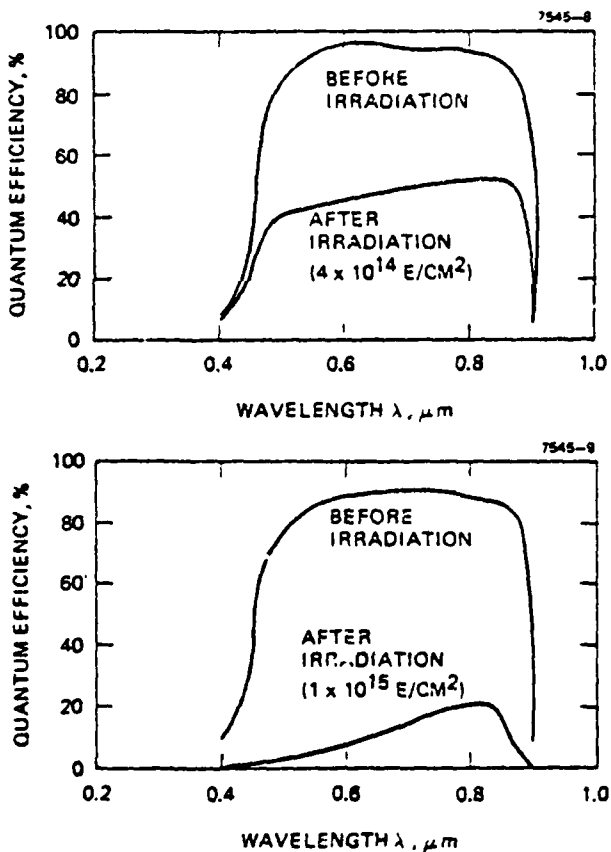


Figure 3. (AlGa)As-GaAs solar cell spectral response before and after 1 MeV electron irradiation

To correlate theory and experiments, Figure 4 shows the (AlGa)As-GaAs solar cell short circuit current density as a function of 1 MeV electron radiation fluence. The continuous curve represents the normalized experimental values.

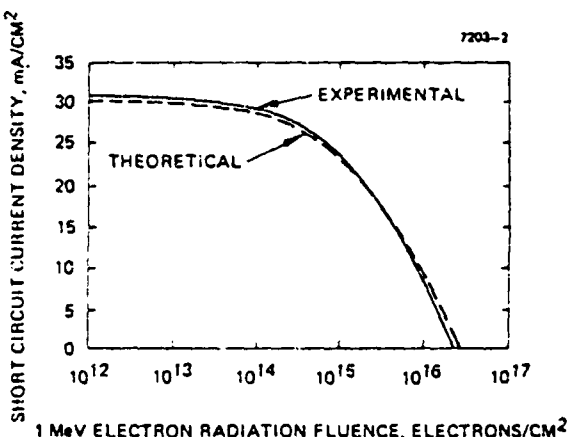


Figure 4. Short circuit current density versus 1 MeV electron radiation fluence, electrons/cm<sup>2</sup>

line is the theoretical curve. Both curves correspond to an (AlGa)As layer thickness of 1  $\mu\text{m}$  and a junction depth of 1  $\mu\text{m}$ . For calculating the theoretical curve, the minority carrier diffusion length  $L$  was related to the fluence  $\phi$  by the usual relation:

$$\frac{1}{L^2} = \frac{1}{L_0^2} + K_L \phi. \quad (1)$$

The initial diffusion lengths for holes ( $L_{po}$ ) and electrons ( $L_{no}$ ) were assumed to be 2 and 5  $\mu\text{m}$ , respectively in these calculations. The damage constant  $K_L$  for the diffusion length used for both p- and n-type GaAs was deduced by matching the theoretical curve to the experimental curve as shown in Figure 4. It was found to be  $K_L = 7 \times 10^{-6}$ , assuming the same value of  $K_L$  for the n- and p-doped GaAs.

Using this value for  $K_L$ , the short-circuit density was calculated for several junction depths as a function of a 1 MeV electron fluence. The results, shown in Figure 5, show that radiation damage decreases as junction depth decreases.

Based on this analysis, we proceeded to fabricate a second-generation of (AlGa)As-GaAs solar cells with the goal of decreased sensitivity to the radiation environment. The window layer thickness was made at 0.5  $\mu\text{m}$  while the junction depth was decreased to  $\sim 0.5 \mu\text{m}$  by readjusting the LPE layer growth parameters.

Figure 6 shows the measured short-circuit current of these shallower junction cells versus 1 MeV electron fluence. The experimentally observed improved radiation resistance is in good agreement

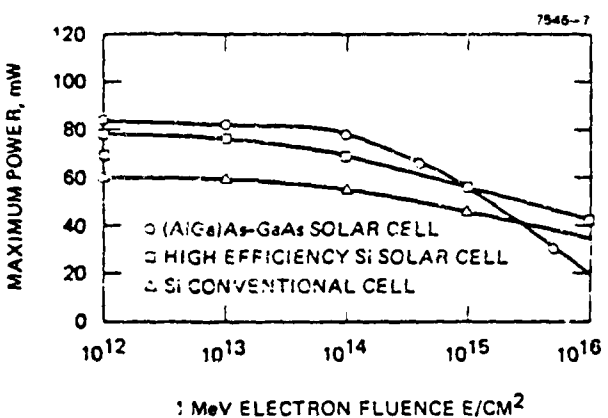


Figure 2. Maximum power as a function of 1 MeV electron fluence

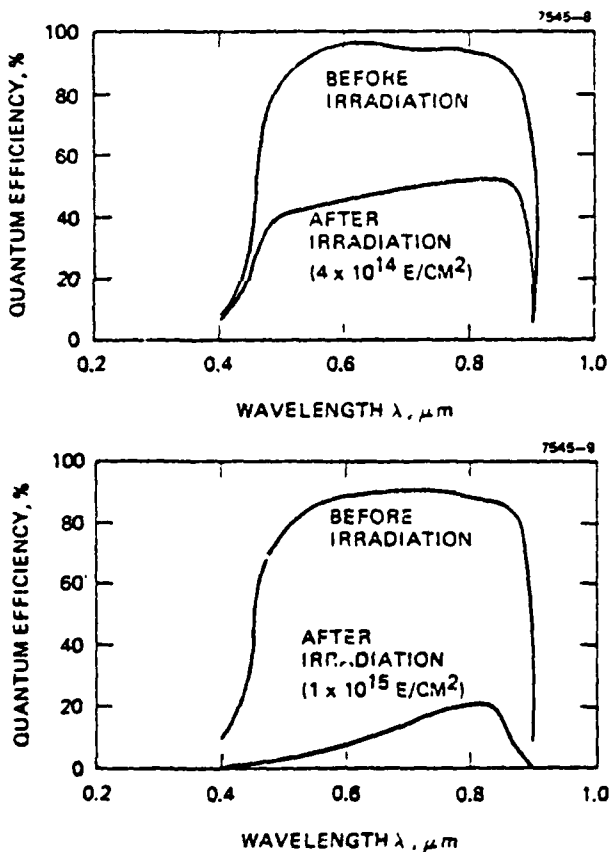


Figure 3. (AlGa)As-GaAs solar cell spectral response before and after 1 MeV electron irradiation

To correlate theory and experiments, Figure 4 shows the (AlGa)As-GaAs solar cell short circuit current density as a function of 1 MeV electron radiation fluence. The continuous curve represents the normalized experimental values.

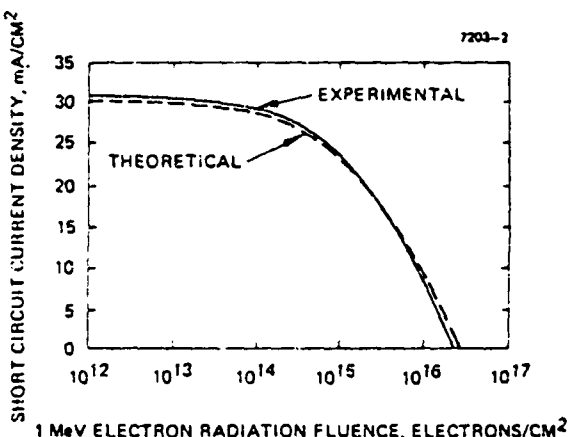


Figure 4. Short circuit current density versus 1 MeV electron radiation fluence, electrons/cm<sup>2</sup>

line is the theoretical curve. Both curves correspond to an (AlGa)As layer thickness of 1  $\mu\text{m}$  and a junction depth of 1  $\mu\text{m}$ . For calculating the theoretical curve, the minority carrier diffusion length  $L$  was related to the fluence  $\phi$  by the usual relation:

$$\frac{1}{L^2} = \frac{1}{L_0^2} + K_L \phi. \quad (1)$$

The initial diffusion lengths for holes ( $L_{po}$ ) and electrons ( $L_{no}$ ) were assumed to be 2 and 5  $\mu\text{m}$ , respectively in these calculations. The damage constant  $K_L$  for the diffusion length used for both p- and n-type GaAs was deduced by matching the theoretical curve to the experimental curve as shown in Figure 4. It was found to be  $K_L = 7 \times 10^{-6}$ , assuming the same value of  $K_L$  for the n- and p-doped GaAs.

Using this value for  $K_L$ , the short-circuit density was calculated for several junction depths as a function of a 1 MeV electron fluence. The results, shown in Figure 5, show that radiation damage decreases as junction depth decreases.

Based on this analysis, we proceeded to fabricate a second-generation of (AlGa)As-GaAs solar cells with the goal of decreased sensitivity to the radiation environment. The window layer thickness was made at 0.5  $\mu\text{m}$  while the junction depth was decreased to  $\sim 0.5 \mu\text{m}$  by readjusting the LPE layer growth parameters.

Figure 6 shows the measured short-circuit current of these shallower junction cells versus 1 MeV electron fluence. The experimentally observed improved radiation resistance is in good agreement

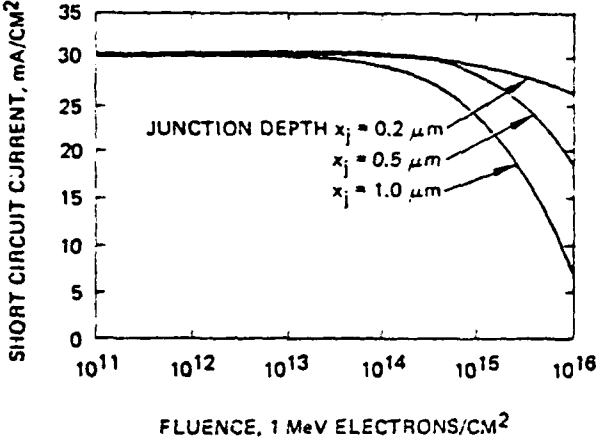


Figure 5. Predicted (AlGa)As-GaAs solar cell short circuit current density versus 1 MeV electron radiation fluence ((AlGa)As layer thickness = 1.0  $\mu m$ , initial diffusion length  $L_{po} = 2 \mu m$ ,  $L_{n0} = 5 \mu m$ , and diffusion length damage constant  $K_L = 7 \times 10^{-8}$ )

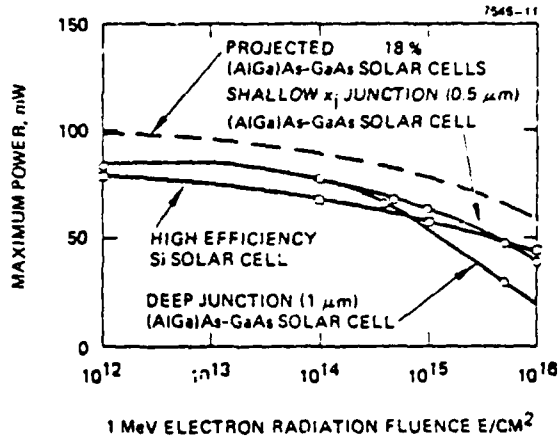


Figure 7. Maximum output power versus 1 MeV electron fluence

The spectral response of the deep-junction and shallower junction cells, both before and after irradiation, are given in Figure 8(a and b). The figure shows that the radiation damage in the deeper junction cells is concentrated in the short-wavelength region, whereas the shallower junction causes the damage to shift to the longer wavelength. This is consistent with our observation that the collection of minority carriers in the p region is not much affected up to the fluence at which the electron diffusion length is reduced to less than the p layer thickness.

Figure 8(c) shows the spectral response of the shallower junction solar cells irradiated at fluences  $1 \times 10^{15} e/cm^2$  with electron energies varying from 0.7 MeV to 1.9 MeV. As expected at higher energies, these cells show more degradation, probably because  $K_L$  increases with increasing electron energy. Figure 9 shows typical dark current-voltage (I-V) characteristics before and after electron irradiation. Although solar cells become more leaky after irradiation, the basic transport mechanism remains the same (as shown by the I-V curves, which remain parallel to each other). This increased leakage current probably results from an increase in the number of recombination centers at the junction.

#### High Energy Proton Damage

Twenty-four (AlGa)As-GaAs solar cells and several representative silicon cells were irradiated with 15.4 MeV to 40 MeV protons at fluences of  $5 \times 10^{10}$  and  $5 \times 10^{11} p/cm^2$  (Table 2).

The baseline structure of the solar cell used for proton irradiation was the same as that of the corresponding solar cell used for electron

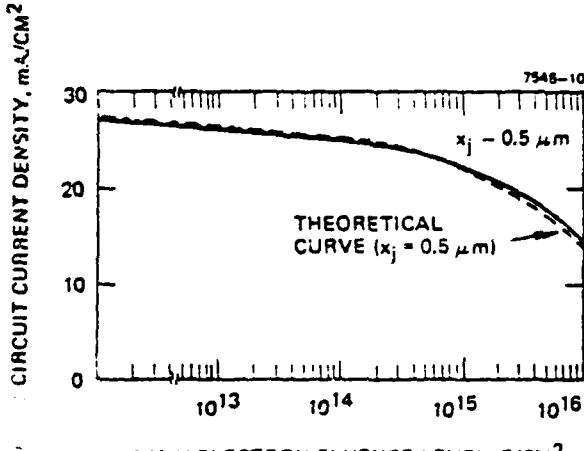


Figure 6. Short circuit current versus electron fluence level (1 MeV)

Figure 7 shows the spectral response of the (AlGa)As-GaAs solar cells with different junction depths before and after electron irradiation. The spectral response of the deep-junction cells is shifted to the shorter wavelength region, whereas the shallower junction cells show a shift to the longer wavelength.

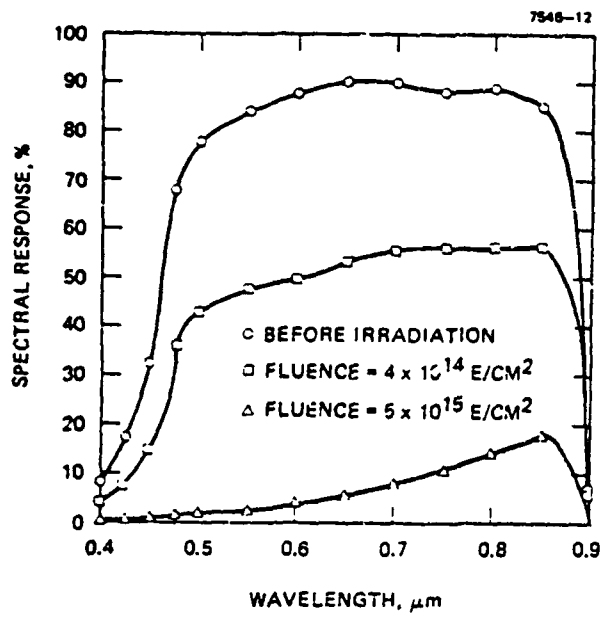


Figure 8(a). (AlGa)As-GaAs solar cell spectral response versus 1 MeV electron radiation fluences

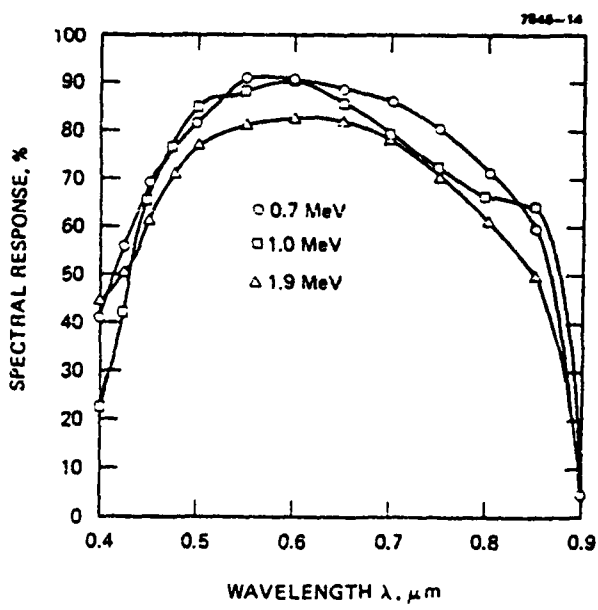


Figure 8(c). (AlGa)As-GaAs solar cell spectral response for several electron energies

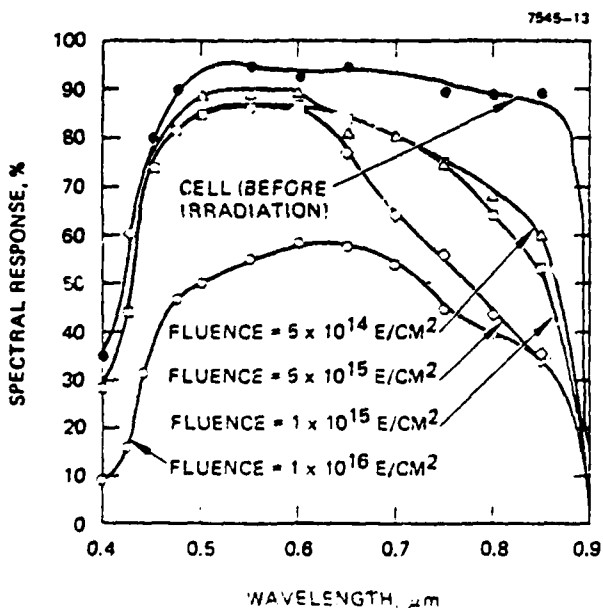


Figure 8(b). (AlGa)As-GaAs solar cell spectral response versus 1 MeV electron radiation fluence

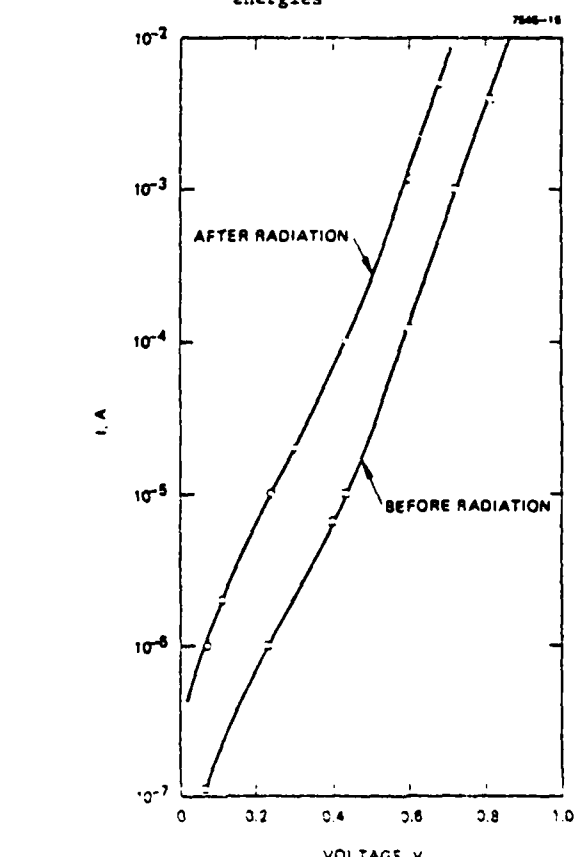


Figure 9. Dark I-V characteristics before and after electron irradiation

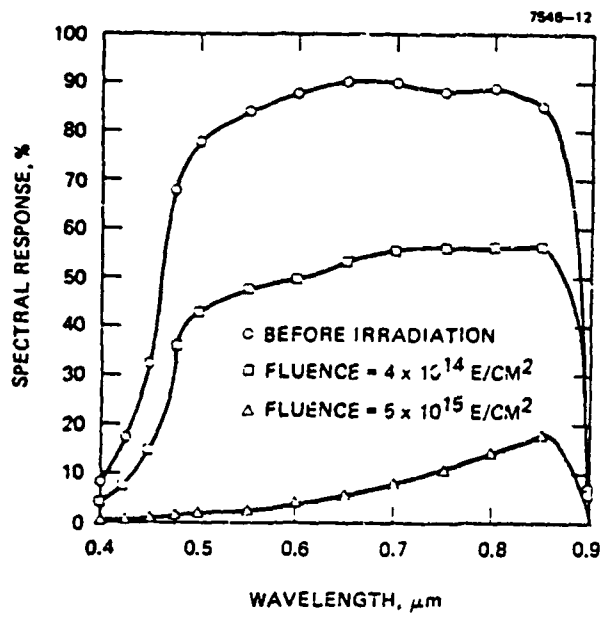


Figure 8(a). (AlGa)As-GaAs solar cell spectral response versus 1 MeV electron radiation fluences

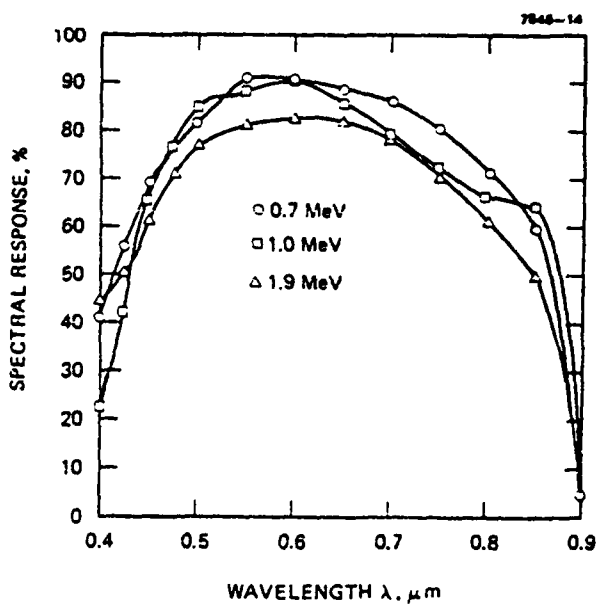


Figure 8(c). (AlGa)As-GaAs solar cell spectral response for several electron energies

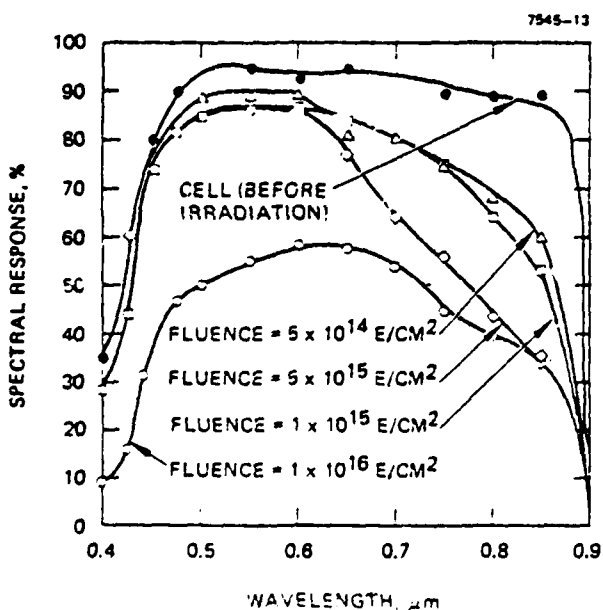


Figure 8(b). (AlGa)As-GaAs solar cell spectral response versus 1 MeV electron radiation fluence

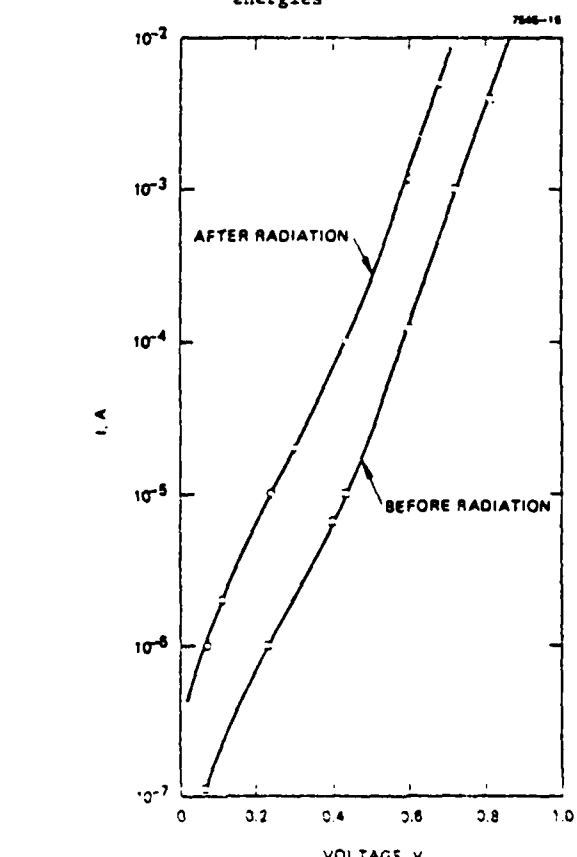


Figure 9. Dark I-V characteristics before and after electron irradiation

irradiation, except that no cover glass was applied to these cells.

The results of these proton irradiation tests are summarized in Figure 10 (a and b), which shows the maximum solar cell output power versus proton irradiation fluence for the three types of cells specified in Table 2. The (AlGa)As-GaAs solar cells are more resistant to high-energy proton radiation damage than the silicon cells. The dotted lines plotted in Figure 10 are extrapolations of our test results; these show the effect expected from proton fluence on an improved (AlGa)As-GaAs solar cell with a beginning-of-life AMO power-conversion efficiency of 18%. This extrapolation is pertinent since the feasibility of an 18% efficiency has already been demonstrated for this type of cell.

Figures 11 and 12 show the average spectral response of the (AlGa)As-GaAs solar cells before and after proton irradiation with proton energies of 15.4 MeV and 40 MeV, respectively. The spectral response in the short wavelength region of these shallow-junction solar cells is almost insensitive to the proton irradiation. A slight decrease in the solar cell spectral response occurs only in the long wavelength region.

Figure 13 shows the dark I-V characteristic before and after irradiation. Again, just as in the case of electron irradiation, the solar cell junction becomes slightly leaky due to the increasing number of recombination centers produced by proton irradiation although the basic transport mechanism remains unchanged.

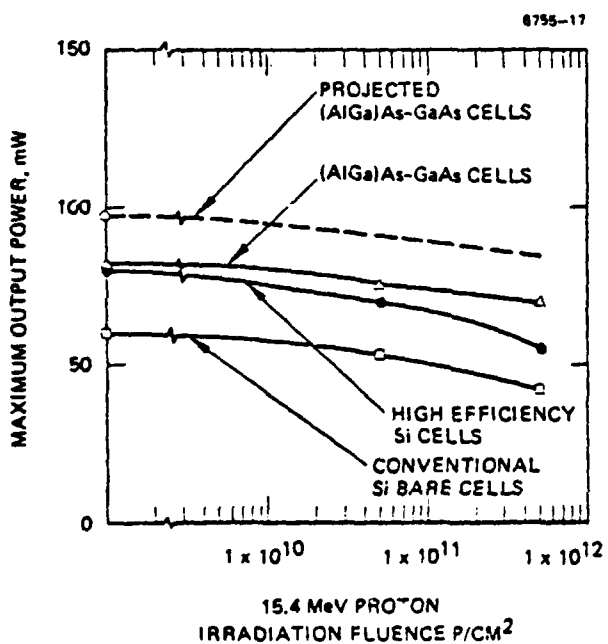


Figure 10(a). Solar cell maximum output power versus 15.4 MeV proton irradiation fluence.

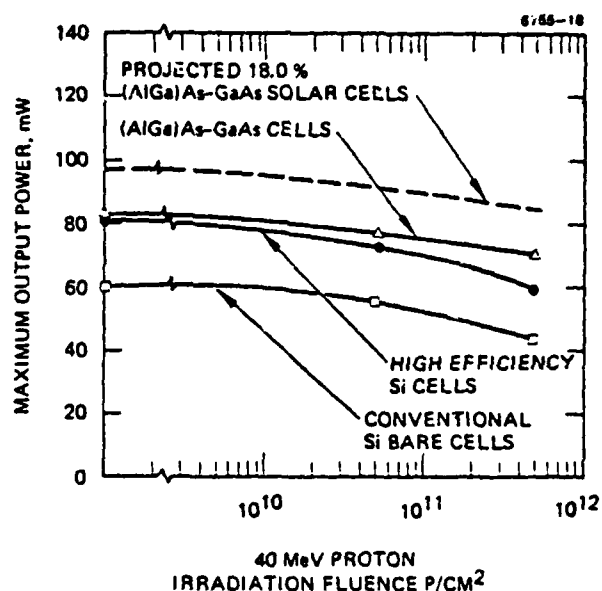


Figure 10(b). Solar cell maximum output power versus 40 MeV proton irradiation fluence

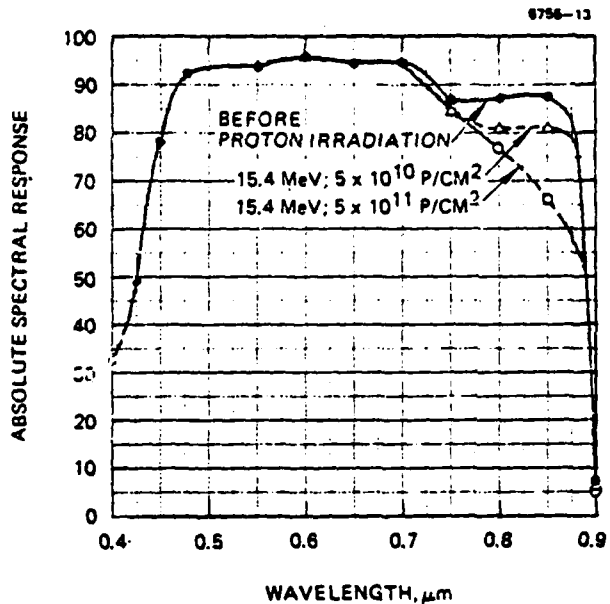


Figure 11. (AlGa)As-GaAs solar cell spectral response before and after 15.4 MeV proton irradiation

#### Radiation Annealing Studies

GaAs solar cells damaged by radiation recover their efficiency when annealed at low temperatures

irradiation, except that no cover glass was applied to these cells.

The results of these proton irradiation tests are summarized in Figure 10 (a and b), which shows the maximum solar cell output power versus proton irradiation fluence for the three types of cells specified in Table 2. The (AlGa)As-GaAs solar cells are more resistant to high-energy proton radiation damage than the silicon cells. The dotted lines plotted in Figure 10 are extrapolations of our test results; these show the effect expected from proton fluence on an improved (AlGa)As-GaAs solar cell with a beginning-of-life AMO power-conversion efficiency of 18%. This extrapolation is pertinent since the feasibility of an 18% efficiency has already been demonstrated for this type of cell.

Figures 11 and 12 show the average spectral response of the (AlGa)As-GaAs solar cells before and after proton irradiation with proton energies of 15.4 MeV and 40 MeV, respectively. The spectral response in the short wavelength region of these shallow-junction solar cells is almost insensitive to the proton irradiation. A slight decrease in the solar cell spectral response occurs only in the long wavelength region.

Figure 13 shows the dark I-V characteristic before and after irradiation. Again, just as in the case of electron irradiation, the solar cell junction becomes slightly leaky due to the increasing number of recombination centers produced by proton irradiation although the basic transport mechanism remains unchanged.

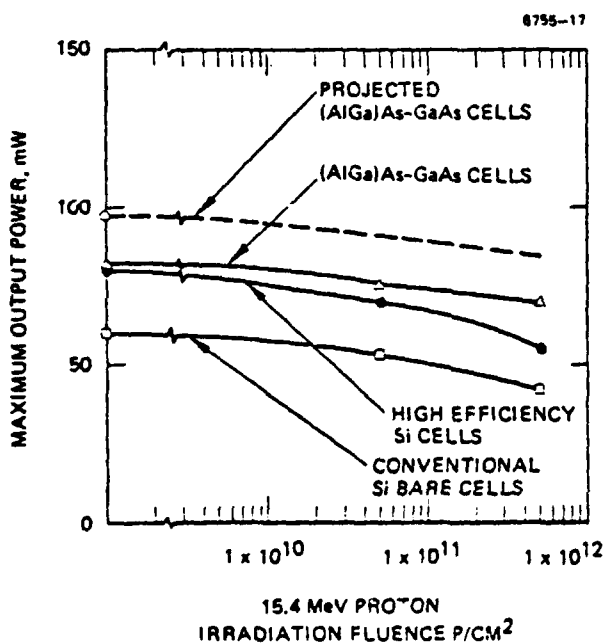


Figure 10(a). Solar cell maximum output power versus 15.4 MeV proton irradiation fluence.

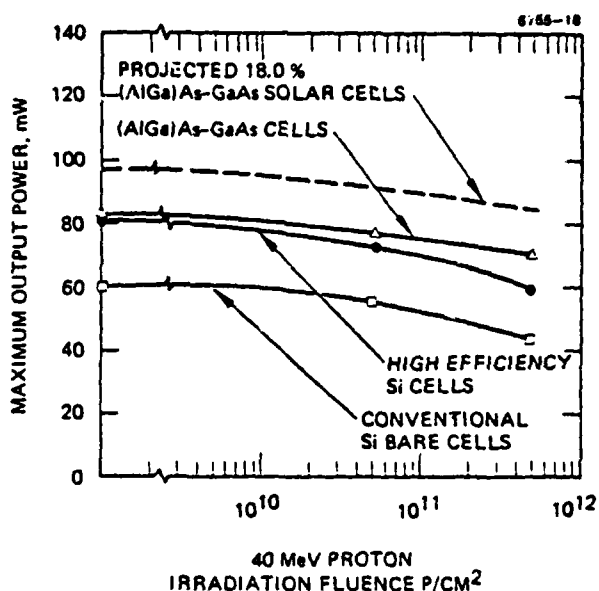


Figure 10(b). Solar cell maximum output power versus 40 MeV proton irradiation fluence

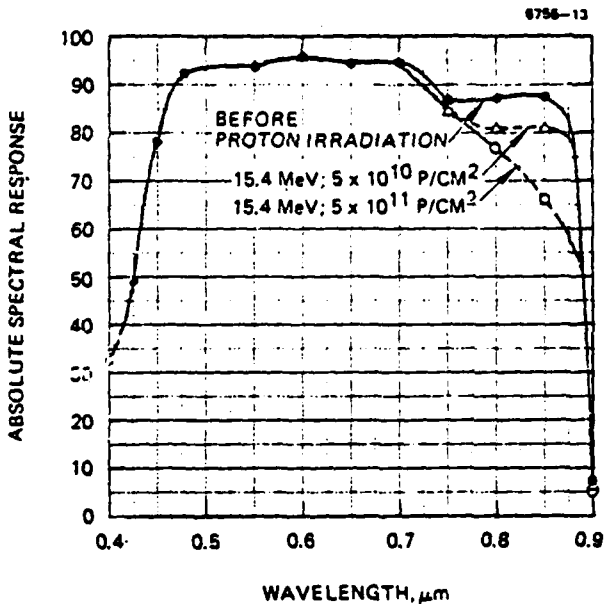


Figure 11. (AlGa)As-GaAs solar cell spectral response before and after 15.4 MeV proton irradiation

#### Radiation Annealing Studies

GaAs solar cells damaged by radiation recover their efficiency when annealed at low temperatures

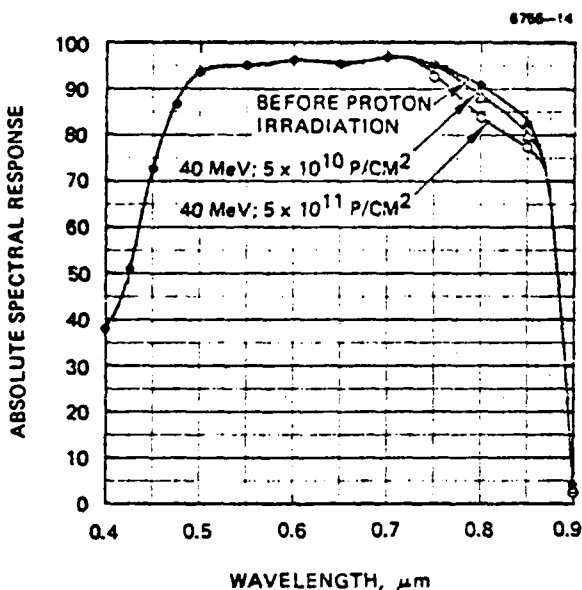


Figure 12. (AlGa)As-GaAs solar cell spectral response before and after 40 MeV proton irradiation

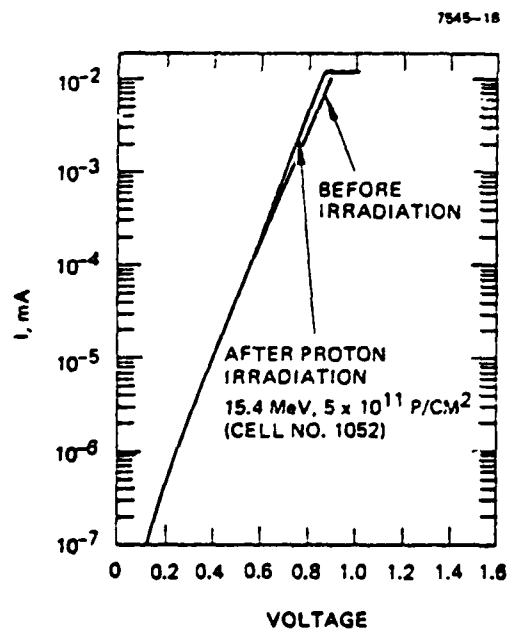


Figure 13. Dark I-V characteristics before and after proton irradiation

Figure 13. Dark I-V characteristics before and after proton irradiation

on the order of 200°C to 300°C (3,4). Some preliminary thermal annealing experiments on the radiation-damaged (AlGa)As-GaAs solar cells were

performed in our laboratory. The cells were irradiated at fluences of  $1 \times 10^{15}/\text{cm}^2$  with electron energies varying from 0.7 MeV through 1.0 MeV to 1.9 MeV. Subsequently, they were annealed in vacuum at temperatures of over 200°C. Figure 14 shows the effect of annealing as a function of annealing time and temperatures.

Figure 15 compares the spectral response of these cells after the annealing step with the spectral response before and after electron irradiation. The long wavelength region shows significant recovery. This suggests that the annealing leads to a significant recovery in the minority carrier diffusion length in GaAs after radiation damage.

Figure 16 shows the dark I-V characteristics of these cells. These cells show leaky p-n junctions after irradiation; however, they almost completely recover to their pre-irradiation condition after annealing at 210°C. These results indicate that (AlGa)As-GaAs solar cells can be annealed at practical temperatures to remove radiation damage. This could be exploited for longer space missions.

#### CONCLUSION AND SUMMARY

Several 2 cm x 2 cm (AlGa)As-GaAs cells were subjected to radiation damage studies using both electrons and protons. The results show that:

- (AlGa)As-GaAs solar cells can be made more resistant to radiation damage than can silicon cells for both electron and proton irradiation.
- The junction depth is a sensitive parameter in determining radiation resistance.
- The (AlGa)As-GaAs solar cells suffer only a moderate amount of degradation at proton energies above 15.4 MeV.
- The efficiencies of electron-radiation-damaged (AlGa)As-GaAs solar cells recover when annealed at temperatures as low as 200°C to 300°C.

#### ACKNOWLEDGMENT

The radiation damage studies reported here were supported in part by contracts from NASA Langley, Contract NAS 1-14727

#### REFERENCES

1. J.M. Woodall and H.J. Hovel, "An Isothermal Etchback - Regrowth Method for High Efficiency GaAlAs-GaAs Solar Cells," *Appl. Phys. Lett.* 30, 492 (1977).
2. R.I. Moon, et al., "Performance of (AlGa)As-GaAs Solar Cells in the Space Environment," 12th IEEE Photovoltaic Specialists Conference, 255 (1975).
3. R.S. Miller and J.S. Harris, "Gallium Arsenide Concentration System," presented at the AIAA Conference on the Future of Aerospace Power System, March 1977.
4. G.H. Walker and E.J. Conway, "Annealing of GaAs Solar Cells Damaged by Electron Irradiation," *J. of Electrical Chemical Society*, Vol. 125, No. 4, p. 576, 1978.

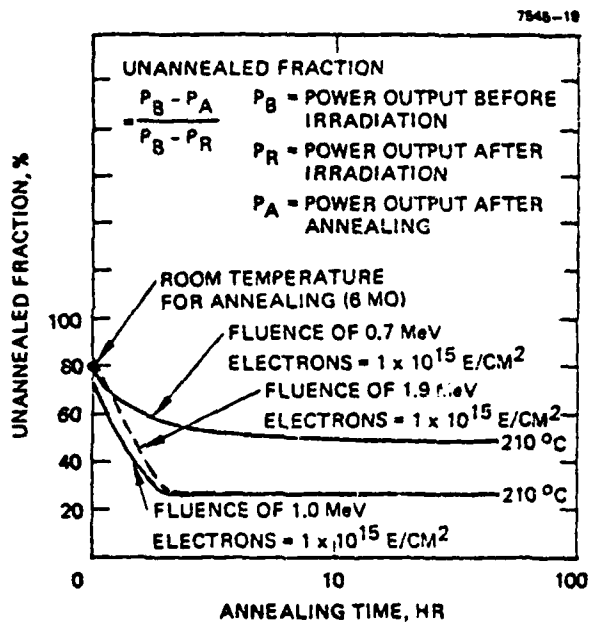


Figure 14. Unannealed fraction versus annealing time

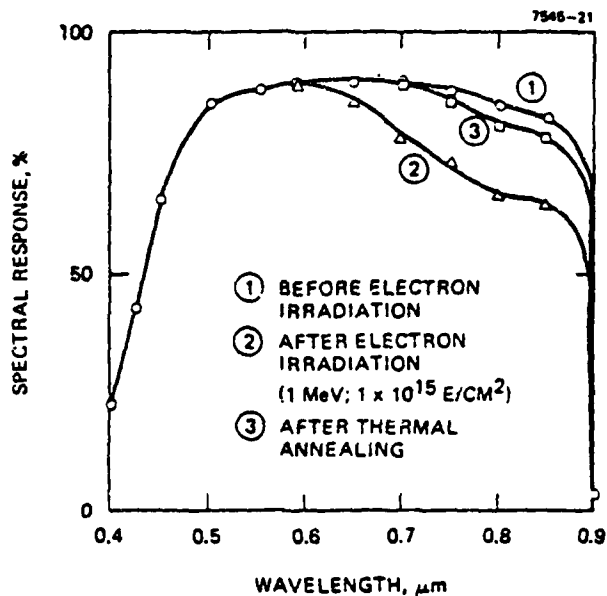


Figure 15(b). Spectral response before and after thermal annealing cell #1008

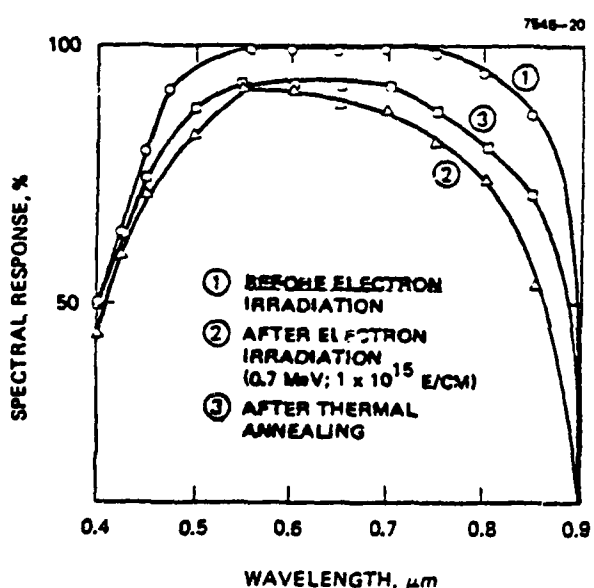


Figure 15(a). Spectral response before and after thermal annealing Call #1222

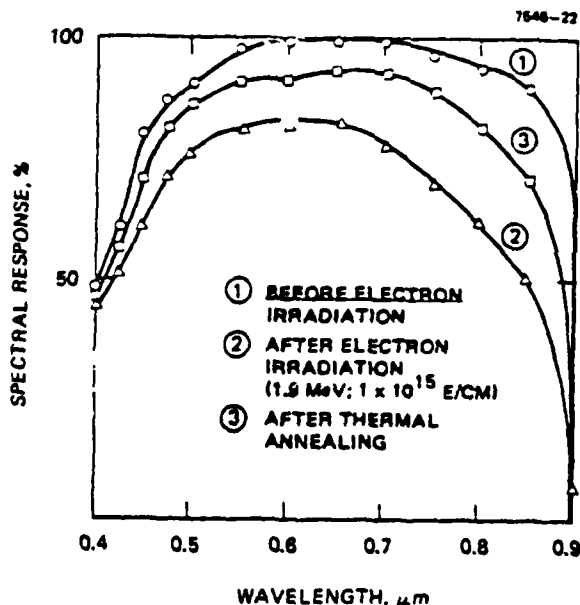


Figure 15(c). Spectral response before and after irradiation and after annealing cell #1278

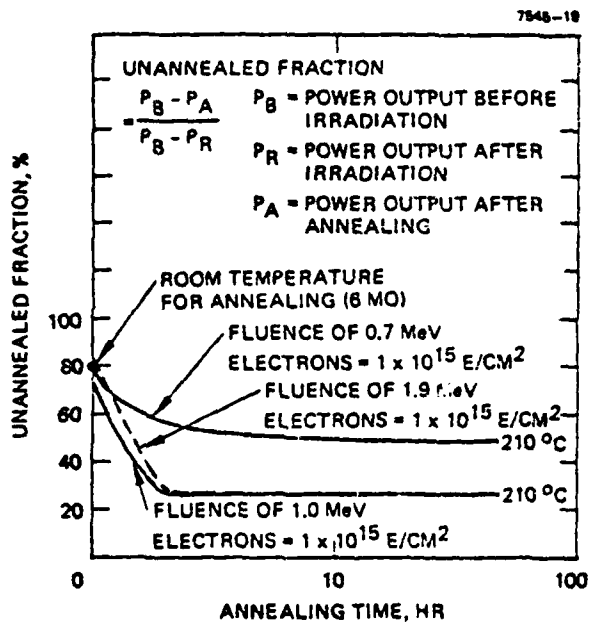


Figure 14. Unannealed fraction versus annealing time

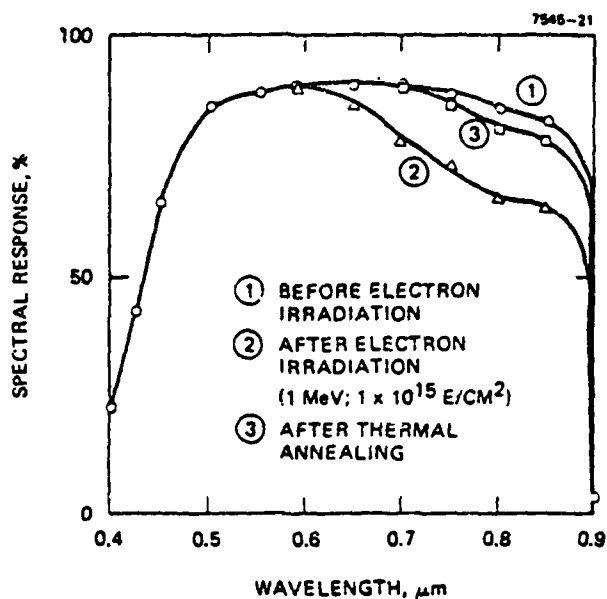


Figure 15(b). Spectral response before and after thermal annealing cell #1008

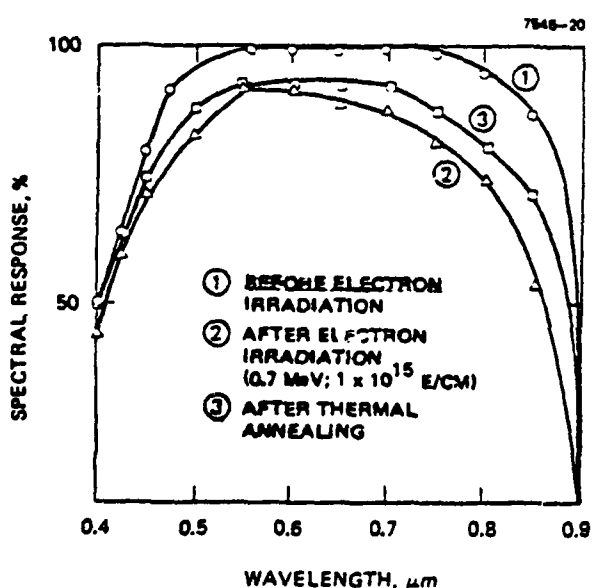


Figure 15(a). Spectral response before and after thermal annealing Call #1222

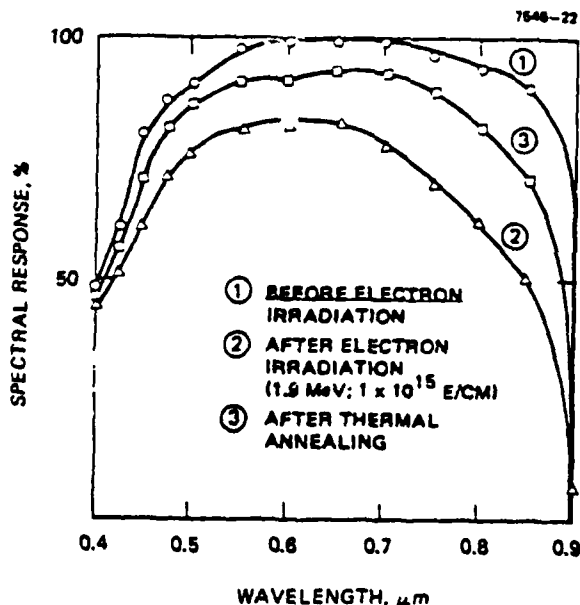


Figure 15(c). Spectral response before and after irradiation and after annealing cell #1278

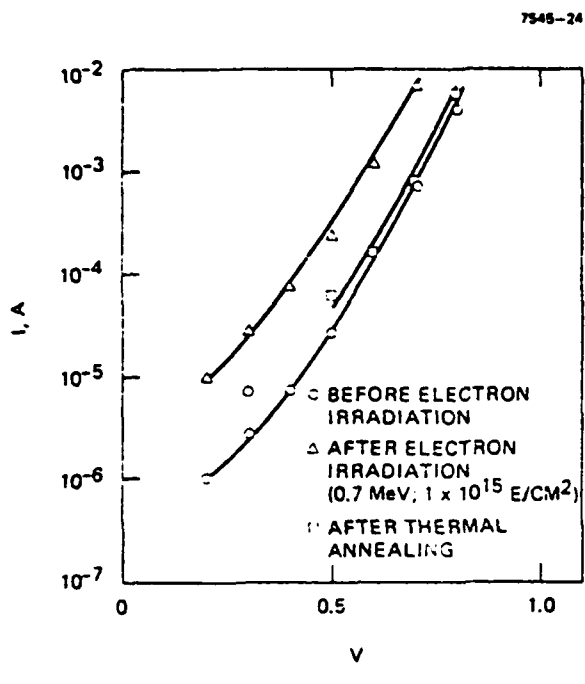


Figure 16(a). Dark I-V characteristic before and after thermal annealing cell #1222

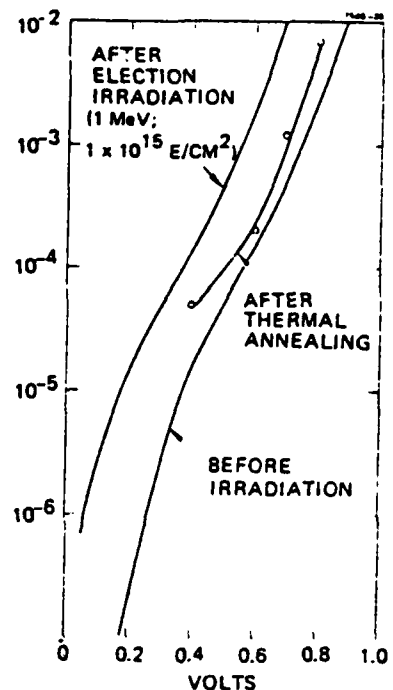


Figure 16(b). Dark I-V characteristic before and after thermal annealing cell #1008

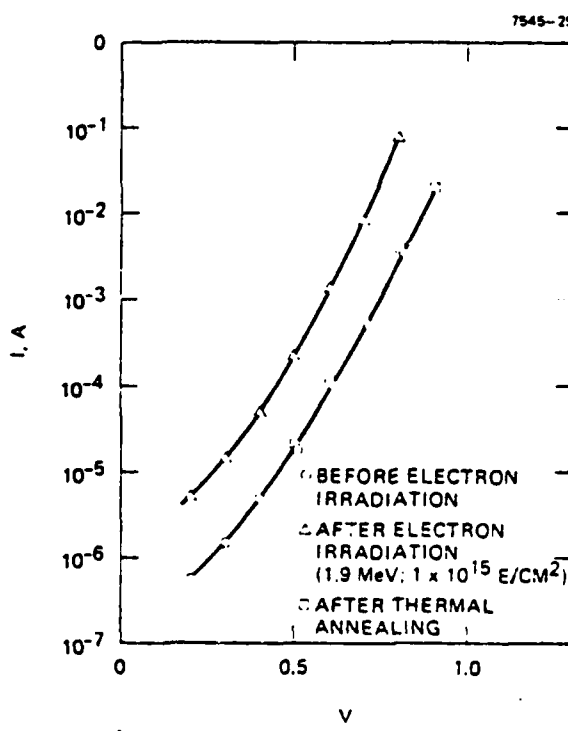


Figure 16(c). Dark I-V characteristic before and after thermal annealing cell #1273

APPENDIX B. GaAs MANUFACTURING CONTROL DOCUMENTATION

PRECEDING PAGE BLANK-NOT FILMED

APPENDIX B. GaAs MANUFACTURING CONTROL DOCUMENTATION

PRECEDING PAGE BLANK-NOT FILMED

## LISTING OF PROCEDURES

1. Gallium Arsenide Inspection
2. Gallium Arsenide Substrate Sizing
3. Gallium Arsenide Cleaning and Etching Substrate
4. Gallium Arsenide Slide Bar Load
5. Gallium Arsenide Reactor Load
6. Gallium Arsenide Buffer Layer Reactor Run
7. Gallium Arsenide Reactor Unload
8. Gallium Arsenide Slide Bar Unload
9. Gallium Arsenide Buffer Layer Measurement and Inspection
10. Gallium Arsenide Substrate Preparation for Window Layer
11. Gallium Arsenide Reactor Run - Window Layer
12. Gallium Arsenide Window Layer Anneal
13. Gallium Arsenide AuZn Sputtered Front Contact
14. Gallium Arsenide Evaporated Front Contact
15. Gallium Arsenide Evaporated Back Contact
16. Gallium Arsenide Sintered Contacts
17. Gallium Arsenide Antireflective Coating

PRECEDING PAGE BLANK-NOT FILMED

## LISTING OF PROCEDURES

1. Gallium Arsenide Inspection
2. Gallium Arsenide Substrate Sizing
3. Gallium Arsenide Cleaning and Etching Substrate
4. Gallium Arsenide Slide Bar Load
5. Gallium Arsenide Reactor Load
6. Gallium Arsenide Buffer Layer Reactor Run
7. Gallium Arsenide Reactor Unload
8. Gallium Arsenide Slide Bar Unload
9. Gallium Arsenide Buffer Layer Measurement and Inspection
10. Gallium Arsenide Substrate Preparation for Window Layer
11. Gallium Arsenide Reactor Run - Window Layer
12. Gallium Arsenide Window Layer Anneal
13. Gallium Arsenide AuZn Sputtered Front Contact
14. Gallium Arsenide Evaporated Front Contact
15. Gallium Arsenide Evaporated Back Contact
16. Gallium Arsenide Sintered Contacts
17. Gallium Arsenide Antireflective Coating

PRECEDING PAGE BLANK-NOT FILMED

## PROCEDURE 1. GALLIUM ARSENIDE INSPECTION

**SCOPE:** This procedure describes the inspection and identification of incoming GaAs substrates as delivered by the vendor for suitability for further processing.

### 1.1 Preliminary Operations

- 1.1.1 Substrates arrive from vendor in glassine (2-3/16 by 2-1/8 inches) bags identified with numbers corresponding to the slide or cut from the GaAs ingot. Transport all substrates into the plastic substrate holder boxes (5-5/16 by 2-3/4 by 2-1/2 inches) in the order that they were sliced. Use a separate box for each ingot.
- 1.1.2 From the invoice accompanying the substrates record the supplier's name, the ingot number, dopant species, level of dopant, and the total number of wafers cut from the ingots into a label (1-1/2 by 3 inches) and attach to the face of the substrate holder box parallel to the surface of the substrates inside.

### 1.2 Visual Inspection

- 1.2.1 Using plastic tweezers, remove the first substrate from its glassine envelope and inspect both sides for obvious flaws: over the major working area of the substrate: breakage, cracks, dislocations, gross imperfections, discoloration, excessively small size, etc.
- 1.2.2 If neither side is acceptable, replace the substrate into the glassine envelope and place in a separate substrate holder box with a label marked "rejects."
- 1.2.3 Repeat procedure for all substrates.

### 1.3 Microscopic Inspection

- 1.3.1 Using plastic tweezers, remove the first substrate from its glassine envelope and place on the x-y stage of the microscope.
- 1.3.2 Move the substrate in the x and y directions to examine the entire surface for flaws.
- 1.3.3 Repeat procedure for all substrates.
- 1.3.4 Remove the boxes of cells to the area designated for cleaving.

## PROCEDURE 2. GALLIUM ARSENIDE SUBSTRATE SIZING

SCOPE: This procedure describes the cleaving of GaAs substrates into units capable of fitting the liquid phase epitaxy slide bar.

### 2.1 Preliminary Operations

- 2.1.1 Take a self-adhering label (1 by 1/2 inch) and fold it over onto the uppermost part of the stem of the glass basket substrate merger. Label the flag with the numeral "1".
- 2.1.2 Repeat procedure for four separate glass baskets. Number them consecutively 1, 2, 3 and 4.

### 2.2 Cell Identification

- 2.2.1 Take the first glassine envelope and remove the substrate, using plastic tweezers.
- 2.2.2 Add the following information to the glassine envelope: supplier's name, ingot number, the date, and the letter "a", which corresponds to the first side of the four-sided slide bar (with sides designated a, b, c, and d) into which the substrate will be mounted.

### 2.3 Substrate Cleaving

- 2.3.1 Place the substrate, good side upwards, onto the glass slide.
- 2.3.2 Align.
- 2.3.3 Using the diamond point scribe, scratch a line onto the excess substrate material.
- 2.3.4 Using a blunt instrument, tap down onto the excess substrate. It will break along the edge of the glass slide sandwich.

### 2.4 Basket Loading

- 2.4.1 Using plastic tweezers, load the "a" substrate into the basket so that the good surface of the substrate faces (in the properly oriented basket) the operator.

### 2.5 Repeat Operations

- 2.5.1 Repeat procedures for three more substrates.

## PROCEDURE 2. GALLIUM ARSENIDE SUBSTRATE SIZING

SCOPE: This procedure describes the cleaving of GaAs substrates into units capable of fitting the liquid phase epitaxy slide bar.

### 2.1 Preliminary Operations

- 2.1.1 Take a self-adhering label (1 by 1/2 inch) and fold it over onto the uppermost part of the stem of the glass basket substrate merger. Label the flag with the numeral "1".
- 2.1.2 Repeat procedure for four separate glass baskets. Number them consecutively 1, 2, 3 and 4.

### 2.2 Cell Identification

- 2.2.1 Take the first glassine envelope and remove the substrate, using plastic tweezers.
- 2.2.2 Add the following information to the glassine envelope: supplier's name, ingot number, the date, and the letter "a", which corresponds to the first side of the four-sided slide bar (with sides designated a, b, c, and d) into which the substrate will be mounted.

### 2.3 Substrate Cleaving

- 2.3.1 Place the substrate, good side upwards, onto the glass slide.
- 2.3.2 Align.
- 2.3.3 Using the diamond point scribe, scratch a line onto the excess substrate material.
- 2.3.4 Using a blunt instrument, tap down onto the excess substrate. It will break along the edge of the glass slide sandwich.

### 2.4 Basket Loading

- 2.4.1 Using plastic tweezers, load the "a" substrate into the basket so that the good surface of the substrate faces (in the properly oriented basket) the operator.

### 2.5 Repeat Operations

- 2.5.1 Repeat procedures for three more substrates.

## PROCEDURE 3. GALLIUM ARSENIDE CLEANING AND ETCHING SUBSTRATE

SCOPE: This procedure describes the cleaning of the substrates just prior to loading into the slide bar assembly for subsequent liquid phase growth of the buffer layer.

### 3.1 Preliminary Operations

- 3.1.1 Prepare the etch solution.
- 3.1.2 Label five clean 300 ml pyrex beakers with the following: trichloroethylene, toluene, isopropyl alcohol, etch, and deionized water.
- 3.1.3 Fill each of the three solvent beakers with 225 ml of the appropriate solvent.
- 3.1.4 Fill the etch beaker with 225 ml from the 500 ml acid bottle.
- 3.1.5 Fill the beaker in the sink with deionized water.

### 3.2 Cleaning Procedure

- 3.2.1 Submerge together all four substrates into the trichloroethylene beaker for 3.0 minutes.
- 3.2.2 Submerge together all four substrates into the toluene beaker for 3.0 minutes and then dry.
- 3.2.3 Submerge together all four substrates into the isopropyl alcohol beaker for 3.0 minutes and then dry.
- 3.2.4 Submerge together all four substrates into the deionized water beaker and then dry.
- 3.2.5 Remove together all four substrates and without drying submerge together into the etch solution for 30 seconds.
- 3.2.6 Remove together all four substrates and without drying submerge together into the running deionized water for 2.0 minutes.

## PROCEDURE 4. GALLIUM ARSENIDE SLIDE BAR LOAD

SCOPE: This procedure describes the loading of the substrates into the slide bar and the proper assembly of the latter onto the slide bar holder.

### 4.1 Preliminary Operations

- 4.1.1 Ensure that the slide bars are oriented properly.
- 4.1.2 All graphite parts should have been thoroughly cleaned during the previous unloading procedure.

### 4.2 Lower Slide Bar Load

- 4.2.1 Loosen the head nut located at end of the rod of the slide bar holder.
- 4.2.2 Extend rod in order to open the first slide panel.
- 4.2.3 Insert the first substrate with good side up without touching the surface.
- 4.2.4 Center the substrate.
- 4.2.5 Close the slide panel.
- 4.2.6 Clamp substrate by gently pressing the pressure bar against the substrate and tightening with a screwdriver the appropriate graphite screw.
- 4.2.7 Insert the second substrate with the good side up in the same manner as the first.
- 4.2.8 Repeat procedures 4.2.4 through 4.2.6.
- 4.2.9 Close the slide panels.

### 4.3 Upper Slide Bar Load

- 4.3.1 Open the appropriate slide panel of the upper slide bar which covers the chamber for the third substrate.
- 4.3.2 Insert third substrate with good side up.
- 4.3.3 Center the substrate using plastic tweezers.

- 4.3.4 Close the slide panel.
- 4.3.5 Clamp substrate.
- 4.3.6 Insert fourth substrate with the good side up.
- 4.3.7 Repeat procedures 4.3.3 through 4.3.5.
- 4.3.8 Close the slide panels.

#### **4.4 Suspend Upper Slide Bar Upon Holder**

- 4.4.1 Align and gently push the upper slide bar onto the metal support posts extending from the slide bar holder.
- 4.4.2 Tighten with a screwdriver.
- 4.4.3 Replace the two graphite L-shaped plates.
- 4.4.4 Reinsert the four graphite thumbscrews.

#### **4.5 Slide Bar Assembly Test**

- 4.5.1 Loosen head nut.
- 4.5.2 Extend rod fully and ensure all four slide panels, G<sup>1</sup>, G<sup>2</sup>, G<sup>3</sup> and G<sup>4</sup>, open smoothly and fully.
- 4.5.3 Close slide panels by manipulating the rod.
- 4.5.4 Tighten head nut, H.

- 4.3.4 Close the slide panel.
- 4.3.5 Clamp substrate.
- 4.3.6 Insert fourth substrate with the good side up.
- 4.3.7 Repeat procedures 4.3.3 through 4.3.5.
- 4.3.8 Close the slide panels.

#### 4.4 Suspend Upper Slide Bar Upon Holder

- 4.4.1 Align and gently push the upper slide bar onto the metal support posts extending from the slide bar holder.
- 4.4.2 Tighten with a screwdriver.
- 4.4.3 Replace the two graphite L-shaped plates.
- 4.4.4 Reinsert the four graphite thumbscrews.

#### 4.5 Slide Bar Assembly Test

- 4.5.1 Loosen head nut.
- 4.5.2 Extend rod fully and ensure all four slide panels, G<sup>1</sup>, G<sup>2</sup>, G<sup>3</sup> and G<sup>4</sup>, open smoothly and fully.
- 4.5.3 Close slide panels by manipulating the rod.
- 4.5.4 Tighten head nut, H.

## PROCEDURE 5. GALLIUM ARSENIDE REACTOR LOAD

SCOPE: This procedure describes the insertion of the substrate loaded slide bar assembly into the buffer layer or window layer reactor for subsequent layer growth.

### 5.1 Preliminary Operations

- 5.1.1 Ensure that the slide rod is extended fully.
- 5.1.2 Ensure that the slide panels are fully closed.
- 5.1.3 Ensure that the star nut is tight.
- 5.1.4 Ensure that the layer reactor entry chamber port is open.

### 5.2 Slide Bar Assembly Load

- 5.2.1 Holding the slide bar assembly in a perfectly vertical position, insert the double slide bar section into the reactor entry chamber port until the face plate covers the port perfectly.
- 5.2.2 Flip up the three bolts and gradually tighten the three wing nuts.

## PROCEDURE 5. GALLIUM ARSENIDE REACTOR LOAD

SCOPE: This procedure describes the insertion of the substrate loaded slide bar assembly into the buffer layer or window layer reactor for subsequent layer growth.

### 5.1 Preliminary Operations

- 5.1.1 Ensure that the slide rod is extended fully.
- 5.1.2 Ensure that the slide panels are fully closed.
- 5.1.3 Ensure that the star nut is tight.
- 5.1.4 Ensure that the layer reactor entry chamber port is open.

### 5.2 Slide Bar Assembly Load

- 5.2.1 Holding the slide bar assembly in a perfectly vertical position, insert the double slide bar section into the reactor entry chamber port until the face plate covers the port perfectly.
- 5.2.2 Flip up the three bolts and gradually tighten the three wing nuts.

AD-A101 317

HUGHES AIRCRAFT CO LOS ANGELES CALIF SPACE AND COMMU--ETC F/6 10/2  
HIGH EFFICIENCY SOLAR PANEL, PHASE II, GALLIUM ARSENIDE.(U)  
MAR 81 B WOLFF, S S KAMATH, B J VENDURA F33615-77-C-3150  
HAC-SCB-00453R AFWAL-TR-80-212A M

UNCLASSIFIED

242  
243  
244

END  
DATE  
FOLDED:  
7-8-81  
DTIC

AD-A101 317

HUGHES AIRCRAFT CO LOS ANGELES CALIF SPACE AND COMMU--ETC F/6 10/2  
HIGH EFFICIENCY SOLAR PANEL, PHASE II, GALLIUM ARSENIDE.(U)  
MAR 81 B WOLFF, S S KAMATH, B J VENDURA F33615-77-C-3150  
HAC-SCB-00453R AFWAL-TR-80-212A M

UNCLASSIFIED

242  
243  
244

END  
DATE  
FOLDED:  
7-8-81  
DTIC

## PROCEDURE 6. GALLIUM ARSENIDE BUFFER LAYER REACTOR RUN

SCOPE: This procedure describes the operation of the liquid phase epitaxial reactor for growing the buffer layer.

### 6.1 Preliminary Operations

- 6.1.1 The buffer reactor must be periodically reprogrammed with each replenishing of melt material or dopant level.

### 6.2 Entry Chamber Evacuation

- 6.2.1 Open the vacuum valve.
- 6.2.2 Observe the vacuum gauge and wait until it reads -30 psi.
- 6.2.3 Close the vacuum valve.
- 6.2.4 Open the lower bypass valve. The vacuum gauge, V, should immediately register -8 psi. (Opening the lower bypass allows the lower chamber to fill with hydrogen).
- 6.2.5 Close the lower bypass valve.
- 6.2.6 Open the vacuum valve.
- 6.2.7 Observe the vacuum gauge and wait until it reads -30 psi.
- 6.2.8 Close the vacuum valve.
- 6.2.9 Open the lower bypass valve.
- 6.2.10 Open the flow valve to 2.0 psi and then tighten to maintain even flow.
- 6.2.11 Open the upper bypass valve.

### 6.3 Lowering the Double Slide Bars

- 6.3.1 Open the gate valve.
- 6.3.2 Loosen the star nut.
- 6.3.3 Lower the rod 5 or 6 inches.
- 6.3.4 Tighten the star nut and wait approximately 30 seconds.

## PROCEDURE 6. GALLIUM ARSENIDE BUFFER LAYER REACTOR RUN

SCOPE: This procedure describes the operation of the liquid phase epitaxial reactor for growing the buffer layer.

### 6.1 Preliminary Operations

- 6.1.1 The buffer reactor must be periodically reprogrammed with each replenishing of melt material or dopant level.

### 6.2 Entry Chamber Evacuation

- 6.2.1 Open the vacuum valve.
- 6.2.2 Observe the vacuum gauge and wait until it reads -30 psi.
- 6.2.3 Close the vacuum valve.
- 6.2.4 Open the lower bypass valve. The vacuum gauge, V, should immediately register -8 psi. (Opening the lower bypass allows the lower chamber to fill with hydrogen).
- 6.2.5 Close the lower bypass valve.
- 6.2.6 Open the vacuum valve.
- 6.2.7 Observe the vacuum gauge and wait until it reads -30 psi.
- 6.2.8 Close the vacuum valve.
- 6.2.9 Open the lower bypass valve.
- 6.2.10 Open the flow valve to 2.0 psi and then tighten to maintain even flow.
- 6.2.11 Open the upper bypass valve.

### 6.3 Lowering the Double Slide Bars

- 6.3.1 Open the gate valve.
- 6.3.2 Loosen the star nut.
- 6.3.3 Lower the rod 5 or 6 inches.
- 6.3.4 Tighten the star nut and wait approximately 30 seconds.

- 6.3.5 Repeat procedure several times until only 6 inches ( $\pm 1$  inch) of the rod remains extended from the face plate.
- 6.3.6 At 5.0 minutes loosen the star nut.
- 6.3.7 Lower the rod 3 additional inches so that only 3.0 inches ( $\pm 0.5$  inch) is exposed.
- 6.3.8 Tighten the star nut.
- 6.3.9 Set the timer for 4.0 minutes.
- 6.3.10 While waiting, push the rotating motor into gear.
- 6.3.11 Hand tighten the wing nut securing the motor.
- 6.3.12 At 4.0 minutes, loosen the star nut.
- 6.3.13 Lower the rod all the way down.
- 6.3.14 Tighten the star nut.

#### 6.4 Melt Cool Down

- 6.4.1 Start the rotating motor.
- 6.4.2 Immediately advance the chart paper about 0.5 inch.
- 6.4.3 Immediately initiate the program by throwing the appropriate toggle switch.

#### 6.5 Temperature and Time Selection

- 6.5.1 In the log book record the following: the date, the run number (the next consecutive number), the four slice numbers, the selected starting temperature, the anticipated time duration of buffer layer growth, the vendor's ingot number, and the speed of the rotating motor.
- 6.5.2 Mark the chart paper at the selected temperature.
- 6.5.3 Determine the anticipated time that the slide bar will be held open. To do this again a review of previous run(s) is necessary.

#### 6.6 Buffer Layer Growth

- 6.6.1 When the pen of the chart recorder reaches the selected temperature, loosen the head nut on the end of the rod of the slide bar holder.

- 6.3.5 Repeat procedure several times until only 6 inches ( $\pm 1$  inch) of the rod remains extended from the face plate.
- 6.3.6 At 5.0 minutes loosen the star nut.
- 6.3.7 Lower the rod 3 additional inches so that only 3.0 inches ( $\pm 0.5$  inch) is exposed.
- 6.3.8 Tighten the star nut.
- 6.3.9 Set the timer for 4.0 minutes.
- 6.3.10 While waiting, push the rotating motor into gear.
- 6.3.11 Hand tighten the wing nut securing the motor.
- 6.3.12 At 4.0 minutes, loosen the star nut.
- 6.3.13 Lower the rod all the way down.
- 6.3.14 Tighten the star nut.

#### 6.4 Melt Cool Down

- 6.4.1 Start the rotating motor.
- 6.4.2 Immediately advance the chart paper about 0.5 inch.
- 6.4.3 Immediately initiate the program by throwing the appropriate toggle switch.

#### 6.5 Temperature and Time Selection

- 6.5.1 In the log book record the following: the date, the run number (the next consecutive number), the four slice numbers, the selected starting temperature, the anticipated time duration of buffer layer growth, the vendor's ingot number, and the speed of the rotating motor.
- 6.5.2 Mark the chart paper at the selected temperature.
- 6.5.3 Determine the anticipated time that the slide bar will be held open. To do this again a review of previous run(s) is necessary.

#### 6.6 Buffer Layer Growth

- 6.6.1 When the pen of the chart recorder reaches the selected temperature, loosen the head nut on the end of the rod of the slide bar holder.

## PROCEDURE 7. GALLIUM ARSENIDE REACTOR UNLOAD

**SCOPE:** This procedure describes the removal of the substrate-loaded slide bar assembly from the buffer layer or window layer reactor after the layer growth cycle.

### 7.1 Preliminary Operations

- 7.1.1 Ensure that the vertical slide rod is extended to the full elevated position.
- 7.1.2 Ensure that the slide rod position is locked.
- 7.1.3 Ensure that the gate valve is completely closed.

### 7.2 Flushing the Entry Chamber

- 7.2.1 Close the upper bypass valve.
- 7.2.2 Close the lower bypass valve.
- 7.2.3 Open the vacuum valve.
- 7.2.4 Observe the vacuum gauge and wait until it reads -30 psi.
- 7.2.5 Close the vacuum valve.
- 7.2.6 Open the inlet valve.
- 7.2.7 Observe the vacuum gauge and wait until it indicates 0 or above.
- 7.2.8 Close the inlet valve.

### 7.3 Slide Bar Assembly Unload

- 7.3.1 Loosen the three wing nuts.
- 7.3.2 With a gloved hand, grasp the extended slide rod and lift the slide bar holder/slide bar assembly up and out of the entry chamber.
- 7.3.3 Immediately cover the entry chamber port with an inverted pietri dish.
- 7.3.4 Remove the slide bar holder/slide bar assembly to the clean hooded area used for loading and unloading substrates and clamp the face plate into the vise.

- 6.6.2 Immediately raise the rod smoothly and fully in order to expose the substrates to the melt.
- 6.6.3 Retighten the head nut.
- 6.6.4 Immediately start the timer.
- 6.6.5 Immediately advance the chart paper about 0.5 inch.

#### 6.7 Raising the Double Slide Bar

- 6.7.1 At exactly the end of the growth period, advance the chart paper to record the final temperature.
- 6.7.2 Immediately loosen the head nut.
- 6.7.3 Immediately drop the rod to 0.25 inch of completely down.
- 6.7.4 Immediately tighten the head nut.
- 6.7.5 Immediately loosen the star nut.
- 6.7.6 Immediately raise the rod 6 full inches.
- 6.7.7 Loosen the head nut.
- 6.7.8 With a smooth, continuous motion, quickly open the slide panels all the way and then close completely.
- 6.7.9 Tighten the head nut.
- 6.7.10 Continue to raise the rod up until the shaft feels too hot to touch.
- 6.7.11 Tighten the star nut and wait approximately 4.0 minutes.
- 6.7.12 After 4.0 minutes, loosen the star nut.
- 6.7.13 Bring the rod up to full extension.
- 6.7.14 Tighten the star nut.
- 6.7.15 Immediately close the gate valve.
- 6.7.16 Allow assembly to cool another ~5.0 minutes.
- 6.7.17 Record the final temperature in the log.

## PROCEDURE 8. GALLIUM ARSENIDE SLIDE BAR UNLOAD

**SCOPE:** This procedure describes the disassembly of the buffer layer or window layer slide bar, the removal of substrates upon which the layers have been growing and the cleaning of the double slide bar components.

### 8.1 Preliminary Operations

- 8.1.1 Ensure that the slide bars are oriented properly.
- 8.1.2 Using various camel hair brushes and/or foam swabs, remove excess material from all outer surfaces of the individual slide bars.

### 8.2 Upper Slide Bar Removal

- 8.2.1 Remove the four graphite thumb screws.
- 8.2.2 Remove the two graphite L-shaped plates.
- 8.2.3 Remove the metal central screw.
- 8.2.4 Pull the loosened upper slide bar to the left off the supporting posts of the holder.

### 8.3 Substrate Removal from Upper Slide Bar

- 8.3.1 Loosen graphite screw.
- 8.3.2 Turn slide bar right side up and release substrate "a" by sliding away (to the right) the pressure bar.
- 8.3.3 Slide the panel to expose the fourth substrate. Lift the substrate from the holder using plastic tweezers.
- 8.3.4 Repeat procedures for the third substrate.

### 8.4 Substrate Removal from Lower Slide Bar

- 8.4.1 Place the screwdriver under the appropriate slide bar and loosen the graphite screw.
- 8.4.2 Release the second substrate.

## PROCEDURE 7. GALLIUM ARSENIDE REACTOR UNLOAD

**SCOPE:** This procedure describes the removal of the substrate-loaded slide bar assembly from the buffer layer or window layer reactor after the layer growth cycle.

### 7.1 Preliminary Operations

- 7.1.1 Ensure that the vertical slide rod is extended to the full elevated position.
- 7.1.2 Ensure that the slide rod position is locked.
- 7.1.3 Ensure that the gate valve is completely closed.

### 7.2 Flushing the Entry Chamber

- 7.2.1 Close the upper bypass valve.
- 7.2.2 Close the lower bypass valve.
- 7.2.3 Open the vacuum valve.
- 7.2.4 Observe the vacuum gauge and wait until it reads -30 psi.
- 7.2.5 Close the vacuum valve.
- 7.2.6 Open the inlet valve.
- 7.2.7 Observe the vacuum gauge and wait until it indicates 0 or above.
- 7.2.8 Close the inlet valve.

### 7.3 Slide Bar Assembly Unload

- 7.3.1 Loosen the three wing nuts.
- 7.3.2 With a gloved hand, grasp the extended slide rod and lift the slide bar holder/slide bar assembly up and out of the entry chamber.
- 7.3.3 Immediately cover the entry chamber port with an inverted pietri dish.
- 7.3.4 Remove the slide bar holder/slide bar assembly to the clean hooded area used for loading and unloading substrates and clamp the face plate into the vise.

- 8.4.3 Loosen head nut, H, and slide panel open by extending the metal rod at H.
- 8.4.4 Lift the substrate from the holder using plastic tweezers.
- 8.4.5 Loosen the pressure bar using a screwdriver.
- 8.4.6 Release the first substrate.
- 8.4.7 Loosen the head nut, H, and slide panel open by extending the metal rod at H.
- 8.4.8 Lift the substrate from the holder using plastic tweezers.
- 8.4.9 Close the slide panels by manipulating the metal rod.

8.5 Upper Slide Bar Clean

- 8.5.1 Brush all areas of the upper slide bar with various camel hair brushes. Dismantle and replace parts as required.
- 8.5.2 Use foam swabs to clean in hard-to-reach areas.

8.6 Lower Slide Bar Clean

- 8.6.1 Brush all areas with various camel hair brushes. Dismantle and replace parts as required.
- 8.6.2 Use foam swabs to clean in hard-to-reach areas.

## PROCEDURE 8. GALLIUM ARSENIDE SLIDE BAR UNLOAD

**SCOPE:** This procedure describes the disassembly of the buffer layer or window layer slide bar, the removal of substrates upon which the layers have been growing and the cleaning of the double slide bar components.

### 8.1 Preliminary Operations

- 8.1.1 Ensure that the slide bars are oriented properly.
- 8.1.2 Using various camel hair brushes and/or foam swabs, remove excess material from all outer surfaces of the individual slide bars.

### 8.2 Upper Slide Bar Removal

- 8.2.1 Remove the four graphite thumb screws.
- 8.2.2 Remove the two graphite L-shaped plates.
- 8.2.3 Remove the metal central screw.
- 8.2.4 Pull the loosened upper slide bar to the left off the supporting posts of the holder.

### 8.3 Substrate Removal from Upper Slide Bar

- 8.3.1 Loosen graphite screw.
- 8.3.2 Turn slide bar right side up and release substrate "a" by sliding away (to the right) the pressure bar.
- 8.3.3 Slide the panel to expose the fourth substrate. Lift the substrate from the holder using plastic tweezers.
- 8.3.4 Repeat procedures for the third substrate.

### 8.4 Substrate Removal from Lower Slide Bar

- 8.4.1 Place the screwdriver under the appropriate slide bar and loosen the graphite screw.
- 8.4.2 Release the second substrate.

## PROCEDURE 9. GALLIUM ARSENIDE BUFFER LAYER MEASUREMENT AND INSPECTION

SCOPE: This procedure describes the cleaning of the substrates after buffer layer growth and the measurement of buffer layer thickness.

### 9.1 Preliminary Operations

- 9.1.1 Fill a 50 ml pyrex beaker with 40 ml of deionized water, cover with a watch glass and heat to 80°C.
- 9.1.2 Examine carefully a pair of disposable gloves for holes, cracks, or any sign of wear or defects.
- 9.1.3 Put on gloves only if they are in excellent condition.
- 9.1.4 Mix a stock solution of the A portion of the universal stain by combining the following into a 100 ml plastic bottle:
  - 40 ml deionized water ( $H_2O$ )
  - 40 ml hydrofluoric acid (HF)
  - 0.3 gms silver nitrate ( $AgNO_3$ )

CAUTION: GREAT CARE MUST BE EXERCISED IN HANDLING HYDROFLUORIC ACID. BECOME FULLY AWARE OF ALL PRE-CAUTIONS BEFORE PREPARING THIS SOLUTION.
- 9.1.5 Mark a self-adhering label with the letter "A" and attach to this bottle.
- 9.1.6 Mix a stock solution of the B portion of the universal stain by combining the following into another 100 ml plastic bottle:
  - 40 ml deionized water ( $H_2O$ )
  - 40 gms chromic trioxide ( $CrO_3$ )
- 9.1.7 Mark a self-adhering label with the letter "B" and attach to this bottle.
- 9.1.8 Mark a self-adhering label with the words "AB STAIN" and attach to the 50 ml plastic container with the cover.

- 8.4.3 Loosen head nut, H, and slide panel open by extending the metal rod at H.
- 8.4.4 Lift the substrate from the holder using plastic tweezers.
- 8.4.5 Loosen the pressure bar using a screwdriver.
- 8.4.6 Release the first substrate.
- 8.4.7 Loosen the head nut, H, and slide panel open by extending the metal rod at H.
- 8.4.8 Lift the substrate from the holder using plastic tweezers.
- 8.4.9 Close the slide panels by manipulating the metal rod.

8.5 Upper Slide Bar Clean

- 8.5.1 Brush all areas of the upper slide bar with various camel hair brushes. Dismantle and replace parts as required.
- 8.5.2 Use foam swabs to clean in hard-to-reach areas.

8.6 Lower Slide Bar Clean

- 8.6.1 Brush all areas with various camel hair brushes. Dismantle and replace parts as required.
- 8.6.2 Use foam swabs to clean in hard-to-reach areas.

## 9.2 Clean Substrates Having Buffer Layers

- 9.2.1 Using plastic tweezers submerge the substrate into the 50 ml beaker of warm deionized water on the hot plate and gently wipe the substrate with a foam swab.
- 9.2.2 Place the substrate into a glass basket substrate holder.
- 9.2.3 Rinse the substrate for at least 1.0 minute in running deionized water.
- 9.2.4 Dry.

## 9.3 Cleave Substrate

- 9.3.1 Place the substrate onto a glass slide so that the bottom of the substrate (the part of the substrate that was lowest in the slide bar chamber when the buffer layer was grown) extends approximately 1/8 inch over the edge of the glass.
- 9.3.2 Using a diamond scribe, notch the substrate.
- 9.3.3 Gently tap the extended section with a small blunt instrument. The 1/8 inch sliver will drop away.

## 9.4 Stain Substrate Sliver

- 9.4.1 In the 50 ml plastic beaker labeled "AB STAIN" mix a 10 ml solution in the following approximate proportions:
  - 1 part stock solution "A"
  - 1 part stock solution
  - 2 parts deionized water
- 9.4.2 Using plastic tweezers place the sliver into the solution.
- 9.4.3 Swish sliver around in the solution for 25 seconds.
- 9.4.4 Remove sliver with plastic tweezers.
- 9.4.5 Rinse thoroughly the sliver in running deionized water for at least 1.0 minute.
- 9.4.6 Dry.

## PROCEDURE 9. GALLIUM ARSENIDE BUFFER LAYER MEASUREMENT AND INSPECTION

SCOPE: This procedure describes the cleaning of the substrates after buffer layer growth and the measurement of buffer layer thickness.

### 9.1 Preliminary Operations

- 9.1.1 Fill a 50 ml pyrex beaker with 40 ml of deionized water, cover with a watch glass and heat to 80°C.
- 9.1.2 Examine carefully a pair of disposable gloves for holes, cracks, or any sign of wear or defects.
- 9.1.3 Put on gloves only if they are in excellent condition.
- 9.1.4 Mix a stock solution of the A portion of the universal stain by combining the following into a 100 ml plastic bottle:
  - 40 ml deionized water ( $H_2O$ )
  - 40 ml hydrofluoric acid (HF)
  - 0.3 gms silver nitrate ( $AgNO_3$ )

CAUTION: GREAT CARE MUST BE EXERCISED IN HANDLING HYDROFLUORIC ACID. BECOME FULLY AWARE OF ALL PRE-CAUTIONS BEFORE PREPARING THIS SOLUTION.
- 9.1.5 Mark a self-adhering label with the letter "A" and attach to this bottle.
- 9.1.6 Mix a stock solution of the B portion of the universal stain by combining the following into another 100 ml plastic bottle:
  - 40 ml deionized water ( $H_2O$ )
  - 40 gms chromic trioxide ( $CrO_3$ )
- 9.1.7 Mark a self-adhering label with the letter "B" and attach to this bottle.
- 9.1.8 Mark a self-adhering label with the words "AB STAIN" and attach to the 50 ml plastic container with the cover.

### **9.5 Measure Buffer Thickness**

- 9.5.1 Mount sliver in tiny spring-mounted microscope clamp.
- 9.5.2 Place clamp holding sliver on x-y stage of the microscope.
- 9.5.3 Focus and align graticule onto the cleaved edge surface.
- 9.5.4 Measure buffer layer depth.
- 9.5.5 Repeat the measuring process for three different areas on the edge of the same sliver.
- 9.5.6 Average the three readings.
- 9.5.7 Record the average on the glassine envelope for the particular substrate under test.
- 9.5.8 Record the average in the buffer reactor log book and traveler under the layer thickness heading.
- 9.5.9 Record the condition of the surface under "remarks" in the buffer layer system log book and traveler. The following criteria should be observed in judging surface condition:
  - Excellent - At least two good cells can be cleaved from the substrate, and there are no surface defects whatsoever.
  - Good - Two good cells can be cleaved from the substrate but there are some surface defects.
  - Fair - Only one good cell can be cleaved from the substrate, and surface defects are more extensive.

### **9.6 Repeat Operations**

- 9.6.1 Repeat all procedures from 9.2.1 through 9.5.9 for the three remaining substrates.

## 9.2 Clean Substrates Having Buffer Layers

- 9.2.1 Using plastic tweezers submerge the substrate into the 50 ml beaker of warm deionized water on the hot plate and gently wipe the substrate with a foam swab.
- 9.2.2 Place the substrate into a glass basket substrate holder.
- 9.2.3 Rinse the substrate for at least 1.0 minute in running deionized water.
- 9.2.4 Dry.

## 9.3 Cleave Substrate

- 9.3.1 Place the substrate onto a glass slide so that the bottom of the substrate (the part of the substrate that was lowest in the slide bar chamber when the buffer layer was grown) extends approximately 1/8 inch over the edge of the glass.
- 9.3.2 Using a diamond scribe, notch the substrate.
- 9.3.3 Gently tap the extended section with a small blunt instrument. The 1/8 inch sliver will drop away.

## 9.4 Stain Substrate Sliver

- 9.4.1 In the 50 ml plastic beaker labeled "AB STAIN" mix a 10 ml solution in the following approximate proportions:
  - 1 part stock solution "A"
  - 1 part stock solution
  - 2 parts deionized water
- 9.4.2 Using plastic tweezers place the sliver into the solution.
- 9.4.3 Swish sliver around in the solution for 25 seconds.
- 9.4.4 Remove sliver with plastic tweezers.
- 9.4.5 Rinse thoroughly the sliver in running deionized water for at least 1.0 minute.
- 9.4.6 Dry.

### **9.5 Measure Buffer Thickness**

- 9.5.1 Mount sliver in tiny spring-mounted microscope clamp.**
- 9.5.2 Place clamp holding sliver on x-y stage of the microscope.**
- 9.5.3 Focus and align graticule onto the cleaved edge surface.**
- 9.5.4 Measure buffer layer depth.**

PROCEDURE 10. GALLIUM ARSENIDE SUBSTRATE PREPARATION  
FOR WINDOW LAYER

SCOPE: This procedure describes the inspection and cleaning of the substrates immediately before loading into the window layer slide bar.

10.1 Preliminary Operations

10.1.1 Into the 3-liter bottle labeled "ETCH #1", mix a stock solution of the following:

- 1600 ml deionized water
- 34 ml ammonium hydroxide
- 14 ml hydrogen peroxide

10.1.2 Into the 3-liter bottle labeled "ETCH #2", mix a stock solution consisting of the following:

- 1 part deionized water
- 1 part hydrogen peroxide
- 5 parts sulphuric acid

10.1.3 Place one self-adhering label on each of seven 300 ml beakers and mark as follows: FREON, TCE #1, TCE #2, TOL, ISO, ETCH #1, and ETCH #2.

10.1.4 Fill each of the seven beakers with 200 ml of the appropriate solvent or acid.

10.2 Visual Inspection

10.2.1 Using plastic tweezers, select the next available substrate.

10.2.2 Examine visually the potential solar cell surface area for the following:

- Excessive narrowness (it must be 0.9 inch)
- Excessive shortness (for 2 cells it must be 2.25 inches)
- Excessive dips in the surface

- 10.3.14 Immediately transfer the substrates to the middle stage for 3.0 minutes.
- 10.3.15 After 3.0 minutes, remove two substrates from the water, shake gently, and place simultaneously into ETCH #2 for exactly 15 seconds.
- 10.3.16 After 15 seconds, remove from the acid and submerge into the lowest stage of the cascading beaker for a  $10 \pm 2$  seconds while stirring constantly.
- 10.3.17 Immediately afterward place substrates into middle stage again for 3.0 minutes.
- 10.3.18 After 3.0 minutes, transfer to the highest stage, cover, and time for 2.0 minutes.
- 10.3.19 After 2.0 minutes, remove each substrate individually and dry exceedingly thoroughly.

- Excessive buffer melt material
- Other defects

### 10.3 Substrate Clean

- 10.3.1 If acceptable, clean both sides and the edges of the substrate as necessary with Freon-soaked cotton swabs.
- 10.3.2 Submerge in trichloroethylene (TCE #1) for 5 seconds and scrub again.
- 10.3.3 Load the substrate into an appropriate glass basket substrate holder.
- 10.3.4 Take the associated glassine bag and add the following information:
  - Date
  - W 10, in which W implies window layer and 10 indicates System X.
- 10.3.5 Repeat steps 10.3.1 through 10.3.4 for four substrates.
- 10.3.6 Place all four substrates again into TCE #1 simultaneously.
- 10.3.7 One-by-one, remove each and quickly dry in N<sub>2</sub>.
- 10.3.8 After drying, place each into TCE #2 for 4.0 minutes. Then dry.
- 10.3.9 Place all four into TOL, cover, and time 3.0 minutes. Then dry.
- 10.3.10 Place all four into ISO, cover, and time 3.0 minutes. Then dry.
- 10.3.11 Place all four into the middle stage of the cascading beaker (with water running) for 3.0 minutes.
- 10.3.12 After 3.0 minutes, place simultaneously into ETCH #1 for exactly 30 seconds.
- 10.3.13 After 30 seconds, remove and submerge into the lowest stage of the cascading beaker, stirring constantly for 10±2 seconds.

## PROCEDURE 11. GALLIUM ARSENIDE REACTOR RUN - WINDOW LAYER

SCOPE: This procedure describes the operation of the liquid phase epitaxial reactor for growing the window layer.

### 11.1 Preliminary Operations

- 11.1.1 The buffer reactor must be periodically reprogrammed with each replenishing of melt material or dopant level.
- 11.1.2 Ensure that the gate valve is fully closed.

### 11.2 Entry Chamber Evacuation

- 11.2.1 Open the vacuum valve.
- 11.2.2 Observe the vacuum gauge and wait until it indicates  $\leq 25$  psi.
- 11.2.3 Close the vacuum valve.
- 11.2.4 Open the lower bypass valve.
- 11.2.5 Close the lower bypass valve.
- 11.2.6 Press button 8, which engages the automatic pumpdown sequence.
- 11.2.7 Press button 9, which actually starts the sequence.
- 11.2.8 Start the chart paper.
- 11.2.9 Advance the chart paper. This defines on the chart paper the beginning point of the cooldown phase.

### 11.3 Lowering the Double Slide Bar

- 11.3.1 Loosen the star nut of the slide bar holder.
- 11.3.2 Lower the rod so that only 6.0 inches extend.
- 11.3.3 Tighten the star nut.
- 11.3.4 Immediately set the timer for 5.0 minutes.
- 11.3.5 After 5.0 minutes, loosen the star nut.

- 10.3.14 Immediately transfer the substrates to the middle stage for 3.0 minutes.
- 10.3.15 After 3.0 minutes, remove two substrates from the water, shake gently, and place simultaneously into ETCH #2 for exactly 15 seconds.
- 10.3.16 After 15 seconds, remove from the acid and submerge into the lowest stage of the cascading beaker for a  $10 \pm 2$  seconds while stirring constantly.
- 10.3.17 Immediately afterward place substrates into middle stage again for 3.0 minutes.
- 10.3.18 After 3.0 minutes, transfer to the highest stage, cover, and time for 2.0 minutes.
- 10.3.19 After 2.0 minutes, remove each substrate individually and dry exceedingly thoroughly.

- 11.3.6 Lower the rod another 3.0 inches.
- 11.3.7 Tighten the star nut.
- 11.3.8 Immediately set the timer for another 5.0 minutes.
- 11.3.9 While waiting, record the following information onto the System X log manual: The date, individual cell numbers, LEPI number (the next consecutive number), the vendor's ingot number, and the starting temperature.
- 11.3.10 After 5.0 minutes, loosen the star nut.
- 11.3.11 Slowly lower the rod all the way down.
- 11.3.12 Quickly engage the motor into gear around the slide bar holder.
- 11.3.13 Translate the selected growth temperature (750°C) into chart paper units. Mark the chart paper at this temperature.
- 11.3.14 Adjust the height of the stopper bar for the rod to extend to just barely expose all four substrates.
- 11.3.15 Swing stopper bar, S, over the top of the rod of slide bar holder.

#### 11.4 Window Layer Growth

- 11.4.1 When the temperature indicated by the chart reaches the 750°C mark, immediately loosen the head nut.
- 11.4.2 Quickly but smoothly open the slide by extending the rod up to the stopper bar.
- 11.4.3 Quickly tighten the head nut.
- 11.4.4 Quickly start the timer.
- 11.4.5 Quickly reset the temperature clock by throwing the reset toggle.
- 11.4.6 Rotate the chart 0.5 inch to mark the exact temperature of growth start.

#### 11.5 Raising the Double Slide Bar

- 11.5.1 After 3.0 minutes ( $\pm 15$  seconds), again rotate the chart paper 0.5 inch to record the specific temperature of growth finish.

## PROCEDURE 11. GALLIUM ARSENIDE REACTOR RUN - WINDOW LAYER

SCOPE: This procedure describes the operation of the liquid phase epitaxial reactor for growing the window layer.

### 11.1 Preliminary Operations

- 11.1.1 The buffer reactor must be periodically reprogrammed with each replenishing of melt material or dopant level.
- 11.1.2 Ensure that the gate valve is fully closed.

### 11.2 Entry Chamber Evacuation

- 11.2.1 Open the vacuum valve.
- 11.2.2 Observe the vacuum gauge and wait until it indicates  $\leq 25$  psi.
- 11.2.3 Close the vacuum valve.
- 11.2.4 Open the lower bypass valve.
- 11.2.5 Close the lower bypass valve.
- 11.2.6 Press button 8, which engages the automatic pumpdown sequence.
- 11.2.7 Press button 9, which actually starts the sequence.
- 11.2.8 Start the chart paper.
- 11.2.9 Advance the chart paper. This defines on the chart paper the beginning point of the cooldown phase.

### 11.3 Lowering the Double Slide Bar

- 11.3.1 Loosen the star nut of the slide bar holder.
- 11.3.2 Lower the rod so that only 6.0 inches extend.
- 11.3.3 Tighten the star nut.
- 11.3.4 Immediately set the timer for 5.0 minutes.
- 11.3.5 After 5.0 minutes, loosen the star nut.

- 11.5.2 Disengage the motor.
- 11.5.3 Quickly raise the outer rod up to the stop bar (which closes the slide panels).
- 11.5.4 Continue to raise the rod to about 6 inches high.
- 11.5.5 Tighten star nut.
- 11.5.6 Loosen the head nut.
- 11.5.7 Extend completely the rod to dump from the slide chambers all melt.
- 11.5.8 Close the slide rod completely.
- 11.5.9 Tighten the head nut.
- 11.5.10 Loosen the star nut.
- 11.5.11 Bring double slide bar up to the point where it can be seen through the glass port in the side of the chamber.
- 11.5.12 Set the timer for approximately 5.0 minutes.
- 11.5.13 Record the following into the lot and traveler by examining the chart:
  - $T_1$  = Temperature at start of the program
  - $T_2$  = Temperature at beginning of window growth
  - $T_3$  = Temperature at the end of window growth
  - $T_g$  = Growth duration (time)
- 11.5.14 After 5.0 minutes open the star nut.
- 11.5.15 Pull the slide bar holder to the limit.
- 11.5.16 Tighten the star nut.
- 11.5.17 Set the timer for 5.0 minutes.
- 11.5.18 Shut the gate valve.

- 11.3.6 Lower the rod another 3.0 inches.
- 11.3.7 Tighten the star nut.
- 11.3.8 Immediately set the timer for another 5.0 minutes.
- 11.3.9 While waiting, record the following information onto the System X log manual: The date, individual cell numbers, LEPI number (the next consecutive number), the vendor's ingot number, and the starting temperature.
- 11.3.10 After 5.0 minutes, loosen the star nut.
- 11.3.11 Slowly lower the rod all the way down.
- 11.3.12 Quickly engage the motor into gear around the slide bar holder.
- 11.3.13 Translate the selected growth temperature (750°C) into chart paper units. Mark the chart paper at this temperature.
- 11.3.14 Adjust the height of the stopper bar for the rod to extend to just barely expose all four substrates.
- 11.3.15 Swing stopper bar, S, over the top of the rod of slide bar holder.

#### 11.4 Window Layer Growth

- 11.4.1 When the temperature indicated by the chart reaches the 750°C mark, immediately loosen the head nut.
- 11.4.2 Quickly but smoothly open the slide by extending the rod up to the stopper bar.
- 11.4.3 Quickly tighten the head nut.
- 11.4.4 Quickly start the timer.
- 11.4.5 Quickly reset the temperature clock by throwing the reset toggle.
- 11.4.6 Rotate the chart 0.5 inch to mark the exact temperature of growth start.

#### 11.5 Raising the Double Slide Bar

- 11.5.1 After 3.0 minutes ( $\pm 15$  seconds), again rotate the chart paper 0.5 inch to record the specific temperature of growth finish.

## PROCEDURE 12. GALLIUM ARSENIDE WINDOW LAYER ANNEAL

SCOPE: This procedure describes the cleaning, annealing, and sizing of the substrate after the window layer growth.

### 12.1 Clean Substrate

12.1.1 Remove excess material by heating on hot plate no higher than 49°C.

12.1.2 Clean with Freon and cotton swab. TAKE CARE NOT TO SWAB CLEAN CELL AREA.

### 12.2 Cleave Substrate

12.2.1 Inspect substrate and identify areas of gallium-substrate interaction.

12.2.2 Scribe and cleave off areas of gallium-substrate interaction near bottom of substrate.

12.2.3 Place the longest and straightest edge of the substrate between two glass slides with self-adhering labels. Scribe and cleave substrate at least 0.95 inches wide.

12.2.4 Align the shortest edge of the substrate onto alignment tool and scribe to 0.9 inch.

12.2.5 Rotate substrate in alignment tool by 90°, scribe and cleave.

### 12.3 Load Slide Bar

### 12.4 Load Slide Bar into Window Layer Reactor

12.4.1 Loosen the star nut of the slide bar holder.

12.4.2 Lower the rod so that only 8.0 inches ( $\pm 0.25$  inch) extends between the rotating gear and the lowest hexagonal nut.

12.4.3 Tighten the star nut.

12.4.4 Immediately set the timer for 5.0 minutes.

12.4.5 After 5.0 minutes, loosen the star nut.

- 11.5.2 Disengage the motor.
- 11.5.3 Quickly raise the outer rod up to the stop bar (which closes the slide panels).
- 11.5.4 Continue to raise the rod to about 6 inches high.
- 11.5.5 Tighten star nut.
- 11.5.6 Loosen the head nut.
- 11.5.7 Extend completely the rod to dump from the slide chambers all melt.
- 11.5.8 Close the slide rod completely.
- 11.5.9 Tighten the head nut.
- 11.5.10 Loosen the star nut.
- 11.5.11 Bring double slide bar up to the point where it can be seen through the glass port in the side of the chamber.
- 11.5.12 Set the timer for approximately 5.0 minutes.
- 11.5.13 Record the following into the lot and traveler by examining the chart:
  - $T_1$  = Temperature at start of the program
  - $T_2$  = Temperature at beginning of window growth
  - $T_3$  = Temperature at the end of window growth
  - $T_g$  = Growth duration (time)
- 11.5.14 After 5.0 minutes open the star nut.
- 11.5.15 Pull the slide bar holder to the limit.
- 11.5.16 Tighten the star nut.
- 11.5.17 Set the timer for 5.0 minutes.
- 11.5.18 Shut the gate valve.

- 12.4.6 Lower the rod another 6.0 inches.
- 12.4.7 Tighten the star nut.
- 12.4.8 Immediately set timer for 5 minutes.
- 12.4.9 After 5.0 minutes, loosen the star nut.
- 12.4.10 Raise the rod 8.0 inches.
- 12.4.11 Tighten the star nut.
- 12.4.12 Immediately set time for 5 minutes.
- 12.4.13 After 5 minutes open gate valve.

12.5 Unload Slide Bar Assembly

12.6 Unload Slide Bar

12.7 Load Wafers into Assembly Mask

- 12.7.1 Assemble top frame, support fingers, and mask.
- 12.7.2 Carefully load one wafer at a time using clean plastic tweezers, inspecting for cleanliness. Ensure that window layer of wafer is facing up.
- 12.7.3 Continue loading till frame pockets are filled with wafers.
- 12.7.4 Carefully place top assembly frame over cells.
- 12.7.5 Insert 6 screws into retainer and tighten down evenly and carefully with nut driver, until a minimum tension is achieved.
- 12.7.6 Check frame to be sure wafers are seated flat.
- 12.7.7 Flip total assembly mask over and place magnet carefully on back of wafers.
- 12.7.8 Check front grid fingers for magnet distortion.
- 12.7.9 Continue loading wafers until amount of frame required for a run is loaded.

## PROCEDURE 12. GALLIUM ARSENIDE WINDOW LAYER ANNEAL

SCOPE: This procedure describes the cleaning, annealing, and sizing of the substrate after the window layer growth.

### 12.1 Clean Substrate

12.1.1 Remove excess material by heating on hot plate no higher than 49°C.

12.1.2 Clean with Freon and cotton swab. TAKE CARE NOT TO SWAB CLEAN CELL AREA.

### 12.2 Cleave Substrate

12.2.1 Inspect substrate and identify areas of gallium-substrate interaction.

12.2.2 Scribe and cleave off areas of gallium-substrate interaction near bottom of substrate.

12.2.3 Place the longest and straightest edge of the substrate between two glass slides with self-adhering labels. Scribe and cleave substrate at least 0.95 inches wide.

12.2.4 Align the shortest edge of the substrate onto alignment tool and scribe to 0.9 inch.

12.2.5 Rotate substrate in alignment tool by 90°, scribe and cleave.

### 12.3 Load Slide Bar

### 12.4 Load Slide Bar into Window Layer Reactor

12.4.1 Loosen the star nut of the slide bar holder.

12.4.2 Lower the rod so that only 8.0 inches ( $\pm 0.25$  inch) extends between the rotating gear and the lowest hexagonal nut.

12.4.3 Tighten the star nut.

12.4.4 Immediately set the timer for 5.0 minutes.

12.4.5 After 5.0 minutes, loosen the star nut.

## PROCEDURE 13. GALLIUM ARSENIDE AuZn SPUTTERED FRONT CONTACT

SCOPE: This procedure describes the process of forming the AuZn ohmic contact on the front of the substrate by a sputtering technique.

### 13.1 Load system

- 13.1.1 Power supply switch on; warm up 15 minutes.
- 13.1.2 Switch on LN<sub>2</sub>.
- 13.1.3 Press start and unload buttons.
- 13.1.4 Open by pressing and holding both lock cover switches.
- 13.1.5 Load cell holders.
- 13.1.6 Close by pressing and holding both lock cover switches.
- 13.1.7 Ensure that system pumps until pressure reads  $1 \times 10^{-7}$ .
- 13.1.8 Check to see that control function switch is set on X.01 Emission and that filament is on.

### 13.2 Sputter Etch

- 13.2.1 Start argon flow by pressing start and gas buttons located on auto pumpdown panel.
- 13.2.2 Switch function control knob to MTORR St 1.
- 13.2.3 Wait until the digital gauge reads 11 MTORR.
- 13.2.4 Set mode selector to sputter etch target selector.
- 13.2.5 Set clock: 1 minute 30 seconds. Close shutter.
- 13.2.6 Set servo control to manual.
- 13.2.7 Turn RF power on by pressing button.
- 13.2.8 Adjust RF power in both the forward and reflected directions.
- 13.2.9 Start clock/ etch 90 seconds at 1000 watts.

- 12.4.6 Lower the rod another 6.0 inches.
- 12.4.7 Tighten the star nut.
- 12.4.8 Immediately set timer for 5 minutes.
- 12.4.9 After 5.0 minutes, loosen the star nut.
- 12.4.10 Raise the rod 8.0 inches.
- 12.4.11 Tighten the star nut.
- 12.4.12 Immediately set time for 5 minutes.
- 12.4.13 After 5 minutes open gate valve.

12.5 Unload Slide Bar Assembly

12.6 Unload Slide Bar

12.7 Load Wafers into Assembly Mask

- 12.7.1 Assemble top frame, support fingers, and mask.
- 12.7.2 Carefully load one wafer at a time using clean plastic tweezers, inspecting for cleanliness. Ensure that window layer of wafer is facing up.
- 12.7.3 Continue loading till frame pockets are filled with wafers.
- 12.7.4 Carefully place top assembly frame over cells.
- 12.7.5 Insert 6 screws into retainer and tighten down evenly and carefully with nut driver, until a minimum tension is achieved.
- 12.7.6 Check frame to be sure wafers are seated flat.
- 12.7.7 Flip total assembly mask over and place magnet carefully on back of wafers.
- 12.7.8 Check front grid fingers for magnet distortion.
- 12.7.9 Continue loading wafers until amount of frame required for a run is loaded.

PROCEDURE 13. GALLIUM ARSENIDE AuZn SPUTTERED FRONT CONTACT

SCOPE: This procedure describes the process of forming the AuZn ohmic contact on the front of the substrate by a sputtering technique.

13.1 Load system

13.2.10 Turn RF power adjustment off.

13.2.11 Turn RF power button off.

13.3 Sputter Au

13.3.1 Set servo control switch to Auto.

13.3.2 Set mode selector to Sputter Deposit.

13.3.3 Set target selector to Target 1, Au.

13.3.4 Press RF power button to on; allow to zero.

13.3.5 Adjust power to 1000 watts.

13.3.6 Start clock and sputter deposit for 2 minutes.

13.3.7 Turn RF adjust off.

13.3.8 Turn RF power off.

13.4 Sputter Zn

13.4.1 Set servo control switch to Auto.

13.4.2 Set target selector switch to Target 3, Zn.

13.4.3 Press RF power button to on; will light when on.

13.4.4 Adjust RF power to 700 watts.

13.4.5 Start clock when amber indicator light goes out and sputter deposit for 2 minutes.

13.4.6 Turn RF power adjust off - counterclockwise to stop, zero.

13.4.7 Turn RF power off. Press light will go off.

13.5 Repeat Operations

Repeat procedures 13.3 and 13.4 THREE CONSECUTIVE TIMES.

13.6 Final Sputter Au

- 13.6.1 Repeat steps 13.3.1 through 13.3.5.
- 13.6.2 Stop rotation; look through porthole to stop rotation when holder is directly under target.
- 13.6.3 Start clock; deposit for 2 minutes.
- 13.6.4 Start rotation; move to next holder deposit for 2 minutes.
- 13.6.5 Repeat steps until each holder has had a 2 minute sputter deposit of Au.
- 13.6.6 Start rotation on.
- 13.6.7 Turn RF power adjust to zero.
- 13.6.8 Turn RF power off.
- 13.6.9 Turn Argon Off.
- 13.6.10 Switch function control knob to X.01.

13.7 Unload System

- 13.7.1 Press start and unload buttons.
- 13.7.2 Press and hold both lock cover switches.
- 13.7.3 Remove holders from system; place in plastic dessicators for transportation to system when metal contacts are completed.
- 13.7.4 Close by pressing and holding both lock cover switches.
- 13.7.5 Switch off LN<sub>2</sub>.
- 13.7.6 Turn off power.

13.6 Final Sputter Au

- 13.6.1 Repeat steps 13.3.1 through 13.3.5.
- 13.6.2 Stop rotation; look through porthole to stop rotation when holder is directly under target.
- 13.6.3 Start clock; deposit for 2 minutes.
- 13.6.4 Start rotation; move to next holder deposit for 2 minutes.
- 13.6.5 Repeat steps until each holder has had a 2 minute sputter deposit of Au.
- 13.6.6 Start rotation on.
- 13.6.7 Turn RF power adjust to zero.
- 13.6.8 Turn RF power off.
- 13.6.9 Turn Argon Off.
- 13.6.10 Switch function control knob to X.01.

13.7 Unload System

- 13.7.1 Press start and unload buttons.
- 13.7.2 Press and hold both lock cover switches.
- 13.7.3 Remove holders from system; place in plastic dessicators for transportation to system when metal contacts are completed.
- 13.7.4 Close by pressing and holding both lock cover switches.
- 13.7.5 Switch off LN<sub>2</sub>.
- 13.7.6 Turn off power.

## PROCEDURE 14. GALLIUM ARSENIDE EVAPORATED FRONT CONTACT

SCOPE: This procedure describes the process of applying the front grid metallization over the sputtered AuZn layer by a thermal evaporation technique.

### 14.1 Load Evapoation Chamber

- 14.1.1 Open air release valve.
- 14.1.2 Open bell jar.
- 14.1.3 Install proper boat (0.010 molybdenum with a 0.010 coating of Al<sub>2</sub>O<sub>3</sub>).
- 14.1.4 Load proper metal.
- 14.1.5 Place frames into chamber position until all are loaded.
- 14.1.6 Fill all necessary information on lot sheet and source sheet.
- 14.1.7 Close bell jar and foreline valve.

### 14.2 Pump Down

### 14.3 Evapoation of Contacts

- 14.3.1 Turn on power.
- 14.3.2 Switch selector switch to silver.
- 14.3.3 Turn bottom variac to 60 moderately slowly.
- 14.3.4 Wait 15 seconds, then open shutter.
- 14.3.5 Gradually increase variac to 72.
- 14.3.6 When current reads 60 ampere (about 1.5 minutes), close shutter; 6 μm layer of silver should be deposited.
- 14.3.7 Turn off power switch.
- 14.3.8 Wait 15 minutes.
- 14.3.9 Close high vacuum valve.
- 14.3.10 Turn range selector switch to 10<sup>-4</sup> range.

## PROCEDURE 14. GALLIUM ARSENIDE EVAPORATED FRONT CONTACT

SCOPE: This procedure describes the process of applying the front grid metallization over the sputtered AuZn layer by a thermal evaporation technique.

### 14.1 Load Evapoation Chamber

- 14.1.1 Open air release valve.
- 14.1.2 Open bell jar.
- 14.1.3 Install proper boat (0.010 molybdenum with a 0.010 coating of Al<sub>2</sub>O<sub>3</sub>).
- 14.1.4 Load proper metal.
- 14.1.5 Place frames into chamber position until all are loaded.
- 14.1.6 Fill all necessary information on lot sheet and source sheet.
- 14.1.7 Close bell jar and foreline valve.

### 14.2 Pump Down

### 14.3 Evapoation of Contacts

- 14.3.1 Turn on power.
- 14.3.2 Switch selector switch to silver.
- 14.3.3 Turn bottom variac to 60 moderately slowly.
- 14.3.4 Wait 15 seconds, then open shutter.
- 14.3.5 Gradually increase variac to 72.
- 14.3.6 When current reads 60 ampere (about 1.5 minutes), close shutter; 6 μm layer of silver should be deposited.
- 14.3.7 Turn off power switch.
- 14.3.8 Wait 15 minutes.
- 14.3.9 Close high vacuum valve.
- 14.3.10 Turn range selector switch to 10<sup>-4</sup> range.

**14.4 Open Chamber**

14.4.1 Open air release valve.

14.4.2 Open bell jar.

14.4.3 Remove frames.

**14.4 Open Chamber**

14.4.1 Open air release valve.

14.4.2 Open bell jar.

14.4.3 Remove frames.

## **PROCEDURE 15. GALLIUM ARSENIDE EVAPORATED BACK CONTACT**

**SCOPE:** This procedure describes the process of applying a highly conductive contact on the back by a thermal evaporation technique.

### **15.1 Load Evaporation Chamber**

- 15.1.1 Open air release valve.
- 15.1.2 Open bell jar.
- 15.1.3 Install proper boat for material to be deposited. In the case of silver use the 0.010 Molybdenum with a 0.010 coating of Al<sub>2</sub>O<sub>3</sub>. In the case of Ni-Au-Ge use tungsten boat.
- 15.1.4 Position boat on terminals and tighten nuts.
- 15.1.5 Load proper metals - both Ni-Ge-Au and Ag.
- 15.1.6 Place frames into chamber until all positions are loaded.
- 15.1.7 Fill all necessary information on lot sheet and source sheet.
- 15.1.8 Close bell jar and foreline valve.

### **15.2 Pump Down**

### **15.3 Evaporation of Contacts**

- 15.3.1 Turn on power.
- 15.3.2 Switch selector switch to Ni-Au-Ge.
- 15.3.3 Turn top variac to 60 moderately slowly.
- 15.3.4 Deposit until the Ni-Au-Ge is depleted.
- 15.3.5 Turn powerstat back to zero.
- 15.3.6 Continue pumpdown 15 more minutes.
- 15.3.7 Switch selector switch to silver.
- 15.3.8 Turn bottom variac to 60 moderately slowly.
- 15.3.9 Wait 15 seconds, then open shutter.

## **PROCEDURE 15. GALLIUM ARSENIDE EVAPORATED BACK CONTACT**

**SCOPE:** This procedure describes the process of applying a highly conductive contact on the back by a thermal evaporation technique.

### **15.1 Load Evaporation Chamber**

- 15.1.1 Open air release valve.
- 15.1.2 Open bell jar.
- 15.1.3 Install proper boat for material to be deposited. In the case of silver use the 0.010 Molybdenum with a 0.010 coating of Al<sub>2</sub>O<sub>3</sub>. In the case of Ni-Au-Ge use tungsten boat.
- 15.1.4 Position boat on terminals and tighten nuts.
- 15.1.5 Load proper metals - both Ni-Ge-Au and Ag.
- 15.1.6 Place frames into chamber until all positions are loaded.
- 15.1.7 Fill all necessary information on lot sheet and source sheet.
- 15.1.8 Close bell jar and foreline valve.

### **15.2 Pump Down**

### **15.3 Evaporation of Contacts**

- 15.3.1 Turn on power.
- 15.3.2 Switch selector switch to Ni-Au-Ge.
- 15.3.3 Turn top variac to 60 moderately slowly.
- 15.3.4 Deposit until the Ni-Au-Ge is depleted.
- 15.3.5 Turn powerstat back to zero.
- 15.3.6 Continue pumpdown 15 more minutes.
- 15.3.7 Switch selector switch to silver.
- 15.3.8 Turn bottom variac to 60 moderately slowly.
- 15.3.9 Wait 15 seconds, then open shutter.

15.3.10 Gradually increase variac to 72.

15.3.11 When current reads 60 amperes (about 1.5 minutes), close shutter; 6  $\mu$ m layer of silver should be deposited.

15.3.12 Turn off power switch.

15.3.13 Wait 15 minutes.

15.3.14 Close high vacuum valve.

15.3.15 Turn range selector switch to  $10^{-4}$  range.

15.4 Open chamber.

15.4.1 Open air release valve.

15.4.2 Open bell jar.

15.4.3 Remove frames.

15.3.10 Gradually increase variac to 72.

15.3.11 When current reads 60 amperes (about 1.5 minutes), close shutter; 6  $\mu$ m layer of silver should be deposited.

15.3.12 Turn off power switch.

15.3.13 Wait 15 minutes.

15.3.14 Close high vacuum valve.

15.3.15 Turn range selector switch to  $10^{-4}$  range.

15.4 Open chamber.

15.4.1 Open air release valve.

15.4.2 Open bell jar.

15.4.3 Remove frames.

## PROCEDURE 16. GALLIUM ARSENIDE SINTERED CONTACTS

SCOPE: This procedure describes the process of sintering the contact metallization.

### 16.1 Standby Preliminary Operations

- 16.1.1 Ensure gate valve is closed.
- 16.1.2 Ensure plate is secured with lock bolts.
- 16.1.3 Ensure furnace temperature is 930°C.
- 16.1.4 Ensure hydrogen gas flow meter at 15.
- 16.1.5 Ensure nitrogen valve closed.
- 16.1.6 Ensure hydrogen valve open.
- 16.1.7 Ensure vacuum valve closed.
- 16.1.8 Ensure hydrogen purge valve closed.
- 16.1.9 Ensure oxygen flow at 38.
- 16.1.10 Ensure fuel cell selector at OUT.
- 16.1.11 Ensure range selector at EXT.
- 16.1.12 Ensure function selector at SHORT.
- 16.1.13 Ensure range selector OFF.

### 16.2 Load System

- 16.2.1 Increase hydrogen flow to 65.
- 16.2.2 Set fuel cell selector to IN.
- 16.2.3 Set range selector to EXT.
- 16.2.4 Set function selector to OPERATE.
- 16.2.5 Set range extender to X1 after 3 ± 1 minutes.

## PROCEDURE 16. GALLIUM ARSENIDE SINTERED CONTACTS

SCOPE: This procedure describes the process of sintering the contact metallization.

### 16.1 Standby Preliminary Operations

- 16.1.1 Ensure gate valve is closed.
- 16.1.2 Ensure plate is secured with lock bolts.
- 16.1.3 Ensure furnace temperature is 930°C.
- 16.1.4 Ensure hydrogen gas flow meter at 15.
- 16.1.5 Ensure nitrogen valve closed.
- 16.1.6 Ensure hydrogen valve open.
- 16.1.7 Ensure vacuum valve closed.
- 16.1.8 Ensure hydrogen purge valve closed.
- 16.1.9 Ensure oxygen flow at 38.
- 16.1.10 Ensure fuel cell selector at OUT.
- 16.1.11 Ensure range selector at EXT.
- 16.1.12 Ensure function selector at SHORT.
- 16.1.13 Ensure range selector OFF.

### 16.2 Load System

- 16.2.1 Increase hydrogen flow to 65.
- 16.2.2 Set fuel cell selector to IN.
- 16.2.3 Set range selector to EXT.
- 16.2.4 Set function selector to OPERATE.
- 16.2.5 Set range extender to X1 after 3 ± 1 minutes.

- 16.2.6 Turn digital multimeter on.
- 16.2.7 Before opening load chamber, observe that gate valve and purge valve are closed.
- 16.2.8 Loosen wing nuts and remove latch bolts from slots.
- 16.2.9 Slide end cover assembly away.
- 16.2.10 Remove moly-holders.
- 16.2.11 Place cells in holder.
- 16.2.12 Replace holder on slide bar.
- 16.2.13 Slide cover assembly back.
- 16.2.14 Put the three latch bolts into slots and tighten wing nuts.
- 16.2.15 Tighten knurled nut connected to cover to prevent oxygen from being pulled into chamber when the chamber is evacuated.

### 16.3 Purge Forechamber

### 16.4 Sinter

- 16.4.1 Loosen knurled nut on end of cover so the slide bar is free to travel into furnace.
- 16.4.2 Push slide bar into furnace.
- 16.4.3 Withdraw slide bar immediately when temperature reaches 480°C. Tighten knurled nut.
- 16.4.4 Close gate valve.
- 16.4.5 Allow to cool to less than 80°C before opening.
- 16.4.6 Open vacuum valve; pump to 30 inches Hg.
- 16.4.7 Close vacuum valve.
- 16.4.8 Open purge valve slightly; purge until vacuum gauge returns to zero.
- 16.4.9 Close purge valve.

**16.5 Unload System**

- 16.5.1 Loosen wing nuts and remove lock bolts from slots.**
- 16.5.2 Slide and cover assembly away from furnace.**
- 16.5.3 Remove holder.**

## PROCEDURE 17. GALLIUM ARSENIDE ANTIREFLECTIVE COATING

SCOPE: This procedure describes the deposition of an antireflective coating on the active area of the solar cell. It also describes the replacing procedure of a crystal.

### 17.1 Standby Preliming Operations

- 17.1.1 Ensure vacuum valve closed.
- 17.1.2 Ensure roughing valve closed.
- 17.1.3 Ensure foreline valve open.
- 17.1.4 Ensure vent valve closed.
- 17.1.5 Ensure thremocouple selector set at TC2.

### 17.2 Load System

- 17.2.1 Vent system.
- 17.2.2 Raise bell jar.
- 17.2.3 Close vent valve.
- 17.2.4 Remove cell holders from system.
- 17.2.5 Loosen screws.
- 17.2.6 Position cells in holder.
- 17.2.7 Tighten screws.
- 17.2.8 Place holders cells down.
- 17.2.9 Lower bell jar.

### 17.3 Program INFICON Rate Meter

- 17.3.1 Switch power on. Meter is automatically placed in the program mode with the following indicator lights on:

Thickness 2  
Limit 1  
Limit 2  
T Limit  
Program  
Shutter opened or closed - Not in use.

17.3.2 Program THICKNESS 2      530 Å Push (7.5.0.E)  
                                        THICKNESS 1      500 Å Push (7.3.5.E)  
                                        DENSITY      8.2 Push (8.2.0.E)  
                                        Z RATIO      1.000 Push (E).  
                                        TOOLING 160 or 0      Push (1.6.0.0.E)

17.3.3 Verify entries.

17.4 Pump Down

- 17.4.1 Close foreline valve.
- 17.4.2 Open roughing valve.
- 17.4.3 Switch thermocouple selector to TC3 to monitor chamber pressure.
- 17.4.4 Close roughing valve when pressure is less than 50 µm.
- 17.4.5 Open foreline valve.
- 17.4.6 Open high vacuum valve.
- 17.4.7 Switch filament on.
- 17.4.8 Switch power E-beam power supply on.

17.5 Tantalum Oxide Deposition

- 17.5.1 Turn key lock on.
- 17.5.2 Turn high voltage on.
- 17.5.3 Turn gun filament on.
- 17.5.4 Increase emission current to 0.65 amperes, wait for two minutes; increase current to 0.75 amperes, wait 2 minutes; increase current to 0.85 amperes, wait 2 minutes.
- 17.5.5 Zero rate monitor.
- 17.5.6 Slowly increase emission current to 0.9. Evaporation of Ta<sub>2</sub>O<sub>5</sub> will begin.

17.3.2 Program THICKNESS 2      530 Å Push (7.5.0.E)  
                                        THICKNESS 1      500 Å Push (7.3.5.E)  
                                        DENSITY      8.2 Push (8.2.0.E)  
                                        Z RATIO      1.000 Push (E).  
                                        TOOLING 160 or 0      Push (1.6.0.0.E)

17.3.3 Verify entries.

17.4 Pump Down

- 17.4.1 Close foreline valve.
- 17.4.2 Open roughing valve.
- 17.4.3 Switch thermocouple selector to TC3 to monitor chamber pressure.
- 17.4.4 Close roughing valve when pressure is less than 50 µm.
- 17.4.5 Open foreline valve.
- 17.4.6 Open high vacuum valve.
- 17.4.7 Switch filament on.
- 17.4.8 Switch power E-beam power supply on.

17.5 Tantalum Oxide Deposition

- 17.5.1 Turn key lock on.
- 17.5.2 Turn high voltage on.
- 17.5.3 Turn gun filament on.
- 17.5.4 Increase emission current to 0.65 amperes, wait for two minutes; increase current to 0.75 amperes, wait 2 minutes; increase current to 0.85 amperes, wait 2 minutes.
- 17.5.5 Zero rate monitor.
- 17.5.6 Slowly increase emission current to 0.9. Evaporation of Ta<sub>2</sub>O<sub>5</sub> will begin.

17.5.7 Continue to evaporate until 530 Å is reached.

17.5.8 Switch gun No. 1 filament off.

17.5.9 Switch high voltage off.

17.5.10 Switch key lock off.

17.5.11 Close high vacuum valve.

17.5.12 Allow to cool 15 minutes.

#### 17.6 Unload System

17.6.1 Ensure that high vacuum and roughing valves are closed,  
foreline valve is open.

17.6.2 Vent system.

17.6.3 Raise bell jar.

17.6.4 Close vent valve.

17.6.5 Remove cell holders.

17.6.6 Losen screws, transfer cells from holder to carrying trays.

## APPENDIX C. SAFETY PLAN

A full spectrum of controls and procedures has been carefully instituted at Hughes Research Laboratory in compliance with OSHA standards to ensure the safety of the operating personnel and the long-term trouble-free operation of all equipment used in the program.

All personnel are instructed in OSHA safety standards and procedures for handling gases, chemicals, and other materials; they are provided with safety equipment such as lab coat, gloves, and safety glasses and have been instructed to use them whenever safety procedures require such use. In addition, the personnel are required to undergo periodic medical checkups for accidental exposure to heavy chemicals or other hazardous materials that they may come in contact with during the course of their work.

The laboratory is provided with monitors and safety alarm systems such as hydrogen alarms to ensure that safety hazards are minimized and all the personnel are instructed in proper procedures in case of emergencies. The laboratory has fully filtered air pumped through it at a high enough level to prevent the accumulation in it of chemicals to levels specified by OSHA requirements, and the air is continuously monitored to ensure that chemical concentrations are well below hazardous levels. Special disposal procedures for hazardous wastes have been instituted to ensure safety of the personnel and the environment.

Hughes Research Laboratory has a safety committee that continuously checks the enforcement of all safety regulations and keeps all the supervisory personnel aware of all new developments to improve laboratory safety.

## APPENDIX C. SAFETY PLAN

A full spectrum of controls and procedures has been carefully instituted at Hughes Research Laboratory in compliance with OSHA standards to ensure the safety of the operating personnel and the long-term trouble-free operation of all equipment used in the program.

All personnel are instructed in OSHA safety standards and procedures for handling gases, chemicals, and other materials; they are provided with safety equipment such as lab coat, gloves, and safety glasses and have been instructed to use them whenever safety procedures require such use. In addition, the personnel are required to undergo periodic medical checkups for accidental exposure to heavy chemicals or other hazardous materials that they may come in contact with during the course of their work.

The laboratory is provided with monitors and safety alarm systems such as hydrogen alarms to ensure that safety hazards are minimized and all the personnel are instructed in proper procedures in case of emergencies. The laboratory has fully filtered air pumped through it at a high enough level to prevent the accumulation in it of chemicals to levels specified by OSHA requirements, and the air is continuously monitored to ensure that chemical concentrations are well below hazardous levels. Special disposal procedures for hazardous wastes have been instituted to ensure safety of the personnel and the environment.

Hughes Research Laboratory has a safety committee that continuously checks the enforcement of all safety regulations and keeps all the supervisory personnel aware of all new developments to improve laboratory safety.

